Hydrogeological Characterization of the Upper Drâa Catchment: Morocco

Dissertation

zur

Erlangung des Doktorgrades (Dr. rer. nat.)

der

Mathematisch-Naturwissenschaftlichen Fakultät

der

der Rheinischen Friedich-Wilhelm-Universität Bonn

vorgelegt von

Sébastien Cappy

aus

Saint Cyr l´Ecole (Yvelines)

Bonn, August 2006

Erste Gutachterin: Prof. Dr. B. Reichert
Geologisches Institut der Universität Bonn

Zweiter Gutachter: Prof. Dr. B. Diekkrüger
Geographisches Institut der Universität Bonn

Tag der Prüfung: 20. November 2006

Diese Dissertation ist auf dem Hochschulschriftenserver der ULB Bonn *http://hss.ulb.uni-bonn.de/diss_online* elektronisch publiziert.

Erscheinungsjahr: 2007

ABSTRACT

The Drâa valley located in the south of Morocco is a typical semi-arid area facing water scarcity problems. This Ph.D. thesis is part of the interdisciplinary research project IMPETUS (integrated approach to the efficient management of scarce freshwater resources in West Africa), which is a project of the universities of Bonn and Cologne (Germany). The IMPETUS project is part of the GLOWA program (global change of the water cycle) funded by the German BMBF (Federal Ministry of Education and Research) and focuses on the development of integrated strategies for an efficient and sustainable freshwater resource management. Groundwater is one of the primordial components of the hydrological cycle. Therefore the aim of this work is to characterize and quantify the hydrogeological properties of the aquifer system prevailing in the Upper Drâa catchment down to the Mansour Eddahbi reservoir (15,200 km^2).

Investigations were carried out between 2001 and 2005 following various approaches (e.g. geological surveys, water balance estimations, groundwater hydrogeochemical classification etc.) at different scales on the three main hydrogeological units of the Upper Drâa catchment: the High Atlas, the Basin of Ouarzazate and the Anti-Atlas domain. The various aquifers of the Upper Drâa catchment are characterized in respect to their dimensions and their hydrodynamical characteristics. The origin of groundwater is assessed by natural labelling using both, the groundwater geochemistry such as major ions and trace elements and the isotopic signatures ($\delta^{18}O$, $\delta^{2}H$). A Local Meteoric Water Line (LMWL; $\delta^{2}H = 8\ \delta^{18}O + 10.6$) is defined, which lies slightly above the Global Meteoric Water Line (GMWL). Based on the weighted $\delta^{18}O$ mean values of the precipitation and the isotopic composition of selected springs, a clear altitude gradient is elucidated ($\delta^{18}O = -0.002$ ”altitude” - 3.0). Tritium and carbon-14 analyses completed by the calculation of saturation indexes for selected minerals allow the estimation of the groundwater residence time. In order to simulate the alluvial aquifer system of the Basin of Ouarzazate, a three dimensional finite-difference groundwater flow model (PMWIN5) is used.

While the Anti-Atlas domain shows poor groundwater storage capacity and low groundwater renewability, the folded Liassic limestones and dolomites of the High Atlas, covering 20 % of the Upper Drâa catchment, represent the main aquifer system in regard to its aquifer qualities, its volume and its recharge. Triassic formations underlying the karstified Liassic aquifer act as an aquitard. With tritium ages younger than 10 years the recharge of the Liassic aquifer system in the High Atlas by recent precipitation is efficient. This important renewability of the groundwater resources in the High Atlas is additionally confirmed by water balance calculations on two different scales giving groundwater recharge rates ranging between 4 % (Assif-n'-Ait Ahmed catchment: 100 km^2) and 11 % (Ifre catchment: 1,240 km^2) of the total precipitation. The “Southern Atlas Marginal Zone” (SAMZ), which is a tectonic compressional zone, acts as the decisive hydrogeological barrier between the aquifers of the High Atlas Mountains and the Basin of Ouarzazate. Therefore, the discharge of the Liassic aquifer of the High Atlas occurs mainly by the surface drainage of the various wadis and the shallow subsurface flow in their adjacent alluvial aquifers. Those wadis have consequently a primordial role for the recharge processes of the aquifer system of the Basin of Ouarzazate. The isotopic signatures of most of the groundwater samples from the alluvial aquifers in the Basin of Ouarzazate reflect mean altitudes of the groundwater recharge area between 2,400 to 2,900 m a.s.l., which localise the recharge area within the High Atlas Mountains. Therefore the recharge by precipitation within

the basin is not significant. Additionally, the steady state simulation with MODFLOW of the alluvial aquifer system of the Basin of Ouarzazate proves an efficient recharge of the alluvial aquifers by river bed infiltration over the whole model domain averaging 85 % of the total recharge (~ 27 Mio m³/a). Only the remaining 15% of the total recharge are provided by the infiltration of precipitation.

The hydrochemical characterization of the groundwater of local aquifers developed in the Mio-Pliocene multi-layer aquifer in the Basin of Ouarzazate shows various origins according to their hydraulic connections with the overlying alluvial aquifers. But, the recharge of those small deeper aquifers is not effective as proved by groundwater ages older than 50 years. The confined aquifer of Infracenomanian in the Tikirt area shows a heterogeneous character in regard to the groundwater chemistry due to some local leakage from the alluvial aquifer of the Imini Wadi. This confined aquifer is mainly recharged in the High Atlas as confirmed by the isotopic composition. Due to the fact that the volume of this confined aquifer is small and that the tritium ages reveal groundwater older than 50 years, the productivity of this aquifer is not suitable for exploitation. Precambrian rocks in the Skoura Mole located in the northern part of the basin embody old groundwater dated between 500 to 2,800 years with the carbon-14 method. The unproductive character of those fissured rocks is explained by a low rate of infiltration and a low permeability confirming the aquitard role of these formations.

The groundwater in the Upper Drâa catchment presents a high variability in quality, which often do not meet the international standards for drinking water due to a high mineralization. This high mineralization results only from the leaching of evaporitic minerals (gypsum, halite and sylvite) naturally present in the various geological formations (Trias, Cretaceous, Eocene and Mio-Pliocene). This is confirmed by the isotopic signatures of the groundwater, which do not show any evaporation effect. In the High Atlas, chemical processes such as dedolomitization associated with the leaching of gypsum influence the groundwater chemistry. In the Basin of Ouarzazate, the exhalation of CO_2 along faults in the Precambrian rocks has also local impact on the composition of the groundwater.

This study provides specific hydrogeological data for the interdisciplinary research. Thus, it supports tasks such as hydrological modelling, anthropological investigations, development of an integrated information system, and the future implementation of Decision Support Systems in the IMPETUS project.

KURZFASSUNG

Das Drâa Tal im Süden Marokkos ist ein typisch semi-arides Gebiet, in dem die Wasserknappheitsproblematik die Motivation der vorliegenden Forschungsarbeit liefert. Diese Dissertation ist eingebettet in das interdisziplinäre Forschungsprojekt IMPETUS (Integratives Management-Projekt für einen Effizienten und Tragfähigen Umgang mit Süßwasser in Westafrika), das gemeinsam von den Universitäten Bonn und Köln durchgeführt wird. Das IMPETUS Projekt ist Teil des GLOWA (Globaler Wandel des Wasserkreislauf) Schwerpunktprogramms der Bundesrepublik Deutschland mit dem Forschungsziel der Entwicklung integrierter Strategien für eine nachhaltige und vorausschauende Bewirtschaftung von Wasser und Gewässern im regionalen Maßstab. Grundwasser ist einer der bedeutsamsten Bestandteile des hydrologischen Kreislaufes. Daher ist es ein Ziel dieser Arbeit die hydrogeologischen Eigenschaften der vom oberen Drâa Einzugsgebiet bis hinunter zum Mansour Eddahbi Stausee (15200 km^2) vorkommenden Aquifere zu charakterisieren und zu quantifizieren.

Die zwischen 2001 und 2005 durchgeführten Untersuchungen wurden auf verschiedenen Skalen in den drei hydrogeologischen Haupteinheiten des oberen Drâa Einzugsgebietes, dem Hohen Atlas, dem Becken von Ouarzazate und der Anti-Atlas Region durchgeführt. Die verschiedenen Aquifere des oberen Drâa Einzugsgebietes wurden hinsichtlich ihrer Ausmaße und ihrer hydrodynamischen Eigenschaften charakterisiert. Die Herkunft des Grundwassers wurde durch die Analyse seiner natürlichen hydrogeochemischen Signatur abgeschätzt. Hierzu wurden sowohl die Hauptionenbestandteile und Spurenelemente, als auch die Zusammensetzung der stabilen Isotope des Wassers ($\delta^{18}O$, $\delta^{2}H$) betrachtet. Es wurde eine lokale Niederschlagsgerade (Local Meteoric Waterline, LMWL; $\delta^{2}H = 8\ \delta^{18}O + 10.6$) definiert, welche geringfügig oberhalb der globalen Niederschlagsgeraden (Global Mean Waterline, GMWL) liegt. Basierend auf den gewichteten $\delta^{18}O$ Niederschlags-Mittelwerten und der isotopischen Zusammensetzung verschiedener Quellen konnte ein eindeutiger Höhengradient abgeleitet werden ($\delta^{18}O$ = -0,002 x „Höhe“ – 3.0). Tritium und ^{14}C Analysen, zusammen mit der Berechnung von Sättigungsindizes ausgewählter Minerale, erlaubten die Abschätzung der Grundwasserverweilzeit. Um das alluviale Aquifer-System des Beckens von Ouarzazate zu simulieren, wurde ein drei-dimensionales Finite-Differenzen Grundwasserströmungsmodell (PMWIN5) verwendet.

Während die Anti-Atlas Region nur eine geringe Grundwasserspeicherkapazität und Grundwasserneubildung aufweist, repräsentieren die gefalteten liassischen Kalksteine und Dolomite, die 20 % des oberen Drâa Einzugsgebietes ausmachen, das Haupt-Grundwasserleitersystem bezüglich der Aquifer-Qualität, seinem Volumen und seiner Grundwasserneubildung. Triassische Einheiten im Liegenden des verkarsteten liassischen Grundwasserleiters fungieren als Aquitarde. Tritium Grundwasseralter des liassischen Aquifersystems zeigen, dass die Grundwasserneubildung durch Niederschlagsinfiltration effizient ist. Dieser wichtige Grundwasserneubildungsmechanismus im Hohen Atlas wird zusätzlich untermauert durch auf zwei Skalen durchgeführten Wasserbilanz-Berechnungen, die Grundwasserneubildungsraten zwischen 4 % (Assif-n'-Ait Ahmed Einzugsgebiet: 100 km^2) und 11 % (Ifre Einzugsgebiet: 1240 km^2) des Gesamtniederschlages ergeben. Die „Southern Atlas Marginal Zone“ (SAMZ), eine tektonische Kompressions-Zone, agiert als maßgebliche hydrogeologische Barriere zwischen den Grundwasserleitern des Hoher Atlas Gebirges und dem Becken von Ouarzazate. Der Grundwasserabfluss des liassischen Aquifers erfolgt daher hauptsächlich über den Baseflow der verschiedenen Wadis und durch flachen unterirdischen Abfluss in den umgebenden alluvialen Grundwas-

serleitern. Diese Wadis haben daher einen nicht zu unterschätzenden Einfluss auf die Grundwasserneubildungsprozesse im Becken von Ouarzazate. Die isotopische Zusammensetzung der Mehrzahl der Grundwasserproben der alluvialen Aquifere spiegeln die mittleren Höhen der Grundwasserneubildungsgebiete zwischen 2400 und 2900 m ü. NN wider und identifizieren so den Hohen Atlas als das Haupt-Grundwasserneubildungsgebiet. Infolgedessen ist die Grundwasserneubildung über Niederschlagsversickerung im Becken von Ouarzazate als nicht signifikant anzusehen. Zusätzlich haben Steady-State Simulationen mit dem Programm MODFLOW im alluvialen Aquifer-System des Becken von Ouarzazate belegt, dass die Grundwasserneubildung dieser Aquifere durch Uferinfiltration ca. 85 % der gesamten Grundwasserneubildung im modellierten Gebiet ausmachen (ca. 27 Mio m^3/a). Nur 15 % der gesamten Grundwasserneubildung werden also durch direkte Niederschlagsinfiltration erzeugt.

Die hydrogeochemische Charakterisierung des Grundwassers ergibt für die lokal ausgebildeten Aquifere im intern gegliederten Aquifer-System der mio-pliozänen Schichten im Becken von Ouarzazate ein komplexes Verbreitungsmuster der Neubildungsgebiete, welches von der jeweiligen hydraulischen Anbindung an die überlagernden alluvialen Aquifer-Bereiche abhängt. Die rezente Grundwasserneubildung für das mio-pliozäne Aquifer-System ist nur sehr eingeschränkt wirksam, was durch ein mittleres Alter des Grundwassers von über 50 Jahren belegt wird. Der gespannte Grundwasserleiter in den Schichten des Infracenoman in der Gegend von Tikirt weist heterogene hydrochemische Bedingungen auf, die durch lokale Zusickerungen aus dem alluvialen Aquifer des Wadi Imini beeinflusst werden. Die Grundwasserneubildung dieses gespannten Aquifers ist hauptsächlich im nördlich gelegenen Bereich des Hohen Atlas wirksam und wird durch die isotopische Zusammensetzung des Grundwassers bestätigt. Da dieser Aquifer relativ klein dimensioniert ist und das Tritiumalter des Grundwassers bei über 50 Jahren liegt, ist seine Produktivität gering und somit nicht zur Ausbeutung geeignet. Das Grundwasser in den präkambrischen Gesteinen der Skoura Mole am nördlichen Rand des des Beckens von Ouarzazate wird mittels der 14-Karbon-Methode auf ein Alter zwischen 500 und 2.800 Jahren datiert. Geringe Kluftweiten, folglich geringe hydraulische Durchlässigkeitswerte, und geringe Grundwasserneubildungsraten weisen diese präkambrischen Gesteine als Aquitarde aus.

Für das obere Drâa-Einzugsgebiet wird eine hohe Variabilität der Grundwasserqualität nachgewiesen, welche durch eine hohe Mineralisation an vielen Probeentnahmepunkten den internationalen Anforderungen für Trinkwasser nicht standhält. Der Grund für die hohe Mineralisation des Grundwassers ist rein geogen und wird durch die Auswaschung evaporitischer Minerale bedingt, die in verschiedenen geologischen Formationen vorkommen (Trias, Kreide, Tertiär–Eozän und Mio-Pliozän). Diese Annahme wird durch die Isotopensignatur im Grundwasser gestützt, welche Evaporationseffekte im Grundwasser ausschließt. Im Hohen Atlas beeinflussen Prozesse wie Entdolomitisierung in Verbindung mit der Auswaschung von Gips die Grundwasserbeschaffenheit. Im Becken von Ouarzazate bedingt die Ausgasung von Kohlendioxid entlang von Störungen im präkambrischen Gestein eine lokale Beeinflussung des Grundwassers hangender Aquifere.

Im Zuge dieser Untersuchungen werden spezifische hydrogeologische Erkenntnisse und Daten für die interdisziplinäre Forschung bereitgestellt. Damit unterstützt diese Arbeit die hydrologische Modellierung, anthropologische Studien, die Entwicklung eines integrierten Informationssystems und die zukünftige Implementierung von Entscheidungshilfesystemen (DSS) im Impetus-Projekt.

RESUME

La vallée du Drâa, située au sud du Maroc, est une zone semi-aride faisant face à des problèmes de pénurie en eau. Cette thèse de doctorat s'est déroulée dans le contexte du projet interdisciplinaire de recherche IMPETUS (approche intégrée pour une gestion durable des ressources en eau en Afrique de l'Ouest) mené en collaboration par les universités de Bonn et Cologne en Allemagne. Le projet IMPETUS fait parti du programme GLOWA (changement global du cycle de l'eau) financé par le German BMBF (Ministère fédéral de l'éducation et de la recherche) qui se concentre sur le développement de stratégies intégratives pour une gestion durable et efficace des ressources en eau douce. Les eaux souterraines représentent une des plus importantes composantes du cycle hydrique. C'est pourquoi, le but de ce travail a été de caractériser qualitativement et quantitativement les propriétés hydrogéologiques du système aquifère du basin versant supérieur du Drâa (15200 km^2), qui correspond à la partie nord de la vallée du Drâa jusqu'au barrage Mansour Eddahbi.

Les recherches ont été menées entre 2001 et 2005 suivant différentes approches et à différentes échelles sur les trois principaux unités hydrogéologiques du basin versant supérieur du Drâa : le Haut Atlas, le bassin de Ouarzazate et l'Anti Atlas. Les différents aquifères qui prévalent dans le bassin supérieur du Drâa sont caractérisés selon leur dimension et leurs caractéristiques hydrodynamiques. L'origine des eaux souterraines est identifiée par la géochimie, telle que les ions majeurs et les éléments traces, et par la composition isotopique des eaux ($\delta^{18}O$, $\delta^{2}H$). Une droite des eaux météoriques locales est définie. Elle est située légèrement au-dessus de la droite des eaux météoriques globales: $\delta^{2}H = 8\ \delta^{18}O + 10,6$. A partir des valeurs moyennes pondérées de $\delta^{18}O$ de la précipitation et de la composition isotopique des eaux de sources sélectionnées, un gradient d'altitude à été trouvé ($\delta^{18}O = -0,002 \cdot$ "altitude" – 3,0). Les analyses de tritium et de carbone-14 complétées par des calculs d'indexe de saturation de certains minéraux ont permis l'estimation des temps de transit des eaux souterraines. Dans le but de simuler le système d'aquifères alluvial dans le bassin de Ouarzazate, un modèle hydrogéologique trois dimensionnel à différence finie (PMWIN5) est utilisé.

Alors que l'Anti Atlas présente de faible réserves hydrogéologiques et un faible renouvellement des eaux souterraines, les calcaires et dolomites plissées et faillées du Haut Atlas, qui couvrent 20% du basin supérieur du Drâa, représentent le système aquifère principal en ce qui concerne ses qualités de stockage et de recharge. Les formations du Trias à la base de l'aquifère karstique du Lias joue un rôle d'aquitarde. La recharge des ressources souterraines par les précipitations dans le Haut Atlas est active comme le prouve les court temps de résidence inférieur à dix ans des eaux souterraines du Lias. De plus, l'importance de cette recharge est confirmée par le calcul du bilan hydrique à deux différentes échelles avec une recharge des eaux souterraines estimées entre 4% (bassin versant du Assif-n'Ait-Ahmed : 100 km^2) et 11 % (bassin versant de Ifre : 1,240 km^2) de la précipitation totale. La « Zone Marginale Sud Atlasique », qui est une zone de compression tectonique, joue un rôle de barrière hydrogéologique décisif entre les aquifères du Haut Atlas et du bassin de Ouarzazate. Par conséquent, l'aquifère liasique du Haut Atlas est drainé par les oueds et par les écoulements de sub-surfaces des aquifères alluviaux associés. Ces oueds ont donc un rôle primordial dans le processus de recharge du système aquifère du bassin de Ouarzazate. La signature isotopique des eaux souterraines des aquifères alluviales dans le bassin de Ouarzazate place

la zone de recharge de ces eaux entre 2400 m et 2900 m. Cela prouve que la recharge des aquifères par précipitation dans le basin est négligeable. Ajouté à cela, la simulation en état stationnaire avec MODFLOW du système aquifère alluvial montre clairement que la recharge par infiltration des eaux des Oueds est efficace et représente 85% de la recharge total sur l'ensemble du domaine (~ 27 Mio m^3/a).

La caractérisation hydrogéochimique des eaux souterraines d'aquifères locaux développés dans l'aquifère multi-couches du bassin de Ouarzazate montre l'existence de plusieurs origines de ces eaux suivant les connections hydrauliques existantes avec les aquifères superficiels. Mais avec un temps de résidence supérieur à 50 ans, la recharge de ces petits aquifères apparaît comme étant non active. L'aquifère captif de l'Infracénomanien dans la zone de Tikirt montre un caractère hétérogène selon la chimie des eaux souterraines due à des infiltrations locales à partir de l'aquifère alluvial de l'Oued Imini. Cet aquifère captif est rechargé dans le Haut Atlas, ce qui est confirmé par la signature isotopique des eaux souterraines. Du fait que le volume de cet aquifère est petit est que les analyses de tritium donne un age des eaux supérieur à 50 ans, la productivité de cet aquifère est donc considéré comme inexploitable. Les roches précambriennes dans le Mole de Skoura, situé dans la partie nord du bassin, montre un temps moyen de résidence des eaux souterraines entre 500 et 2800 ans selon la datation au carbone 14. Le caractère improductif de ces roches fissurées résulte d'un faible taux d'infiltration et d´une faible perméabilité qui confirme le rôle d'aquitarde de ces formations.

La qualité des eaux souterraines dans le bassin versant supérieur du Drâa présente une grande variabilité souvent en dehors des normes internationales de potabilité du à une forte minéralisation. Les analyses isotopiques ne révèlent pas d'important effet d'évaporation de ces eaux souterraines. Donc, la minéralisation est seulement due au lessivage de minéraux évaporitiques (gypse, halites et sylvites) qui sont présents naturellement dans les différentes formations géologiques (Trias, Crétacé, Eocène et Mio-Pliocène). Les processus géochimiques affectant les eaux souterraines sont identifiés tels que l'effet de dédolomitisation associé à la dissolution de gypse dans le Haut Atlas ou l´influence sur la chimie des eaux de l'afflux de CO_2 gaz remontant le long de fractures des roches précambriennes dans le bassin de Ouarzazate.

Cette étude fournit des données spécifiques d'hydrogéologie qui sera utilisées pour les recherches interdisciplinaires. Les résultats de ces travaux serviront à la modélisation hydrologique, aux recherches ethnologiques, au développement d'un système d'information géographique, et à la création d'un système de support à la décision développé par le projet IMPETUS.

ACKNOWLEDGMENTS

This research was supported by the Federal German Ministry of Education and Research (BMBF) under grant No. 01 LW 0301A and by the Ministry of Science and Research (MWF) of the federal state of Northrhine-Westfalia under grant No. 223-21200200.

I would like to express my deepest thanks and gratitude to my supervisor Prof. Dr. Barbara Reichert for offering me the opportunity to do my PhD in Germany. I thank for her guidance, constructive criticism and her supervision. I am especially grateful for her continual support during the redaction with helpful suggestions.

I thank Dipl.-Phys. W. Stichler of GSF (Neuherberg) who supervised the isotope analysis, for his collaboration and for useful helping in the interpretation of the isotope data. I am grateful to Prof. Dr. B. Diekkrüger who helped me with fruitful discussions and prosperous ideas during the development of the hydrogeological model.

Special thanks go to colleagues and friends of the Department of Hydrogeology, Dipl.-Geol. Kerstin Kremer, Dr. Fathy Ahmed, Dr. Christian Derer, Dr. Wolfram Watenberg, Dr. Frederike Bungenstock and Dr. Kai Witthüser. I am especially indebted to Dr. Thorsten Faß, Dipl.-Geol. Stephan Klose and Dipl.-Geol. Tobias El Fahem who give useful contributions at various times during the development of this thesis. I thank also the laboratory personal of the institute of geology of Bonn, Mrs. Bettina Schulte-van Berkum, Mrs. Camilla Kurth and the student helpers for their work.

Sincere thanks are extended to the IMPETUS researchers for the interesting multidisciplinary works and their help during the field investigations, Dr. H. Kirscht, Dr. Carmen de Jong, Dr. Manfred Finckh, Dipl. Christina Rademacher, Dr. Oliver Schulz, Dipl.-Geog. Anna Zeyen, Dipl.-Agrar. Frank Gresens, Dr. Benedikt Weber and Dipl. Andreas Roth. I acknowledge the master students Dipl.-Geol. Simone Bell, Tim Budewig, Dipl.-Geol. Harald Hofmann, Dipl.-Geol. Volker Osterholt and Dipl.-Geol. Christine Ewen, who contributed at this study with hard work in the field. Special thanks to Dr. Barbara Casciari and Brahim Elkrateka for the efficient common work in a nice atmosphere at Tagounite. I thank also the coordinators at Ouarzazate Jamal Ait El Hadj and Andreas Preu, especially for the complex administrative work during the samples exportation, which made things easier for me. I extend my thanks to Omar Abdelaoui (ORMVAO) and to the staff of the Direction Hydraulique de Ouarzazate for their important collaboration. I am grateful for the welcome of the friendly people of Tichki, Ameskar, Tizi Tounza, Taoujgalt, Bouskour, Trab Labied, El Miyit, Tiraf and Iriki. They played an important role for this study with the regular collecting of rain water for isotope, which would not be possible without their collaboration.

I thank also Prof. Dr. P. Speth and Dr. M. Christoph who managed the IMPETUS project.

I wish to express my deep gratitude to Prof. Dr. Michel Bakalowicz for his encouragements and his contribution to the first contact with Prof. Dr. Barbara Reichert.

Lastly, very special thanks go to my girlfriend Uli, Paula for her energy and of course my family who gave me an important support during this work.

TABLE OF CONTENTS

Appendices (CD)

LIST OF FIGURES AND TABLES

LIST OF FIGURES

LIST OF TABLES

NOTATION

$\alpha_{A/B}$	fractionation factor
δ [‰]	isotopic deviation
$\varepsilon_{A/B}$	enrichment factor
γ_i	activity coefficient of the ion i
λ	decay constant
µS	micro siemens
Ω	saturation state
ρ_s	snow density
τ	mean transit time
[i]	ion activity
^{2}H	deuterium
$^{2}R_{(H2O)}$	isotope ratio of deuterium for the water molecule
^{3}H	tritium
^{13}C	carbon-13
$^{13}R_{(H2O)}$	isotope ratio of carbon-13 for the water molecule
^{14}C	carbon-14
^{18}O	oxygen-18
$^{18}R_{(H2O)}$	isotope ratio of oxygen-18 for the water molecule
A	radioactivity
$a^{14}C$	activity of carbon-14
C_{RIV}	river hydraulic conductance
d or d-excess	deuterium excess
h	potentiometric head
IAP	activity product
K	equilibrium constant of a reaction (hydrochemical)
K	hydraulic conductivity (hydrodynamic)
K_H	horizontal hydraulic conductivity
K_{RIV}	effective hydraulic conductivities of the river bed
K_V	vertical hydraulic conductivity
Q	discharge or flow rate
m_i	molality of the ion i
m a.s.l.	meter above sea level
meq	milliequivalent
mg	milligram
Mio	million
Pd	dispersion parameter
pmC	percent modern carbon
q	dilution factor
R^2	correlation coefficient
S_S	specific storage
swe	snow water equivalent
W	volumetric flux per unit volume (sources and/or sinks of water)
$T_{1/2}$	half time
T	time

Abbreviations

AAS	Atom Absorption Spectrometer
ARG	Argium
BSK	Bouskour
DEM	Digital Elevation Model
DIC	Dissolved Inorganic Carbon
DM	Dispersion Model
DRH	Direction Regional de l'Hydraulique
EC	Electric Conductivity
EM	Exponential Model
EMY	El Miyit
ET	Evapotranspiration
ETp	Potential Evapotranspiration
GIS	Geographic Information System
GMWL	Global Meteoric Water Line
GPS	Global Positioning System
HCA	Hierarchical Cluster Analysis
IAEA	International Energy Atomic Agency
IC	Ion Chromatograph
IRK	Iriki
IMS	Imeskar
LMWL	Local Meteoric Water Line
MGN	M'Goun
P	precipitation
PCA	Principal Component Analyse
PFM	Piston Flow Model
SAMZ	Southern Atlas Marginal Zone
SD	Standard Deviation
SI	Saturation Index
SMOW	Standard Mean Ocean Water
TAO	Taoujgalt
TIC	Tichki
TRB	Trab Labied
TU	Tritium Units
TZT	Tizi Tounza

1 INTRODUCTION

1.1 IMPETUS project

Since the early 1970s the occurrence of drought years increases in the Northwest and West Africa which may represent a major obstacle to the development of these regions in the future. Therefore the IMPETUS West Africa project (**I**ntegratives **M**anagement-**P**rojekt für einen **E**ffizienten und **T**ragfähigen **U**mgang mit **S**üßwasser in Westafrika) investigates water as a scarce resource in West Africa in the context of the BMBF GLOWA (”Global change of the water cycle”). Hence, IMPETUS is directed towards an efficient and sustainable freshwater resource management, the scientific approaches are interdisciplinary and application-orientated. With the assessment that the droughts North and South of the Sahara are probably related (SPETH et al. 2002), two river catchments have been investigated: the river Drâa in the South-east of Morocco and the Ouémé in Benin (Fig. 1.1). The Drâa valley is one of the ten driest catchments of the world (RAVENGA 1998). It is a typical semi-arid area facing water scarcity problems. With an integrated approach the IMPETUS project deals with all aspects of the hydrological cycle. Added to the analyses of the different components and interactions of the hydrological cycle (e.g. meteorology, hydrology, hydrogeology, botany, agriculture etc.) governing the availability of fresh water, the socio-economic and medical issues are also considered. The IMPETUS project is carried out in three phases. The aim of the first phase (2000-2003) was the identification and analysis of the influencing factors in respect to various aspects of the water budget. Based on this, different global change scenarios are compiled in the second phase (2003-2006) in order to assess management options and to install operational tools for the decision-making processes which will be carried out during the third phase (SPETH et al. 2002). This present study is the result of investigations of the first and the second phase.

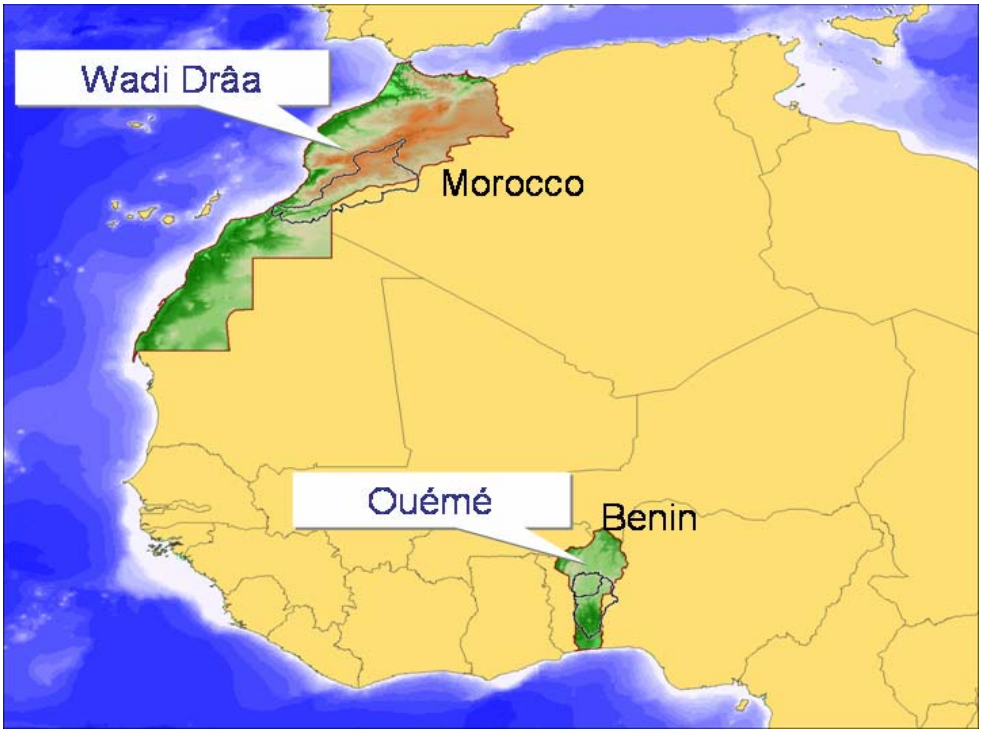

Fig. 1.1: The IMPETUS project is an integrated approach to the efficient management of scarce water resources in West Africa. Two catchments are investigated: the river Drâa in the south east of Morocco and the Ouémé in Benin (SPETH et al. 2002).

1.2 Context and aim of the study

Due to the aridity of the Drâa basin, the population, the infrastructure and the husbandry are concentrated around rivers and oases. The ephemeral flows of the rivers force people to use groundwater to provide for water demand. Consequently, the groundwater is of significant importance regarding the water management of this region. The Upper Drâa valley is a semi-arid area where groundwater recharge is low and strongly depending on the limestone covered High Atlas Mountains which represent only 20 % of the Upper Drâa catchment. Moreover, the groundwater in this area presents a high variability in quality, often beyond the international drinking water standards. Therefore, groundwater quality is an additional deciding factor regarding water-use strategies. In this context, this study attempts to identify the potential of the scarce groundwater resource in order to provide the necessary knowledge to do an efficient and sustainable water resource management in this region. Hence, it is necessary to understand the groundwater system and to estimate the groundwater availability including storage, recharge and the potential sustainable exploitation rate. Regional focus of the present study is the Upper Drâa catchment.

1.3 Strategies of investigations

The complex aquifer system of the semi-arid Upper Drâa catchment is not well known, rarely described and almost not monitored. Therefore, this study attempts to provide the basic hydrogeological knowledge necessary for an efficient groundwater management. Investigations were carried out following various approaches and at different scales on the three mains hydrogeological units of the Upper Drâa catchment: the High Atlas Mountains which represent the recharge areas of the catchment, the sedimentary Basin of Ouarzazate and the Anti-Atlas domaine. The various methods include:

- **Geological surveys**: Detailed geological investigations were carried out in the field to characterize the structural pattern and the lithology of specific geological area within the catchment. These investigations allow the estimation of dimensions and the hydrodynamic characteristics of the various aquifers in dependence to their stratigraphic and tectonic features. The knowledge of the geology of the Upper Drâa catchment was also completed by a synthesis of the existing literature.
- **Water balance estimations**: various components of the water budget are defined for selected parts of the High Atlas which represents the main recharge area of the Upper Drâa catchment.
- **Hydrodynamics measurements**: hydrodynamic parameters were provide by the data set of the Direction Régionale de l'Hydraulique (DRH) and were completed with water level measurements.
- **Hydrogeochemical analyses of groundwater:** geochemistry of the groundwater with analyses of the major ions, trace elements, and isotopic elements allows the understanding of the movements and origins of the groundwater, and an estimation of the residence time (GÜLER et al. 2002, TÓTH 1998, CLARK and FRITZ 1997, FRITZ & FONTES 1980 & IAEA 1980, 1987, 1991, 1995, 2001). Two different approaches can be distinguished:
    - The "signature method" based on chemical (dissolved ions) and isotopic species (^{2}H, ^{3}H, ^{18}O) allow the definition of recharge areas and an understanding of the

groundwater mixing processes. This method takes into account the temporal and spatial variations.

- The "dating method" with the use of ^{3}H and ^{14}C as time markers for the assessment of water ages and of the circulation time.

The sampling of groundwater for chemical and isotopic analyses and measurements of the water levels were carried out throughout the Upper Drâa catchment during low and high water conditions between 2001 and 2005.

- **Modelling using a three dimensional finite-difference groundwater flow model (PMWIN5):** a three dimensional finite-difference groundwater flow model (PMWIN5) is used to simulate in steady state the groundwater of the alluvial aquifer system of the Basin of Ouarzazate.

2 CHARACTERIZATION OF THE AREA UNDER INVESTIGATION

2.1 The Drâa valley

The Drâa basin with an area of 115,000 km^2 is a large arid catchment stretching across Morocco, Algeria and Western Sahara (Fig. 2.1-A). The Drâa River reaches the Atlantic Ocean in a continuing flow only during some very exceptional flood events. The research area investigated by IMPETUS includes the Upper and Middle Drâa catchment (Fig. 2.1-B), an area of approximately 42,000 km^2. This catchment is limited in the north by the southern slope of the High Atlas range culminating between 2,000 m and 4,000 m a.s.l. (Jbel Toubkal: 4,167 m a.s.l. and Jbel M'Goun: 4,071 m a.s.l.). The Basin of Ouarzazate with approximately 150 km in length and 40 km in width spreads east-west between the High Atlas and the Anti Atlas ranges (Fig. 2.1-B). With an altitude around 1,100 m a.s.l. the relatively flat topography of the Ouarzazate Basin contrasts with the surrounding mountains.

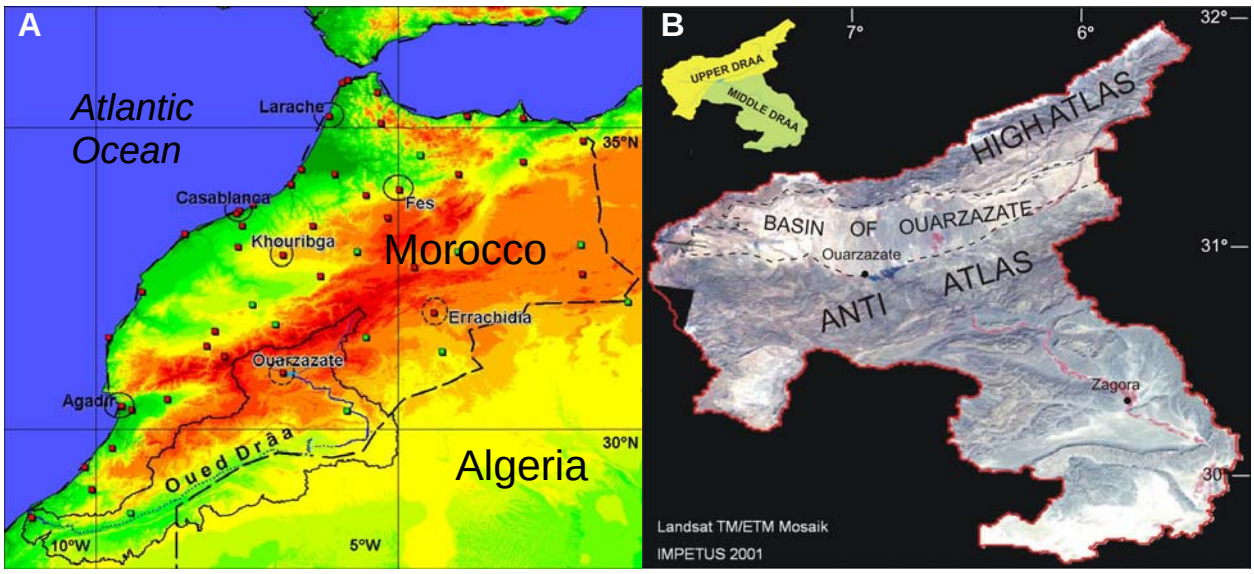

Fig. 2.1: Location of the Drâa catchment within Morocco (A) and the Upper and Middle Drâa catchment (SCHMIDT 2003) (B).

The Anti Atlas, a lower mountain range (Jbel Siroua: 3,304 m a.s.l.) than the High Atlas mountains forms with the Jbel Saghro (Fig. 2.2) the southern boundary of the Upper Drâa catchment and constitutes with the Saharan forelands the Middle Drâa catchment (Fig. 2.1-B). The Upper Drâa catchment which corresponds to the northern part of the basin until the Mansour Eddahbi reservoir has an area around 15,200 km^2 (Fig. 2.2). The study area comprises the administrative regions of Ouarzazate and Zagora with a population around 655,500 inhabitants in 1990 (DIRECTION DE LA RECHERCHE ET DE LA PLANIFICATION DE L' EAU 1994). The density of population is low with 15.6 people/km^2. The agriculture sector of traditional type represents 70 % of the human activity. In order to develop this area economically, the Mansour Eddahbi dam was built in 1972 near Ouarzazate and controls now the discharge of the Drâa for the irrigation of 26,000 ha of fields distributed between Agdz and M'Hamid in six palmgroves (Fig. 2.2).

2.2 IMPETUS meteorological stations and test sites

In order to monitor climatic parameters along a gradient of altitude and aridity, the IMPETUS project installed 12 Automatic Weather Stations (AWS) spread out from the highest altitude of the High Atlas in the north (i.e. M'Goun station at 3,900 m a.s.l) to the former terminal Iriki Lake situated in the Saharan forelands in south (i.e. Iriki at 500 m a.s.l.) (Fig. 2.2 and 2.3). Since 2001, the stations measure standard meteorological variables such as air temperature and humidity, soil temperatures, wind speed and direction, solar irradiance, net radiation and precipitation. The three highest stations are equipped with ultrasonic snow depth sensors, infrared temperature sensors for surface temperature measurements and temperature probes for snow pack temperatures (SCHULZ & DE JONG 2004).

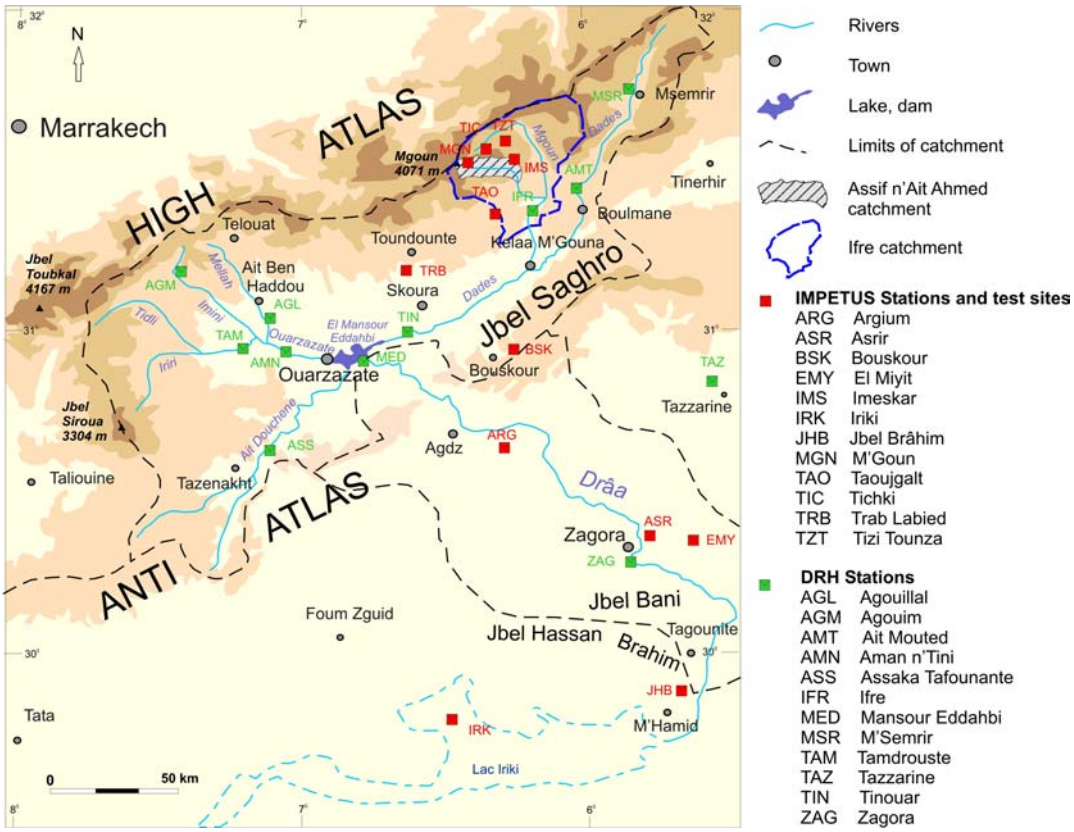

Fig. 2.2: IMPETUS has installed 12 climatic stations and test sites to complete the Moroccan climate and surface flow monitoring network (DRH stations). The IMPETUS investigations focus at various test-sites with an interdisciplinary approach in the Upper and Middle Drâa catchment. (DRH: Direction Régionale de l'Hydraulique).

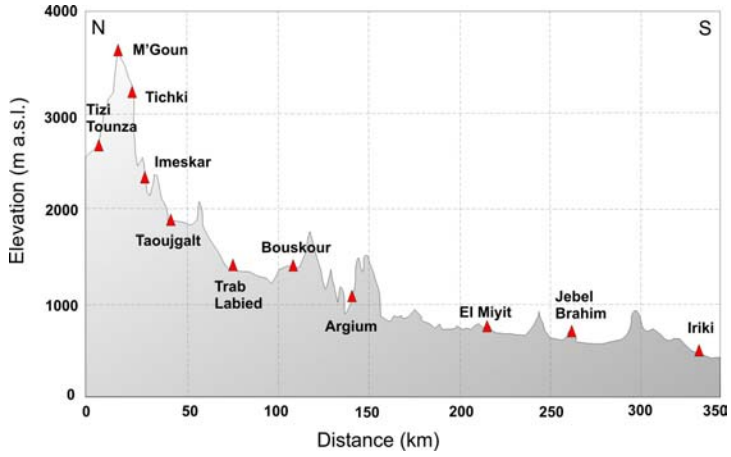

Fig. 2.3: The climatologic IMPETUS stations and test-sites are localised along a gradient of aridity and altitude (see Fig. 2.2 for location).

The IMPETUS project has also selected communally various test sites representative for specific areas of the Drâa basin, where interdisciplinary investigations have been carried out (Fig. 2.2). Most of these test-sites are small sized study areas (from 1 to 10 km^2) situated at the climatologic stations:

- Ameskar, Tichki and Taoujgalt in High Atlas.
- Trab labied in the Basin of Ouarzazate.
- Bouskour in Jbel Saghro.
- Argium, Jbel Brâhim and El Miyit in the Anti-Atlas.
- Iriki in the Saharan forelands.

The hydrogeological investigations were performed at different scales: *local*-, *meso*- and *regional-scale*. At *local scale*, investigations focus on the IMPETUS's test-sites in order to define the hydrogeological characteristics of each specific geological area of the Drâa catchment. As an intermediary step in up-scaling, hydrogeological investigations focus on the Assif-n'Ait-Ahmed catchment (110 km^2) and on the Ifre catchment (1,240 km^2) in order to understand the aquifer system prevailing in the High Atlas (Fig. 2.2). These catchments represent the *sub regional scale* approach. Taking the size of the Basin of Ouarzazate into account a different investigation strategy was chosen. The hydrogeological screening was carried out along four profiles trending more or less N-S from the High Atlas to the Anti Atlas.

2.3 Climatic conditions

Starting in 1962 the Direction Générale de l'Hydraulique (DRH) installed climatic stations and gauges monitoring the discharges of rivers which are distributed mainly in the Upper Drâa catchment (Fig. 2.4). The data show that the Upper Drâa catchment is a semi-arid zone showing a "humid season" between September and April with two precipitation peaks in October-November and February-March (Fig. 2.5). The number of raining days per year monitored at the DRH stations varies between 18 and 40 days. The whole Drâa catchment shows notable spatial and temporal variability of precipitation.

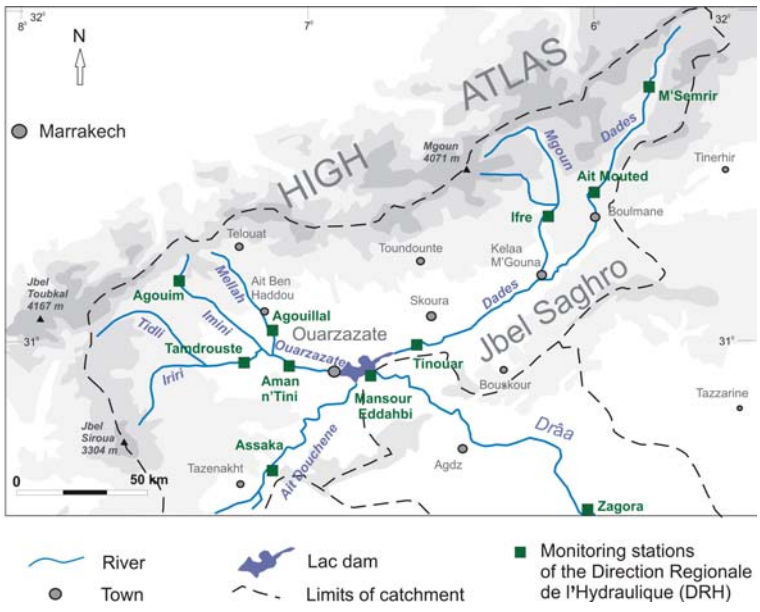

Fig. 2.4: The monitoring stations (climate and discharge of rivers) of the Direction Régionale de l'Hydraulique (DRH) in the Upper Drâa catchment.

A strong gradient of aridity and altitude exists along a north-south profile. Precipitations measured at the IMPETUS stations in the M'Goun valley reach 900 mm/a above 2,500 m of altitude. At the foothills of the High Atlas the precipitations decrease to 274 mm/a at Agouim (1,648 m a.s.l.) and 176 mm at Ifre (1,505 m a.s.l) respectively in the north-west and north-east of the Basin of Ouarzazate. The Basin of Ouarzazate and the Anti Atlas show clear arid conditions with 107 mm/a of precipitation at Ouarzazate (1,135 m a.s.l.), 121 mm/a at Assaka station (1,372 m a.s.l.) near Tazenakht and 61 mm/a at Zagora station (707 m a.s.l.).

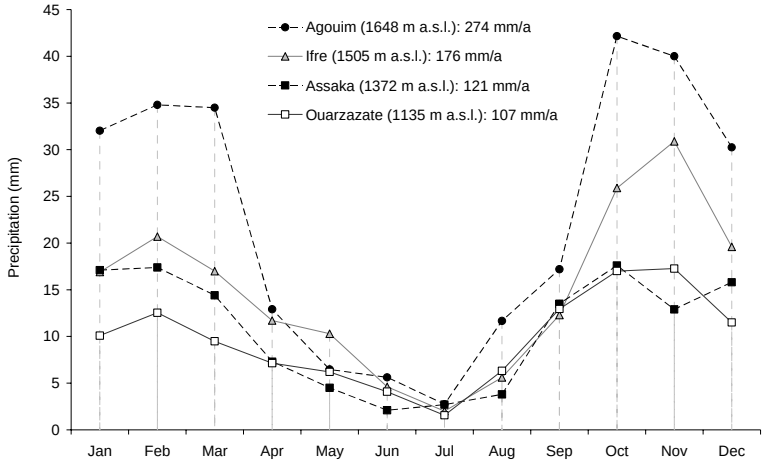

Fig. 2.5: Monthly mean of the precipitation at 4 stations for the period 1965 to 2001 depending on availability of the DRH-data). For the locations see Fig. 2.4. (Data from: DRH)

The monitoring of precipitation between 1962 and 2001 shows a high inter-annual variability of precipitation (Fig. 2.6). For example, at the Agouim station (1,648 m a.s.l.) the annual precipitation varies between a minimum of 52 mm (1982-1983) and a maximum of 682 mm (1970-1971), at the Ouarzazate station (1135 m a.s.l.) between 18 mm (1983-1984) and 227 mm (1987-1988) and in the lower altitude at the Zagora station (707 m a.s.l.) between 9 mm (1983-1984) and 212 mm (1979-1980).

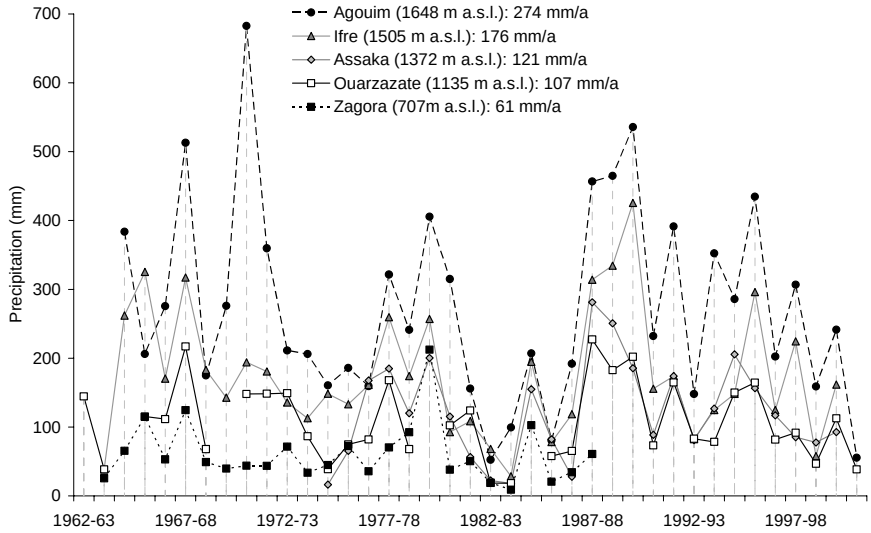

Fig. 2.6: Annual mean precipitation (Sept - August) for the period 1962-2001 at 5 DRH stations; for the locations see Fig. 2.4, (Data from: DRH).

The catchment shows also a high potential evaporation which was measured monthly by Piche and Bac methods at selected DRH stations since 1970 (Fig. 2.7). An annual mean of the potential evaporation of 4,250 mm (Piche method) is measured at the Assaka station, 4,557 mm

at Zagora, 3,557 mm at Agouilal, 3,064 m at Agouim, 3,175 mm/a at the Mansour Eddahbi dam, 3,026 mm at Ifre and 2,570 mm at M'Semrir (Fig. 2.7). It is obvious, that the monthly mean of precipitation is largely below the monthly potential evaporation measured. Nevertheless, those data exclude any information about the real evaporation. Additionally they disregard the heavy rain events occurring during very short time.

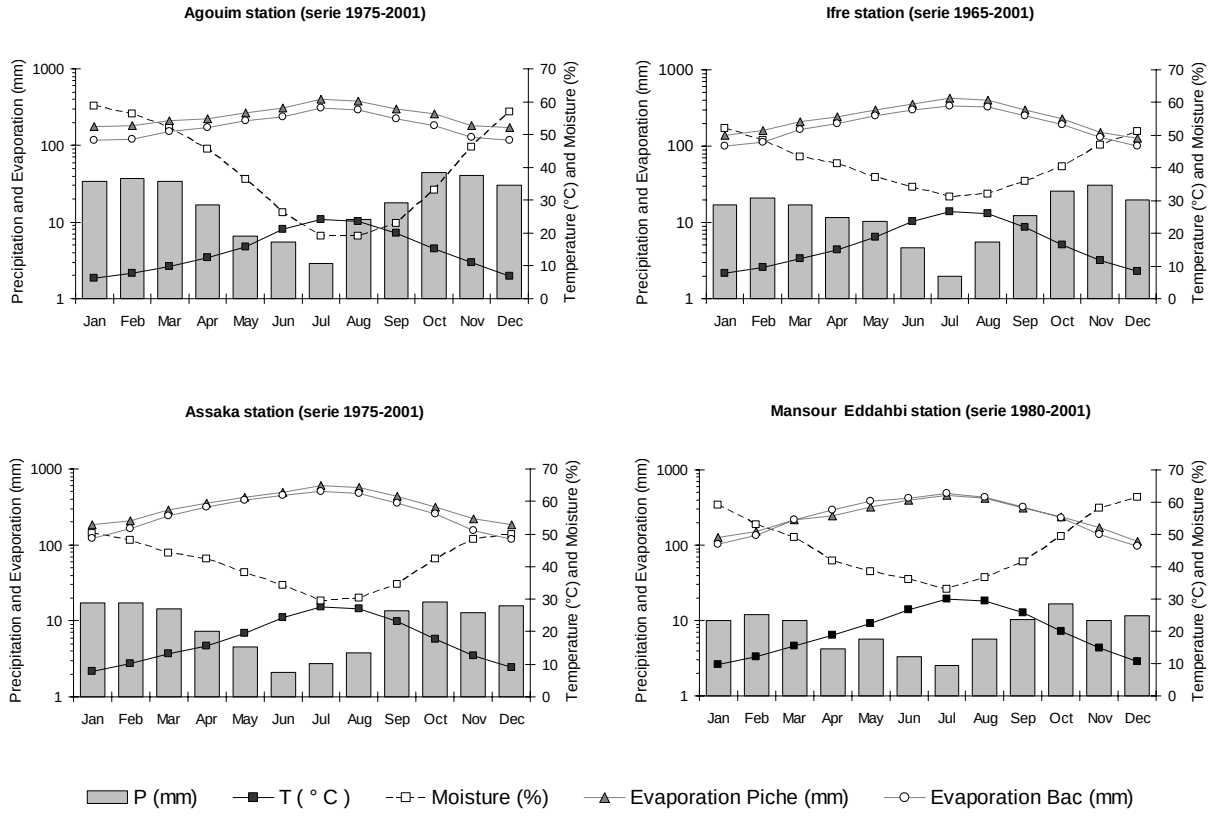

Fig. 2.7: Monthly mean of climatic parameters at 4 DRH stations in the Upper Drâa catchment, precipitation and evaporation with Piche and Bac methods (Y-axe 1), temperature and moisture (Y-axe 2); for the locations compare Figure 2.2, (Data from: DRH).

Comparison between the daily measurements of rain and the potential evaporation (Piche method) at the Ifre station for the period 01/10/94 to 31/05/99 (Fig. 2.8) clearly shows that short but intensive rain events have a potential to recharge aquifers. Examples are the 31/10/94 event with 39 mm of precipitation compared to an evaporation of 0.6 mm, or the 07/02/98 event with 45 mm with an evaporation value of 2.4 mm. For the period considered (01/10/94 to 31/05/99), a total sum of 839 mm precipitation was registered at the Ifre station. Daily subtraction between precipitation and evaporation results in a potential recharge amount of respectively 592 mm precipitation for the Bac evaporation data and 629 mm for the Piche evaporation data by neglecting evapotranspiration and runoff.

Snow is also an important factor determining the water availability of the Upper Drâa catchment. Based on an energy balance model to assess the snow melt and sublimation processes in the Assif-n'Ait-Ahmed catchment, SCHULTZ & DE JONG (2004) showed that the relation between snow and rain increases with altitude from a ratio of 1:4 to 4:1 between 2,250 to 3,850 m a.s.l. and that large amounts of snow (averaging 44 %) are removed by sublimation during cold and dry climatic conditions in winter.

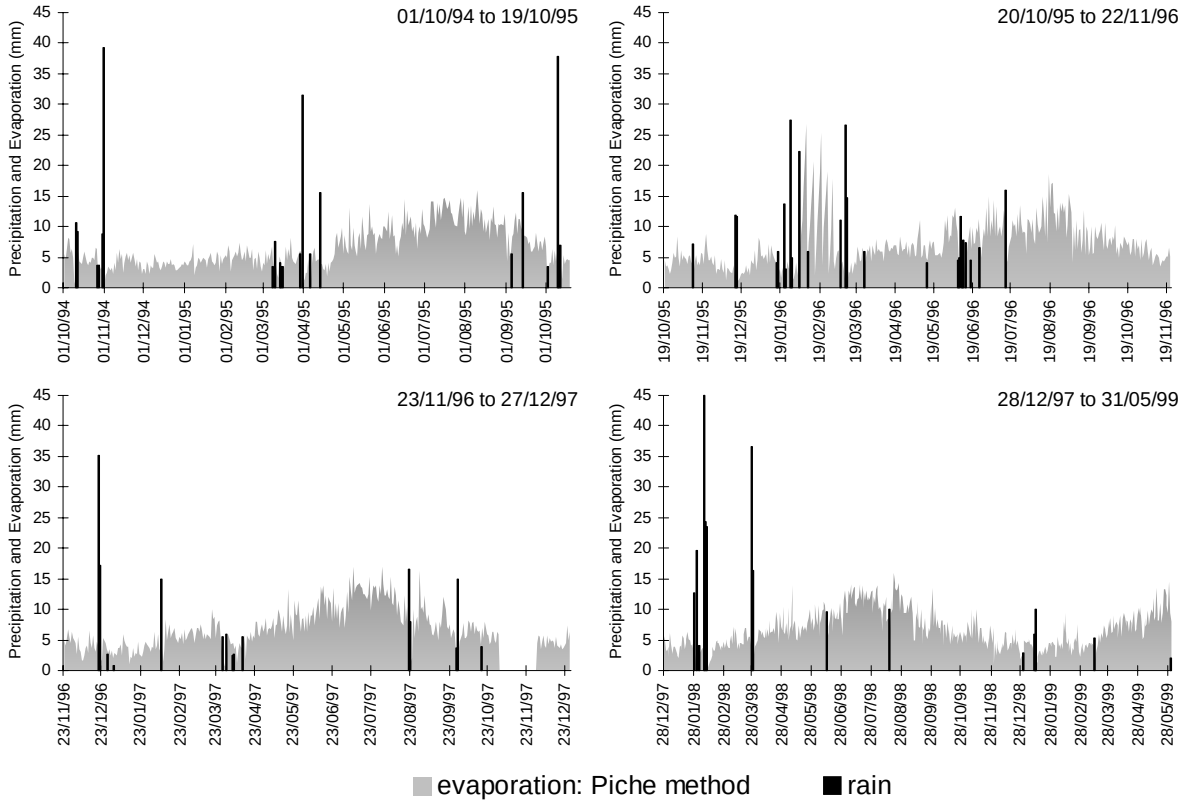

Fig. 2.8: Daily measurement of precipitation and Piche evaporation at the Ifre station (see Fig. 2.2 for location) between 01/10/94 to 31/05/99 (Data from: DRH).

2.4 Hydrological features

The Mansour Eddahbi reservoir is the decisive hydrographic feature of the Upper Drâa catchment. The reservoir collects the water of three different hydrographic networks (Fig. 2.4):

- The Dades Wadi with its tributary the M'Goun Wadi drains the calcareous High Atlas range in the north-east. The catchment size of both rivers is 7,170 km^2 (EL BOUARI, 1990). The Dades Wadi shows a mean slope of 1.1 % (CHAMAYOU et al. 1977). It receives the irregular flows of Imassine, Skoura and Izerki rivers between Kelaa M'Gouna and Ouarzazate.
- The Ouarzazate Wadi (catchment size 4,630 km^2) with three main tributaries drains the western part of the Ouarzazate Basin and the southern slope of the High Atlas. The tributaries are from east to west: the Mellah, Imini and Iriri-Tidili Wadis (Fig. 2.4). The Mellah and Imini Wadis take their spring close the Tichka pass and have similar hydrological characteristics. The main slope of the Ouarzazate Wadi including its tributaries is 2.0 % (CHAMAYOU et al. 1977).
- The Ait Douchene Wadi with a catchment size of 2,930 km^2, drains the low permeable rocks of the Anti-Atlas (Fig. 2.4).

Except the M'Goun and Dades Wadis, all rivers of the Upper Drâa catchment present discontinuous flows during the year. While the Dades Wadi annually discharges 243 million m^3 (Tinouar station), the Ouarzazate River drains 121 million m^3 (Aman n'Tizi station) and the Ait Douchene River only 9 million m^3 (Assaka station) (Tab. 2.1).

Tab. 2.1: Hydrological characteristics of surface flow in the Upper Drâa catchment: mean annual discharge ($Q_{mean\ annual}$) and specific discharge ($Q_{specific}$) at 8 DRH stations. (Location Fig. 2.4).

River / Station	Catchment (km^2)	$Q_{mean\ annual}$ (10^6 m^3)	$Q_{specific}$ (10^3 m^3/km^2)
Imini / Agouim	max. 300	37	~ 120
Iriri / Tamdroust	undefined	41	-
Mellah / Agouilal	undefined	48	-
Ouarzazate / Aman N'Tini	4,500	121	27
Dades / Ait Moutade	1,525	116	76
M'Goun / Ifre	1,239	136	110
Dades / Tinouar	6,680	243	36
Ait Douchene / Assaka	1,390	9	6
Total of the measured discharges	12,570	373	30
Mansour Eddahbi reservoir*2	14,900	378	-

*1 MINISTERE DE L'EQUIPEMENT, 2002 *2 DIRECT. RECH. PLAN. EAU, 1994

The specific discharge for the whole Upper catchment (at Mansour Eddahbi dam) averages 30,000 $m^3/km^2/a$. Nevertheless, significant differences exist within the catchment. While the drainage of the Anti-Atlas by the Ait Douchene Wadi shows a specific discharge of approximately 6,000 $m^3/km^2/a$ at the Assaka station, the High Atlas presents specific discharge around 110,000 $m^3/km^2/a$ at the Ifre station. It is also important to notice that the cumulated discharges of Imini, Iriri and Mellah rivers (126 $\cdot 10^6$ m^3/a) are higher than the discharge measured downstream in the Ouarzazate river (121 $\cdot 10^6$ m^3/a). Similar results are known for the cumulated discharges of the Dades and M'Goun rivers (252 $\cdot 10^6$ m^3/a) and downstream at the Tinouar station (243 $\cdot 10^6$ m^3). These differences can be explained by the use of surface water for irrigation, the recharges of alluvial aquifers and evaporation effects occurring along the various rivers. The Mansour Eddahbi dam receives approximately 378 million m^3 in total per year (DIRECTION DE LA RECHERCHE ET DE LA PLANIFICATION DE L'EAU 1994).

Due to the aridity of the Drâa catchment and of the poor cover of vegetation runoff is important during rain events. The rivers react rapidly showing a high variability in discharge and the presence of floods (Fig. 2.9).

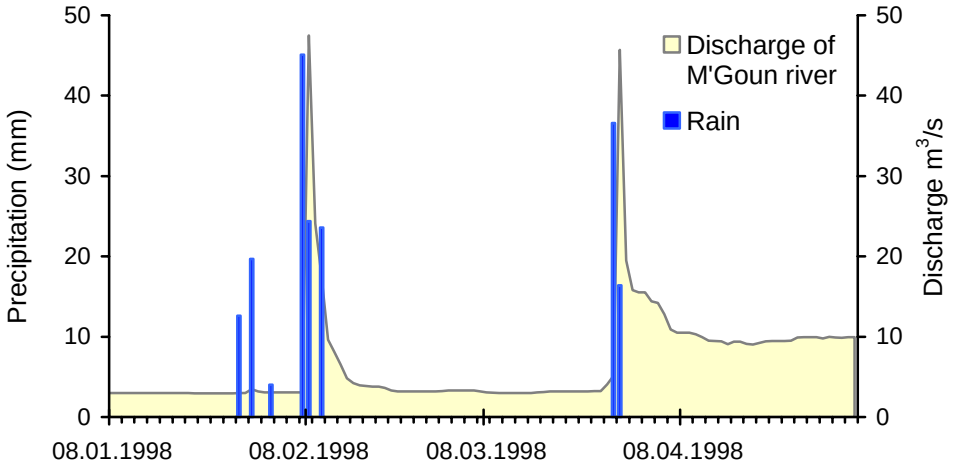

Fig. 2.9: Floods of the M'Goun River during two rain events; discharge and precipitation measurements at Ifre station (Data from: DRH; Location Fig. 2.4).

The Drâa river discharge mainly depends on the management of the Mansour Eddahbi reservoir by the "Office Régional de Mise en Valeur Agricole de Ouarzazate" (ORMVAO). For an efficient recharge of the downstream palm-grove aquifers, it is considered that 250 $\cdot 10^6$ m^3 should be released from the dam in seven "lâchers" spread over the year (DIRECTION DE LA RECHERCHE ET DE LA PLANIFICATION DE L'EAU 1994).

2.5 Geological overview

Morocco can be divided into four structural geological domains from south to north (Fig. 2.10):

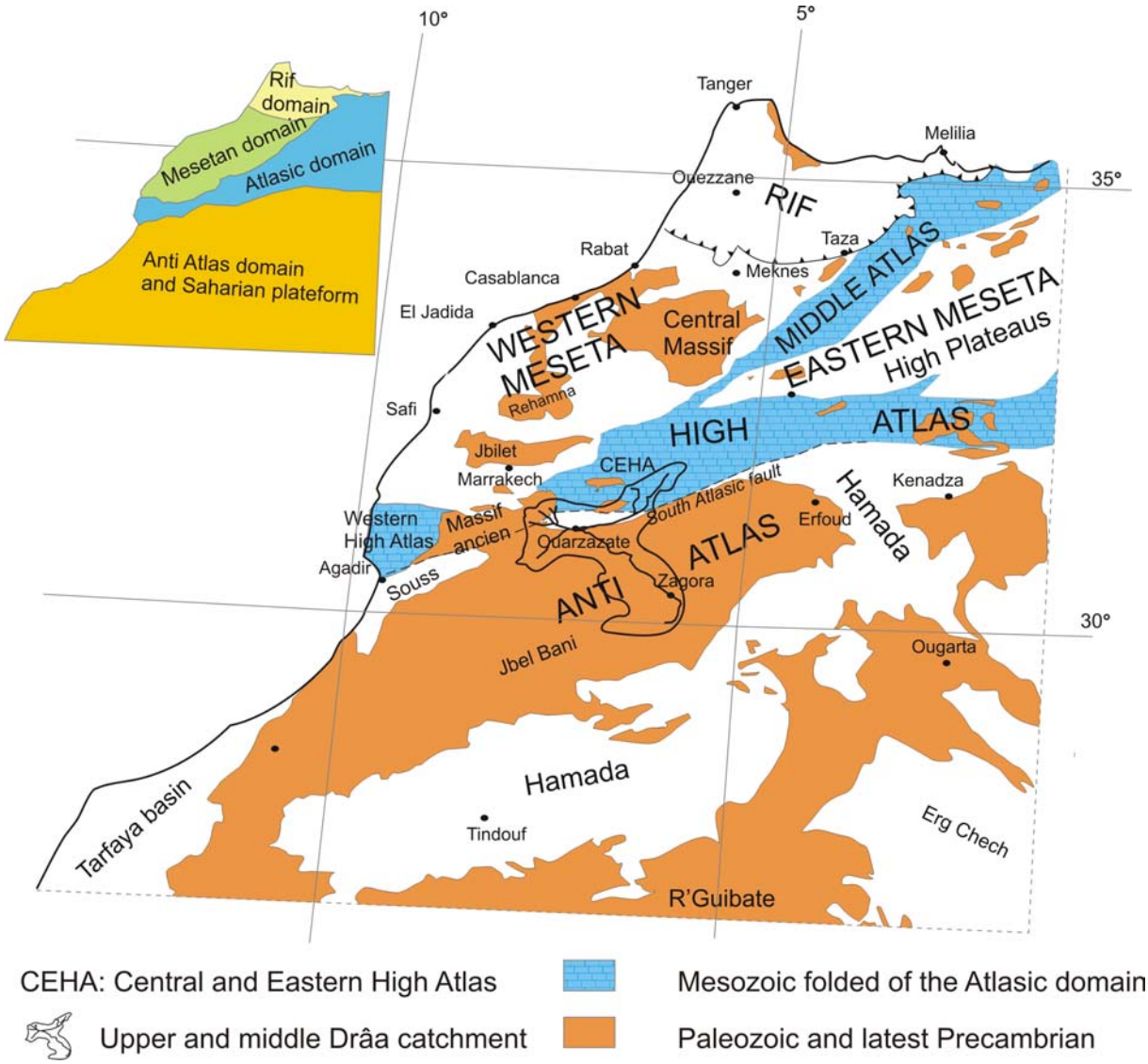

Fig. 2.10: The main geological domains of Morocco (modified after MICHARD 1976).

- The Anti-Atlas and the Saharian platform belong to the northern border of the West-African Craton in which the major deformation is dated to the end of the Precambrian. This domain was stable during the major post Jurassic tectonics (PIQUÉ 2001).
- The Atlasic domain is characterized by a Paleozoic basement which was deformed in the Mesozoic and by a Cenozoic cover. It is represented by the mountains of the Middle and the High Atlas uplifted during the Alpine phase. While the Middle Atlas is located between the Mesetan domains, the High Atlas range split the Mesetan domains from the Anti Atlas. The High Atlas is composed from west to east of the Western High

Atlas, the Paleozoic “Massif Ancien” and the Central and Eastern High Atlas (Fig. 2.10).

- The plains and plateaus of the Mesetan domains where the Paleozoic terrains are covered by thin tabular successions of Mesozoic and Cenozoic sediments.
- The thrusted Rif belt located along the Mediterranean Sea.

The Upper and Middle Drâa catchment is located between the southern margin of the Central High Atlas and the Anti-Atlasic domain (Fig. 2.10). This catchment presents rock series from Precambrian up to recent (Fig. 2.11). It is characterised by an important “Hercynian unconformity” at the base of the Mesozoic series which divides the sedimentary cover into two “Super Cycles”: Paleozoic (i.e. Gondwanien) and Meso-Cenozoic (i.e. Atlantic and Tethyan), respectively (PIQUÉ 2001).

From a geological and a structural point of view, the Upper Drâa catchment can be divided in four specific units (Fig. 2.11):

- The Anti Atlas as a stable domain of Precambrian basement with Paleozoic cover.
- The High Atlas Mountains composed of a Variscan basement and a Mesozoic limestone cover.
- The “Southern Atlas Marginal Zone”, a compressional deformation zone forming the northern rim of the Ouarzazate Basin.
- The foreland Basin of Ouarzazate with Tertiary continental infilling, which is an asymmetrical synclinorium of approximately 150 km length and 40 km widths.

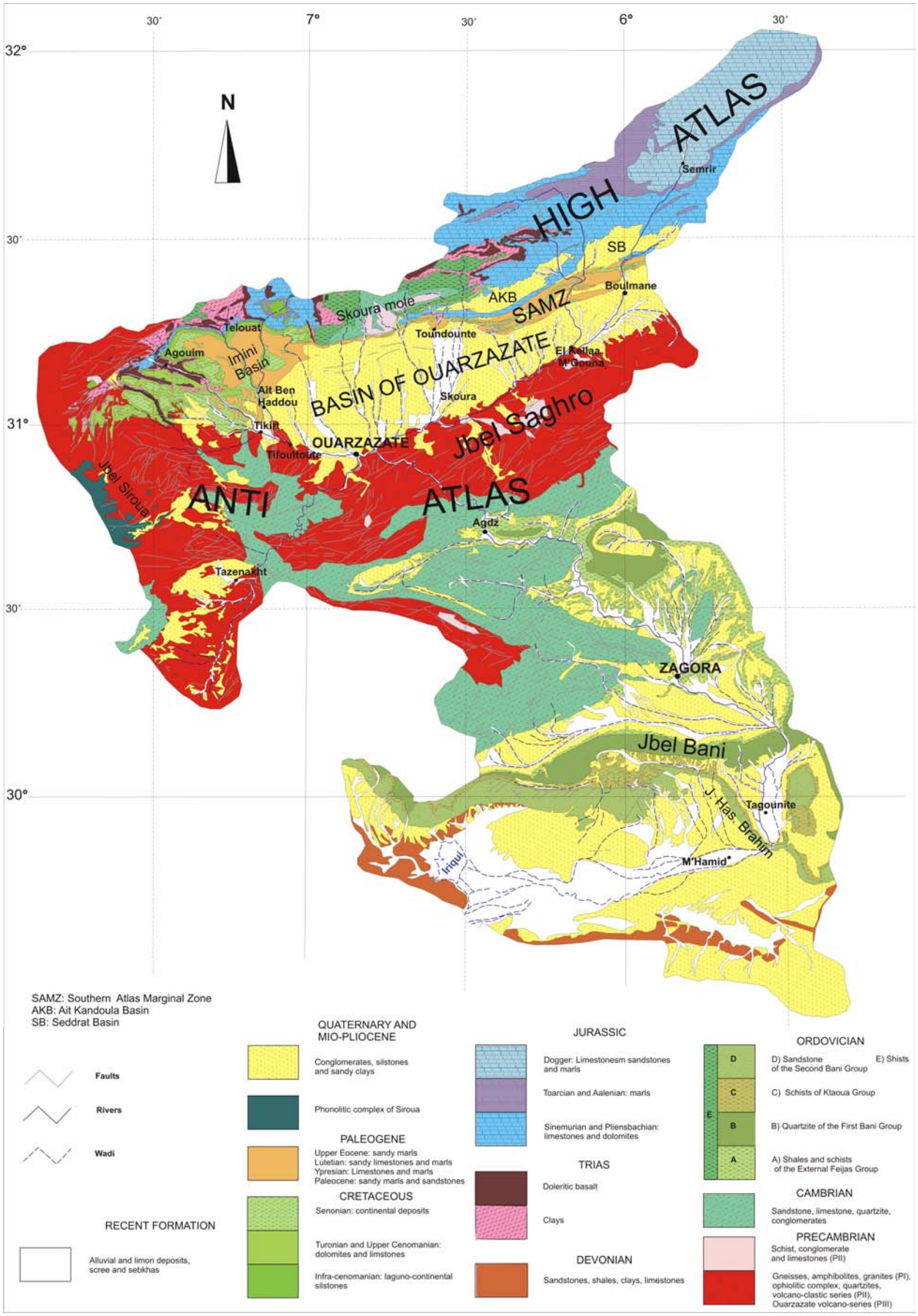

Fig. 2.11: Simplified geological map of the Upper and Middle Drâa catchment after the 1/500,000 Ouarzazate sheet (CHOUBERT 1959).

3 METHODS OF INVESTIGATION

3.1 Overview

Geological and hydrogeological investigations were undertaken in the Upper Drâa between 2000 and 2004. Local studies were carried out at the IMPETUS test-sites such as detailed geological mapping including hydrogeological characterization. The meso-scale catchment of the Assif-n'Ait-Ahmed Wadi has been chosen to characterize the aquifer system prevailing in High Atlas. In order to understand the groundwater provenance, its renewability and the subsurface processes affecting quality and quantity, hydrochemical and environmental isotopes (^{18}O, ^{2}H, ^{3}H,^{13}C and ^{14}C) analyses were performed on surface water and groundwater throughout the whole Upper Drâa catchment and at every test-site. Rain water has also been sampled and analysed for the stable isotopes (^{18}O and ^{2}H) at the IMPETUS climatic stations which are located along a gradient of aridity and altitude (Paragraph 2.2).

Regarding the methods of interpretation, various approaches and software are used. The partitioning of water chemistry is done with various graphical and statistical techniques such as pie diagram, Schoeller plot, Piper diagram, hierarchical cluster analysis and principal components analysis (with the program SPSS: LEVESQUE 2004) as described by GÜLER et al. (2002) or BAKALOWICZ (1994). The calculation of the saturation indexes of selected minerals based on equilibrium chemistry of aqueous solutions is computed with the program PHREEQC (PARKHURST & APPELO 1999). The residence time of the groundwater has been estimated based on radio-isotopes using the low parameter model BoxmodelV3 (KINZELBACH et al. 2002) (www.unep.org/water/ groundwater/). In order to simulate the groundwater flow of the basin of Ouarzazate, the three-dimensional finite-difference groundwater flow model PMWIN5 (www.unep.org/water/ groundwater/) developed by the U.S. Geological Survey (MC DONALD & HARBAUGH 1988a) was used in a first phase of parameterization.

3.2 Hydrogeological investigations

3.2.1 Geological investigations

To access the basic requirements for a reliable hydrogeological characterization of the geological structure, detailed geological and structural maps (1:25,000), geological profiles and lithological descriptions for selected test-sites result from various master thesis: Taoujgalt (MARTAU 2002) and Tichki and Ameskar in the Assif-n'Ait-Ahmed catchment (OSTERHOLT 2002, HOFMANN 2002, BELL 2005 and BUDEWIG *in progress*). The eastern and western part of the Assif-n'Ait-Ahmed catchment were mapped in the context of this study based on existing geological maps of the area, remote sensing data and investigations in the field.

3.2.2 Groundwater and surface water sampling

Between November 2000 and November 2004, 8 sampling campaigns for chemical analyses of groundwater and surface water were carried out in autumn and spring seasons in order to register the low and high water conditions (Tab. 3.1). Figure 3.1 shows the climatic conditions in the Upper Drâa catchment (monthly averages of precipitation) during the sampling periods between Mai 2001 and September 2004. In the Drâa valley, the period between June and August is usually considered as being the driest season (compare Fig. 2.5), and thus the sampling carried out in autumn is representative for low water conditions. But it should be

noticed that the summer 2003 was relatively rainy, therefore the campaign carried out during the autumn 2003 (IMP6) does not reflect properly a period of low water.

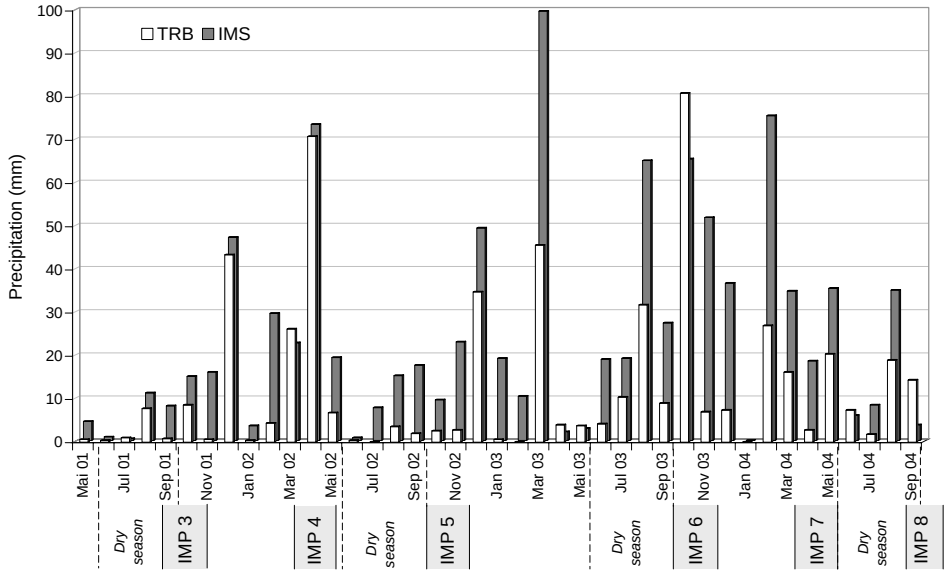

Fig. 3.1: Campaigns IMP3 to IMP8 in comparison with precipitation (monthly averages of precipitation) monitored at two IMPETUS stations; TRB = Trab Labied (Basin of Ouarzazate, 1,380 m a.s.l.) and IMS = Imeskar (High Atlas, 2,245 m a.s.l.).

Tab. 3.1: Sampling strategy

Campaign / season	Periods	Number of samples	Types of water	Type of analyses
IMP 1 / Autumn 2000	17/11/00 to 29/11/00	52 for ion analysis, 11 for stable isotopes	18 Springs / 32 Wells/ 2 Surface Waters	Major ions, SiO_2, Fe_{total}, Mn^{2+}, PO_4^{3-}, ^{18}O, ^{2}H.
IMP 2 / Spring 2001	25/02/01 to 13/03/01	93 for ion analysis, 93 for stable isotopes	38 Springs/ 45 Wells/ 10 Surface Waters	Major ions, SiO_2, Fe_{total}, Mn^{2+}, NH_4^+, PO_4^{3-}, ^{18}O, ^{2}H.
IMP 3 / Autumn 2001	21/09/01 to 10/11/01	69 for ion analysis, 69 for stable isotopes	22 Springs/ 42 Wells/ 5 Surface Waters	Major ions, SiO_2, Fe_{total}, Mn^{2+}, NH_4^+, PO_4^{3-}, ^{18}O, ^{2}H.
IMP 4 / Spring 2002	18/03/02 to 16/05/02	88 for ion analysis, 88 for stable isotopes	39 Springs/ 39 Wells/ 10 Surface Waters	Major ions, SiO_2, Fe_{total}, Mn^{2+}, NH_4^+, PO_4^{3-}, ^{18}O ,^{2}H.
IMP 5 / Autumn 2002	12/09/02 to 12/12/02	96 for ion analysis, 103 for stable isotopes, 10 for ^{14}C, 50 for ^{3}H	45 Springs/ 43 Wells/ 8 Surface Waters	Major ions, SiO_2, Fe_{total}, Mn^{2+}, NH_4^+, PO_4^{3-}, Sr, ^{18}O, ^{2}H, ^{14}C ,^{3}H
IMP 6 / Autumn 2003	30/09/03 to 02/12/03	80 for ion analysis, 97 for stable isotopes	30 Springs/ 48 Wells/ 2 Surface Waters	Major ions, SiO_2, Fe_{total}, Mn^{2+}, NH_4^+, PO_4^{3-}, Sr, ^{18}O, ^{2}H.
IMP 7 / Spring 2004	28/02/04 to 21/04/04	72 for ion analysis, 82 for stable isotopes	22 Springs/ 48 Wells/ 2 Surface Waters	Major ions, SiO_2, Fe_{total}, Mn^{2+}, NH_4^+, PO_4^{3-}, Sr, ^{18}O and ^{2}H.
IMP 8 / Autumn 2004	17/09/04 to 08/11/04	64 for ion analysis, 74 for stable isotopes	18 Springs/ 44 Wells/ 2 Surface Waters	Major ions, SiO_2, Fe_{total}, Mn^{2+}, NH_4^+, PO_4^{3-}, Sr, Cd, As, Cu, Pb, Ni, ^{18}O, ^{2}H.

Surface waters, wells and springs were sampled throughout the Upper Drâa catchment. The sampling in the Upper Drâa catchment started in autumn 2000. The sampled points are distributed in the following way (Fig. 3.2):

- Anti Atlas: 3 wells around the Bouskour test-site.
- The High Atlas: 43 springs in the meso-scale Assif-n'Ait-Ahmed catchment (Fig. 3.3), 4 springs in the Taoujgalt test-site, 10 wells and 3 springs in the Ait Kandoula basin, 2

springs in the Cambrian Skoura mole (only spring 2001: IMP 2) and 2 wells in the Dades Canyon (only autumn 2002: IMP 5).

- The Basin of Ouarzazate: 34 wells and 4 springs.

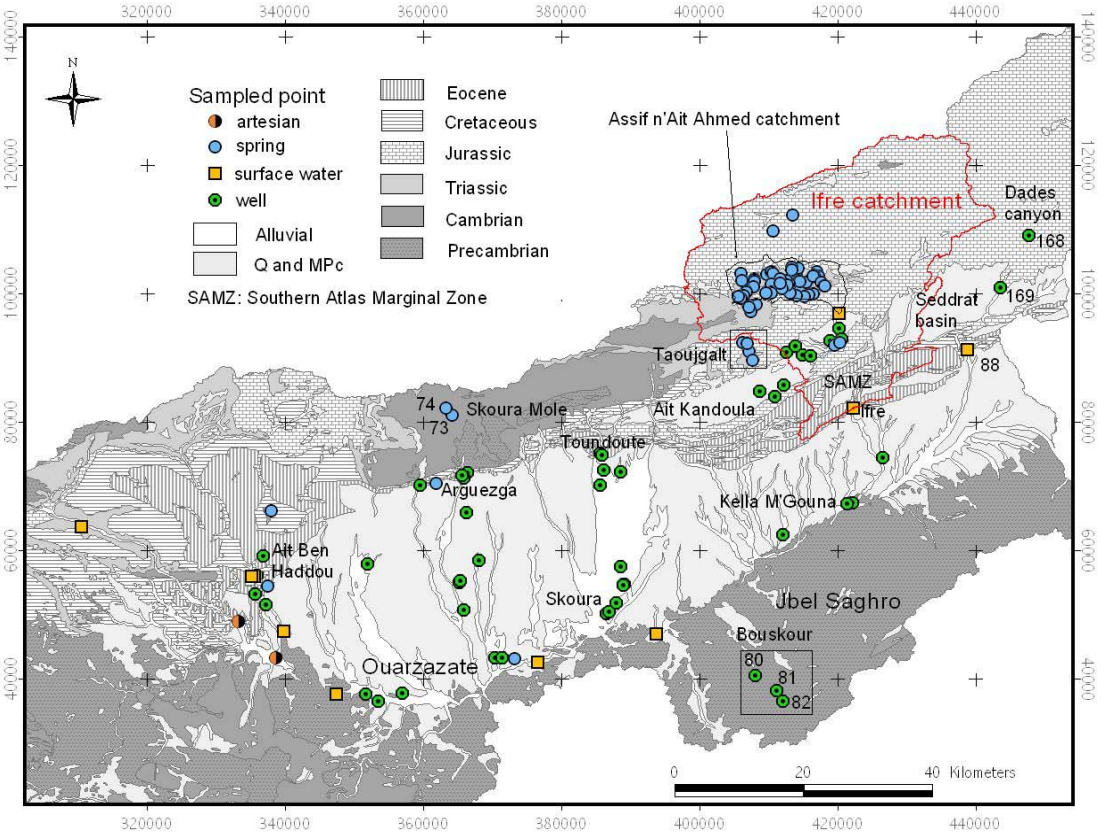

Fig. 3.2: Localisation and type of the sampled groundwater and surface water in he Upper Drâa catchment; location of the Ifre and Assif-n'Ait-Ahmed catchments; Q = quaternary and MPc = Mio-Pliocene (projected GCS Merchich, Lambert conformal conic).

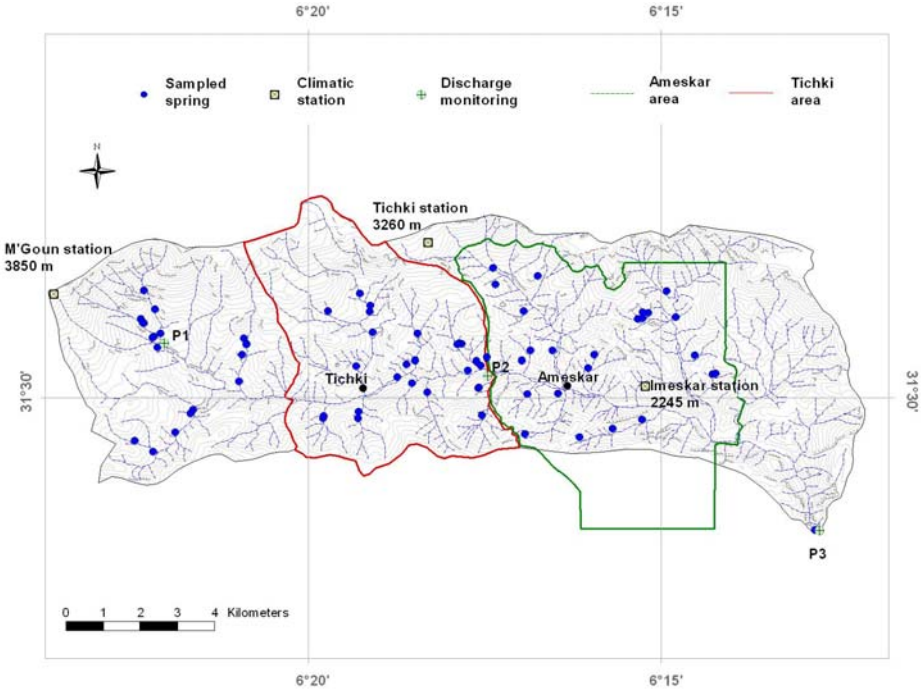

Fig. 3.3: The meso-scale Assif-n'Ait-Ahmed catchment (110 km^2): sampled springs, IMPETUS climatic stations and discharge monitoring; the precise geological mapping (1:25,000) of the delimited areas were carried out by OSTERHOLT (2002) and HOFMANN (2002) for the Ameskar area, and by BELL (2005) and BUDEWIG (in progress) for the Tichki area.

3.2.3 Rain and snow sampling

Collecting of rain for stable isotope analyses (^{18}O and ^{2}H) was done between summer 2002 and autumn 2004 at 8 IMPETUS climatic stations: Iriki (IRK), El Miyit (EMY), Argium (ARG), Bouskour (BSK), Trab Labied (TRB), Taoujgalt (TAO), Imeskar (IMS), Tichki (TIC) M'Goun (MGN) and Tizi Tounza (TZT) (compare Fig. 2.2 and Fig. 2.3). The rain events in the Drâa catchment are generally short and it usually does not rain more than three days without stop. Therefore, with the help of people living close to the climatic stations, the rain water has been collected after each event or even every day when it was possible. Figure 3.4 shows the system used for the rain sampling. This system reduces the contact between the atmosphere and the air within the bottle and it avoids in this way too much evaporation effect. In order to have the isotopic signature of the snow, some samples have been taken in the Assif-n'Ait-Ahmed catchment. The snow sampling has been carried out at different periods and at various altitudes.

Fig. 3.4: Example of rain collector for stable isotope analyses.

3.2.4 Hydrogeochemical analyses

In-situ measurements have been carried out including pH, electrical conductivity (µS/cm), temperature (°C), redox potential (mV) and oxygen (mg/l and %). Bicarbonate (HCO_3^-) and dissolved CO_2 was analysed in the field employing the titration method. The collected samples were analysed for (Tab. 3.1):

- Major ions: Na^+, K^+, Mg^{2+}, Ca^{2+}, Cl^-, NO_3^-, SO_4^{2-}.
- SiO_2, NH_4^+, PO_4^{3-}, Fe_{total}, Mn^{2+}, Sr^{2+}.
- Cd, As, Cu, Pb, Ni, Cd, As, Cu, Pb and Ni: only in autumn 2004 (IMP 8).
- Stable isotopes: ^{18}O and ^{2}H.
- Tritium, Carbon-13 and Carbon-14: only in autumn 2002 (IMP5).

Sampling and analytical methods followed the guidelines of the DVWK (DWVK 1999) (Tab. 3.2). To preserve the samples, they were filtered and treated with HNO_3 and H_2SO_4. In some cases, the high concentration of sulphates in the groundwater was problematic for the analysis of

nitrates with the IC. Therefore, a portable set from MERK was used to directly measure the nitrates in the field.

To measure ^{14}C and the $^{13}C/^{12}C$ ratio of water, it is necessary to obtain the Dissolved Inorganic Carbon (DIC) by precipitation which has to be carried out in the field (OLIVE 1999, RUEEDI 2002). The volume of water to obtain the necessary quantity of DIC is calculated according to the alkalinity measured beforehand by the titration method. The volume of the sample varies between 60 and 80 litres and the sampling is carried out after 30 minutes of pumping. In order to fix all the dissolved carbon in the form of CO_3^{2-}, the pH is raised above 10 with a strong base (NaOH). Then, addition of $BaCl_2$ allows capturing the CO_3^{2-} as $BaCO_3$ as an insoluble phase. To accelerate the precipitation process, a flocculation reagent ($FeSO_4$) is added. The precipitate is stored in a sampling bottle of 1 litre, which is well sealed against the atmosphere.

Tab. 3.2: Methods of conservation and technique of analyses

Parameter	Amount	Treatment	Analysis techniques
Anions: Cl^-, NO_3^-, SO_4^{2-}	20 ml	Macro-filtration and micro-filtration (0,45 µm)	IC
Anion : PO_4^{3-}	100 ml	Macro-filtration and micro-filtration (0,45 µm) + drops of pure H_2SO_4 until Ph<2	Photometry
Hydrogencarbonates: HCO_3^-	500 ml	Macro-filtration	Titration
Cations : Na^+, K^+, Mg^{2+}, Ca^{2+}, Fe_{total}, Mn^{2+}, Sr, Cd, As, Cu, Pb, Ni	100 ml	Macro-filtration and micro-filtration (0,45 µm) + drops of pure HNO_3 until Ph<1	AAS
Cations : NH_4^+ and SiO_2	100 ml	Macro-filtration and micro-filtration (0,45 µm) + drops of pure H_2SO_4 until Ph<2	Photometry
Stable isotopes: ^{18}O and ^{2}H	30 ml	-	Masses spectrometer
Tritium[*1]	500 ml	Macro-filtration	LCP
Carbon-14[*1] and Carbon-13[*1]	60 to 80 l. of water	NaOH until pH > 10.3 + $BaCl_2$ (precipitation) + $FeSO_4$ (flocculation reagent)	Fluid scintillation counters

[*1] analyses performed at the GSF Institute of Hydrology in Neuherberg by W. Stichler

For the analyses of Na^+, K^+, Mg^{2+}, Ca^{2+}, Fe_{total}, Sr^{2+}, Mn^{2+}, Cd, As, Cu, Pb, Ni, Cd, As, Cu, Pb and Ni, an Atom Absorption Spectrometer (Perkin-Elmer AAS 3030 B) is used (Tab. 3.2). Concentrations of Cl^-, NO_3^-, SO_4^{2-} are determined with a Ion Chromatograph (Shimadzu IC-A1) and SiO_2, NH_4^+, PO_4^{3-} with a Spectral Photometer (DR. Lange Cadas 100). The isotope analyses (^{18}O, ^{2}H, ^{3}H, ^{13}C and ^{14}C) were carried out by Mr. W. Stichler (Dipl.-Phys.) at the GSF Institute of Hydrology in Neuherberg. The analysis of ^{18}O and ^{2}H are done with an Isotope Ratio Mass Spectrometer. Tab. 3.3 shows the analytic detection limits of the analysed elements.

Tab. 3.3: Errors due to the detection limits

Element	Detection limit	Element	Detection limit	Element	Detection limit
Na^+	0.01 mg/l	NH_4^+	0.5 mg/l	Cu	0.002 mg/l
K^+	0.04 mg/l	PO_4^{3-}	0.5 mg/l	Pb	0.002 mg/l
Mg^{2+}	0.02 mg/l	SiO_2	0.5 mg/l	Ni	0.002 mg/l
Ca^{2+}	0.09 mg/l	Sr^{2+}	0.025 mg/l	As	0.005 mg/l
Cl^-	0.2 mg/l	Fe_{total}	0.001 mg/l	δ^2H	1.0 ‰
NO_3^-	0.5 mg/l	Mn^{2+}	0.002 mg/l	$\delta^{18}O$	0.1 ‰
SO_4^{2-}	0.6 mg/l	Cd	0.002 mg/l	$\delta^{13}C$	+/- 0.2 ‰

3.2.5 Interpretation of the hydrogeochemical data

Statistical methods

Hierarchical Cluster Analysis (HCA) is used to group groundwater samples into hydrochemical groups. The variables used for the HCA are weighted (standardization: z-scores) and the linkage rule applied is the Ward's method.

In order to understand the correlation between the variables, Principal Component Analyse (PCA) is performed using the software SPSS (LEVESQUE 2004). This technique reduces the number of dimensions present in data to an easily interpretable form. A correlation coefficient matrix is computed, which gives the inter correlations among the set of variables. "Components" representative of the total variance are calculated as well as the "component loading" of each variables as a measure of the degree of closeness between the variables and the component (GÜLER 2002). For a better interpretation, the component loading matrix is rotated with the "varimax rotation" method. This procedure gives a new rotated matrix in which each component is better described by the variables, although the total variance is generally not as well explained.

Saturation Index

The saturation index (SI) of various minerals is calculated in order to characterise the chemical evolution of the groundwater. The SI of a mineral in groundwater is calculated from the activities of ions based on pH, temperature and the major ion concentrations of the solution (LANGMUIR 1971, APPELO & POSTMA 1999). Activities are used to reflect the chance that ions react together and form a precipitate. The activity [i] of the ion i is:

$$[i] = \gamma_i \cdot m_i \qquad \text{[Eq. 1]}$$

γ_i is the activity coefficient which depends on the ionic strength of the solution and m_i is the molality of the ion i.

The saturation state (Ω) of a groundwater sample for any mineral is obtained with the comparison between the solubility product of the considered mineral (K) and the product of activities of the solution (or activity product: IAP) such as:

$$\Omega = \frac{IAP}{K} \qquad \text{[Eq. 2]}$$

The saturation index (SI) is defined as:

$$SI = \log \Omega \qquad \text{[Eq. 3]}$$

The calculation of saturation indexes requires iterative computations between each species content and total ion content given by analysis. Calculations of the saturation indexes were computed with Phreeqc (PARKHURST & APPELO 1999). Dissolution can occur for negative SI (under-saturation) and precipitation for positive SI (over-saturation). A solution is at equilibrium (or saturation) at -0.5 < SI < 0.5 (BAKALOWICZ 1994). The calculation of the saturation index (SI) of minerals allows the estimation of the degree of evolution of the groundwater. In fact, the dissolution of minerals depends on the time of contact between the solution and these minerals and on the initial saturation of the solution. Consequently, in homogeneous aquifers the degree of saturation of groundwater in regard to a mineral reflects partly the transit time. The time of contact necessary to acquire the equilibrium of a solution in regard to a mineral depends also on the kinetic of the involved reactions. Negative SI values in regard to calcite are related to short

residence time of water in contact with carbonate rock, while equilibrium values reflect longer residence time more than a few weeks (BAKALOWICZ 1994). The solubility of calcite is higher than dolomite which is higher than quartz. But, the solubility of these minerals is low in comparison to gypsum. The dissolution process of gypsum under natural conditions is very rapid and brings Ca^{2+} in the solution, which increases the saturation of calcite and dolomite. Dolomite and quartz do not precipitate under normal conditions of pressure and temperature (BAKALOWICZ 1979) and quartz is not affected so much by the common ion effect. Saturated water with respect to quartz can reveal groundwater with high residence time from magmatic rocks, quartzite and sandstones. The SI_{CO2} gives information about the saturation of CO_2 gas of the groundwater. A positive SI_{CO2} reveals a degassing of CO_2.

3.2.6 Digital elevation model of the Upper Drâa catchment

A Digital Elevation Model (DEM) of the Upper Drâa catchment derived from SRTM by P. Poete (IMPETUS) is used. The horizontal accuracy is 2 seconds (78 x 92 m) and the vertical precision is about 25 m.

3.2.7 Discharge and water level measurements

Discharges of springs and rivers in the Assif-n'Ait-Ahmed catchment were measured with a magnetic-induction discharge sensor: Nautilus C2000 (Ott Messtechnik GmbH, Kempten). During each campaign, the water level of the monitored wells was measured. In autumn 2003 (IMP 6), a precise water level map was carried out in the Ait Kandoula basin in the Ifre catchment using a "Differential GPS" (GPS Pathfinder, Pro XRS, Timble Co., USA), which allows localisation with a precision of +/- 0.2 m laterally and about +/- 0.5 m vertically.

3.2.8 Water budget

The water budget is estimated in the Assif-n'Ait-Ahmed catchment and in the Ifre catchment (Fig. 3.2). The amount of precipitation for the year 2002-2003 is defined by SCHULTZ (2006). He uses the IMPETUS climatic data which were extrapolated through the DEM of the Drâa catchment. The evapotranspiration was defined in the Ifre catchment by Machauer with the MMS model (personal communication).

3.3 Environmental Isotopes

Regarding the environmental isotopes, analyses of groundwater in this study focus on the stable isotopes ^{2}H, ^{18}O and ^{13}C, and the radioisotopes ^{3}H and ^{14}C. These geochemical tools can provide information on the hydrogeological characteristics of aquifers such as: origin of water, hydraulic discontinuities or interconnections, replenishment processes, mixing proportions of component flows originating from different sources and residence times. This paragraph gives an overview of the isotope techniques applied in hydrogeology (FONTES 1976, FRITZ & FONTES 1980, CLARK & FRITZ 1997, KENDALL & CALDWELL 1998, ROZANSKI et. al 2001, GEYH 2000, KINZELBACH et al. 2002).

3.3.1 Stable isotopes

The concerned stable isotopes are the abundant and rare isotopes (except ^{17}O) of the water molecule (H and O) and the Carbon atom (Tab. 3.4).

Tab. 3.4: Masse abundances in the hydrological cycle of the stable isotopes of Hydrogen, Oxygen and Carbon atoms (GAT et al. 2001).

Hydrogen		Oxygen			Carbon	
^{1}H	^{2}H	^{16}O	^{17}O	^{18}O	^{12}C	^{13}C
99.985 %	0.015 %	99.759 %	0.037 %	0.204 %	98.892 %	1.108 %

3.3.1.1 Isotope ratios

The isotopes ratios of molecules are defined by the ratio (R) of the heavy (or rare) to light (or abundant) molecular concentrations. Regarding the water molecule, the ratios of ^{1}H and ^{2}H can be defined by equation Eq. 4 and ^{16}O and ^{18}O by equation Eq. 5. The ratio between ^{12} C and ^{13}C in the molecule of CO_2 will be defined by the equation Eq. 6.

$$^{2}R\left(H_2O\right)=\frac{\left[^{2}H^{1}HO\right]}{\left[^{1}H_2O\right]} \quad \text{[Eq. 4]} \qquad ^{18}R\left(H_2O\right)=\frac{\left[H_2{}^{18}O\right]}{\left[H_2{}^{16}O\right]} \quad \text{[Eq. 5]} \qquad ^{13}R\left(CO_2\right)=\frac{\left[^{13}CO_2\right]}{\left[^{12}CO_2\right]} \quad \text{[Eq. 6]}$$

3.3.1.2 Deviation value (δ), standards

Isotopic concentrations are often expressed as the difference between the measured ratios of the sample (spl) and an international standard (std) reference (CLARK & FRITZ 1997):

$$\delta_{spl/std}\left[‰\right]=\left[\frac{R_{spl}}{R_{std}}-1\right]\cdot 1000 \qquad \text{[Eq. 7]}$$

If the sample has lower abundance of rare isotope in respect to the standard, then δ (‰) < 0, and δ (‰) > 0 for a higher abundance. The standard reference used for $\delta^{2}H$ and $\delta^{18}O$ measurements is the V-SMOW (Vienna-Standard Mean Ocean Water). The $\delta^{13}C$ measurements are reported relative to the VPDB (Vienna-Pee Dee Belemnite).

3.3.1.3 Isotopes fractionation

An isotope fractionation occurs when a chemical compound (molecules containing different isotopes of the same element) changes from one state to another (i.e. liquid to vapour) or into another compound (i.e. carbon dioxide into plant organic carbon). This is the consequence of the mass differences of the atomic nuclei. For two molecules with the same kinetic energy ($E_k = 1/2mv^2$ = constant when T = constant) the heavier isotopic molecule has a lower mobility and a lower diffusion velocity which involves that it reacts slower than the lighter molecule. Moreover, heavier isotopic particles have in general higher binding energies than the lighter. Hence, the molecules containing heavy isotopes are more stable during physical or chemical transition process. For instance, the molecule $^{1}H^{2}H^{16}O$ evaporates less easily than $^{1}H_2{}^{16}O$ because it has lower vapour pressures and the molecule $Ca^{12}CO_3$ dissolves faster than the molecule $Ca^{13}CO_3$. However, it should be noticed that it is not true with the molecule of $^{13}CO_2$ which shows higher vapour pressure in the liquid phase and lower solubility in water than $^{12}CO_2$ (compare Tab. 3.6). For reversible process between two phases or two compounds, the dense phase (i.e. liquid rather than vapour) or the compound having the largest molecular masse (i.e. $CaCO_3$ versus CO_2) usually contains the highest abundance of the heavy isotope (MOOK 2000).

3.3.1.4 Kinetic and equilibrium isotope fractionations

To assess the change in isotopic composition in a one-way process (A→B), the ratio $\alpha_{A/B}$ was defined as the fractionation factor (Eq. 8).

$$\alpha_{A/B} = \frac{R_A}{R_B} \qquad \text{[Eq. 8]}$$

The fractionation for irreversible processes (such as evaporation without condensation, rapid calcite precipitation etc.) is called the "kinetic fractionation". The fractionation for reversible chemical reactions (Eq. 9) or reversible physical processes ("thermodynamic isotopic equilibrium" reactions) is defined as the "equilibrium fractionation".

$$*A + B \leftrightarrow A + *B \qquad \text{[Eq. 9]}$$

(*=presence of rare isotope in the molecule)

In the Eq. 9, A and B can be two different compounds or two phases of the same compounds. The equilibrium fractionation factor α is defined by the equilibrium constant K of the following exchange reaction (CLARK & FRITZ 1997):

$$K(T) = \frac{[A]\cdot[*B]}{[*A]\cdot[B]} = \frac{[*A]/[A]}{[*B]/[B]} = \frac{R_A}{R_B} = \alpha_{A/B}(T) \qquad \text{[Eq. 10]}$$

The equilibrium isotopic fractionation is temperature (T) dependent. The fractionation can also be expressed with the "enrichment factor" $\varepsilon_{A/B}$ (Eq. 11). An enrichment of the rare isotope in B with respect to A will involve $\varepsilon_{A/B} < 0$, while $\varepsilon_{A/B} > 0$ means depletion.

$$\varepsilon_{A/B} = \left[\alpha_{A/B} - 1\right]\cdot 1000 \ [‰] \qquad \text{[Eq. 11]}$$

3.3.1.5 Temperature effect on fractionation

The isotopic equilibrium fractionation is strongly dependent on the temperature of the reaction. The correlation between α and the absolute temperature (T) is represented by the following equation form:

$$\ln\alpha_{A/B} = -\ln\alpha_{B/A} = a\cdot T^2 + b\cdot T^{-1} + c \quad \text{with} \quad a,b,c = \text{constants} \qquad \text{[Eq. 12]}$$

The fractionation term is often expressed with the form: $10^3\ln\alpha_{A/B}$. Then, the "enrichment factor" $\varepsilon_{A/B}$ can be approximated to $10^3\ln\alpha_{A/B}$ under specific conditions. The Table 3.5 shows the fractionation between water and vapour at different temperatures for ^{18}O and ^{2}H. When the temperature decreases, the fractionation $10^3\ln\alpha_{w/v}$ increases.

Tab. 3.5: Values for fractionation relationships for ^{18}O and ^{2}H in water-vapour-ice reactions (CLARK & FRITZ 1997).

	T [°C]	$10^3\ln\alpha^{18}O$	$10^3\ln\alpha^{2}H$
Water/vapour: $10^3\ln\alpha_{w/v}$	-10	12.8	122
	10	10.6	93
	25	9.3	76
Ice/vapour: $10^3\ln\alpha_{i/v}$	0	14.7	126

3.3.1.6 The Rayleigh process

The Rayleigh fractionation considers chemically open systems where the isotopic species are removed. At every instant, these removed species are in thermodynamic and isotopic equilibrium with those remaining in the system at the moment of removal (KENDALL & CALDWELL 1998). The simplest case is the reservoir with one sink (Fig. 3.5.A). In this case, the isotopic composition δ_r of the reservoir after the removal of an amount of N_0 – N molecules can be approximated by:

$$\delta_r = (1+\delta_0)\cdot\left(\frac{N}{N_0}\right)^2 - 1 \qquad \text{[Eq. 13]}$$

The δ_f of the compound formed by the process can be approximated by:

$$\delta_f = (1+\delta_0)\cdot\frac{1-\left(\frac{N}{N_0}\right)^{\alpha}}{1-\frac{N}{N_0}} - 1 \qquad \text{[Eq. 14]}$$

With: N_0 = initial total number of molecule in the reservoir, N/N_0 = remaining fraction of the original reservoir, α = equilibrium or kinetic fractionation factor involved (with $\varepsilon = \alpha - 1$) and δ_0 = initial δ in the reservoir.

Figure 3.5.B shows the enrichment of rare heavy isotopes in a reservoir by the Rayleigh process as a function of the fraction removed. In this case, $\alpha_{removed/remaining} < 1$($\varepsilon_{removed/remaining}$ = -10 ‰), which is accompanied by a preferential removing of the light istopic species during this process. This example can describes the variation of $^{18}O/^{16}O$ of a confined water body under evaporation.

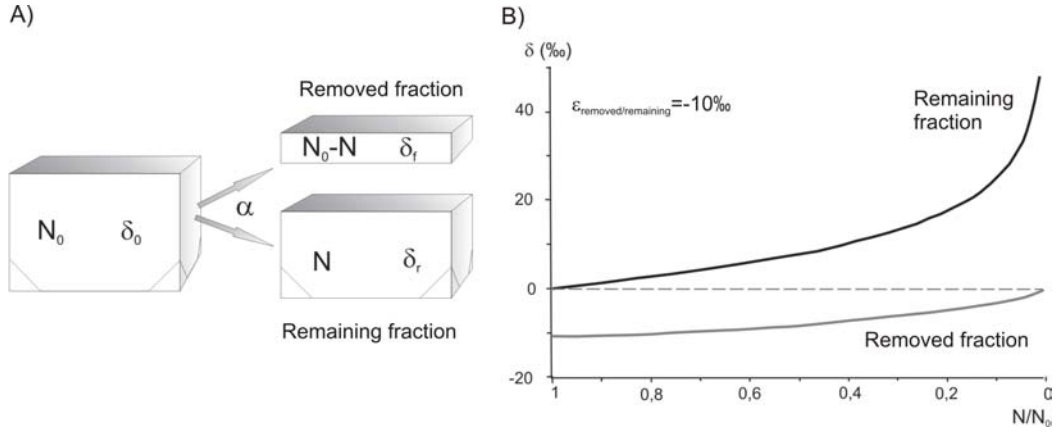

Fig. 3.5: A) Schematic representation of the Rayleigh process for a reservoir with one sink. N_0: initial number of molecule in the reservoir, δ_0: initial δ in the reservoir, δ_r: δ in the reservoir after the removal of an amount of N_0-N molecules, δ_f: δ of the removed fraction, α: fractionation factor involved in the process. B) Enrichment of a rare heavy isotope in a reservoir by the Rayleigh process as a function of the fraction removed (MOOK 2000). The lower line presents the average cumulative isotopic composition of the compound formed by the process (δ_f).

3.3.1.7 Oxygen-18 and Deuterium

The Global Meteoric Water Line and the d-excess

The use of isotopes for tracing groundwater involves that the input signal which is the isotopic concentration in the precipitations. CRAIG (1961) plotted in first the isotopic compositions (δ^2H, versus $\delta^{18}O$) of precipitation samples from all over the world and defined the *Global Meteoric Water Line* (GMWL) described by the equation:

$$\delta^2H = 8\,\delta^{18}O + 10\ ‰\ (SMOW) \qquad [Eq.\ 15]$$

Later, the IAEA with a world wide monitoring (Global Network for Isotopes in Precipitation-GNIP) refined this relationship (Fig. 3.6).

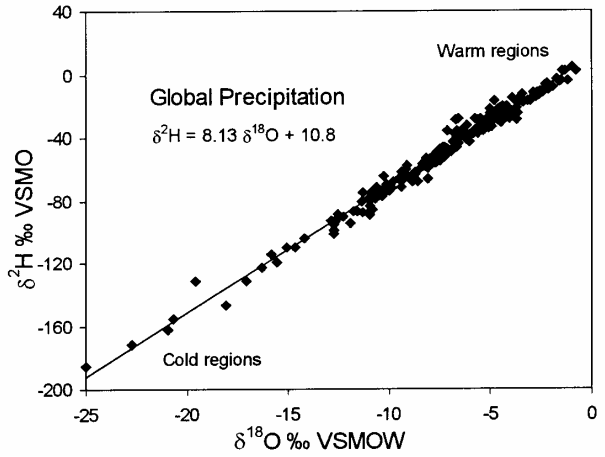

Fig. 3.6: The meteoric relationship for ^{18}O and ^{2}H in precipitation. Data are weighted average annual values for precipitation at stations in the IAEA global network compiled in (CLARK & FRITZ 1997).

The slope of 8 reflects the ratio of the equilibrium fractionation factors for H and O isotopes at 25 to 30°C ($10^3 \ln\alpha_{w/v}{}^2H$ / $10^3 \ln\alpha_{w/v}{}^{18}O$ = 8.2 at 25°C, Tab. 3.5) and the equilibrium Rayleigh condensation of rain at about 100% humidity (KENDALL & CALDWELL 1998). The interception with the y-axe is called the deuterium excess (d or d-excess) which is equal to 10 for the GMWL defined by CRAIG. More generally, the d value is defined for a slope of 8 as:

$$d = \delta^2H - 8\,\delta^{18}O \qquad [Eq.16]$$

The evaporation effect and the Local Meteoric Water Line

Considering a volume of water under strong kinetic evaporation, the isotopic composition of the residual water and the produced vapour evolves according to a slope lower than 8 which would be the slope under equilibrium fractionation (Fig. 3.7.A). The residual water will be enriched in heavy isotopes, while the vapour will have a depletion plotting to the opposite of the initial composition of water.

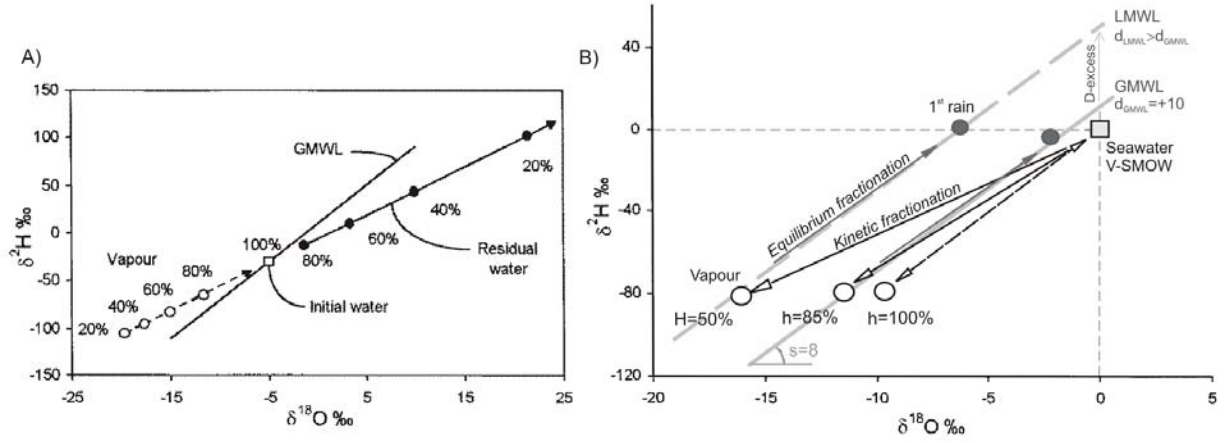

Fig. 3.7: A) Isotopic evolution of a finite volume of water during evaporation with 50% humidity. Residual water and accumulating vapour are in percentages of the initial reservoir (CLARK & FRITZ 1997). B) Kinetic isotope effects during evaporation of seawater to form vapour for various humidities (h) at 25°C and first rain formed by equilibrium condensation (modified after CLARK & FRITZ 1997); GMWL Global Meteoric Water Line, LMWL: Local Meteoric Water Line.

Figure 3.7.B shows the kinetic isotope effects for various humidities during evaporation of seawater. The first precipitation of the produced vapours is also shown, which is positively displaced along a line with the slope 8 (condensation under equilibrium). The GMWL (d = +10 ‰) corresponds to the kinetic evaporation of seawater under humidity about 85% following by the equilibrium condensation of the produced vapour. When humidity is lower (i.e. h = 50 %) the vapour is strongly depleted and the precipitation plots above de GMWL ($d_{GMWL} < d_{h=50\%}$). Therefore, on a local scale the precipitation can plot on a line which differs of the GMWL. This line is called the Local Meteoric Water Line (LMWL). The slope of the LMWL can also differ from 8 due to local climatic factors which are described in the next paragraph.

The isotopic variations of precipitation

In the atmosphere, the evolution of isotopic composition of air masses, which comes from the ocean and moves across continents loosing water by rainout is well described by the Rayleigh process (Paragraph 3.3.1.6). The air masses become depleted in the heavy isotopes because the rain is enriched in the heavy isotopes relative to the vapour phase. In other words, the process of rainout distills the heavy isotopes from the vapour. Hence, when clouds move inland from the ocean, the δ values of rain become lighter (KENDALL & CALDWELL 1998). It is the "continental effect".

Moreover, due to the fact that the isotopic fractionation is strongly dependent on the temperature (Paragraph 3.3.1.5), the Rayleigh process is accentuated for lower temperature of condensation (Fig. 3.8).

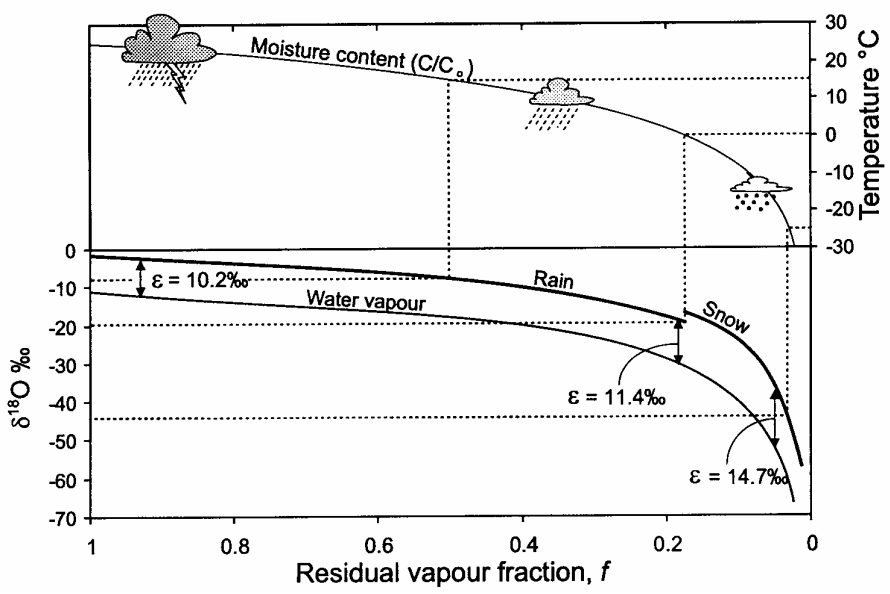

Fig. 3.8: The change in the ^{18}O content according to Rayleigh distillation; f = residual vapour fraction in the cloud (CLARK and FRITZ, 1997).

Due to the fact that the temperature of condensation is correlated with ground temperature, the isotopic composition of the precipitation shows various variations such as (GONFIANTINI et. al. 1998):

- Seasonal variation ("season effect"): summer precipitations are enriched in heavy isotopes.
- Variation due to the altitude ("altitude effect"): high altitude precipitations are depleted in heavy isotope.

The isotopic concentration in the precipitation can also be a result of the local weather system. For example, the investigated area can be influenced by the mixing of several vapour masses having different origins. Each vapour masse having its own source (i.e. Atlantic Ocean or Mediterranean Sea) will show different isotopic composition. Moreover, these vapour masses will be more or less affected by the "continental effect" according to their trajectories. It exists also the "amount effect", which describes the relation between the intensity of precipitation and $\delta^{18}O$ values. Heavy rains are extremely depleted in heavy isotopes. In arid areas, light rains can be enriched in heavy isotopes due to partial evaporation of raindrops during the fall.

The mixing processes of groundwater

The δ value of mixture of two quantities of a compound with different δ values (δ_1 and δ_2) (Fig. 3.9) can be approximated (with an error of ± 0.03 ‰ for natural abundance) from the simple masse balance equation (MOOK 2000):

$$\delta \approx f_1\delta_1 + f_2\delta_2 \qquad \text{[Eq.17]}$$

with N=number of molecules and $f_1 = N_1/N$ and $f_2 = N_2/N$.

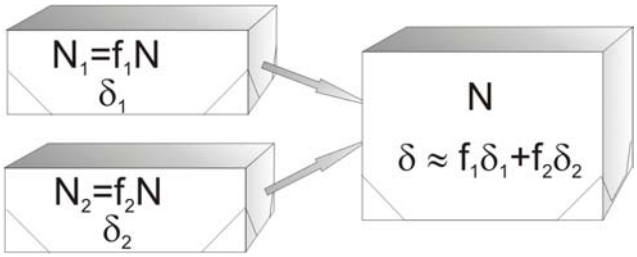

Fig. 3.9: Schematic representation of the mixing of two quantities of one compound with different isotopic compositions; δ can be approximated as $\delta = f_1\delta_1+f_2\delta_2$ (MOOK 2000); N1, N2 and N are the number of molecules.

Figure 3.10-A shows examples of the mixing of two different groundwater types defined by a "mixing line" (A). The mixing of three compounds is described by a ternary mixing diagram (Fig. 3.10-B).

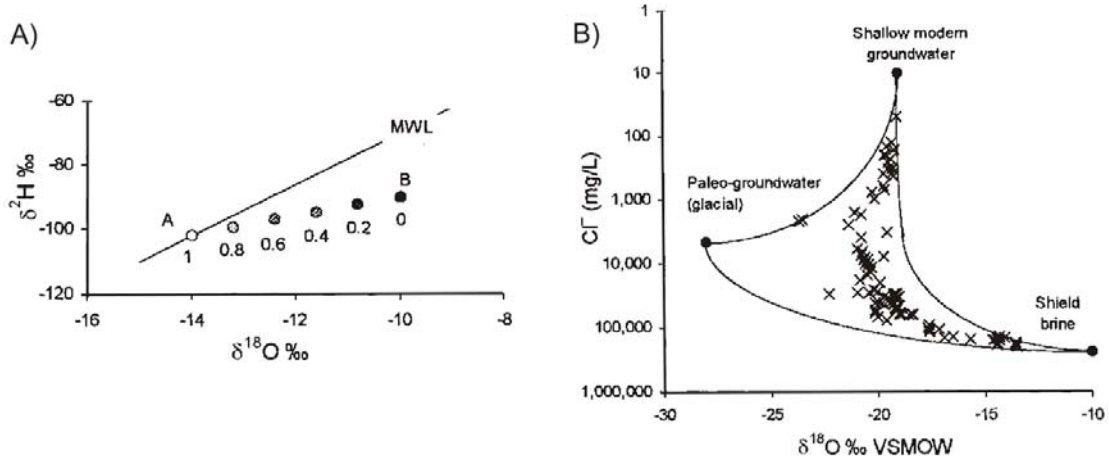

Fig. 3.10: A) The fractional mixing of two groundwater quantified on the basis of their stable isotope contents, shown as the fraction of groundwater "A" in the "A-B" mixture (CLARK & FRITZ 1997); MWL: Meteoric Water Line. B) Ternary mixing diagram for groundwater from crystalline rocks of the Canadian Shield (DOUGLAS 1997 in: CLARK & FRITZ 1997).

3.3.1.8 Carbon-13

^{13}C is an excellent tracer associated with all the processes intervening in carbonate geochemistry.

The carbonate geochemistry and the carbon sources of the groundwater

The dissolved inorganic carbon (DIC) of water is present in four main species (Eq. 18).

$$DIC = \left[CO_{2(aq)}\right] + \left[H_2CO_3\right] + \left[HCO_3^-\right] + \left[CO_3^{2-}\right] \qquad \text{[Eq. 18]}$$

The distribution of the species is a function of the pH (Fig. 3.11) according to the equilibrium equation [Eq. 19] with thermodynamic reaction constants (K) for T = 25°C..

$$CO_{2(g)} + H_2O \xleftrightarrow{K_{CO_2}} H_2CO_3 \xleftrightarrow{K_1} H^+ + HCO_3^- \xleftrightarrow{K_2} 2H^+ + CO_3^{2-} \qquad \text{[Eq. 19]}$$

with: $K_{co_2} = \dfrac{\left[H_2CO_3\right]}{P_{CO_2} \cdot \left[H_2O\right]} = 10^{-1.47}$ $K_1 = \dfrac{\left[H^+\right]\left[HCO_3^-\right]}{\left[H_2CO_3\right]} = 10^{-6.36}$ $K_2 = \dfrac{\left[H^+\right]\left[CO_3^{2-}\right]}{\left[HCO_3^-\right]} = 10^{-10.33}$

The pH of groundwater is usually between 6 and 8. Within this range of pH values the dominant carbonate species is bicarbonate (HCO_3^-) (Fig. 3.11).

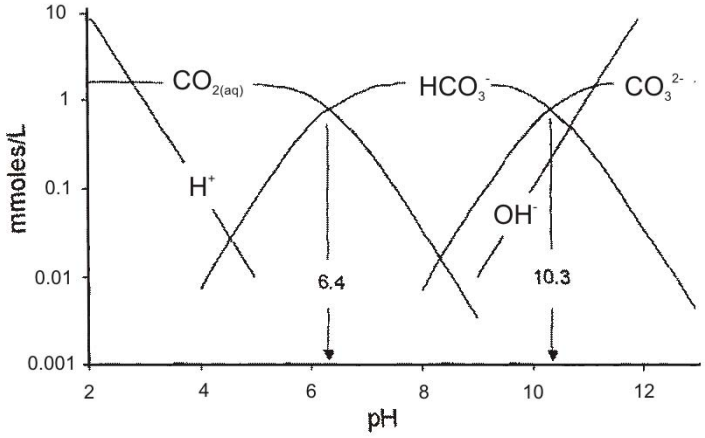

Fig. 3.11: Distribution of carbonate species in pure water as a function of pH at 25°C, calculated for a total dissolved inorganic carbon content of 1.6 mmol/L (CLARK & FRITZ 1997).

The groundwater will be mainly influenced by two sources of carbon, the CO_2 of the soil and the carbonates of aquifers:

- The atmosphere presents a small concentration of CO_2 ($p_{CO2} \approx 10^{-3.5}$) in comparison to the concentration of CO_2 in the soil ($p_{CO2} \approx 10^{-3}$ to 10^{-1}) due to the biogenic activity (CLARK and FRITZ 1997). Therefore, the first main input of C in the aquifer system will occur during the infiltration, when the water equilibrates with soil CO_2.
- In carbonated environment, the dissolution of calcite or dolomite provides an additional source of carbon to the groundwater system. Moreover, in open systems the calcite dissolution is enhanced by carbonic acid from soil CO_2 according to the reaction of equation Eq. 20: the higher p_{CO2} of the soil, the more effective is the dissolution of the calcite.

$$CO_{2(g)} + H_2O + CaCO_3 \leftrightarrow Ca^{2+} + 2HCO_3^- \quad K = 10^{-6.41} \qquad \text{[Eq. 20]}$$

$\delta^{13}C$ values of the main carbon reservoirs

Besides the knowledge of the reactions involved and the sources of carbon, it is necessary to define the $\delta^{13}C$ values of the various reservoirs. Four main carbon reservoirs can be distinguished (Fig. 3.12):

- The $\delta^{13}C$ content of **atmospheric CO_2** was about -6.4 ‰ (FRIEDLI et al. 1986), but it is now decreasing due to the burning of fossil fuels and reached values of -8.2 ‰ in 1992 (LEVIN et al. 1995).
- **Biogenic CO_2** results from photosynthesis processes. The amount of fractionation depends on the photosynthetic cycles:

  - The Calvin or C_3 cycle which concern 85 % of plant species. The $\delta^{13}C$ value of C_3 plants varies between -24 to -30 ‰ with an average value of about -27 ‰ (VOGEL 1993).

  - The Hatch-Slack or C_4 cycle plants represent less than 5% of all plant species. They represent for example tropical and temperate grasslands, sugar cane or corn are also typical C_4.plants. The $\delta^{13}C$ value of C_4 plants varies between -10 to -16 ‰ with an average value of about -12.5 ‰ (VOGEL 1993).

  - The CAM cycle plants combine the C_3 and C_4 photosynthesis. Therefore, the $\delta^{13}C$ values of CAM plants are intermediate and are close -17‰. These plants represent 10% of plant species and are mainly from desert ecosystems (e.g. cacti).
- **Mantelic CO_2** shows $\delta^{13}C$ values between -5 to -8 ‰ (CLARK & FRITZ 1997).
- **Marine carbonates** show $\delta^{13}C$ values between -2 to +2 ‰ (CLARK & FRITZ 1997).

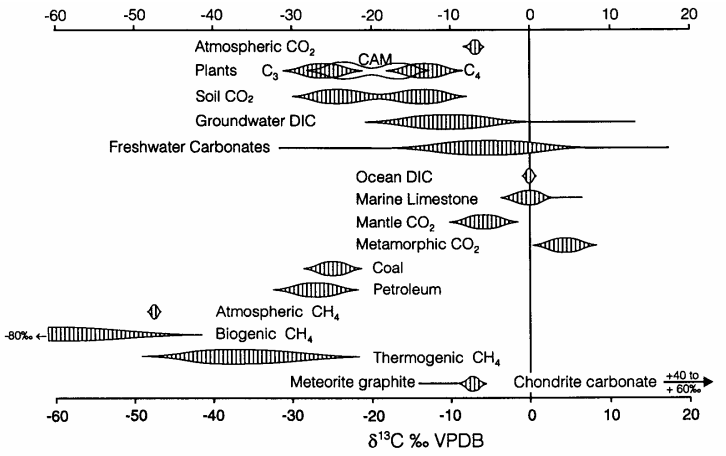

Fig. 3.12: Ranges for $\delta^{13}C$ values in selected natural compounds (CLARK & FRITZ 1997).

The fractionation of ^{13}C

^{13}C measured in groundwater corresponds to the ^{13}C of the dissolved inorganic carbon (DIC) (Eq. 18). Fractionation of the ^{13}C in groundwater occurs between the carbonate species (Eq. 19) according to the fractionation factors given in the Table 3.6.

Tab. 3.6: ^{13}C fractionation in the system $CO_{2(aq)}$-$CO_{2(g)}$-HCO_3^--CO_3^{2-}-$CaCO_3$.

T°C	$\varepsilon^{13}C_{CO2(aq)/CO2(g)}$	$\varepsilon^{13}C_{HCO3/CO2(g)}$	$\varepsilon^{13}C_{CO3/CO2(g)}$	$\varepsilon^{13}C_{CaCO3/CO2}$	$\varepsilon^{13}C_{CaCO3/HCO3}$
10	-1.1	9.6	9.2	12.7	3.0
20	-1.1	8.5	8.1	11.1	2.6
25	-1.1	7.9	7.6	10.4	2.4

Figure 3.13 shows the schematic of fractionation of ^{13}C during equilibrium exchange of carbon between CO_2, DIC and calcite. It should be noticed that in this theoretical example, the carbon of the precipitated calcite ($\delta^{13}C_{calcite}$= -14.6 ‰) comes only from the soil CO_2 ($\delta^{13}C$= -23 ‰). But it is remained that marine carbonates has $\delta^{13}C_{calcite}$ close 0 ‰. In the case of the example, the processes of dissolution of calcite will increase the $\delta^{13}C_{DIC}$ of the groundwater. But the rate of this enrichment will depend of the openness of the system.

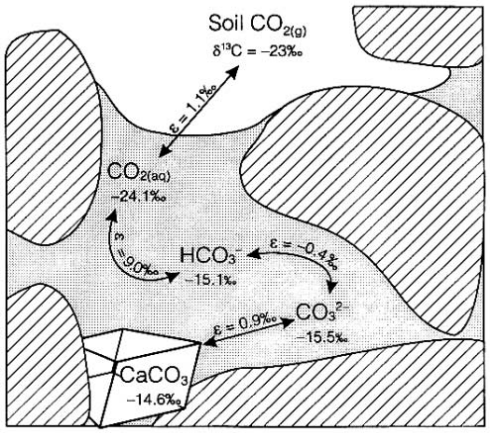

Fig. 3.13: Schematic fractionation of $\delta^{13}C$ during equilibrium exchange of carbon between CO_2, DIC and calcite at 25°C and under geochemical equilibrium and calcite saturation (CLARK & FRITZ 1997).
Radioactive Isotopes

3.3.2 Radioactive isotopes

Regarding the groundwater availability of an aquifer system, the renewal capacity of the groundwater is an important factor. Therefore, radioactive isotopes such as Tritium and Carbon-14 are used to define the "groundwater mean residence time" of an aquifer which is defined as the time elapsed since the water parcel had its last contact with the atmosphere. Tritium as a part of the water molecule can "date" the modern water showing a recharge of few decades (CLARK & FRITZ 1997). With the carbon-14 activity measured on the dissolved carbon of water, it is possible to "date" old groundwater from several hundred years to a maximum of 30 000 years (FONTES 1985).

3.3.2.1 Equation of radioactive decay

Each radioactive nuclide has its specific degree of instability which is expressed by the half-life assigned to this nuclide. The law of radioactive decay is derived by statistical processes. The probability of decay per nucleus per unit of time (λ = *decay constant*) is expressed as (MOOK 2000):

$$\lambda = \frac{\left(-dN/dt\right)}{N} \qquad \text{[Eq. 21]}$$

N = number of radioactive nuclei

The "radioactivity" (A) is defined as the number of disintegrations per unit of time:

$$A = -dN/dt = \lambda N \qquad \text{[Eq. 22]}$$

Integration assuming $N = N_0$ or $A = A_0$ at $t = 0$ results in:

$$N = N_0 \cdot e^{-\lambda t} \quad \text{or} \quad A = A_0 \cdot e^{-\lambda t} \qquad \text{[Eq. 23]}$$

Then the age (T) of the material is:

$$T = \left(\frac{-1}{\lambda}\right) \cdot \ln\left(\frac{A}{A_0}\right) \qquad \text{[Eq. 24]}$$

The time in which half of the nuclei have desintegrated ($T_{1/2}$ = half-life) is:

$$T_{1/2} = \left(\frac{-1}{\lambda}\right) \cdot \ln\left(\frac{1}{2}\right) \qquad \text{[Eq. 25]}$$

3.3.2.2 Tritium

The radioactive hydrogen isotope tritium has a half-life ($T_{1/2}$) of 12.32 years. The tritium (^3H) values are given in Tritium Units (TU) where 1 TU corresponds to 1 atom of tritium per 10^{18} hydrogen atoms. The precision of measurement is generally: $\sigma(^3H)$ = +/- 0.7 TU.

The tritium is produced naturally by cosmic radiation on nitrogen molecules and its natural level in precipitation is a few TU. But due to the atmospheric nuclear weapons tests between 1951 and 1980 the level of tritium in precipitation increased showing a peak of 2000 TU in 1963/64 (Fig. 3.14). Then after the atom bomb moratorium, tritium has been greatly attenuated by the buffer effect of oceans and nowadays its concentration is close to the natural atmospheric production.

The IAEA established a global network of about 125 stations throughout the world to collect precipitation for isotope analysis providing reliable input curves (www.iaea.org/ programs/ri/gnip/gnipmain.htm). With this input function and taking into consideration the decay equation (Eq. 24), it is possible to determine the mean residence time using a lumped parameter approach (see Paragraph 3.4.1).

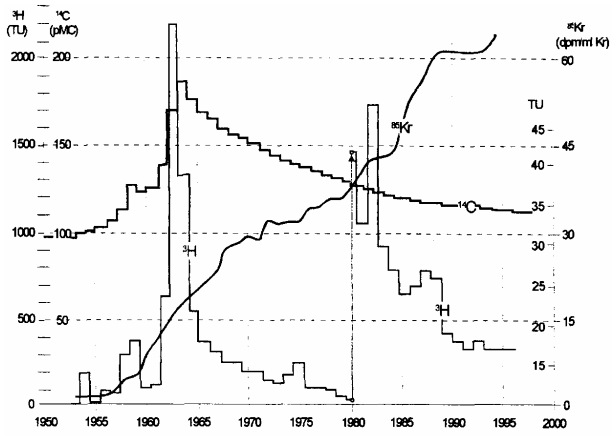

Fig. 3.14: Imput curves of the radioactive tracers (^{14}C, ^3H) from nuclear weapon tests with a peak injection at 1963/64 and from the continuous emissions of the nuclear industry (^{85}Kr) (GEYH 2000).

3.3.2.3 Carbon-14

Half life, standard and measurement

^{14}C is a radioactive isotope of carbon with a half life ($T_{1/2}$) of 5,730 years. The ^{14}C is calibrated against an NBS (National Bureau of Standards) oxalic acid standard. The radiocarbon dating reference is 95% of the activity of the NBS oxalic acid in 1950. The factor of 0.95 adjusts the oxalic acid to the activity of pre-industrial wood (from 1840 to 1860). For groundwater studies,

the activity of ^{14}C ($a^{14}C$) is given in pmc (percent modern carbon) which depends on this reference. The measurement precision is +/- 0.3 pmC on dissolved inorganic carbon convert to C_6H_6 (LSC) (CLARK & FRITZ 1997).

Origin of the atmospheric ^{14}C

^{14}C is naturally produced in the upper atmosphere due to the collision between high-speed particles of cosmic rays and atmospheric gases. Once oxidized to carbon dioxide, ^{14}C is dissolved in the ocean or it is used by the vegetation during photosynthesis processes. In the past, the production of ^{14}C in the atmosphere knew great natural variations (at least between 97 pmC and 140 pmC) due to the changing of the Earth's geomagnetic field (Fig. 3.15) (CLARK & FRITZ 1997). Moreover, some anthropogenic effects on the variation of the ^{14}C in atmosphere were also observed. While the use of fossil fuel free of active ^{14}C decreases the ^{14}C activity in the atmosphere by a dilution effect, the atmospheric nuclear weapons tests strongly increased it (Fig. 3.14).

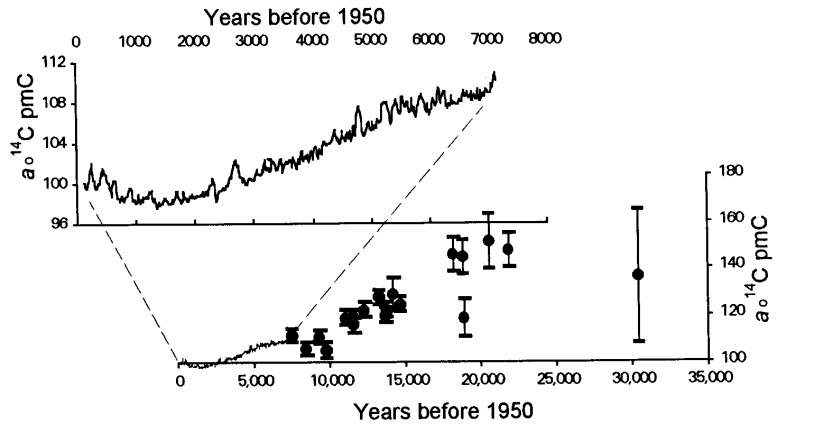

Fig. 3.15: Composite of atmospheric ^{14}C activity from tree rings using the dendrochronological method and U/Th ages of marine corals. Due to the Earth's geomagnetic field change a strong decreasing occurred from ca. 30,000 years to present (CLARK & FRITZ 1997).

Groundwater ^{14}C, soil CO_2 and calcite dissolution

The mechanisms, which are responsible for the incorporation of the atmospheric ^{14}C into the groundwater, are the same as for ^{13}C (Paragraph 3.3.1.8). Two main processes have to be taken into account (Fig. 3.16):

- After incorporation of the atmospheric ^{14}C into the vegetation by photosynthesis and later release in the soil by decay and root respiration, equilibrium occurs between the soil CO_2 and the infiltrated water from precipitation which will recharge the aquifer. For recent soil the ^{14}C activity of the CO_2 is about 100 pmC (CLARK & FRITZ 1997).
- The processes of dissolution and precipitation of carbonates. Dissolution can occur in an open system (in contact with the soil CO_2) or in closed system. The marine carbonates have ^{14}C activities equal to 0 pmC.

The processes of dissolution of carbonates (Eq. 20) will input "dead carbon" (0 pmc) into the DIC of groundwater. Then, due to a dilution effect, the apparent ^{14}C groundwater ages will appear older than in reality. Under closed system conditions and according to the Eq. 20 with $a_{0soilCO2}$ = 100 pmc and a_{0CaCO3} = 0 pmc, the calcite dissolution will imply a dilution about 50 % of the initial ^{14}C. Under open system, the $a_0{}^{14}C_{DIC}$ stays close 100 pmc due to the constant exchange between the DIC and the soil CO_2.

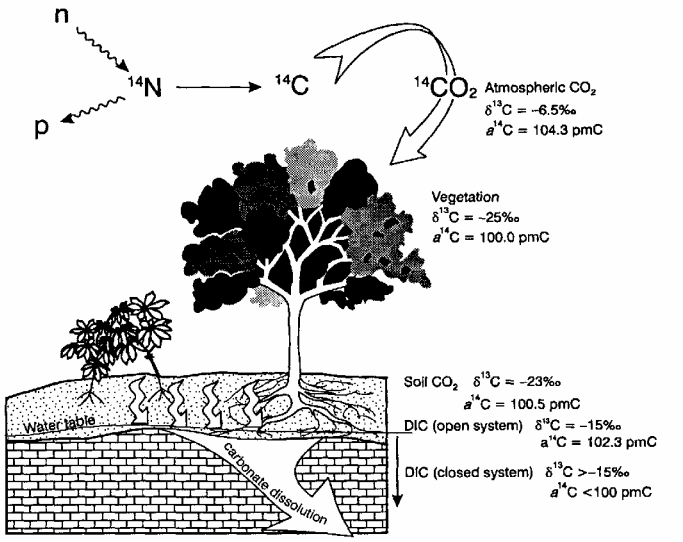

Fig. 3.16: The pathway and associated fractionation of ^{14}C and ^{13}C in CO_2 during photosynthesis, respiration in soils, and dissolution by groundwater (CLARK & FRITZ 1997).

Models of correction

The dilution of ^{14}C through calcite dissolution will lead to an error in the age calculation. To correct this "apparent ^{14}C water ages" a "dilution factor" (q) is introduced which allows the estimation of $a^{14}C$ of the recharge area ($a^{14}C_{rech}$) (CLARK & FRITZ 1997):

$$a^{14}C_{rech} = q \cdot a_0{}^{14}C \qquad \text{[Eq. 26]}$$

VOGEL (1970) reports "characteristic" q values:

- 0.65 to 0.75 for karst system.
- 0.75 to 0.90 for sediment with fine-grained carbonate such as loess.
- 0.90 to 1.00 for crystalline rocks

Several models of correction can be found in the literature (FONTES et.al. 1992, CLARK & FRITZ 1997, OLIVE 1999, HUNEAU 2000):

- The model of Tamers based on chemical balance (for pH close to 7) (*after* HUNEAU 2000):

$$a^{14}C_{rech(Tamers)} = \frac{\left(H_2CO_3 + \tfrac{1}{2}HCO_3\right) \cdot a^{14}C_{soil} + \tfrac{1}{2}HCO_3 \cdot a^{14}C_{carb}}{\left(H_2CO_3 + HCO_3^-\right)} \qquad \text{[Eq. 27]}$$

- The model of Pearson based on isotopic balance ($\delta^{13}C$) (*after* HUNEAU 2000):

$$a^{14}C_{rech(Pearson)} = \left[\frac{\left(a^{14}C_{soil} - a^{14}C_{carb}\right)\left(\delta^{13}C_{DIC} - \delta^{13}C_{carb}\right)}{\left(\delta^{13}C_{DIC} - \delta^{13}C_{carb}\right)}\right] + a^{14}C_{carb} \qquad \text{[Eq. 28]}$$

Both models assume that carbonate dissolution occur under closed system conditions and neglect the isotopic exchange between $CO_{2\ soil}$ and DIC-Carbonates. The computed values of $a^{14}C_{rech}$ with these models are low.

- The model of MOOK based on isotopic exchange (*after* HUNEAU 2000):
  This model takes into account the isotopic exchange between $CO_{2\ soil}$ and DIC-Carbonates by including a correction factor (k_{Mook}) to the model of Tamers:

$$a^{14}C_{rech(Mook)} = a^{14}C_{rech(Tamers)} + k_{Mook} \quad \text{[Eq. 29]}$$

$$k_{Mook} = \frac{\frac{1}{2}\left[\left(a^{14}C_{soil} - a^{14}C_{carb}\right)\left((A+B)\cdot\delta^{13}C_{DIC} - \left(a+\frac{1}{2}B\right)\cdot\delta^{13}C_{soil} - \frac{1}{2}B\delta^{13}C_{carb}\right)\right]}{\left[\frac{1}{2}\cdot\left(\delta^{13}C_{soil} - \delta^{13}C_{carb}\right) - \varepsilon_{co_2/HCO_3^-}\right]\cdot(A+B)} \quad \text{[Eq. 30]}$$

  with $A = H_2CO_3$ and $B = HCO_3^-$ in mol/l

- The IAEA model based on isotopic exchange (SALEM et al. 1980): [Eq. 31]

$$a^{14}C_{rech(IAEA)} = \frac{\left(\delta^{13}C_{DIC} - \delta^{13}C_{carb}\right)\left(a^{14}C_{soil} - a^{14}C_{carb}\right) + \left(\delta^{13}C_{soil} - \varepsilon_{CO_2/HCO_3^-} - \delta^{13}C_{carb}\right)\cdot a^{14}C_{carb}}{\left(\delta^{13}C_{soil} - \varepsilon_{CO_2/HCO_3^-} - \delta^{13}C_{carb}\right)}$$

  This model considers that in first the bicarbonate and soil CO_2 are in equilibrium and then the dissolution of the carbonates occur.

- The Fontes-Garnier model based on matrix exchange (FONTES & GARNIER 1979 in CLARK & FRITZ 1997):
  This model calculates a "dilution factor" ($q_{F\text{-}G}$) based on concentrations in mol/l by correcting the measured DIC (DIC_{meas}) with both the DIC, which has exchanged with soil CO_2 in an open system ($DIC_{CO2exch}$) as well as the DIC which has exchanged with the carbonate matrix (DIC_{carb}):

$$q_{F-G} = \frac{DIC_{meas} - DIC_{carb} + DIC_{co_2\ exch}}{DIC_{meas}} \quad \text{[Eq. 32]}$$

  Calculation of DIC_{carb} takes into account the dissolution based on Ca and Mg with a correction for evaporite dissolution and cation exchanges:

$$DIC_{carb} = Ca^{2+} + Mg^{2+} - SO_4^{2-} + \frac{1}{2}\left(Na^+ + K^+ + Cl^-\right) \quad \text{[Eq. 33]}$$

  The $DIC_{CO2exch}$ is calculated from the following mass-balance:

$$DIC_{CO_2\ exch} = \frac{\delta^{13}C_{meas}\cdot DIC_{meas} - \delta^{13}C_{meas}\cdot DIC_{carb} - \delta^{13}C_{soil}\left(DIC_{meas} - DIC_{carb}\right)}{\delta^{13}C_{soil} - \varepsilon^{13}C_{co_2/CaCO_3} - \delta^{13}C_{carb}} \quad \text{Eq. 34]}$$

3.4 Modelling

Various approaches of modelling were used:

- A lumped-parameter model based on a linear systems approach (transfer-function type) (*BoxmodelV3*) is applied to estimate the groundwater age from tritium data.
- A three-dimensional finite-difference groundwater flow model (PMWIN5) is used to simulate the groundwater flow in the alluvial aquifer system of the Basin of Ouarzazate.

3.4.1 Groundwater dating using lumped-parameter approach

A Black Box Model approach can be use for the interpretation of environmental tracer data such as ^3H to estimate the groundwater residence time (ZUBER 1986, MALOSZEWSKI & ZUBER 1993, ZUBER & MALOSZEWSKI 2000). The lumped-parameter approach considers that the system is

linear and the flow system is constant (steady state). For a given tracer input function $c_{in}(t)$, the Black Box Model calculates the convoluted theoretical output $c_{out}(t)$ depending on (KINZELBACH et al. 2002):

- A "transfer function" f(t,t'), which has to be defined for the various model types (Piston Flow-, Exponential- or Dispersion Model) (Fig. 3.17).
- The main fitting parameters of this particular "transfer function" are the mean transit time (τ) and the dispersion parameter (Pd).

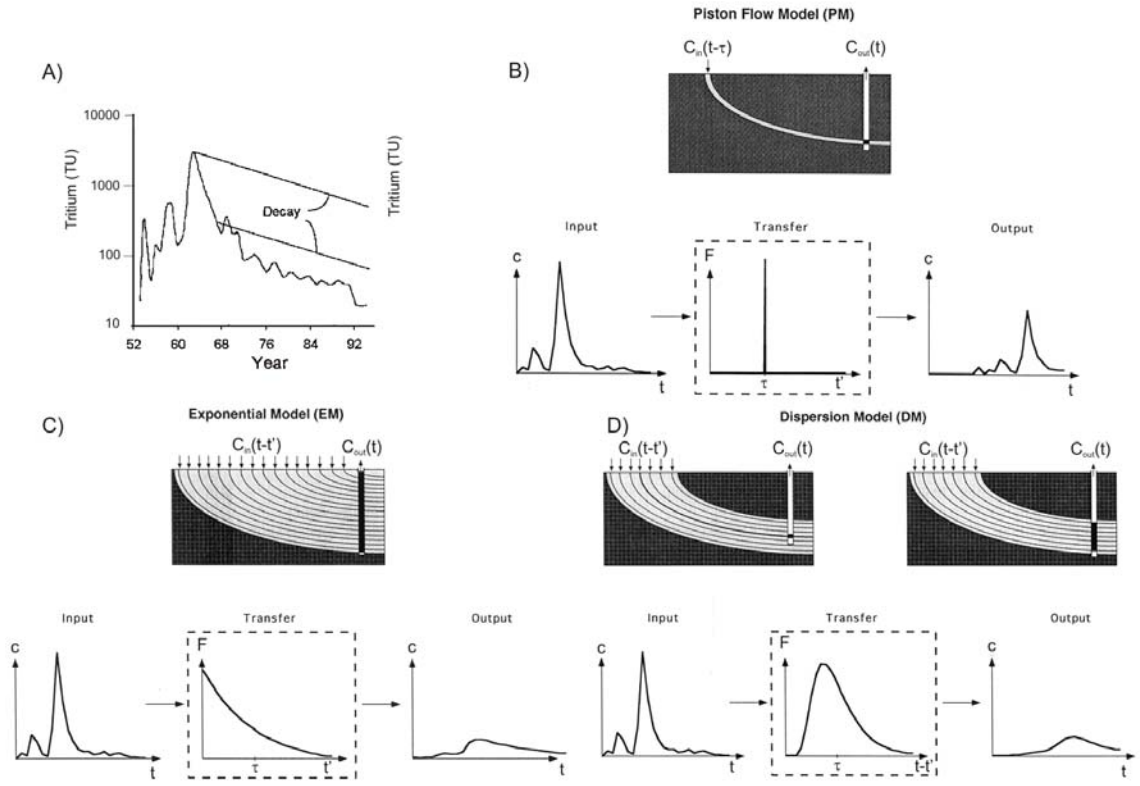

Fig. 3.17: (A) Decay of tritium from given inputs from precipitation (semi-log plots) (CLARK & FRITZ 1997); Piston flow model (B), Exponential model (C) and Dispersion model (D) with corresponding transfer functions. The output concentration is additionally influenced by radioactive decay (KINZELBACH et al. 2002).

The relation between the variable input $c_{in}(t')$ and output $c_{out}(t)$ is:

$$C_{out(t)} = \int_0^{\infty} C_{in(\tau)} \cdot e^{-\lambda t'} \cdot f(t') \cdot dt' \qquad \text{[Eq. 35]}$$

where t' is the time of entry, τ the transit time ($\tau = t - t'$), f(t') the transfer function and λ the decay constant.

The Piston Flow Model (PFM) is based on the idea**,** that the flow lines have the same transit time, and that hydrodynamic dispersion and diffusion are negligible. The output concentration is equal to the input concentration and change only by radioactive decay (Fig. 3.17-A and B).

$$C_{out(t)} = C_{in(t-\tau)} \cdot e^{-\lambda\tau} \qquad \text{[Eq. 36]}$$

In the Exponential Model (EM), the flow lines are assumed to have an exponential distribution of transit times (ZUBER & MALOSZEWSKI 2000) with the shortest line having the theoretical transit time equal to zero (Fig. 3.17-C). There is no exchange between the flow lines. The "response function" is:

$$f(t') = \frac{1}{\tau} \cdot e^{\left(\frac{-t'}{\tau}\right)} \qquad \text{[Eq. 37]}$$

In the Dispersion Model (DM), the dispersion effect is considered (Fig. 3.17-D). The dispersion equation is for a semi-infinite medium and concerns an uni-dimensional solution. The "response function" is given according to the "apparent dispersion parameter" P_D:

$$f(t') = \left(4\pi P_D \frac{t'}{\tau}\right)^{-1/2} \cdot \frac{1}{t'} \cdot e^{\left(\frac{-\left(1-\frac{t'}{t}\right)^2}{\frac{4P_D t'}{\tau}}\right)} \qquad \text{[Eq. 38]}$$

The higher the P_D values are, the wider and more asymmetrical is the distribution of the travel times.

3.4.2 The three-dimensional finite-difference groundwater flow model PMWIN5

3.4.2.1 Overview

The U.S. Geological Survey developed a modular three dimensional groundwater flow simulation program (Modflow PWIN 5) that uses the finite-difference approximation: MCDONALD & HARBAUGH (1988a and 1988b), KINZELBACH & RAUSCH (1995), CHIANG et al. (1998) and CHIANG & KINZELBACH (2000).

The aquifer system is discretized with a mesh of blocks called cells (Fig. 3.18). The model may be visualized in terms of a three dimensional assemblage of cells in which the hydraulic properties, such as hydraulic conductivity and storage coefficient are defined. The center of each cell correspond to a "node" at which head is calculated. The size of the model array is specified by the user in terms of the number of rows (i), columns (y) and number of layers (k). The three-dimensional array of cells has the form of a rectangular box. This model program simulates steady and unsteady flow in a system. Hydraulic conductivities or transmissivities for any layer may differ spatially and the storage coefficient may be heterogeneous. Flow from external stresses, such as flow to wells, recharge, evapotranspiration, flow to drains, and flow through river beds, can be simulated.

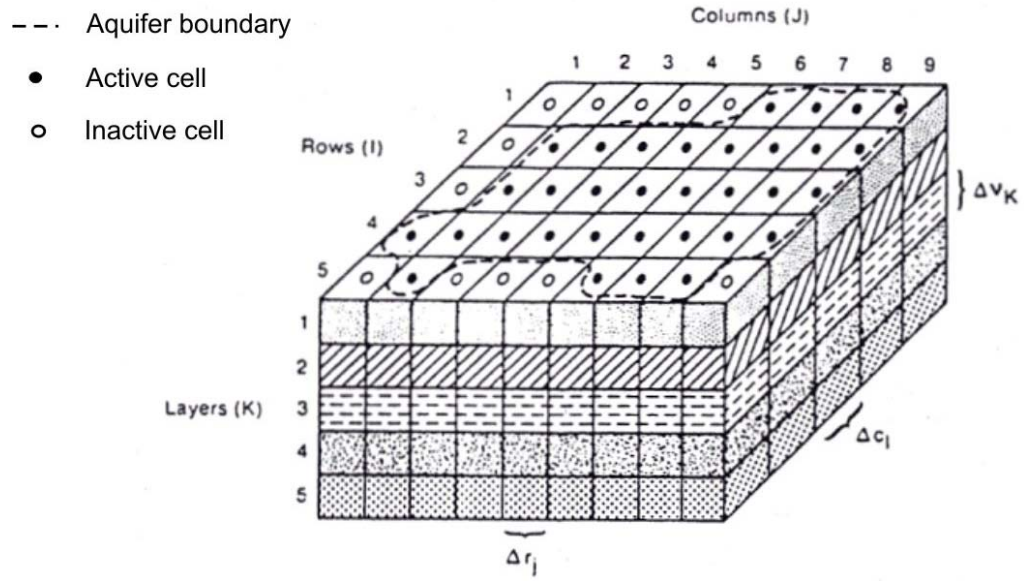

Fig. 3.18: A discretized hypothetical aquifer system (MCDONALD & HARBAUGH 1988b).

3.4.2.2 Equations considered in the model program

The theory about the numerical equations and their embedding into the model framework are not repeated in this chapter. Only a short introduction of the main equations considered in the model program is presented. The numerical equations are derived from the partial-differential equation, the continuity equation and the Darcy's law.

- The **partial-differential equation** (MCDONALD & HARBAUGH, 1988b) describes the three dimensional movement of groundwater through porous material:

$$\frac{\partial}{\partial x}\left(K_{xx}\frac{\partial h}{\partial x}\right)+\frac{\partial}{\partial y}\left(K_{yy}\frac{\partial h}{\partial y}\right)+\frac{\partial}{\partial z}\left(K_{zz}\frac{\partial h}{\partial z}\right)-W=S_s\frac{\partial h}{\partial t} \qquad \text{[Eq. 39]}$$

  where:

  K_{xx}, K_{yy} and K_{zz} are values of hydraulic conductivity along x, y and z coordinate axes, which are assumed to be parallel to the major axes of hydraulic conductivity (L/t); h is the potentiometric head (L); W is a volumetric flux per unit volume and represents sources and/or sinks of water (1/t); S_S is the specific storage of the porous material (1/L); and T is time (t).

  Equation 39 describes groundwater flow under nonequilibrium conditions in a heterogeneous and anisotropic medium taking into account the flow and/or head conditions at the boundaries and the initial head conditions of the aquifer system (MCDONALD & HARBAUGH 1988b). A time-varying head distribution characterizes the flow system, considering both the energy of flow and the volume of water in storage. Directions and rates of water movement can be then calculated.

- The **continuity equation** expresses the balance of flow for a cell which implies that the sum of all flows into and out of the cell must be equal to the rate of change in storage within the cell (MCDONALD & HARBAUGH 1988b):

$$\sum Q_i = S_S \cdot \frac{\Delta h}{\Delta t} \cdot V \qquad \text{[Eq. 40]}$$

  where:

  Q_i is a flow rate into or out to the cell (L^3t^{-1}); S_S is the specific storage and represents the volume of water which can be injected per unit volume of aquifer material per unit change in head (L^{-1}); V is the volume of the cell (L^3); and Δh is the change in head over the time interval of length Δt.

- The **Darcy's law** describes one-dimensional steady state flow occurring in a volume of porous material. Figure 3.19 shows two cells (cell i,j,k and cell i, j -1,k) where a flow ($q_{i, j -1/2, k}$) occurs into cell i,j,k in the row direction from cell i, j -1. From the Darcy's law the flow $q_{i, j-1/2, k}$ is defined as (after MCDONALD & HARBAUGH 1988b):

$$q_{i,j-1/2,k} = K_{i,j-1/2,k} \cdot A \cdot \frac{h_{i,j-1,k} - h_{i,j,k}}{D} \qquad \text{[Eq. 41]}$$

  Where:

  $q_{i, j-1/2, k}$ is the volumetric fluid discharge through the face between cells i, j, k and i, j -1, k (L^3t^{-1}); $K_{i, j - 1/2, k}$ is the hydraulic conductivity along the row between nodes i, j, k and i, j -1, k (Lt^{-1}); A is the area of the cell faces normal to the row direction (L^2); $h_{i, j, k}$ and $h_{i, j-1, k}$ are the heads at nodes i, j, k and i, j -1, k (L); and D is the distance between nodes i, j, k and I, j -1, k (L).

The flows from adjacent cells through each face of the cell are also expressed by the equation 41.

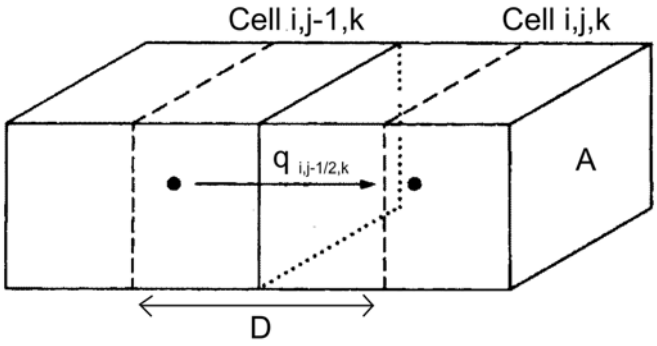

Fig. 3.19: Flow into cell i, j, k from cell i, j-1, k (after McDONALD & HARBAUGH 1988b).

To account for flows into cell from features or processes external to the aquifer, such as steams, drains, recharge, evapotranspiration or wells, additional terms are used which are dependent or not on the head. The details of these additional terms are not developed here.

3.4.2.3 Conception of a model

The spatial discretization of the model domain should be based on a conceptual model of the groundwater system. In first, the user need to generate the mesh of cell which will reflects the geometry of the aquifer. The mesh size (number of rows and columns and size of cells) and the number of layers have to be specified as well as the type (unconfined, confined, or partially/fully convertible between confined and unconfined) and the geometry of layers (elevation of the top and bottom). In order to simulate conditions along various hydraulic boundaries, the user can choose two types of cells: “constant head” cells and “inactive” (or no flow) cells. In constant-head cells, the head is specified in advance and stay constant during the simulation (in steady or unsteady states). In the “inactive” cells no flow are simulated.

For the groundwater flow modelling, input of spatial and temporal parameters is required for the simulation such as: the time, the initial hydraulic head, the horizontal and vertical conductivity.

Various codes called packages are integrated in MODFLOW PMWIN in order to simulate the effects of evapotranspiration, recharge, rivers and wells (CHIANG & KINZELBACH 2000):

- Evapotranspiration package: The evapotranspiration (ET) package simulates the effects of plant transpiration and direct evaporation in removing water from the saturated zone. The maximum ET rate (LT^{-1} per unit surface area), the elevation of the ET surface (L) and the ET extinction depth (L) have to be specified.
- Recharge package: The recharge package simulates the distributed recharge to the groundwater system. The recharge flux (LT^{-1} per unit surface area) has to be specified.
- River package: The River package simulates the flow between an aquifer and a river (or a lake). Head in the river (L), elevation of the bottom of the riverbed (L) and the hydraulic conductance of the riverbed (C_{RIV}) (L^2T^{-1}) have to be specified. The conductance (C_{RIV}) is generally defined as (CHIANG & KINZELBACH 2000):

$$C_{RIV} = \frac{K \cdot L \cdot W}{M} \quad \text{[Eq. 42]}$$

Where K is the hydraulic conductivity of the riverbed material, L the length of the river within a cell, W the width of the river and M is the thickness of the riverded.

- Well package: The well package simulates an injection or a pumping well. The recharge rate of the well has to be specified.

3.4.2.4 The water budget calculator

The model program calculates a water budget for the whole model as a check on the acceptability of the solution, and in order to provide summarized information on the flow system. Flow to or from rivers, constant head cells or wells are all included in the overall budget terms. Calculations of flow terms for various subregions are possible.

3.4.2.5 Calibration, validation and sensitivity analysis

In steady state, parameters have to be adjusted in order to reach a water budget over the whole catchment close to zero. The water budget calculator can be use for this purpose. The results of the steady state will be used as the initial conditions for an unsteady state model. A calibration phase has to be done in unsteady state in order to make the model match real-world data. It involves making several model runs, varying parameters until the ‘best fit’ is achieved. A validation should be done in order to confirm the validity of the calibration by using the model to fit an independent set of data.

To ensure the best model, the accuracy of the most sensitive parameters needs to be checked. Sensitive parameters are defined after the Sensitivity Analysis which is the process of changing parameters to see the effects on the model results.

4 GEOLOGY OF THE DRÂA CATCHMENT

4.1 Introduction

In order to define the various aquifer systems, it is important to acquire a precise knowledge of the geology including the lithology and the structural pattern. Therefore, this chapter attempt to synthesize the current geological knowledge of the Upper and Middle Drâa catchment. In a first step, a geological overview of each main geological domain of the catchment is given including the geological history and the important paleogeographical aspects. Then, the precise litho-stratigraphic and tectonic descriptions are presented.

4.2 General Features

The Upper and Middle Drâa catchment is characterised by three main geological units formed during different orogenic events (compare Fig. 2.11): the Precambrian Anti Atlas with its Paleozoic cover, the Atlasic domain with Mesozoic depositions that was mainly deformed during the Cenozoic, and the Basin of Ouarzazate in which sedimentation and structure strongly depend on the alpine orogenese.

4.2.1 The Anti Atlas

The Anti-Atlas exposes Precambrian through Paleozoic age rocks of the West African Craton in a vast anticline of ENE-WSW axis plunging eastward, which extends from the mouth of the Drâa to Tafilalt (PIQUÉ 2001) (Fig. 4.1). The Precambrian crystalline terrains crop out in inliers along its axis (Lower Drâa (fig. 4.1 Bas Drâa), Ifni, Kerdous, Igherm, Siroua, Bou-Azzer, Saghro). The Late Proterozoic rocks were affected by the Pan-African orogeny, which occurred between 680 and 570 Ma (PIQUÉ et al. 1993). The Paleozoic terrains were part of Paleozoic Gondwana and spread out broadly on the southern flanks of the Anti Atlas anticlinorium.

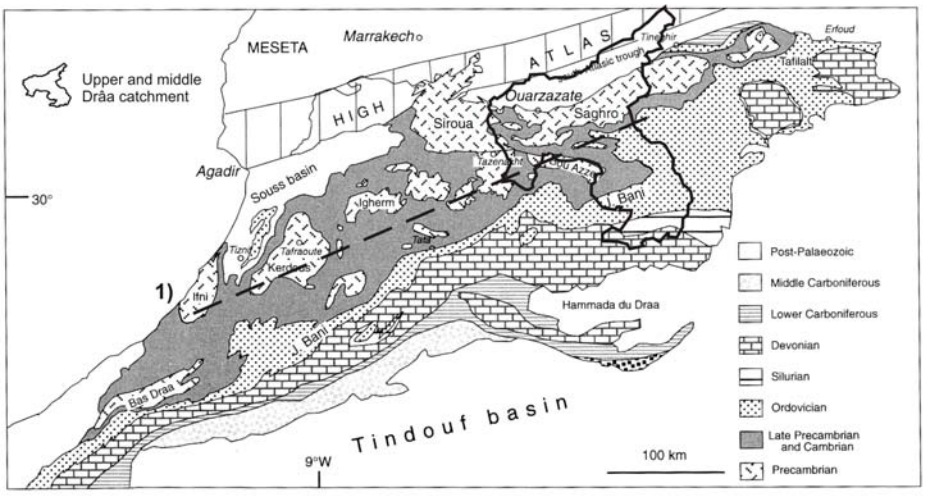

Fig. 4.1: Simplified geological map of the Anti Atlas (PIQUÉ 2001); 1): profile of the Cambrian in Fig. 4.9.

4.2.2 The High Atlas

The High Atlas range is an intracratonic belt extending from the Moroccan West coast to eastern Tunisia (Fig. 4.2-A). The geological history of the Central High Atlas is synthesized by WARME (1988) in Table 4.1. The High Atlas Mountains were formed by the reactivation of a major intracontinental rift system which was associated with the opening of both the Atlantic Ocean and the Thethyan Ocean (STETS & WURSTER 1977, MATTAUER et al. 1977, LAVILLE & PETIT 1984, BREDE et al. 1992, STETS 1992, PIQUÉ 2001) (Fig. 4.2-B).

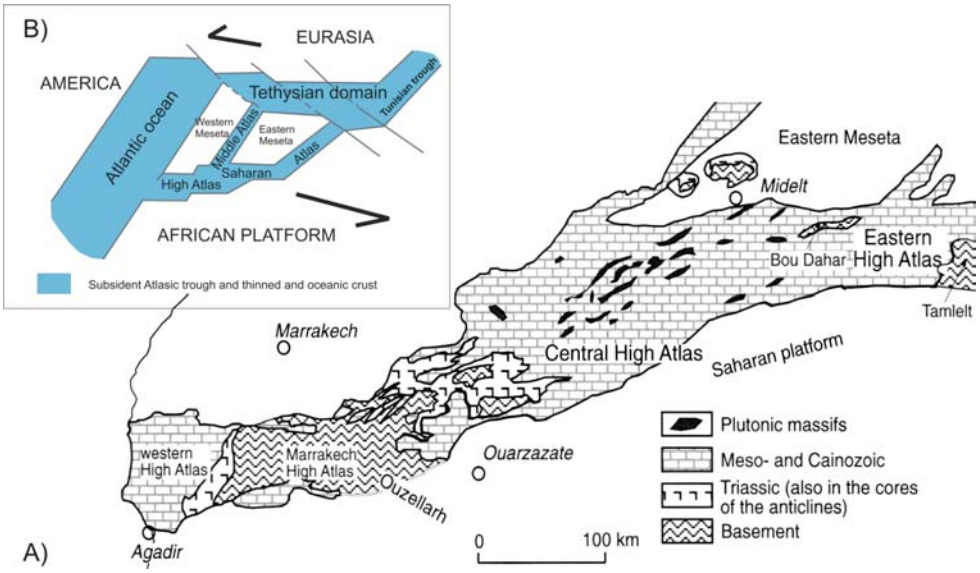

Fig. 4.2: A) The High Atlas (PIQUÉ 2001); B) The northern margin of Africa during the Jurassic (after PIQUÉ 2001).

During the Trias the Pangea was broken-up forming the Atlas rift system of transtensional type (STETS & WURSTER 1981, BEAUCHAMP 1988, LAVILLE 1988, LAVILLE & PIQUÉ 1991). This rift system evolved along weaknesses of the Panafrican substratum and Paleozoic rocks (STETS 1992). The Triassic sediments were deposited in a horst and graben environment where fault systems guided the subsidence of ENE-WSW basins (Fig. 4.3.A). The basins were filled with detritic continental red beds and evaporitic sediments, locally overlain by thoelitic basalt floods (MANSPEIZER et al. 1978, BEAUCHAMP 1988).

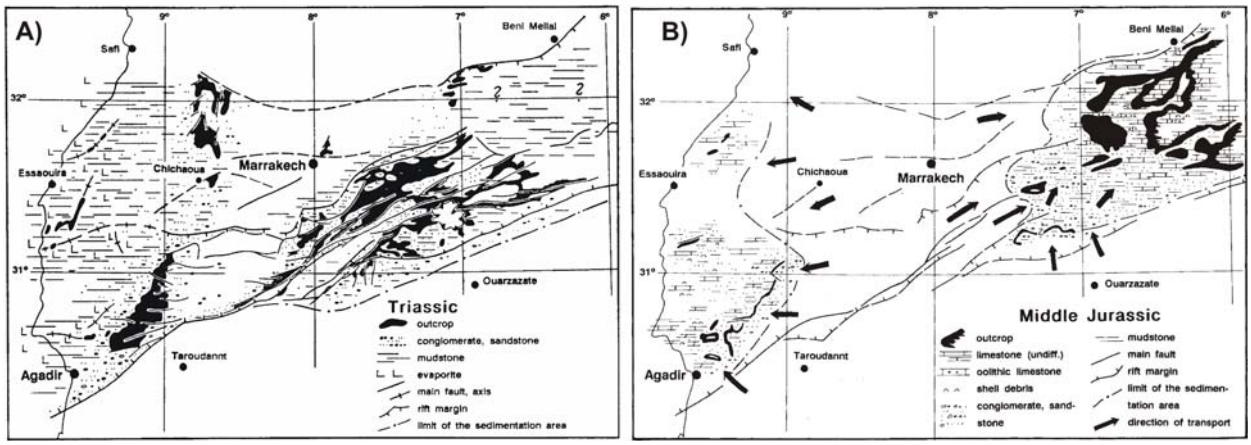

Fig. 4.3: Paleogeographic map of the Trias (A) and Middle Jurassic (B) in the Western High Atlas belt (STETS 1992).

The Atlasic rift system showed very active deposition through the Early-Middle Jurassic (MICHARD 1976, MANSPEIZER et al. 1978, du DRESNAY 1979, LAVILLE 1988, WARME 1988). The Jurassic sediments rocks deposited mainly within the boundaries of the present High Atlas Mountains (Fig. 4.3-B). The very active subsidence explains the complex facies distributions of the Jurassic sediments (Fig. 4.4). The Lower and Middle Lias are characterized by massif tidal dolomites and limestones. At the Late Pliensbachian-Toarcian boundary, the shelf was dislocated and the trough reaches its maximum depth which explains the sedimentation of marls during Toarcian and Aalenian times (Tab. 4.1). In Bajocian the marls pass up into Limestones followed by a detrital succession of Bathonian-Callovian resulting of the build-up of a deltaic unit and the development of coastal lagoons and fluviatile system (PIQUÉ 2001) (Tab. 4.1).

Tab. 4.1: Geological history of Central and Eastern High Atlas (WARME 1988)

Age	Geologic events
Late Cenozoic	Uplift and erosion - High Atlas Mountains
Cenozoic	"Alpine" deformation – compression; faults rejuvenated and reversed along "en echelon" folds and up-thrusts
Late Mesozoic (Malm – Cretaceous)	Mild deformation, uplift, erosion; Cretaceous shallow marine deposits
Middle to late Dogger – Malm	Continental deposits; fluvial, floodplain
Middle Dogger (Late Bajocian – Bathonian)	Trough filled – end of carbonate deposition; "wet" rift filled
Early Dogger (Aalenian – Bajocian)	Subsidence greater than sedimentation, then equal to sedimentation, followed by less than sedimentation.
Late Lias (Toarcian)	Abrupt eustatic deepening; marls ubiquitous
Middle Lias (Sinemurian- Pliensbachian)	Subsidence generally greater than sedimentation – development of entire facies mosaic controlled by fault blocks, with deep- and shallow-marine deposits
Early Lias (Hettangian – Sinemurian)	Rifting continues; abrupt initiation of "wet" rift; stratified water column
Late Triassic – Early Liassic	"Dry" rift – fault-block mosaic with redbeds, evaporites and basalts
Permo-Triassic	Erosion and peneplanation
Permo-Carboniferous	Variscan Orogeny – mild metamorphism of sandstones and mudstones; late orogenic fault-troughs.

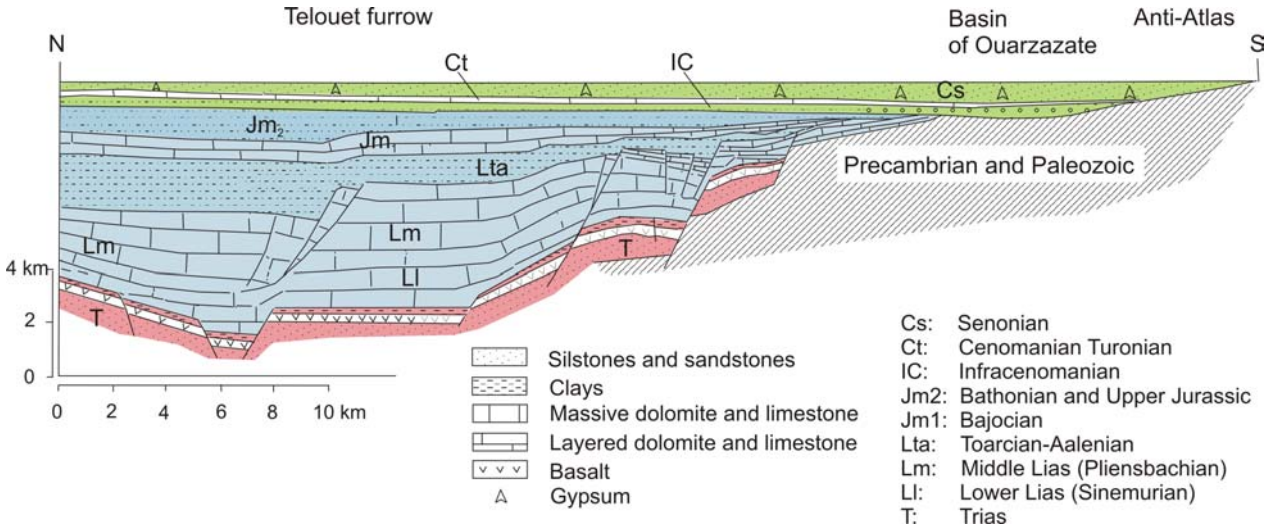

Fig. 4.4: Paleogeographic profile showing Jurassic and Cretaceous series in the southern range of the Atlas Gulf (modified after JOSSEN & FILALI 1988).

Due to the convergence of the African and Eurasian plates an inversion phase of the Atlas rift began in the Early Cretaceous and extended into the present (PIQUÉ 2001). The Cretaceous formation, which is weak in thickness, shows three types of facies: the sandstones and red marls of Lower Cretaceous (Infracenomanian which is similar in facies to Upper Jurassic), the Cenomano-Turonian limestones, and the red continental formation of Upper Cretaceous (Senonian). The major uplift phases of the High Atlas occurred between the Late Eocene and the lower Quaternary and correspond to the Alpine orogenic event (GÖRLER et al. 1988, EL HARFI et al. 1996, 2001). It is responsible for the uplift of the entire Atlas system and for the development of important thrust-related structures in the southern range of the High Atlas. After

BEAUCHAMP et al. (1999) the generalized stratigraphic section of the Central High Atlas can be distinguished in prerift-, synrift- and postrift-sediments (Fig. 4.5).

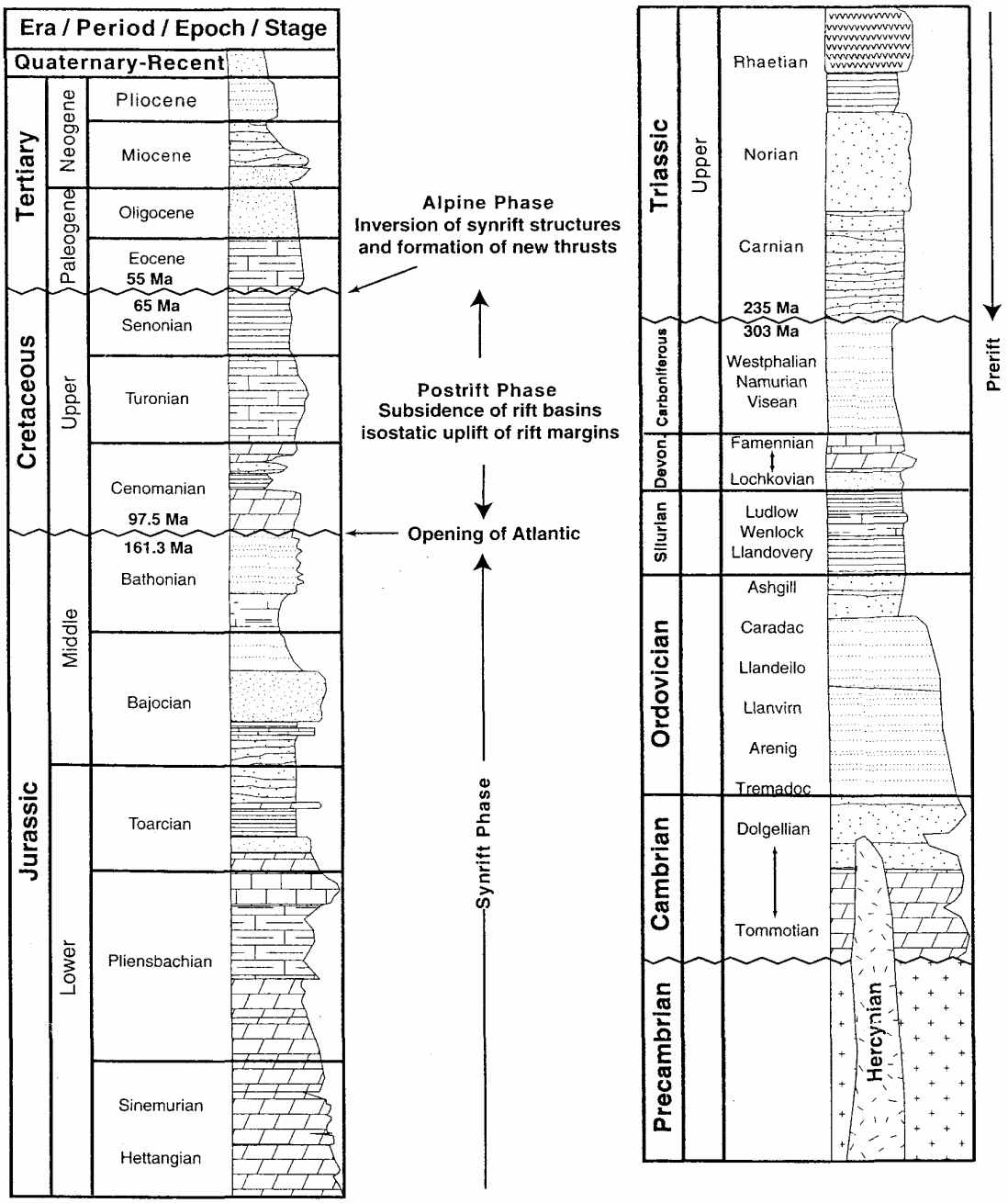

Fig. 4.5: Generalized stratigraphic section of the central High Atlas Mountains compiled from geological maps (BEAUCHAMP et al. 1999).

4.2.3 The Basin of Ouarzazate

The uplift of the High Atlas was limited in its southern margin by the presence of the stable Precambrian African basement. Consequently, the subsidence of the Basin of Ouarzazate began as a foreland basin which evolved with an axe parallel to the High Atlas chain. The basin is filled with mainly Cenozoic formations lying on the Paleozoic and Precambrian basement in an asymmetrical synclinorium form. The sedimentation of the basin is the result of a complex geological history between transgressions and orogenic events. Two major stratigraphic units can be distinguished corresponding to two distinct periods of sedimentation. The first period occurred from the Late Cretaceous to the Mid Eocene when a transgressive megacycle controlled by

eustatic sea-level changes deposited marine sediments in an epicontinal sea (Herbig 1986, TRAPPE 1991, BREDE et al. 1992) (Fig. 4.6). This stratigraphic unit is divided in various formations: the red Lower Cretaceous sandstone and siltstone, the Cenomanian-Turonian marine limestones and the Upper Cretaceous continental siltstone passing upward in lower and middle Eocene carbonates. The marine sediments from Paleocene to Middle Eocene are defined as the “Subatlas Marin Group” (TRAPPE 1991, HERBIG 1991, EL HARFI et al. 2001) (Fig. 4.7-A).

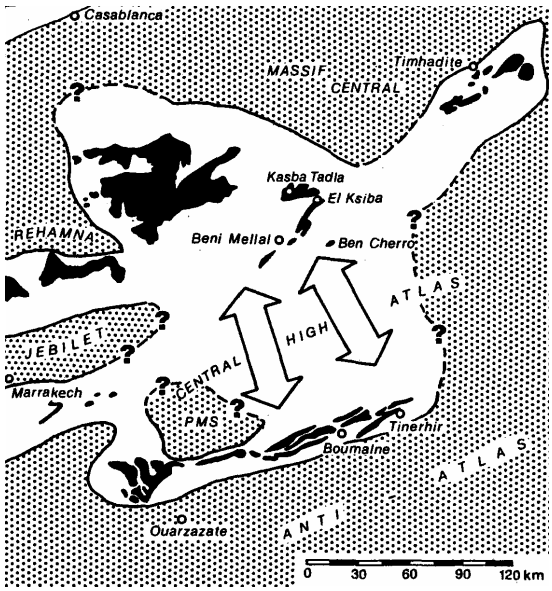

Fig. 4.6: Paleogeographic map of the paleogene epicontinental seas of middle and southern Maroc; PMS: Paleozoic Skoura Massif (HERBIG 1986).

The second period began after the regression of the sea at the end of Mid Eocene when the basin became a separated entity and was filled with thick continental series that were distinctly affected by the uplift of the Central High Atlas Mountains (GÖRLER & ZUCHT 1986, FRAISSINET et al. 1988, EL HARFI 2001). This stratigraphic unit which is more important in thickness is called the “Imerhane Continental Group” (Fig. 4.7-A) (GÖRLER & ZUCHT 1986, FRAISSINET et al. 1988, GÖRLER et al. 1988, EL HARFI 2001). The basin evolved from a margino-littoral environment composed of coastal sabkhas and fluviatile systems (Upper Eocene), to a palustro-lacustrine deposits in a context of alluvial fans and fluviatile environments (Mio-Pliocene), and ended with a vast conglomeratic pediment, forming the alluvial plain and the terraces (Quaternary) (EL HARFI et al. 2001) (Fig. 4.7). The syntectonic molasses of Oligocene to Pliocene ages overlay n discordance the fluviatile and coastal sediments of Upper Eocene. Sediment analyses in the Basin of Ouarzazate show two main stages of the High Atlas uplift (GÖRLER 1988, EL HARFI 1996, EL HARFI et al. 2001). The first occurred in the Late Eocene-Oligocene after the retreat of the sea. Then after a period of tectonic inactivity characterised by the widespread lake deposits of Miocene (Fig. 4.7), a second stage occurred in the Mid Pliocene.

Addional to the strong structural asymmetry which affected the Basin of Ouarzazate during its subsidence, strong vertical and lateral variations in facies of the Cenozoic sediments is noted due to the paleogeography (Fig. 4.7). Advance and retreat of alluvial fan systems are closely related to the tectonic movement of the uplift of High Atlas. A strong variation in thickness along a north-south profile is observed. While the Tertiary sedimentary filling is up to 1,200 m thick (GÖRLER et al. 1988) in the northern edge of the basin, the Paleogene and late Cretaceous age rocks onlap Paleozoic and Proterozoic rocks along the southern margin of the Ouarzazate Basin (Fig. 4.8). The Triassic and Jurassic sediments were not deposited in the Basin of Ouarzazate.

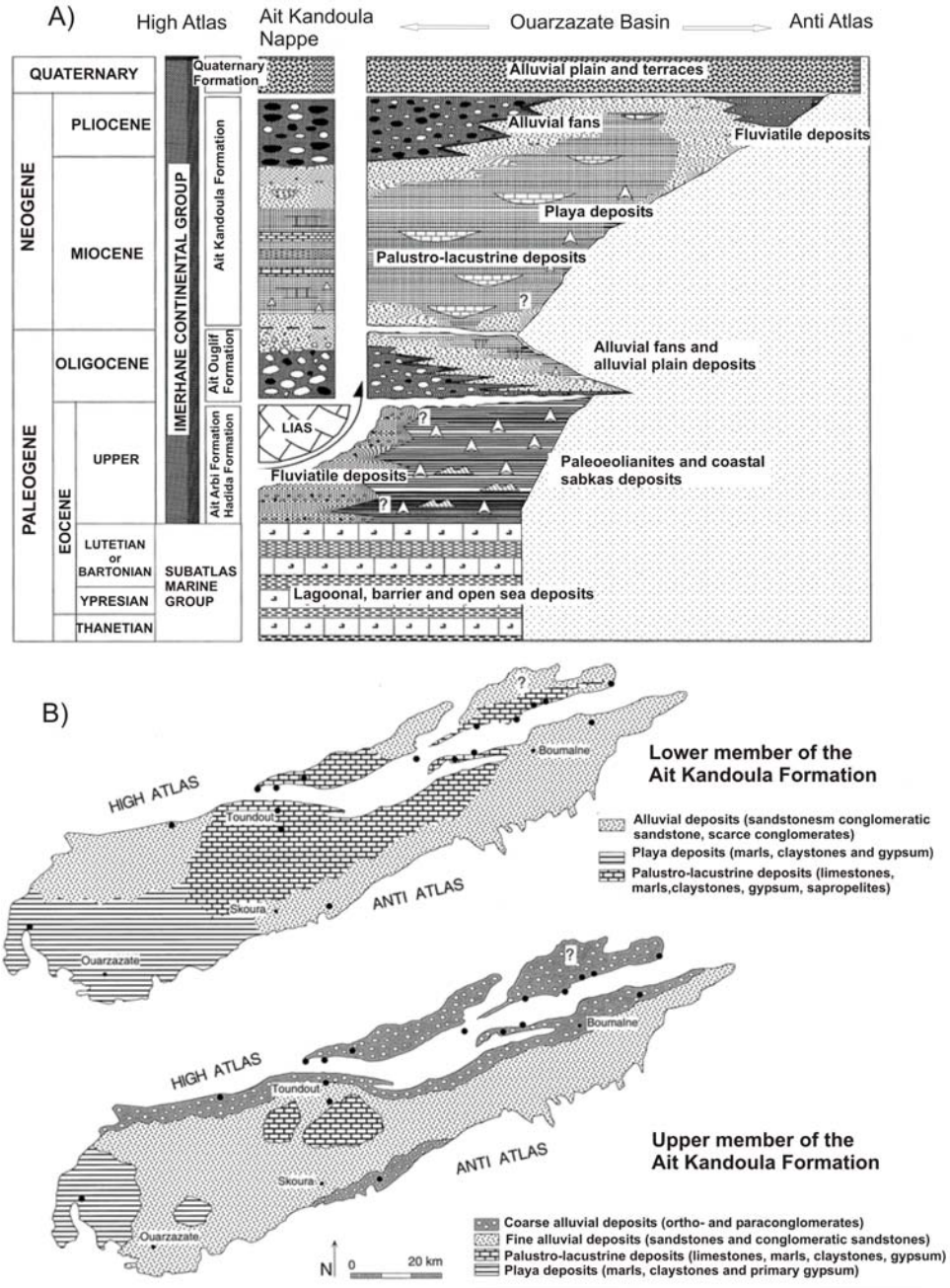

Fig. 4.7: Chronostratigraphic diagram showing the vertical and lateral changes in the different lithostratigraphic units of the Basin of Ouarzazate (A) and facies distribution of the palustro-lacustro-alluvial plain system in the Lower Member of the Ait Kandoula formation and alluvial fan facies prograding over it in the Upper Member of the Ait Kandoula formation (B) (EL HARFI et al. 2001).Litho-stratigraphic description

4.3 Litho-stratigraphic description

4.3.1 The Precambrian

The Precambrian rocks crop out mainly in the Anti-Atlas from the Siroua massif to the Jbel Saghro (Fig. 4.8). After PIQUÉ (2001) the following successive lithostratigraphic units of the Precambrian terrains are described:

- **The Precambrian I or the Zenaga and Kerdous series** (CHOUBERT 1963) which is a unit of augen gneisses, metadolerites and metamorphic rocks.
- **The Precambrian II (Quartzite Series)** is a detrital unit with siltstone, sandstones, conglomerates and especially thick quartzitic layers intruded by dolerites and tholeiitic

gabbros. From the Siroua to Bou-Azzer the abundance of quartzites gradually decreases with the development of black shales and volcanic flows. In the Bou-Azzer inlier an ophiolitic complex which is the relic of an oceanic crust is described (LEBLANC 1976) (Fig. 4.8-B). In the Jbel Saghro the formations are of sandy-pelitic terrigenous type with turbiditic facies which were describes by MARINI & OUGUIR (1990) as deposits from the base of a continental margin with clastic supply coming from the north (Fig. 4.8-A).

- **The Precambrian III (Tanalt-Ouarzazate Series)** consists of an alternation of continental detrital rocks: breccias and conglomerates, sandstones and siltstones and rhyo-ignimbritic volcanic rocks. To the east, in the Jbel Saghro, the fluvio-lacustrine Ouarzazate Group comprises a unit of andesites, dacites and aluminous basalts (BOYER et al. 1978) (Fig. 4.8-A).

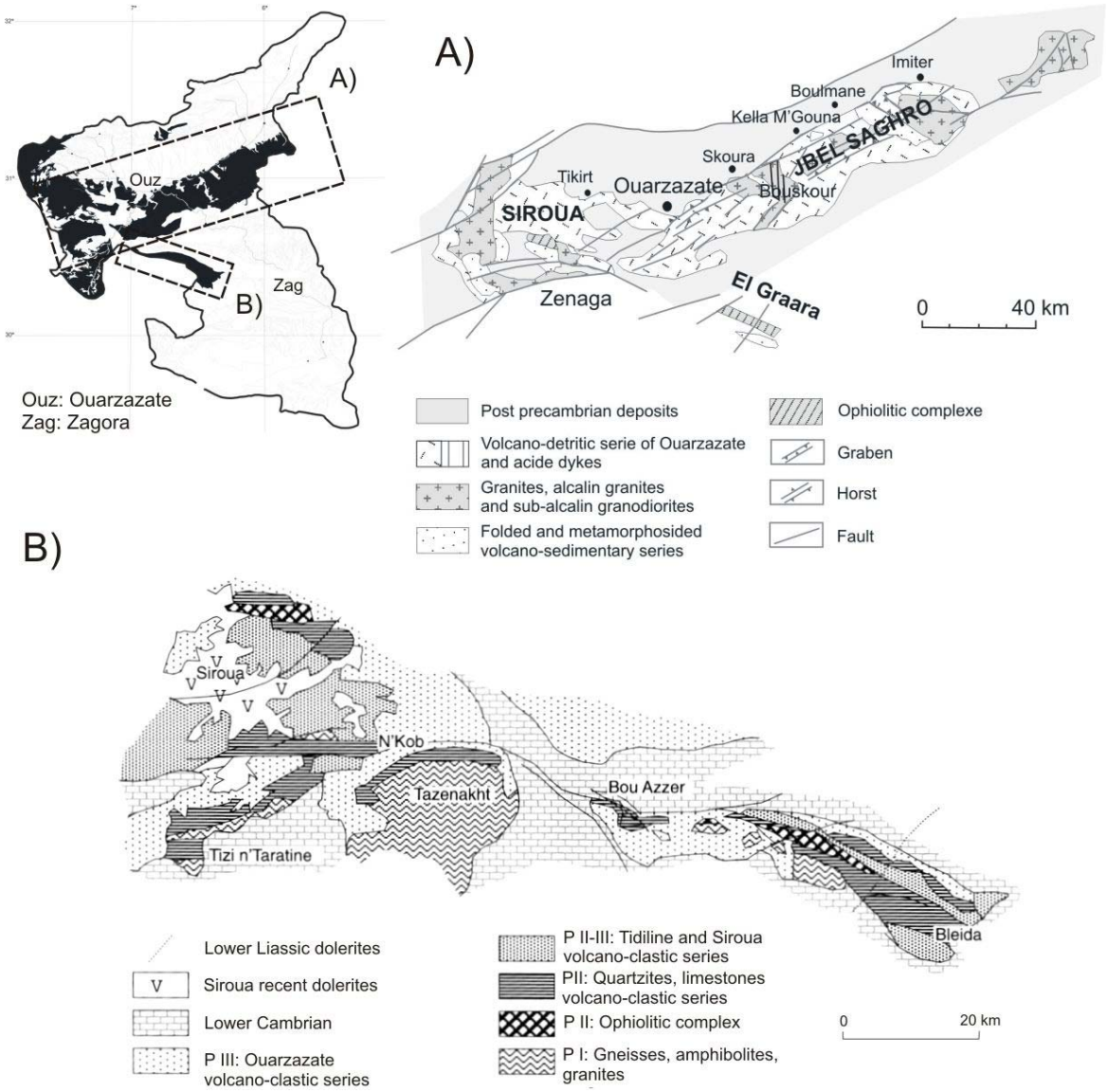

Fig. 4.8: Outcrop map of the Precambrian rocks. A): Precambrian facies and tectonic map of Siroua and Jbel Saghro (after AGUTTES et al. 1993). B): Simplified map of the Bou Azzer and Siroua inliers (PIQUÉ 2001).

4.3.2 The Paleozoic

During the Early Paleozoic to Middle Devonian, western and central Morocco was a shallow platform with the deposition of epicontinental facies. The Paleozoic rocks crop out mainly in the Middle Drâa catchment (Fig. 4.9).

The Lower Cambrian

The end-Protozoic-Lower Cambrian succession of the western and Central Anti Atlas represents a complete sedimentary cycle with a transgression directed toward the east and starting from the Gulf of Souss. The base of the Cambrian is represented by the Adoudounian succession which consists of the following series (PIQUÉ 2001) (Fig. 4.9):

- The transgressive basal member consists of conglomerates, dolomites and siltstones.
- The "Lower Limestones" reaches a thickness of 1,000 m in the western Atlas.
- The regressive deposits of purplish shales ("serie lie-de-vin") with crystals of gypsum and salt, which were deposited under a hot climate.
- The "Upper limestones" which is a transgression unit of dolomites and limestones.
- The shale and limestone of Amouslek Formation, with a thickness of 400 m in west and resting directly on the Precambrian III beds in Jbel Saghro.
- The green and red mudstones and limestones of the "Issafene Formation".
- And the regressive "Upper Sandstones formation"

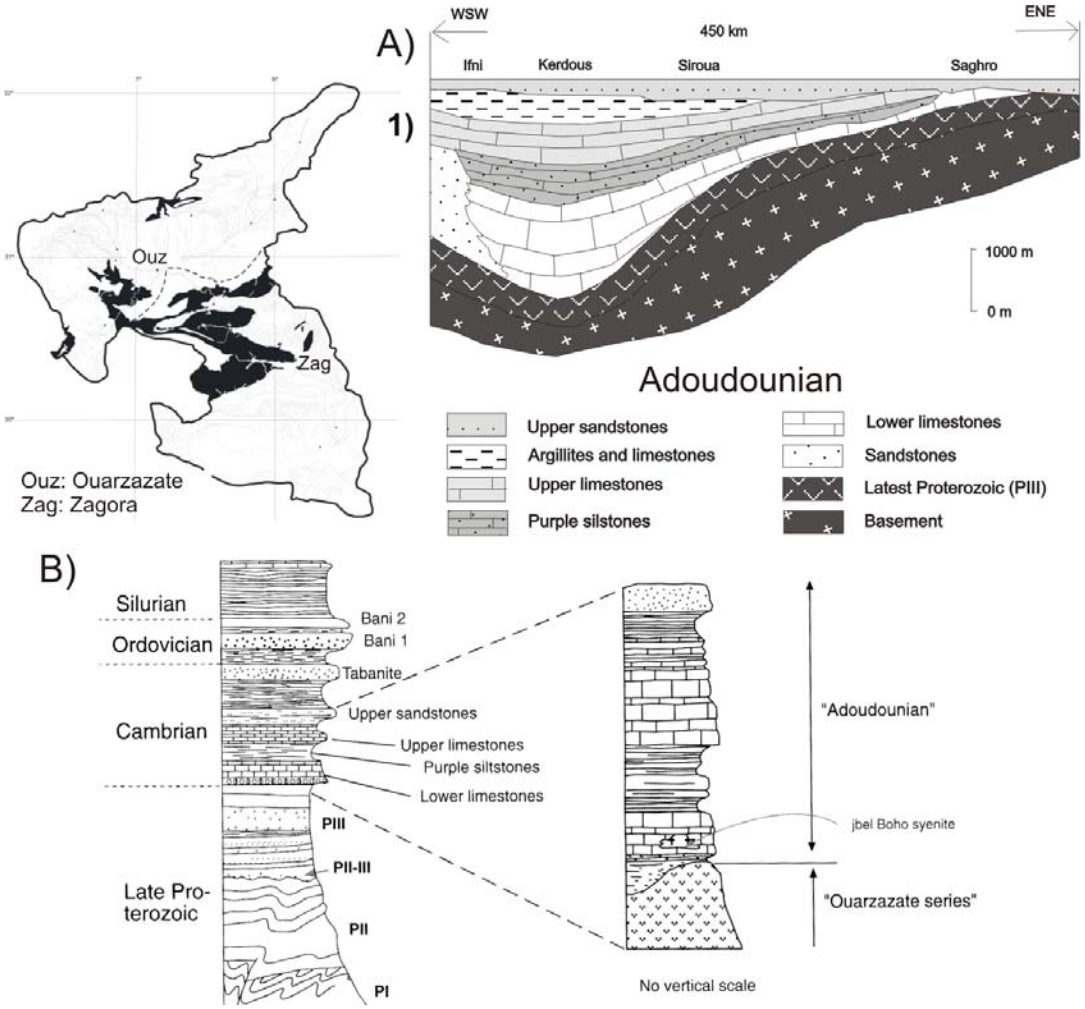

Fig. 4.9: Outcrop map of the Cambrian. A): E-W section through the Anti Atlas of the Andoudounian formations, (PIQUÉ 2001); location of the profile 1): Fig. 4.1.; B): Lithostratigraphic column of the Upper Proterozoic and the Lower Paleozoic of the Anti Atlas (PIQUÉ 2001).

The Ordovician

The Ordovician is represented by epicontinental and detritic series. This alternation of fine pelitic talus and quartzite-sandstone ridges are described in different groups (DESTOMBES 1963, MICHARD 1976) (Fig. 4.10):

- The external Feijas group (1,100 m at Zagora): shales and mudstones forming the low plains of the middle Drâa between Agdz and Zagora.
- The first Bani group (400 m at Zagora): sandstones.
- The Ktaoua group (400 m in the Ktaoua palm grove): clays and argilites.
- The second Bani group (100 m at Zagora): sandy beds forming an upper resistant band above the low valley of the Drâa. Quartzite at the base of this group is concordant on the Ktaoua mudstones.

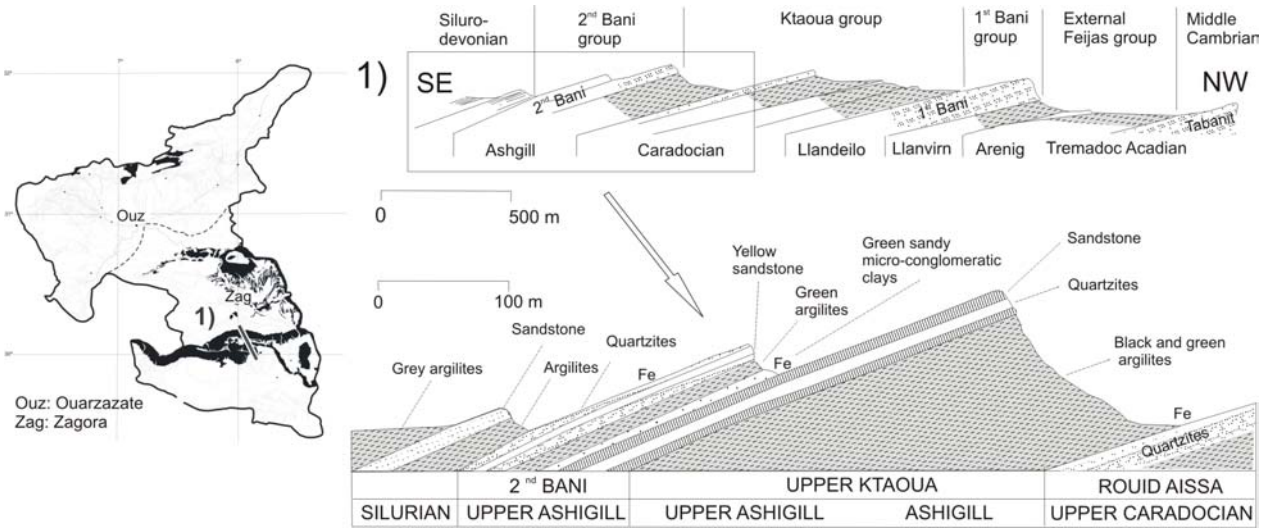

Fig. 4.10: Outcrop map of the Ordovician. Simplified profiles of the Upper Ordovician in the Central Anti Atlas between Foum-Zguid and M'Hamid (DESTOMBES 1968 modified by MICHARD 1976).

4.3.3 The Mesozoic

The Trias

The Triassic rocks crop out in the West of the Ouarzazate Basin (Imini basin) and in the southern flank of the High Atlas within anticlines of the Toudout nappe (e.g. the M'Goun anticline in the Assif-n'Ait-Ahmed catchment) (Fig. 4.11). The Triassic sequence consists of a continental facies of interbedded sandstones and silstones from alluvial fans and fluvial and deltaic red beds overlain by thoelitic basalt floods (MANSPEIZER et al. 1978, BEAUCHAMP 1988, VAN HOUTEN 1977). The whole sequence can reach a thickness of 1,000 m in the Central High Atlas. At the southern margin of the High Atlas it is less than 500 m thick. Triassic formations are absent in the Ouarzazate Basin and in the Anti-Atlas. JENNY (1988) distinguished different formations in the Upper Trias in the Central High Atlas (Fig. 4.11):

- The continental basal conglomerates.
- The siltstones of the **Anouffig formation** (max. 200 m).
- The red sandstones (80 % of quartz) of the **Oukaimeden formation** (max. 500 m).
- The siltstones of the **Tafilalt formation** (max. 300 m).
- And the tholeitic basalts of the **Ait-Aadel formation** (max. 500m). This facies is intercalated with, and overlain by a sabkha facies with evaporitic minerals.

In the western part of the Basin of Ouarzazate and at the southern range of the High Atlas the Triassic series are not complete and know important variations in thickness and facies due to the environment of sedimentation in Horst and Graben (Fig. 4.11).

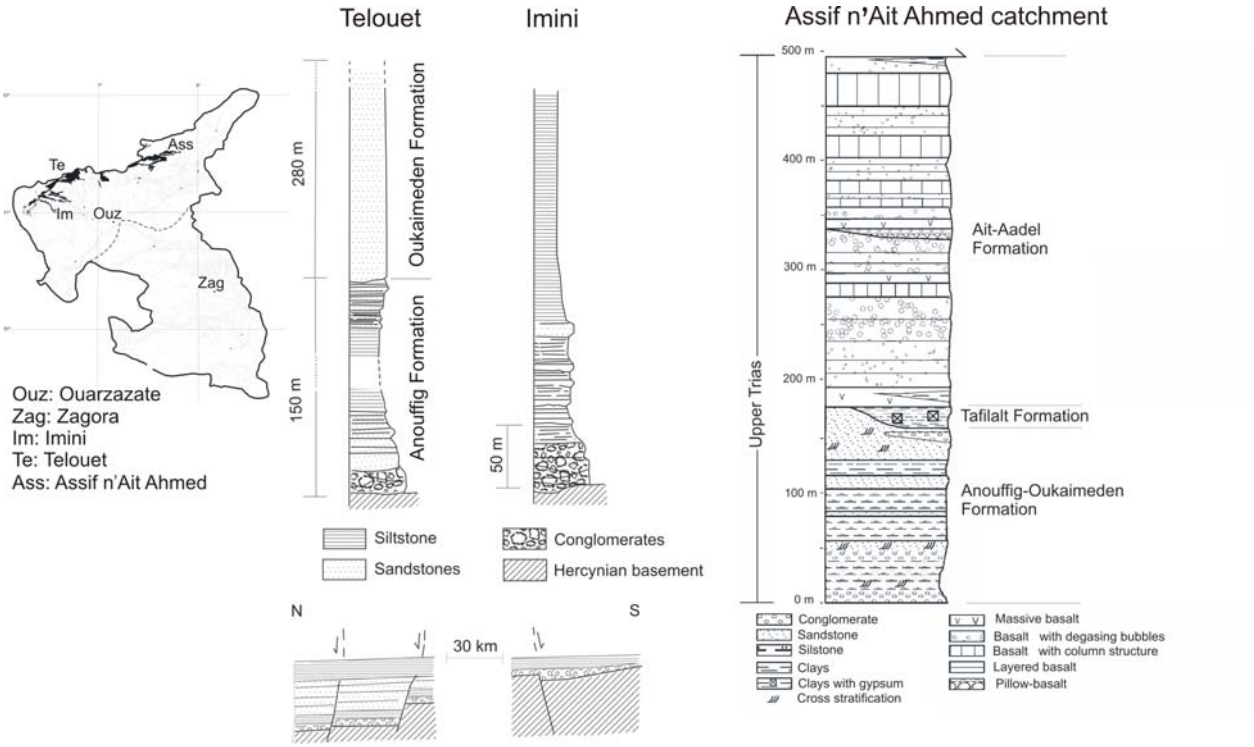

Fig. 4.11: Outcrop map of the Trias, stratigraphic logs of the Upper Triassic series of Telouet and Imini and hypothetical reconstruction of Triassic basin during deposition of evaporitic siltstones (BEAUCHAMP et al. 1983); Triassic series observed in the Assif-n'Ait-Ahmed catchment by BELL (2005).

The Jurassic

The Jurassic sediments are present only in the north and northeast of the Upper Drâa catchment (Fig. 4.12) and constitute the nappe unit of Toundoute. The Lower Liassic consists of massif dolomites and thick limestones, which are sedimented on a marine platform established in the Atlasic gulf (MICHARD 1976, JACOBSHAGEN et al. 1988). In the Todrha canyon, the Pliensbachian is constituted by 800 m thick, shallow-water, intertidal and supratidal dolomites and limestones (Fig. 4.12-A). Due to the dislocation of this shelf and the creation of a central trough with deposition of fine clastic sediments, the Late Pliensbachien limestones of shelf facies are overlain by Toarcian-Aalenian green marls. The Jurassic sequence of 1,800 m thick from Aalenian to Upper Jurassic is observed in the M'semrir syncline (Fig. 4.12-A). The Aalenian marls pass up into shelf carbonates in the Upper Bajocian. Then a remarkable change of depositional conditions took place during the Bathonian where shaly-sandy continental sequence is deposited (1,000 m). The detrital succession from Bathonian to Upper Jurassic reflects the build-up of a deltaic unit, followed by the development of coastal lagoons and fluviatile system (JENNY et al. 1981). Most of the Atlasic domain became emergent. HOFMANN (2002), OSTERHOLT (2002), BELL (2005) and BUDEWIG (in progress) described a thrusted unit called the Toundoute Nappe (Paragraph 4.4) localised in the anticline of M'Goun (Assif-n'Ait-Ahmed catchment). In this area the Toundoute Nappe is made up by the limestones and dolomites of Lower Lias and reaches a thickness of more than 700 m (Fig. 4.12-B). The observation of autochthonous continental Jurassic sediments laying in direct discordance on Paleozoic rocks in the North of the Toundoute village proves both, that it was no Jurassic

deposition in the Ouarzazate Basin, and that this region corresponds to the southern limit of the Jurassic Atlas golf (JOSSEN & FILALI 1988) (Fig. 4.4).

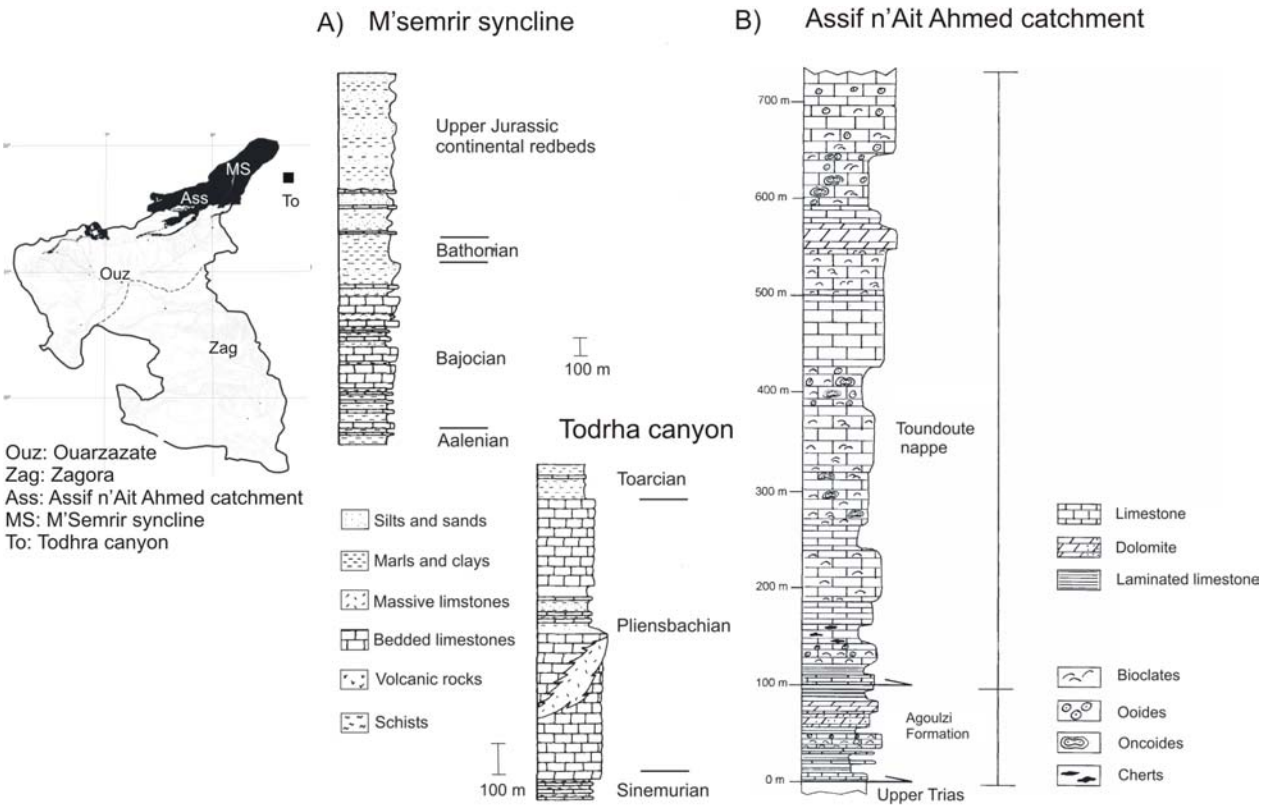

Fig. 4.12: Outcrop map of the Jurassic and stratigraphic columns of the Jurassic of the Central High Atlas. A): M'semrir syncline and Todrha canyon (JACOBSHAGEN et al. 1988); B): The Lower Lias of the Toundoute nappe in the Assif n'Ait Ahmed catchment (BELL 2005).

The Cretaceous

Cretaceous sediments crop out only in the Upper Drâa catchment, in the folded and thrusted "Southern Atlasic Marginal Zone" (Paragraph 4.4.2) and in the Imini and Tikirt sub-basins (Fig. 4.13). Investigations about Cretaceous deposits in High Atlas were carried out by several authors who defined the stratigraphy and the paleogeography (among other: GENTIL 1915, MORET 1933, CHOUBERT 1948, GAUTHIER 1957, STAMM 1981, THEIN 1985, 1989).

The Cretaceous series show four types of facies:

- The red lagoon-continental siltstones of Lower Cretaceous (Infracenomanian). This formation which is similar in facies to Upper Jurassic contains gypsum. GAUTHIER (1957) observed a thickness of about 350 m of this formation in the north of the Basin of Ouarzazate. KHALIL and RACHACH (1986) described the Infracenomanian in the sub-basin of Tikirt as a 40 m thick unit of conglomerates with calcareous matrix passing upward to red sand and silstones.
- The massive marine limestones and dolomites of Cenomano-Turonian with a thickness varying between 10 m in the Imini basin (THEIN, 1989) (Fig. 4.13-A) and 30 m in the Dades canyon.
- The red sandy marls of Senonian with a thickness varying between 50 to 120 m deposited in a lagoon environment after the sea regression in Upper Turonian.

The Cretacous series is not complete in the whole Basin of Ouarzazate. In the South of the Tikirt sub-basin, the Mio-pliocene sediments rest directly in discordance on the Infracenomanian (Fig. 4.13-B).

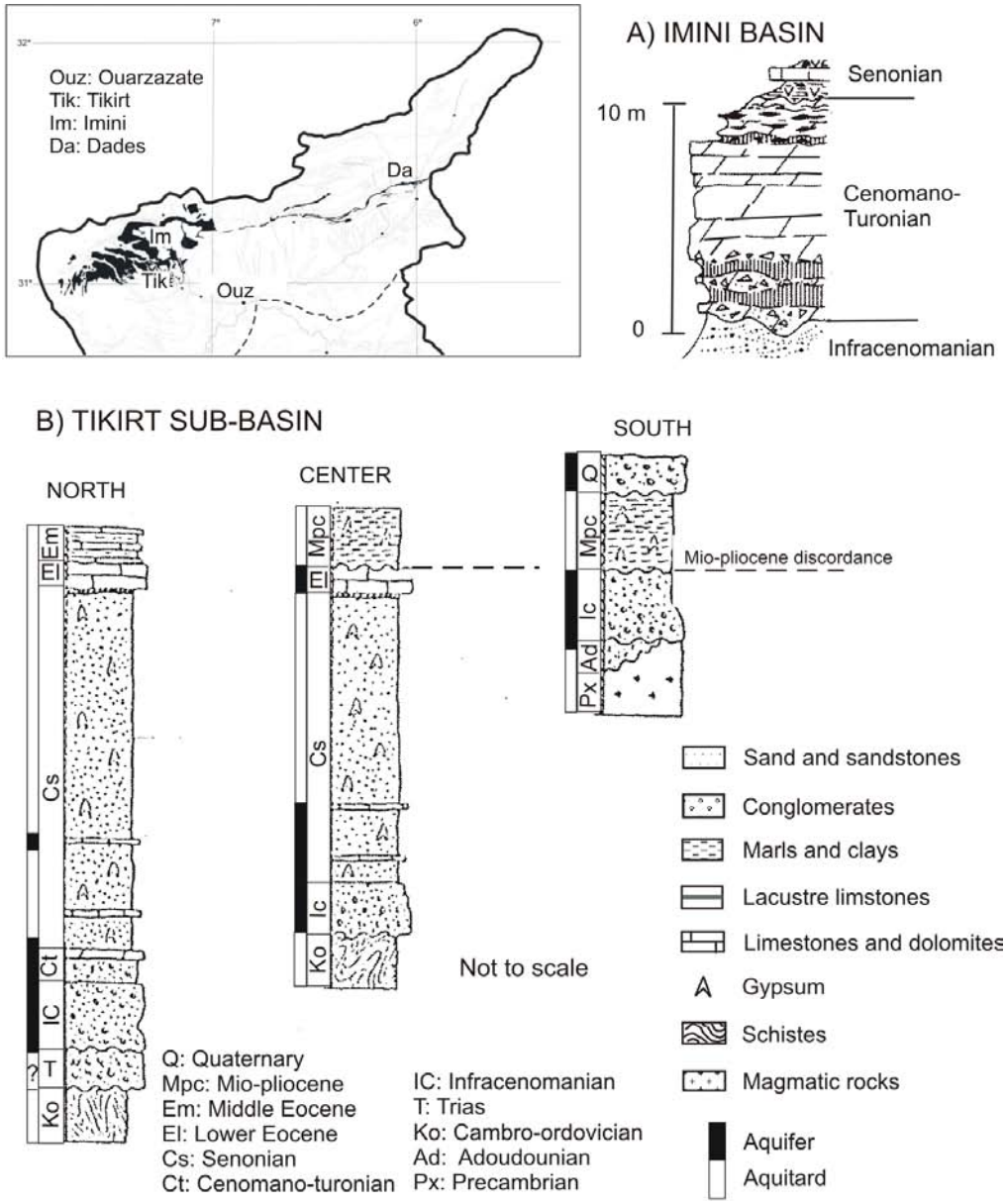

Fig. 4.13: Outcrop map of the Cretaceous; A) Type section through the Cenomano-Turonian carbonate sequence in the Imini basin (THEIN 1989); B) Stratigraphic columns in the Tikirt sub-basin (JOSSEN & FILALI 1988).

4.3.4 The Cenozoic

The Cenozoic sediments were deposited in thick sequences in the Basin of Ouarzazate. EL HARFI et al. (2001) distinguishes the marine and the continental Cenozoic formations, respectively the "Subatlas Marine Group" defined by TRAPPE (1989, 1991) and HERBIG (1991), and the "Imerhane Group" studied by GÖRLER and ZUCHT (1986), FRAISSINET et al. (1988), GÖRLER et al. (1988), HERBIG (1991) and EL HARFI (1994).

The "Subatlas Marine Group"

The "Subatlas Marine Group" corresponds to Paleocene (Danian and Thanetian) and Lower and Middle Eocene (Ypresian and Lutetian) sediments (Fig. 4.7-A). These sediments crop out along the "Southern Atlas Marginal Zone" (Paragraph 4.4.2) and in the western part of the Basin of Ouarzazate (Fig. 4.14). The deposits are almost all of marine or at least near-coastal origin. It is a complete transgressive-regressive megacycle, composed of phosphatic and carbonated sediments, marls, siltstones and regionally sandstones (HERBIG & TRAPPE 1994).

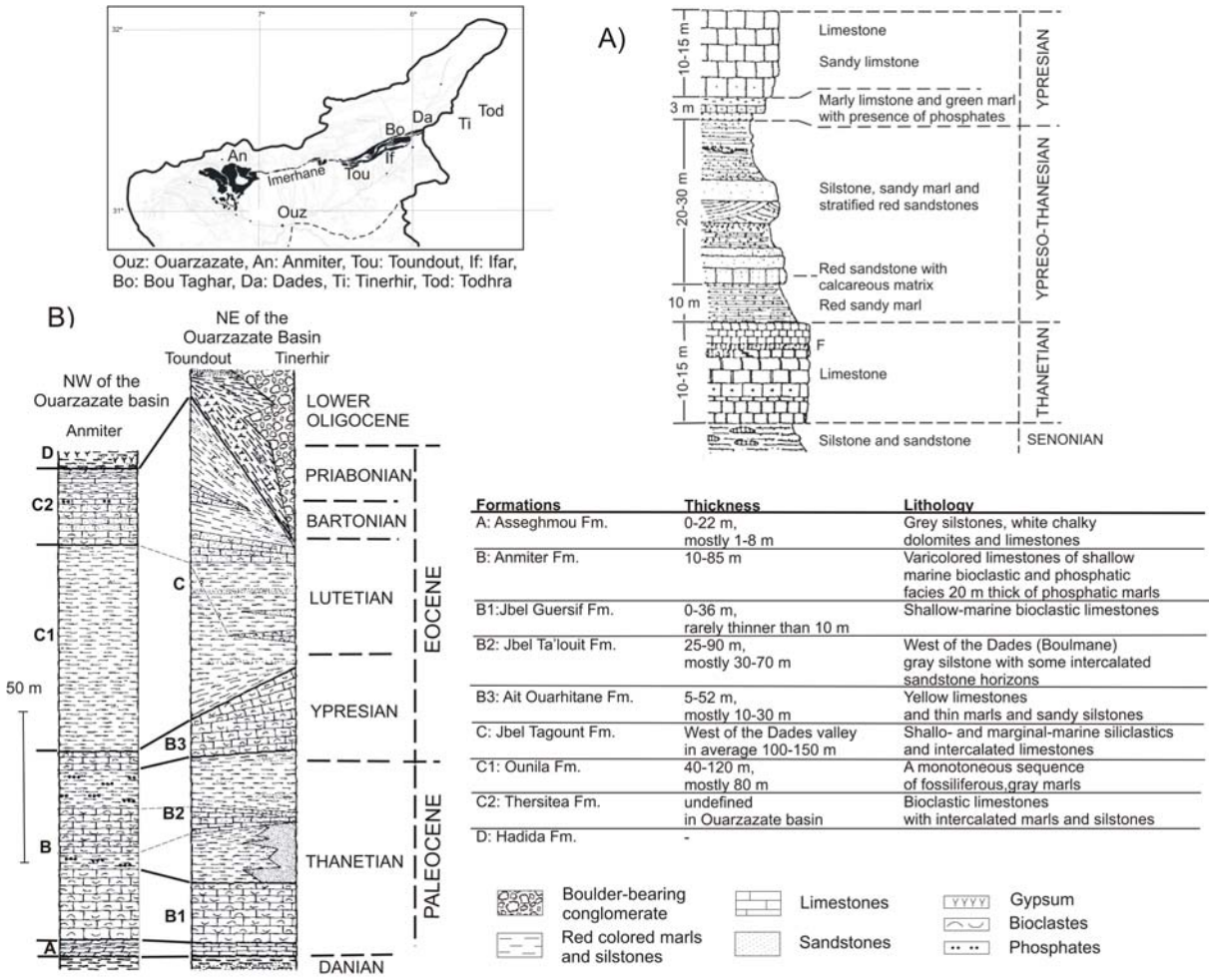

Fig. 4.14: Outcrop map of the Paleogene. A) Synthetic stratigraphy of the Upper Paleocene and the Lower Eocene of the Ouarzazate Basin (CAPPETTA et al. 1987); B) Stratigraphic column of the Subatlas Group in the northwestern and eastern Ouarzazate Basin (HERBIG & TRAPPE 1994) and lithology of the various formations compiled after HERBIG & TRAPPE (1994).

CAPPETTA et al. (1987) define the synthetic stratigraphy of the Thanetian and Ypresian prevailing in the Basin of Ouarzazate (Fig. 4.14-A). But due to the high variability of the "Subatlas Marine Group" facies within the basin, it is necessary to consider these series of sediments more in detail. HERBIG and TRAPPE (1994) made a synthesis of lithologies and thicknesses of the various formations of the "Subatlas Marine Group" defined in the Basin of Ouarzazate (Fig. 4.14-B). In addition to the variability of facies, strong variations in thickness of the series are observed. GAUTHIER (1957) notices a thickness about approximately 170 m of the Cenozoic marine sediments in the Imerhane area and about 280 m at Bou Taghar (Fig. 4.15).

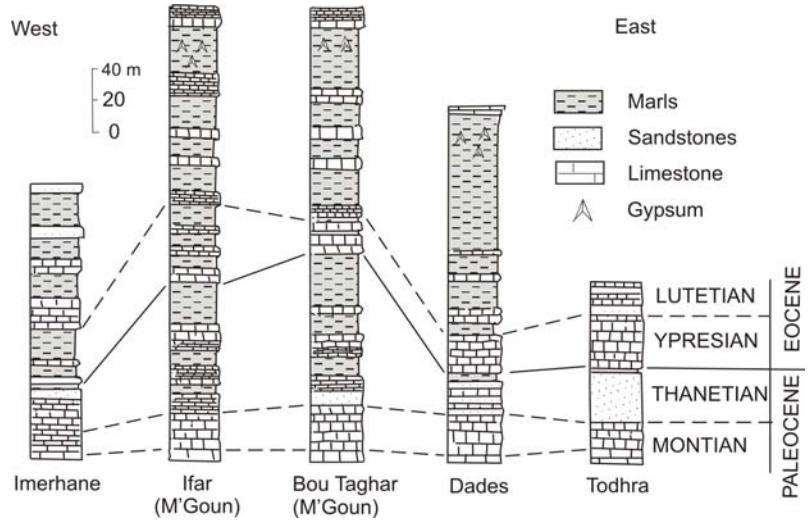

Fig. 4.15: Stratigraphy of the Upper Paleocene and Lower and Middle Eocene between Imerhane and Todhra (in JOSSEN & FILALI 1988 after GAUTHIER 1957); Localisation Fig. 4.14.

The "Imerhane Continental Group"

The "Imerhane Group" described in the Basin of Ouarzazate (Fig. 4.7-A) corresponds to the continental deposits from Upper Eocene to Quaternary (EL HARFI et al. 2001). In the Upper Drâa catchment the sediments of Neogene age have been deposited in a large basin between the rising High Atlas and the Anti-Atlas and Jbel Sarho. GÖRLER (1988) suggests that the basins of Ait Kandoula, Seddrat and Ouarzazate have been part of a single large basin during the Miocene. The sedimentation occurred in paleo-valleys cut respectively into Precambrian and Paleozoic rocks and Eocene limestones. Then today, due to the tectonics and erosions these sediments crop out separately (Fig. 4.16). GÖRLER (1988) notices the pronounced asymmetry of the Basin of Ouarzazate where continental Neogene sediments show moderated thickness in the western and southern margins of the Ouarzazate Basin but are 1,200 m thick in the north at Amekchoud. He proposes a schematic stratigraphic section of the thick Imerhane Continental Group of the northern Ouarzazate Basin and Ait Kandoula regions (Fig. 4.16). The series began with sabkha deposits passing up to lacustrin and afterwards to alluvial sediments.

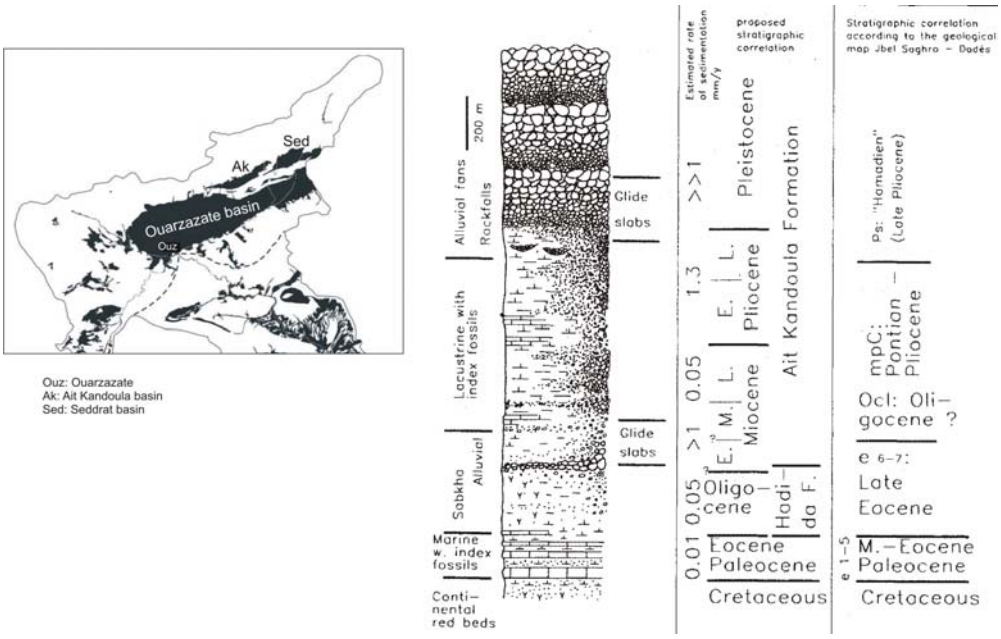

Fig. 4.16: Outcrop map of the Neogene and Quaternary in the Upper Drâa catchment and schematic stratigraphic section of the Imerhane Continental Group of the northern Ouarzazate Basin and Ait Kandoula region (GÖRLER 1988).

EL HARFI et al. (2001) made a synthesis of the lithology of the "Imerhane Continental Group" of the Ait Kandoula and Seddrat basins and the Ouarzazate Basin (Fig. 4.17 and Tab. 4.2).

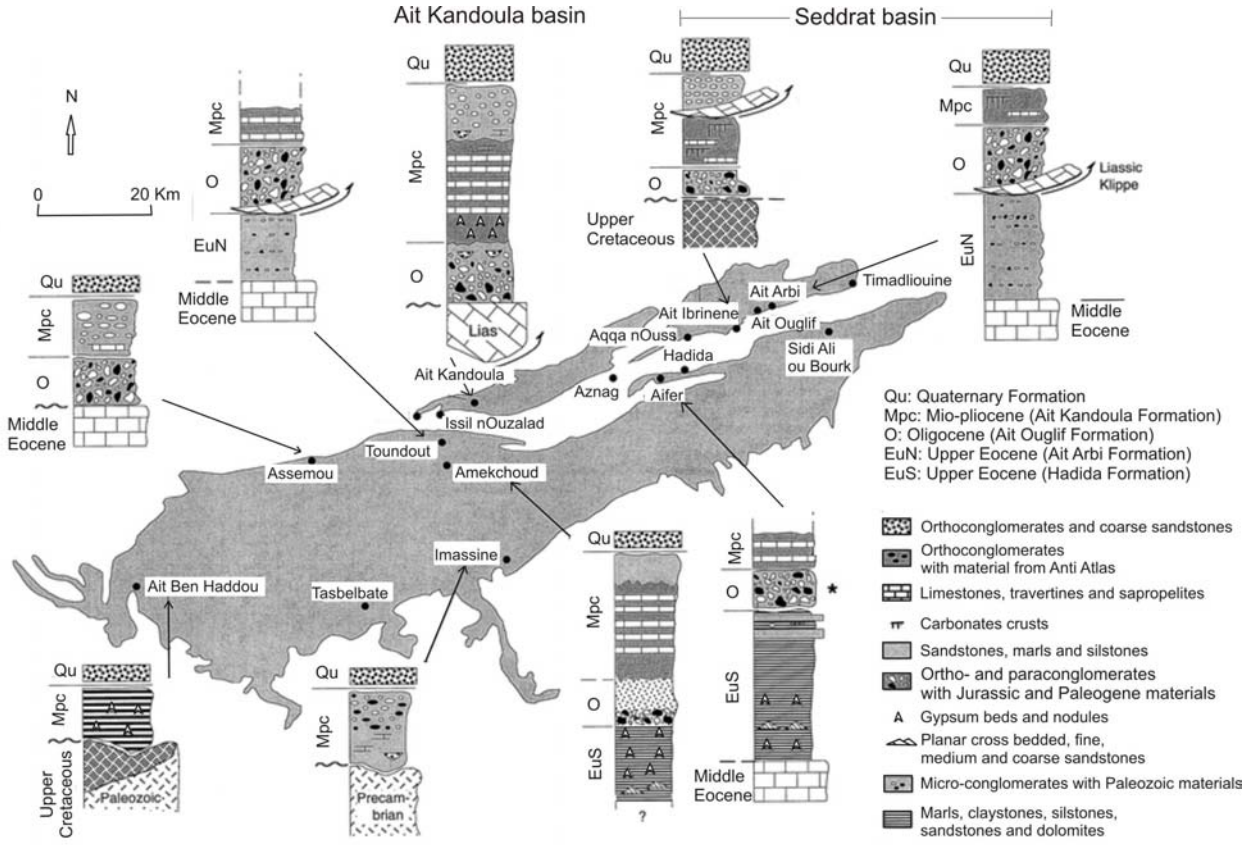

Fig. 4.17: Geological sections of the Imerhane Continental Group: Ouarzazate Basin and subatlas Zone (after EL HARFI 2001).

The Upper Eocene is defined by the conglomeratic "Ait Arbi Formation" and the marly "Hadida formation" which overlay conformably the Sub Atlas Marine Group. Although both crop out in the North of the Basin of Ouarzazate and along the "South Atlasic Marginal Zone" (Paragraph 4.4.2), the "Hadida formation" is observed southern of the "Ait Arbi Formation" (Fig. 4.17). The Oligocene crops out in the "South Atlas Marginal Zone" overlaying unconformably the Liassic limestones, the Lower Cretaceous and the Eocene. It is described as the "Ait Ouglif Formation" showing sandy and conglomeratic facies. The Mio-Pliocene or the "Kandoula Formation" crops out in the Ait Kandoula and Seddrat basins and over almost the whole Basin of Ouarzazate. Overlaying unconformably all the previous terrains, this formation is divided by a basal palustro-lacustrine unit and an upper conglomeratic unit (Fig. 4.7). Its thickness shows great variations with 700 m in north of the Basin of Ouarzazate and sediments fining out on the Precambrian rocks of the Anti-Atlas. The Quaternary terraces and pediments cover the Mio-Pliocene with a relative constant thickness about 30 m.

In the Middle Drâa catchment, the Neogene sediments were less deposited. Along the Drâa valley the Mio-pliocene and Quaternary sediments constitute the various alluvial aquifers of the palm groves overlaying the Ordovician schists of the Ktaoua and the External Feijas Groups.

Tab. 4.2: Lithology of the Imerhane Continental Group based on the description of EL HARFI et al. (2001).

Age	Formations	Lithology: Facies/Thickness	Paleogeography
QUATERNARY		Coarse and heterometric conglomerates / 30 m in the Basin of Ouarzazate.	Alluvial terraces and consolidated pediments.
MIO-PLIOCENE	Ait Kandoula	**Basal palustro-lacustrine unit** *:* Limestones, travertines, marls, clay-silstones, sapropelites and primary gypsum; **Upper conglomeratic unit***:* sandstones and mainly conglomerates High variability in thickness in the Basin of Ouarzazate, while sediments are 700 m thick in north (500 m for the basal unit), they pinch out on the precambrian basement in south; layers locally vertical close the Subatlasic zone and horizontal southwards.	Prograding alluvial fans in the context of a palustro-lacustrine alluvial plain system; *North-south trend:* reduced conglomerate-to-sandstone and siliciclastic-to-carbonate ratios and decreasing maximum grain size.
OLIGCENE	Ait Ouglif	**Ait Seddrat basin:** Breccia, paraconglomerates beds with clasts of up to 1.20 m separated by coarse sandstone and silt-sandstone beds / 40 to 60 m thick. **Ait Kandoula basin:** paraconglomerates and coarse breccia with material floating in a sand-silt-clay matrix / 30 m south Ait Kandoula nappe. **Ouarzazate basin:** sandstone and conglomerate (Aïfer, Hadida and Amekchoud)/ 30 m of conglomerates overlaid by 150 m-200 m of sandstones at Amekchoud.	**Ait Seddrat basin:** proximal part of braided river system adjoining alluvial fans. **Ait Kandoula basin:** mudflow facies of alluvial fan system. **Ouarzazate Basin:** braided fluviatile system.
UPPER EOCENE	Hadida	Clays, marls, red siltstones, sandy dolomites and fine sandstones with primary gypsum lenses; massive sandstones toward the top of the formation / 600 m at Hadida with an average about 300 m.	Coastal sabkha deposits cut by eolian dune sediments.
	Ait Arbi	Conglomeratic sandstones, orthoconglomerates with highly indurated carbonate sandstone cement / 600 m with a mean of 400 m.	Proximal braided fluviatile system.

4.4 Tectonic features

4.4.1 The main fault systems of the Upper and Middle Drâa catchment

The Upper and Middle Drâa catchment is affected by two main fault systems (Fig. 4.18): the Anti Atlas Major Fault and the South Atlas Front.

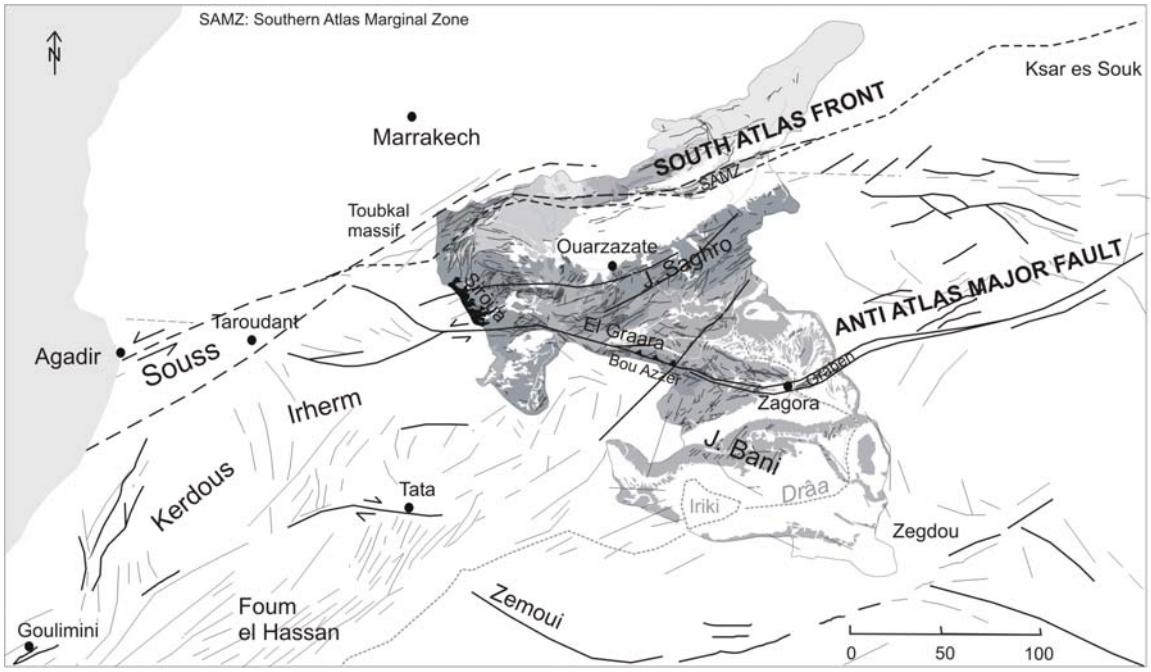

Fig. 4.18: Structural features of South Morocco (modified after MICHARD 1976) and the Upper and Middle Drâa catchment.

In the Middle Drâa catchment, the Anti Atlas Fault crosses the Anti Atlas from the Jbel Siroua to Zagora with a WNW-ESE strike and turns NE-SW to the east of Zagora. This tectonic structure is delineated by the Bou Azzer anticline inlier (Fig. 4.1-B) and the Graben of Zagora.

The South Atlas Front is a major thrust front running continuously from Agadir to Tunis (FRIZON DE LAMOTTE et al. 2000). At the northern boundary of the Basin of Ouarzazate, it corresponds to a compressional zone, the "Southern Atlas Marginal Zone" (SAMZ) (Fig. 4.18). In the west of the Basin of Ouarzazate, it separates the High Atlas domain (Toubkal massif) from the Anti Atlas domain (Jbel Siroua) (Fig. 4.18).

4.4.2 Tectonic features of the Upper Drâa catchment

The Upper Drâa catchment can be divided into four structural units (Fig. 4.19 and 4.20): the Anti Atlas, the High Atlas, the Southern Atlas Marginal Zone and the Basin of Ouarzazate.

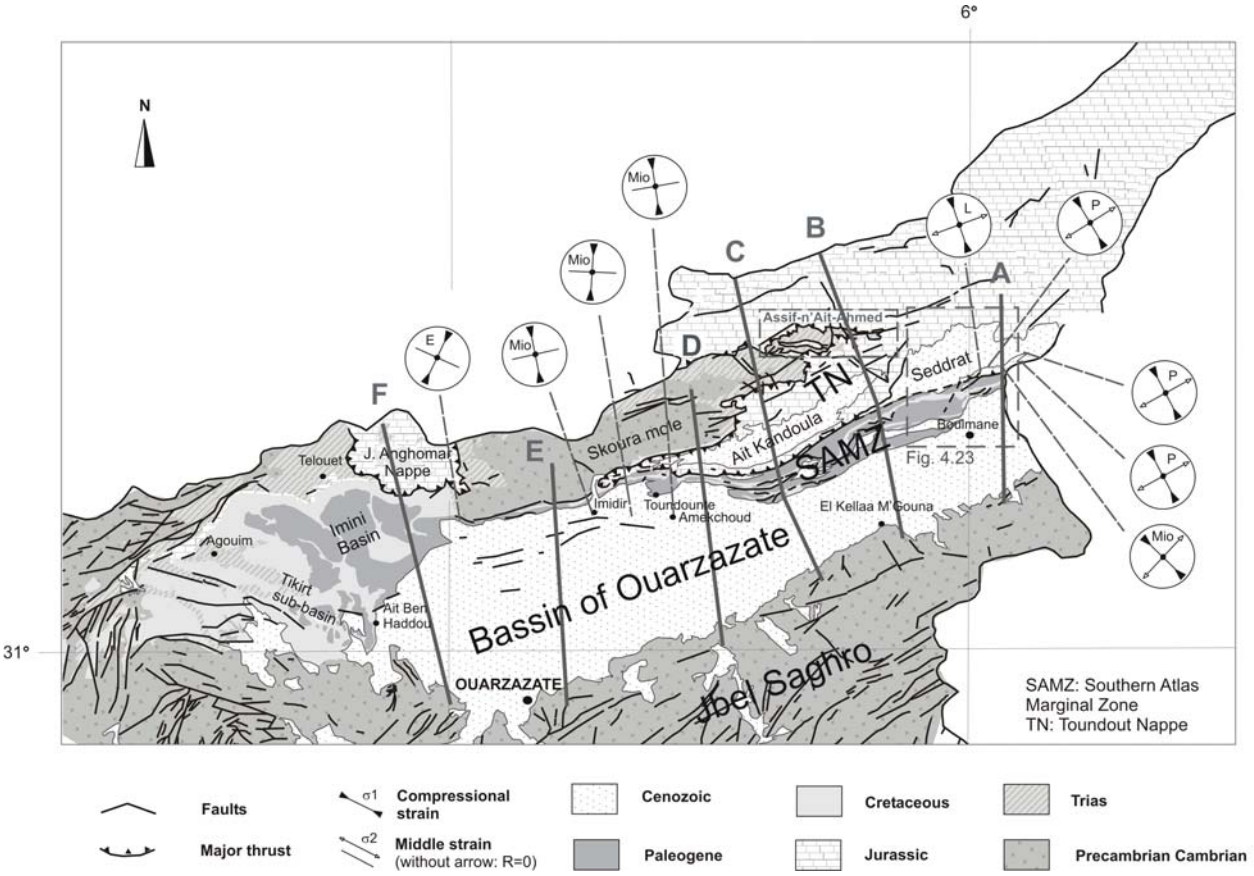

Fig. 4.19: Simplified tectonic map of the Upper Drâa catchment (based on the 1/500,000 Ouarzazate sheet, CHOUBERT 1959) and microtectonic results after LAVILLE (1980); L: Lias, E: Eocene, Mio: Miocene and P: Pliocene.

The Anti Atlas

The Anti Atlas belongs to the West African craton margin which was moderately affected by the Pan-African orogeny. Moreover, due to the lack of important Meso-Cenozoic deformation the Precambrian and Paleozoic rocks are weakly deformed. The Jbel Saghro (Fig. 4.19) is an anticlinorial structure of NE-SW axis with faults of the same direction. In the Jbel Siroua the predominated directions of the faults are WNW-ESE, N-S and SW-NE.

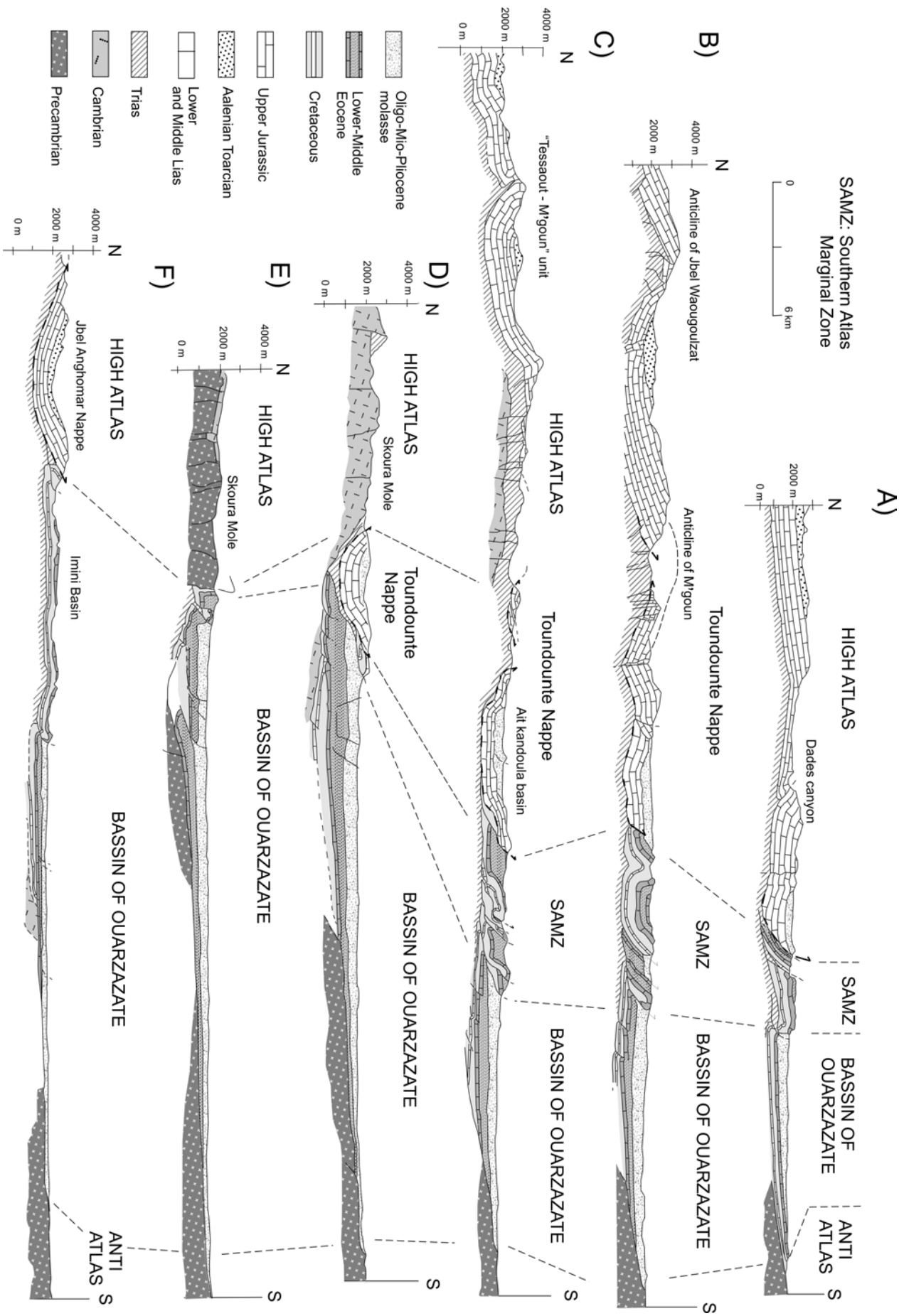

Fig. 4.20: North-south geological profiles of the Upper Drâa catchment (after JOSSEN & FILALI 1988); localisation of the profiles Fig. 4.19.

The High Atlas

The High Atlas Mountains show large synclines of N70 axes separated by narrow anticlines like the M'Goun anticline in the Asif-n'Ait-Ahmed catchment (Fig. 4.20, profile B). The N70 main folds and faults are sometimes deformed by sinistral N30 wrench faults (FRAISSINET 1988). Due to the uplift of the High Atlas, the Jurassic strata were decoupled from its basement and has been thrusted since the end of Cretaceous times along the weak Triassic series and moved southward in a thin-skinned tectonic style, forming the Toundoute Nappe (Fig. 4.20 and Fig. 4.21) (LAVILLE et al. 1977, LAVILLE 1980, GÖRLER & ZUCHT 1986). The thrusted Liassic carbonates of the Toundoute Nappe override locally with a southward vergence the Neogene and Quaternary of the northern range of the Basin of Ouarzazate. In the Ait Kandoula and Ait Seddrat basins, the molasses of Miocene rest directly on the Liassic carbonates in piggyback basin type overlying the Toundoute Nappe (Fig. 4.21).

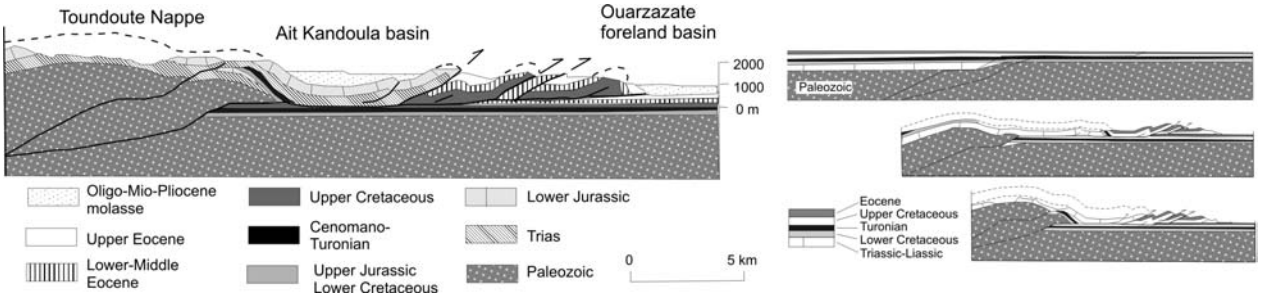

Fig. 4.21: Cross section through the Ait Kandoula basin (localisation: Fig. 4.20, profile C) and schematic kinematic evolution of the cross-section (FRIZON DE LAMOTTE et al. 2000).

In the north of the Taoujgalt village, the Toundoute Nappe overlies the Cretaceous series, which proves a minimum throw about 10 km (LAVILLE et al. 1977). In spite of this displacement, the internal deformation within the thrusted unit is low. HOFMANN (2002), OSTERHOLT (2002), BELL (2003) and BUDEWIG (in progress) carried out structural and geological investigations of the Toudout Nappe in the M'Goun anticline. The stereo-projections of the fractures (Fig. 4.22) show high variability of the density and direction of fractures between the autochthonous, the para-autochtonous and the Toundoute Nappe. While the red sandstones of the Triassic autochthonous show low density of fracturing with NE-SW direction, the basalt is densely fracturated. The calcareous para-autochthonous shows a dense fracturing with various directions due to the movement of the Toundoute Nappe. The Toundoute Nappe itself shows an ENE-WSW main striking direction.

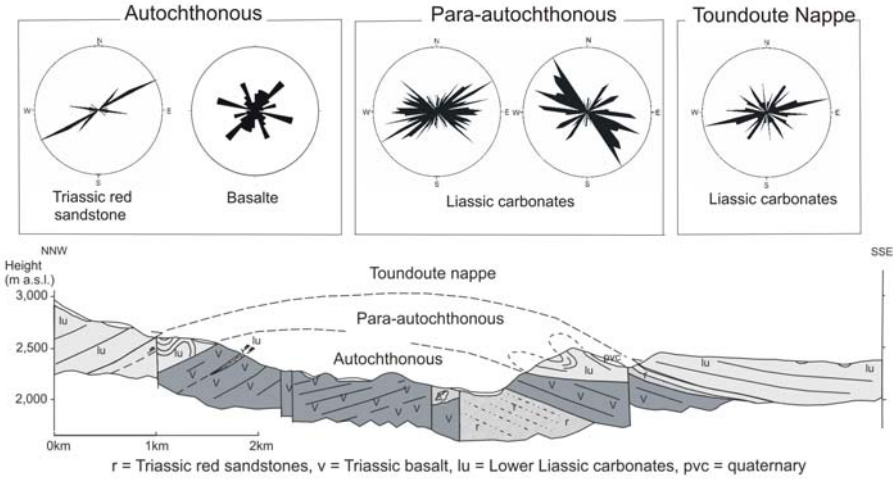

Fig: 4.22: Profile of the Toudoute Nappe and stereo-projections of the fractures in the Assif-n'Ait-Ahmed catchment: M'Goun Anticline (after HOFMANN 2002 and BELL 2005); localisation Fig. 4.20.

The "Southern Atlas Marginal Zone"

A fold- and thrust-belt with a width of approximately 10 km was formed in front of the Toundoute Nappe. This compressional deformation zone is called by various authors: "the Southern Atlas Marginal Zone" (LAVILLE 1980, GÖRLER & ZUCHT 1986, FRIZON DE LAMOTTE et al. 2000), (Fig. 4.19, 4.20). This zone includes narrow and asymmetrical anticlines and synclines oriented E-W and NE-SW, reversed faults, folds, scales, thrusts and tectonic slabs (GAUTHIER 1957, ERRARHOUI 1997, BEAUCHAMP 1999) (Fig. 4.23). The fault pattern shows directions varying between N45-N90. ERRARHOUI (1997) and BEAUCHAMP et al. (1999) show in this zone a frontal tectonic repetition of the Upper Cretaceous-Eocene sequence (Fig. 4.21). Some flat south-verging thrust sheets override the Neogene sediments of the Basin of Ouarzazate. The amount of shortening in this zone is ~ 60% (FRIZON DE LAMOTTE 2000).

The Basin of Ouarzazate

The Basin of Ouarzazate is an asymmetrical synclinorium (Fig. 4.20). It seems only to be affected by faults striking N70 in its northern part. LAVILLE (1980) and FRAISSINET et al. (1988) investigated the younger tectonic events registered in the most recent deposits in order to know what could have been the directions of the stresses during the early history of the belt (Fig. 4.19). In the Dades region, the Pliocene, the Lias and the Miocene show the same stress state which indicates a N150 direction of shortening with thrusts and strike slip faults structures. In the Basin of Ouarzazate, the Miocene and the Eocene registered only a sub-meridian shortening.

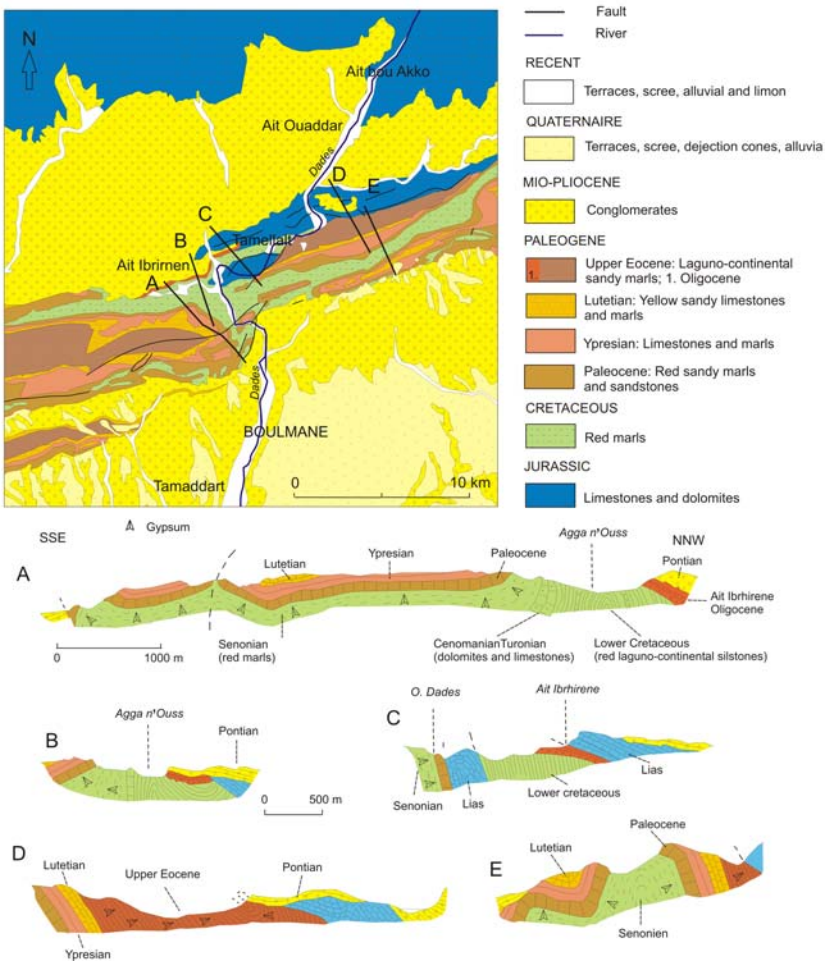

Fig. 4.23: The Southern Atlas Marginal Zone between the Seddrat basin and the Ouarzazate Basin, profiles from GAUTHIER (1957) in MICHARD (1976). Localisation map of the profiles from the geological map of Saghro Dades 1/200,000 (SAADI et al. 1977); localisation Fig. 4.19.

5 WATER BALANCE OF THE ASSIF-N'AIT-AHMED AND IFRE CATCHMENTS

5.1 Introduction

Due to relative high precipitation, the High Atlas Mountains represent the recharge area of the Upper Drâa catchment. But how effective is this recharge? In order to give a first answer, this chapter attempts to give a water balance estimation of two catchments of the High Atlas: the Assif-n'Ait-Ahmed catchment (110 km^2) and the Ifre catchment (1,240 km^2) (Fig. 5.1). Due to the availability of the meteorological data, the water balance of the Assif-n'Ait-Ahmed catchment is carried out for the year 2002 (January to December), while the water balance of the Ifre catchment is carried out for the year 2002-2003 (September to August).

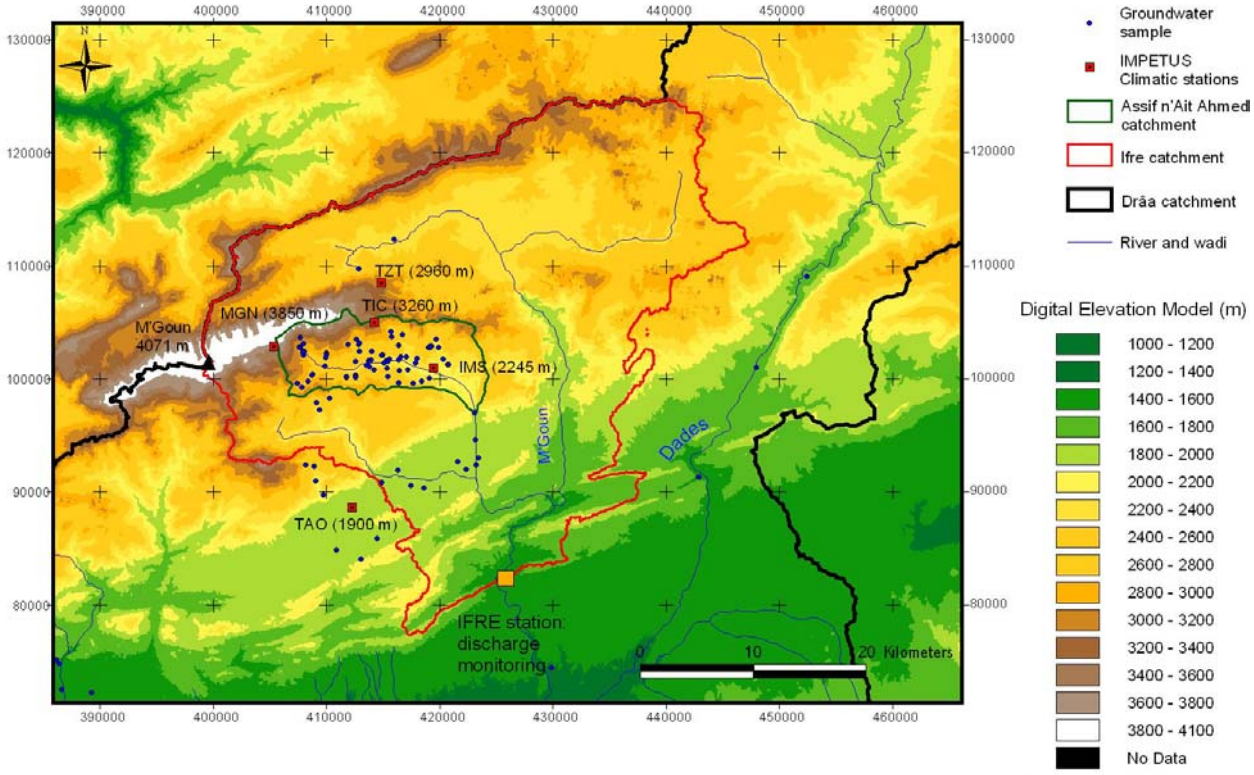

Fig. 5.1: The Assif n'Ait Ahmed catchment (110 km^2) and the Ifre catchment (1,240 km^2) in the High Atlas Mountains (localisation Fig. 3.2); Digital Elevation Model of the northern part of the Upper Drâa catchment and IMPETUS climatic stations: MGN = M'Goun, TIC = Tichki, TZT = Tizi Tounza, IMS = Imeskar and TAO = Taoujgalt.

5.2 Water balance of the Assif-n'Ait-Ahmed catchment (2002)

5.2.1 Characterization of the catchment

The Assif-n'Ait-Ahmed catchment located within the M'Goun Range (4,071 m) of the High Atlas Mountains covers an area of approximately 110 km^2. Its altitude lies between 2,000 m and 4,000 m with a mean of 2,500 m. Vegetation is scarce and dominated by scattered *Juniperus* trees and cushion shrubs above 2,400 m. The Assif-n'Ait-Ahmed Wadi is a tributary of the M'Goun Wadi (Fig. 5.1). Geomorphologically, the basin has extensive scree slopes, debris flow channels, debris fans, ancient and active landslides and gravely river beds (DE JONG et al. 2004).

5.2.2 Estimation of the total precipitation: snow and rain

Three climatic stations were installed within the catchment: Imeskar station (2,250 m.), Tichki station (3,260 m.) and M'Goun station (3,850 m.) (Fig. 5.1). At these altitudes, the snow falls are important in winter and can play a significant role in the recharge processes. In the context of his PhD-Thesis, Schulz estimated the quantity of water precipitated during snow falls and the rate of sublimation (SCHULZ & DE JONG 2004). To take into account the snow in the total precipitation, the thickness of snow monitored at the climatic stations is transformed in snow water equivalent (swe) according to DYCK & PESCHKE (1995):

$$swe(mm) = 0.01 \cdot \rho_S \cdot h_S$$

with ρ_s (kg/m^3) the density and h_s (cm) the thickness of the snow.

The measured density of new snow (ρ_s) ranges between 100 kg/m^3 (Imeskar station) and 150 kg/m^3 (M'Goun and Tichki stations) (SCHULZ 2006). SCHULZ (2006) showed the importance of the snow fall by simulation of the snow cover compared to the total precipitation. He calculated for the period between October 2001 and September 2002 that the snow component represented 86 % of the total precipitation at the M'Goun station, 50 % at the Tichki station and 25 % at the Ameskar station (Fig. 5.2).

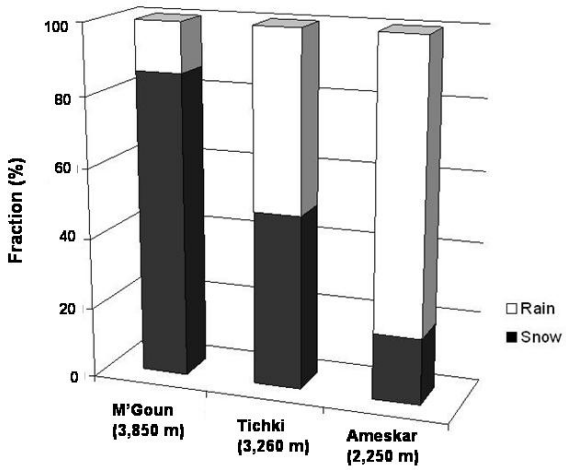

Fig. 5.2: Proportion of snow and rain within the total precipitation of the Assif-n-Ait-Ahmed catchment for October 2001 to September 2002 (after SCHULZ 2006).

For the estimation of the water balance in Assif-n'Ait-Ahmed catchment, climatic data of the year 2002 is used. The monthly precipitation (Fig. 5.3-A) takes into account the rain and the snow components (SCHULZ 2006). In 2002, a high precipitation period occurred during April.

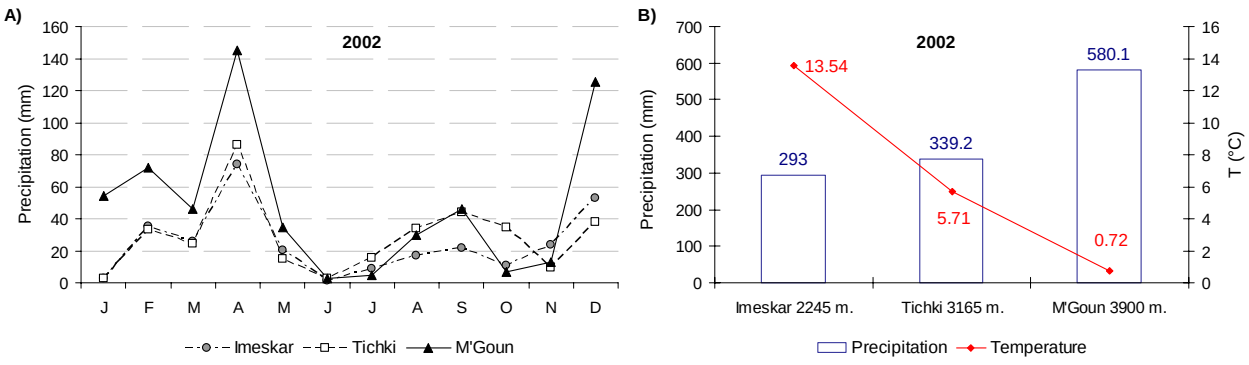

Fig. 5.3: A) Monthly precipitation (rain and snow) at the IMPETUS climatic stations in the Assif-n'Ait-Ahmed catchment for the year 2002 (data after SCHULZ; personal communication); B) Altitude gradient of temperature and precipitation; Gradient of temperature: -0.78 °C/100 m (after BELL 2005).

Due to the orographic effect, strong gradients of temperature and precipitation exist with the altitude (Fig. 5.3-B). Therefore, the catchment is subdivided into three zones represented by the three climatic stations (M'Goun (MG), Tichki (T) and Imeskar (I)) (BELL 2005) (Fig. 5.4). Precipitation data from each station is weighted with the area of each zone. For the year 2002, the total volume of precipitation in the catchment (Pt) is:

$$Pt = \frac{(P_{MG} \cdot A_{MG})(P_T \cdot A_T)(P_I \cdot A_I)}{A_{MG} + A_T + A_I}$$

P_x is the precipitation measured at each climatic station "x" (MG = M'Goun, T = Tichki and I = Imeskar) and A_n the area of each zone which is associated to one meteorological station.

Following this method, the estimation of the total volume of precipitation in the Assif-n'Ait-Ahmed catchment for the year 2002 is equal to 32.5 $\cdot 10^6$ m^3 (Fig. 5.4).

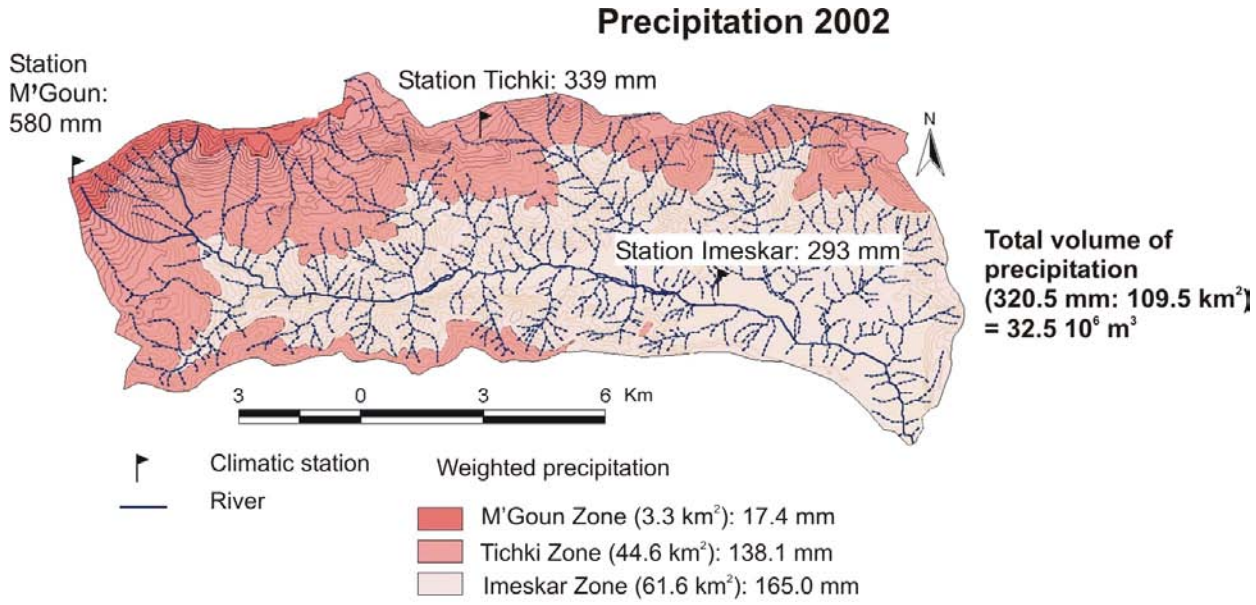

Fig. 5.4: Assif-n'Ait-Ahmed catchment: three zones were defined following the gradient of altitude to be representative of each climatic station. For the year 2002, weighted precipitation was calculated according to these zones and a total precipitation of 320.5 mm for the whole catchment has been calculated (modified after BELL 2005).

5.2.3 Estimation of the evapotranspiration

BELL (2005) calculated the monthly potential evapotranspiration (ETp) at the three IMPETUS climatic stations of the catchment according to THORNTHWAITE (1948) and TURC (1963):

- THORNTHWAITE (1948) is based on monthly data to estimate the potential evapotranspiration (ETp_{Thorn}):

$$ETp_{Thorn} = 0.533 \cdot n \cdot \frac{S_0}{12} \cdot \left(\frac{10 \cdot t}{5}\right)^a \quad \text{(mm/month)}$$

n = number of day, S_0 = mean duration of sunshine per day (h), t = mean of the air temperature (t=0°C for negative temperatures), a = (0.0675 J^3 – 7.71 J^2 + 1792 J + 49,239) x 10^{-5} and

$$J = \sum_{Jan}^{Dec} \left(\frac{t}{5}\right)^{1.514}$$

- TURC (1963) is based on daily data to estimate the potential evapotranspiration (ETp_{Turc}):

$$ETp_{Turc} = 0.027 \cdot C \cdot (R_G + 24) \cdot \frac{t}{t+15} \text{ (mm/day)}$$

$$RF \geq 50 \Rightarrow C = 1 + \frac{(50 - RF)}{70}$$

$$RF \leq 50 \Rightarrow C = 1$$

RF = daily mean of the relative humidity (%), R_G = sum of the global radiation (W/m^2) and t = daily mean of the air temperature (°C) for $t > 5$°C

This estimation of the potential evapotranspiration considers only the periods with daily temperature above 5°C. For $t < 5$°C, ETp is calculated from monthly data according to Ivanov (in DYCK & PESCHKE 1995):

$$ET_P = 0.0011 \cdot (t + 25)^2 \cdot (100 - RF) \text{ (mm/month)}$$

To take into account the real evapotranspiration, BELL (2005) calculated the difference between the amount of precipitation and the potential evapotranspiration (P-ETp) for each month of the year 2002 according to Turc and Thornthwaite. Based on these results the total P–ETp for the year 2002 is calculated for each meteorological station (Tab. 5.1). The extrapolation of these values to the whole catchment was carried out with the method already described for the precipitation. For the year 2002 evapotranspiration was estimated to 14.4 $\cdot 10^6$ m^3 according to Thornthwaite and 3.8 $\cdot 10^6$ m^3 according to Turc. The difference of results is high between both methods. Hence, Turc takes into account the humidity and daily data, the lower values of his estimation seems to be more realistic.

Tab. 5.1: Calculation of P - ETp (P = precipitation, ETp = potential evapotranspiration) according Turc & Thornthwaite (Thorn) for the year 2002 based on monthly mean values.

Station	Altitude (m a.s.l.)	$P_{station}$ (mm)	P - ETp_{Turc} (mm)	P - ETp_{Thorn} (mm)	area (km^2)	P - ETp_{Turc} (mm) weigthed	P - ETp_{Thorn} (mm) weighted
Imeskar	2,245	293	0	91.6	61.60	0	51.6
Tichki	3,165	339	61.4	163.2	44.55	25	66.4
M'Goun	3,900	580	328.3	456	3.30	9.9	13.7
Mean for the whole catchment (year 2002)						34.9 mm 3.8 Mio m^3	131.7 mm 14.4 Mio m^3

5.2.4 Discharges of the Assif-n'Ait-Ahmed Wadi and springs

The Assif-n'Ait-Ahmed Wadi flows over a highly porous bed. An IMPETUS gauge has been installed in order to monitor the discharge of the wadi at the outlet of the catchment, which is located in a small canyon of fracturated carbonates of the Toundoute nappe (Paragraph 4.4.2). Due to vandalism it was necessary to remove it before a sufficient data set was obtained. The available data were completed with punctual measurements. An average discharge of 0.05 m^3/s equivalent to 1.6 $\cdot 10^6$ m^3/a is estimated. This low discharge is explained by the presence of subsurface flow and by high infiltration which occurs in the canyon. It is observed that during flow events, the discharge of the Wadi at the end of the canyon stay almost constant.

Although some springs show karstic features, their discharges don't have important variations during the year. The total discharge of springs for the whole catchment is estimated to 2.24 $\cdot 10^6$ m^3/a, which is more than the estimated discharge of the Assif-n'Ait-Ahmed Wadi. The

difference of discharge between the wadi and the springs is due to sub-surface flows, infiltration and evaporation occurring in the river bed itself which cannot be measured.

5.2.5 Water balance

The water balance of the Assif-n'Ait-Ahmed is based on the simple approximation:

$$P- ETp = Runoff + Subsurface\ flows + Infiltration$$

Subsurface flows being difficult to estimate, the total outflow of surface and subsurface water at the outlet of the catchment is estimated to be equal to the total discharge of the springs (QT springs). Then:

$$Infiltration \approx P - Etp - Q_T\ springs$$

Of course this estimation does not take into account floods of the wadi which are rare in the canyon. Table 5.2 shows the estimation of the infiltration rate for the year 2002 according to the values of $P\text{-}ET_P$ calculated with Turc and Thornthwaite methods. The Thornthwaite method overestimates obviously the P-ET value (44.3 % of the total precipitation) which results to a too high infiltration rate (37.4 % of the total precipitation). With the more accurate method of Turc, the infiltration rate is estimated to 4.8 % of the total precipitation which is more realistic.

Tab. 5.2: Estimation of the infiltration rate in the Assif-n'Ait-Ahmed catchment for the year 2002 calculated from the values of P - ET_P (monthly values of precipitation - potential evapotranspiration) based on Turc and Thornthwaite and the total discharge of springs (Q_T springs). The values are given in m^3/a and in % in regard to the total precipitation of the year 2002.

Year 2002	P		P - ETp		Q_T springs		Infiltration	
	10^6 m^3 /a	%	10^6 m^3 /a	%	10^6 ^{3} /a	%	10^6 m^3 /a	%
Turc	32.50	100.0	3.80	11.7	2.24	6.9	1.56	4.8
Thornthwaite	32.50	100.0	14.40	44.3	2.24	6.9	12.16	37.4

Using Turc for the estimation of the evapotranspiration results in about 29 millions m^3 representing 88 % of the total precipitation for 2002 (Fig. 5.5.). The groundwater recharge during the year 2002 in the Assif-n'Ait-Ahmed catchment is estimated only around 1.6 millions m^3 representing 5 % of the total precipitation.

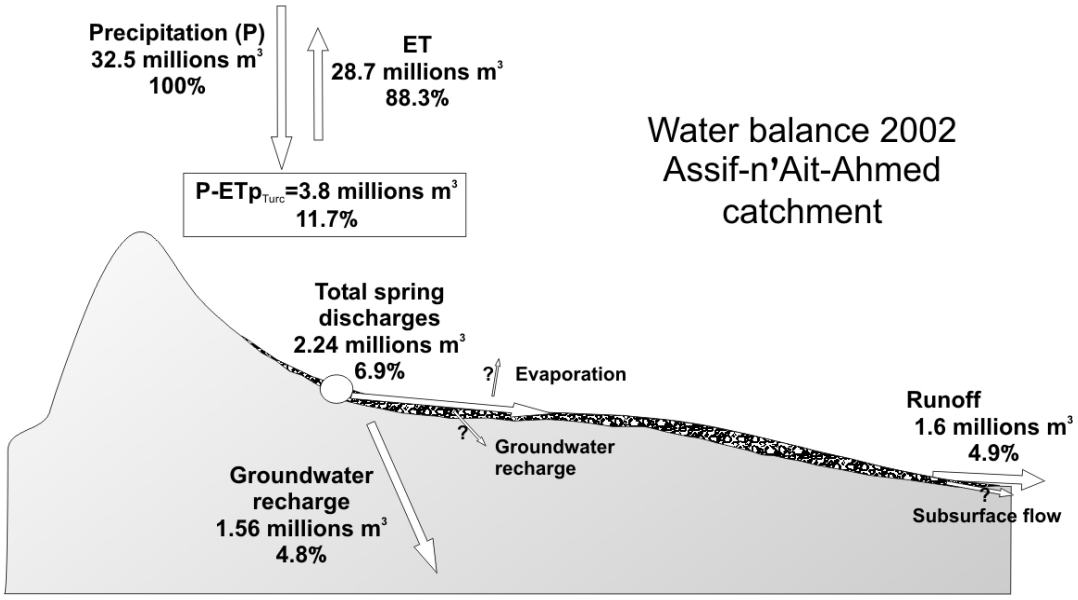

Fig. 5.5: Assif-n'Ait-Ahmed catchment: estimation of the water balance for the year 2002 (millions m^3 and % of the total precipitation).

5.3 Water balance of the Ifre catchment (2002-2003)

5.3.1 Characterization of the catchment

The Ifre catchment is the basin of the M'Goun Wadi up to the village "Ifre" (Fig. 5.1). At Ifre, a DRH monitoring station measures the daily discharge of the M'Goun River. Its area covers approximately 1,240 km^2 between 1,530 m and 4,000 m altitude. The Ifre catchment includes the Assif-n'Ait-Ahmed catchment. For the Ifre catchment, a different approach than for the Assif-n'Ait-Ahmed catchment was chosen to estimate the water balance. Due to the data availability a period between September 2002 and August 2003 is considered.

5.3.2 Estimation of the total precipitation

SCHULZ (2006) defined a gradient of precipitation against altitude (P = 0.285·Alt) from precipitation data at five IMPETUS climatic stations in the Ifre catchment (Fig. 5.6-A). With this gradient and the Digital Elevation Model of the Drâa catchment, the precipitation data was extrapolated at the whole catchment scale and a mean precipitation equals to 407.7 mm (504 millions m^3) was calculated (Fig. 5.6-B).

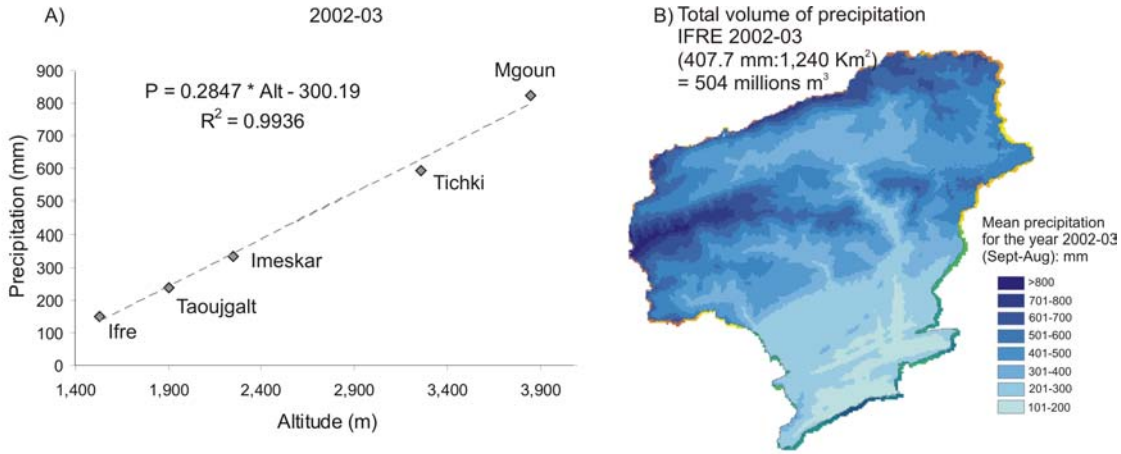

Fig. 5.6: Gradient of the precipitation according to the altitude in the Ifre catchment calculated from the IMPETUS station data (A), and calculation of the total precipitation for the year 2002-03 extrapolated from this gradient and the Digital Elevation Model (DEM) (SCHULZ 2006).

5.3.3 Estimation of the evapotranspiration

Machauer (personal communication) calculated the effective evapotranspiration for the same period (2002-03) with the MMS model using the Jensen-Haise methods (JENSEN & HAISE 1963): ET = 304 mm (377 millions m^3).

5.3.4 Discharge and base flow component of the M'Goun Wadi

The Ifre station measured a total discharge about 65 millions m^3 for the period 2002-03 (from the DRH data). Based on discharge measurements of the M'Goun Wadi at the Ifre station between 1963 and 1987, YOUBI (1990) defined the base flow and runoff components of the surface flow by hydrograph separation method as (Fig. 5.7):

$$Q_{Ifre} = Q_{base\ flow} + Q_{runoff}$$

The proportion of the base flow component ($Q_{base\ flow}$) in comparison to the total discharge at Ifre (Q_{Ifre}) varies between 47% (November) and 90% (July). Taking the mean for one year, the base flow represents 75% of the total measured discharge.

A quantity of the surface water is lost upstream to the Ifre station due to irrigation (evaporation and infiltration) which is evaluated to 8% of the measured annual discharge. At Ifre, the discharge of surface flow is corrected by the irrigation component such as:

$$Q_{\text{Ifre corrected}} = Q_{\text{irrigation}} + Q_{\text{Ifre}}$$

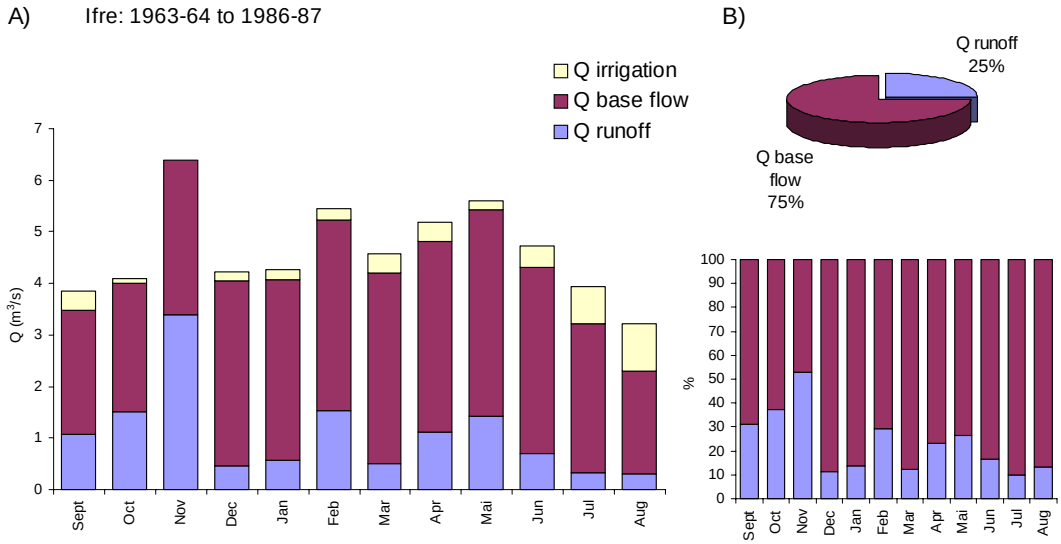

Fig. 5.7: Monthly means of total discharge of the M'Goun River at Ifre (period 1963-87) corrected by losses due to the irrigation (8% of the measured discharge in one year) and base flow and runoff components calculated by hydrograph separation (in m^3s^{-1}) (A); and proportion in % of the base flow and runoff of the real discharge without the irrigation correction, monthly and mean for one year (B) (after YOUBI 1990).

5.3.5 Water balance

Figure 5.8 shows the estimation of water balance for the year 2002-2003 (Sept-Aug) in the Ifre catchment. The evapotranspiration is estimated to approximately 75% of the total precipitation (377 millions m^3). The runoff at the Ifre station represents approximately 13% (65 millions m^3) of the total precipitation and loses of surface water due to the irrigation is estimated to 1% (5.2 millions m^3). The groundwater recharge is estimated at approximately 11% (56.8 millions m^3).

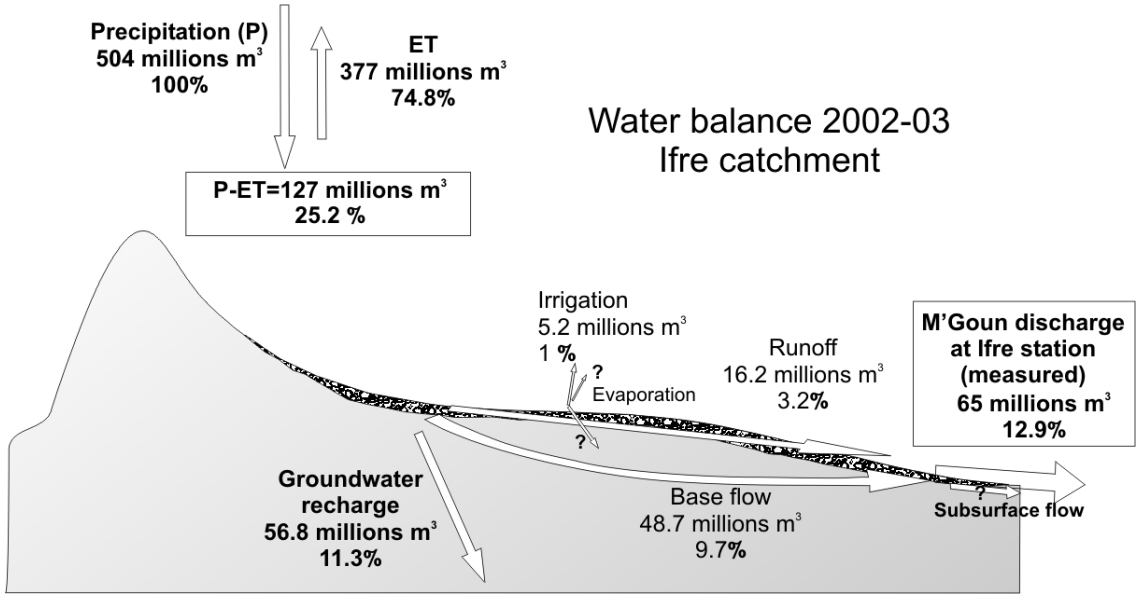

Fig. 5.8: Ifre catchment: estimation of the water balance for the year 2002-03 (Sept-Aug) (millions m^3 and % of the total precipitation).

5.4 Conclusion

The estimation of water balances in the High Atlas has been carried out at two different scales in the Assif-n'Ait-Ahmed catchment (110 km^2) and the Ifre catchment (1240 km^2). The lack of evapotranspiration data does not allow a precise water balance calculation. Moreover, the processes of sublimation of snow are difficult to assess and the soil moisture storage was not taken into account. In the Assif-n'Ait-Ahmed catchment, the discharge of the wadi is not reliable due to technical problem, which makes difficult the estimation of the runoff component. Two different approaches and observation periods have been chosen for the evaluation of the water balance calculation of these basins due to the availability of data, which makes difficult the comparison of the results.

The evapotranspiration in the Assif-n'Ait-Ahmed catchment is roughly estimated with the Turc method to about 90% of the total precipitation. The estimation of the potential evapotranspiration according to Tornthwaite is not accurate in our case. In the Assif-n'Ait-Ahmed catchment, the groundwater recharge is estimated to 5 % of the total precipitation for the year 2002. In the Ifre catchment, the evapotranspiration is calculated with the MMS model using the Jensen-Haise method and represents about 75 % of the total precipitation for the year 2002-2003. The groundwater recharge in this sub-catchment is estimated to 11% of the total precipitation.

These results reflect a high recharge rate of the groundwater in the Ifre catchment (57 millions m^3 for the year 2002-03). This recharge concerns mainly the carbonated aquifer of the Lias. The sink of this aquifer is not known. To validate these estimations, water budgets should be calculated from long data series. Moreover, the evapotranspiration rate is the primordial factor which should be estimated with better accuracy.

6 ISOTOPES OF THE WATER MOLECULE IN RECHARGE PROCESSES

6.1 Introduction

The definition of the isotopic composition of the water molecule (^{1}H, ^{2}H, ^{3}H, ^{16}O and ^{18}O) in precipitation and in groundwater allows the understanding of the recharge processes of aquifers. While the stable isotope ratios $\delta^{2}H$ and $\delta^{18}O$ reflect the origin of groundwater (Paragraph 3.3.1), the content of the radionuclide ^{3}H reveals the mean residence time (Paragraph 3.3.2).

4.2 Stable isotopes (^{2}H and ^{18}O) as natural tracers

The stable isotope composition of groundwater at an observed point represents an integration of the infiltrated precipitation over the recharge area and over time. Thus the isotopic signature of precipitation is of major interest to understand the recharge processes of an aquifer system. In this paragraph, a local meteoric water line (LMWL) is defined and various processes involved in the changes of the isotopic signature of precipitation are described. An isotopic altitude gradient for precipitation and groundwater prevailing in the investigation area is calculated.

6.2.1 Climatic conditions at the IMPETUS meteorological stations

The isotopic composition of the precipitation depends on the various climatic conditions prevailing in the different parts of the Upper and Middle Drâa catchment. Strong temperature and humidity gradients exist between the highest station close to the summit of M'Goun (3,850 m. a.s.l.) in the north (T = 0.7°C and humidity = 50.8 %) and the Iriki station (445 m. a.s.l.) in the south (T = 23.8 °C and humidity = 24.3 %) (Fig. 6.1). Consequently, the Upper and Middle Drâa catchment shows clearly a high variability of the climatic conditions according a gradient of altitude and aridity which will have a high impact on the isotopic composition of the precipitation. Bouskour station (1,420 m. a.s.l.) in the Jbel Saghro shows intermediary values (T = 19.5 °C and humidity = 28.8 %).

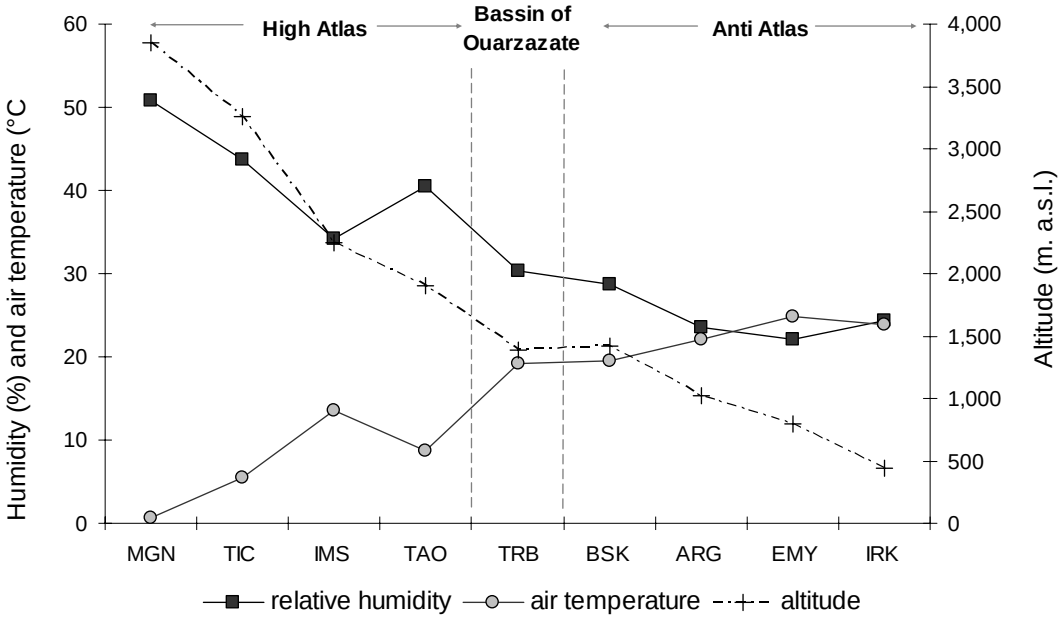

Fig. 6.1: Mean values for the years 2002 and 2003 of the relative humidity (%) and air temperature (°C) in comparison with altitude of 9 IMPETUS climatic stations (MGN = M'Goun, TIC = Tichki, IMS = Imeskar, TAO = Taoujgalt, TRB = Trab Labied, BSK = Bouskour, ARG = Argium, EMY = El Miyit and IRK = Iriki; localisation see Fig. 2.2).

6.2.2 Local Meteoric Water Line (LMWL)

A high variability of the isotopic composition is observed in rain events over the whole catchment with values between -21.4 ‰ and 4.3 ‰ for $\delta^{18}O$ and between -161 ‰ and 28 ‰ for $\delta^{2}H$ (Fig. 6.2). Based on 280 samples of precipitation collected at the IMPETUS climatic stations between summer 2002 and autumn 2004 (Paragraph 3.2.3), a Local Meteoric Water Line (LMWL) (Paragraph 3.3.1.7) was defined:

$$\delta^{2}H = 7.12\ \delta^{18}O + 1.54\ (R^{2}=0.95)$$

The slope of 7.12 reflects the evaporation effect occurring during rainfalls due to the aridity conditions prevailing in the southern part of the catchment (Argium, El Miyit and Iriki), clearly expressed by low relative humidity values around 23 % (Fig. 6.1).

Assuming that the condensation of vapour occurs under equilibrium conditions the LMWL is defined as (Fig. 6.3):

$$\delta^{2}H = 8\ \delta^{18}O + 10.6\ (R^{2}=0.92)$$

where the slope of 8 reflects the equilibrium conditions. In this case the LMWL has an excess value of 10.6 which is close to the GMWL.

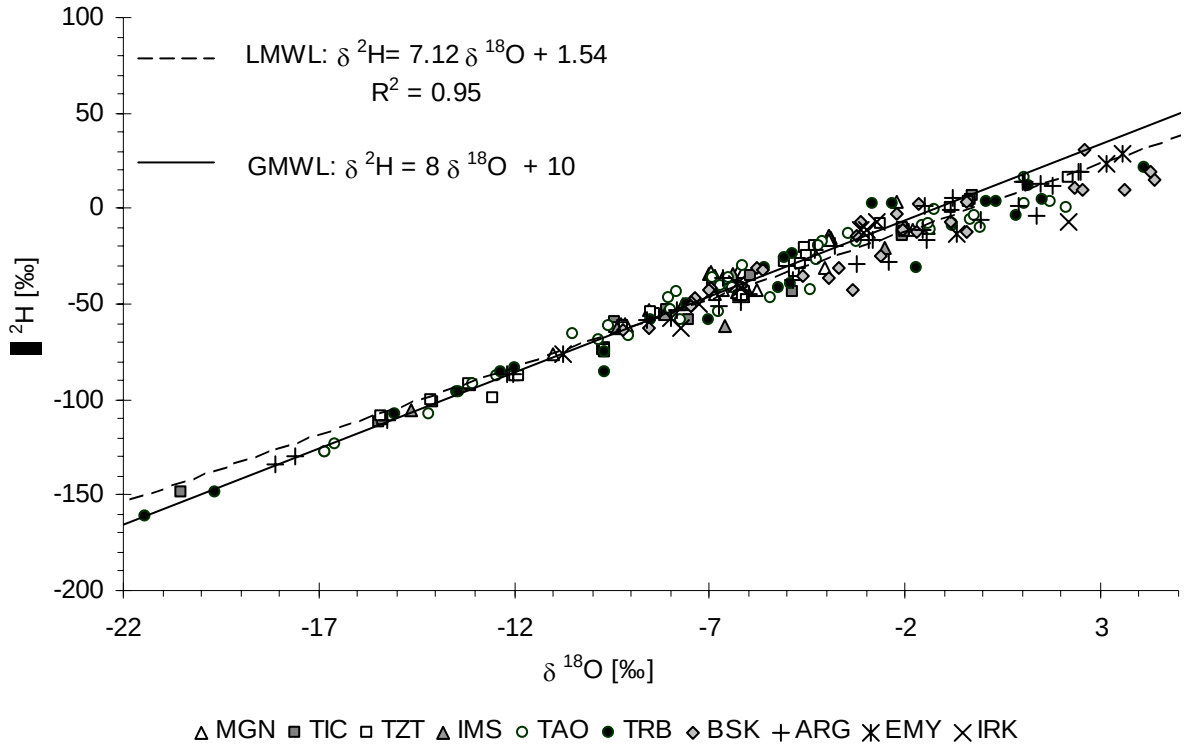

Fig. 6.2: Stable isotopic composition of 280 precipitation samples collected at the IMPETUS climatic stations between summer 2002 and autumn 2004 (MGN = M'Goun, 3,850 m; TIC = Tichki, 3,260 m; TZT = Tizi Tounza, 2,960 m; IMS = Imeskar, 2,245 m; TAO = Taoujgalt, 1,900 m; TRB = Trab Labied, 1,383 m; BSK = Bouskour, 1,420 m; ARG = Argium, 1,020 m; EMY = El Miyit, 792 m and IRK = Iriki, 445 m; localisation see Fig. 2.2), resulting Local Meteoric Water Line (LMWL) and the Global Meteoric Water Line (GMWL, after CRAIG 1961); R^2 = correlation coefficient.

From the weighted mean value of the isotopic composition of precipitation (in regard to the precipitation amount) (Fig. 6.3) is clear that the rain collected at the El Miyit station is the most enriched in heavy isotopes ($\delta^{18}O$ = 2.2‰ and $\delta^{2}H$ = 19‰) due to the high aridity of this zone represented in a relative low humidity of 22%, which is the lowest value recorded at the IMPETUS stations (Fig. 6.1). Due to the altitude effect, the northern stations in the High Atlas

are the most depleted in heavy isotopes (M'Goun: $\delta^{18}O$ = -6.0 ‰ and $\delta^{2}H$ = -35 ‰, Imeskar: $\delta^{18}O$ = -6.4 ‰ and $\delta^{2}H$ = -41‰, Tizi Tounza: $\delta^{18}O$ = -6.5 ‰ and $\delta^{2}H$ = 43 ‰) (Fig. 6.3). It should be noted that for the highest stations (M'Goun 3,850 m and Tichki 3,260 m) technical problems occurred during the sampling. Due to the difficult accessibility during winter, no continuous sampling was possible, which might explain the relative enrichment in heavy isotopes of the weighted mean values in comparison to the lower stations. Moreover, at these altitudes snow can fill the funnel of the rain collector and due to the high variability of the temperature between night and day, alternating melting and icing can occur on this snow changing the isotopic composition of the water by fractionation.

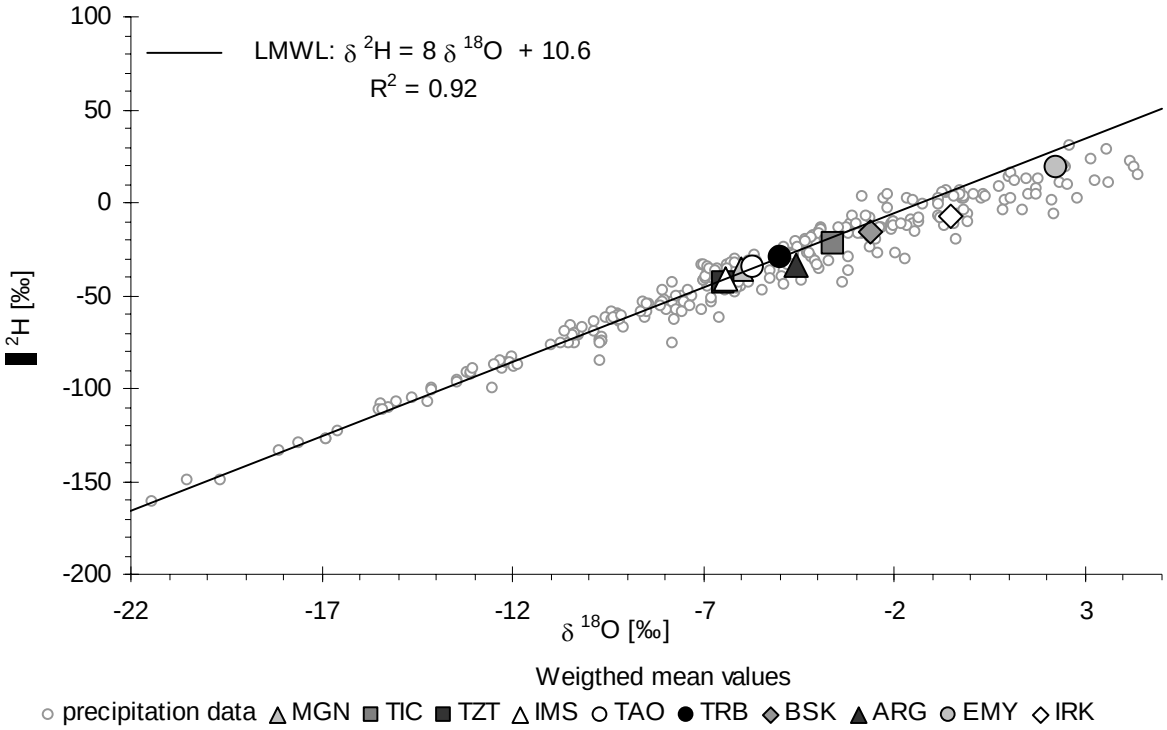

Fig. 6.3: Local Meteoric Water Line defined for a slope of 8 reflecting condensation of vapour under equilibrium conditions: $\delta^{2}H = 8\ \delta^{18}O + 10.6$ and weighted mean values in regard to the precipitation amount; R^2 = correlation coefficient. (MGN = M'Goun, 3,850 m; TIC = Tichki, 3,260 m; TZT = Tizi Tounza, 2,960 m; IMS = Imeskar, 2,245 m; TAO = Taoujgalt, 1,900 m; TRB = Trab Labied, 1,383 m; BSK = Bouskour, 1,420 m; ARG = Argium, 1,020 m; EMY = El Miyit, 792 m and IRK = Iriki, 445 m; localisation see Fig. 2.2).

6.2.3 Seasonal variation

Seasonal variations in the isotopic signature of precipitation have been evaluated using the two main climatological seasons: the humid period from October to April and the dry period from May to September (Fig. 6.4). As representative for all Impetus stations the seasonal effects are described for Imeskar (2,245 m), Taoujgalt (1,900 m), Trab Labied (1,383 m) and Argium (1,020 m). An important enrichment in heavy isotopes during the dry season compared to the humid period occurs. This enrichment in regard to $\delta^{18}O$ is almost similar over the whole catchment with an increasing of the weighted mean between + 6.1‰ (Imeskar) and + 6.6 ‰ (Argium) (Tab. 6.1). The enrichment of heavy isotopes in the summer precipitation can be explained by the fact that the summer precipitation contains more recycled water condensed at a warmer temperature. While the rain events of the humid period plot close to the LMWL (d-excess from 10.7 and 12.1), a clear shifting under the LMWL is observed at the stations of Taoujgalt, Trab Labied and Argium for the precipitations of the dry period (d-excess from -5.3 and -1.9) (Tab. 6.1). This

shifting is due to evaporation effects occurring during the rainfall. The highest station Imeskar is less affected by this evaporation effect (d-excess = 8.3).

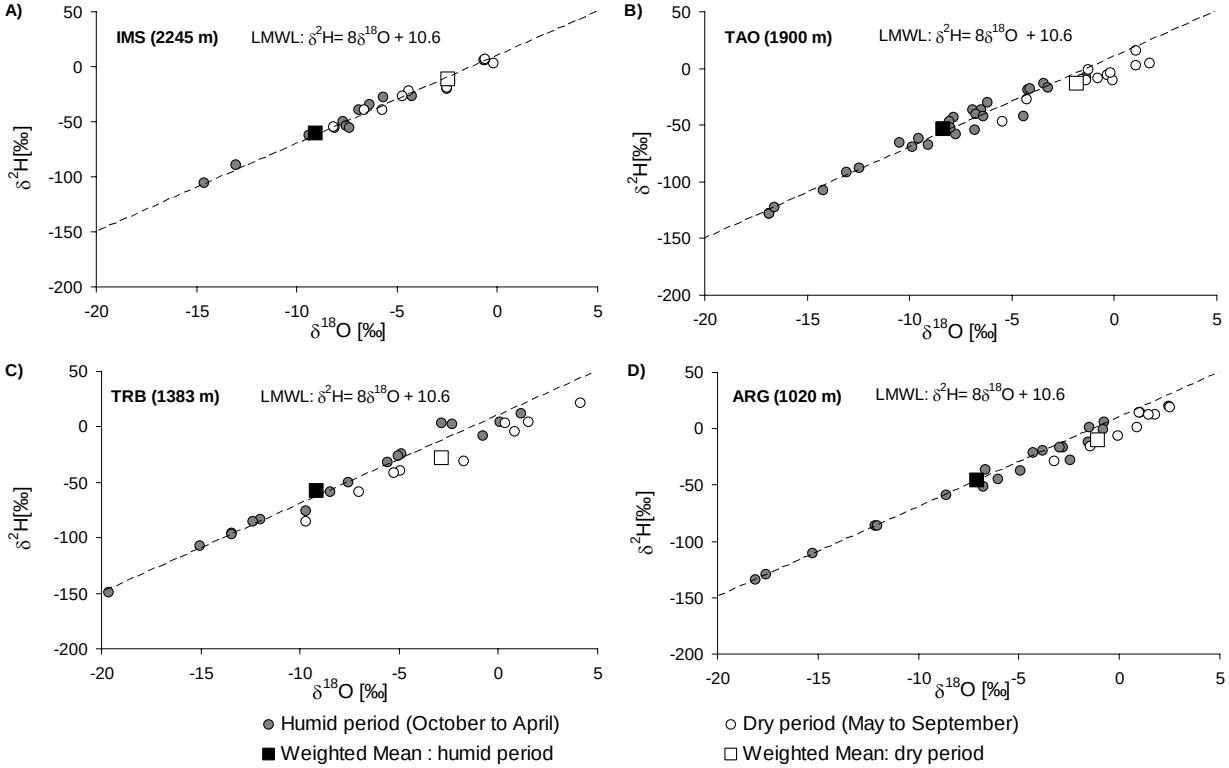

Fig. 6.4: Seasonal variations of stable isotopes in precipitation observed in rain events of the humid (October to April) and the dry period (May to September) collected between summer 2002 and autumn 2004 at the climatic stations IMS = Imeskar, TAO = Taoujgalt, TRB = Trab Labied and ARG = Argium. The weighted mean values in regard to the precipitation amount for the humid and dry season at each climatic station are also given.

Tab. 6.1: Seasonal variations observed in precipitation at 4 climatic stations: weighted mean values characterizing the humid (October to April) and dry periods (May to September).

Stations	Humid period			Dry period			Variation: dry – humid		
	$\delta^{18}O$ (‰)	$\delta^{2}H$ (‰)	d-excess	$\delta^{18}O$ (‰)	$\delta^{2}H$ (‰)	d-excess	$\delta^{18}O$ (‰)	$\delta^{2}H$ (‰)	d-excess
Imeskar	-9.1	-60	12.1	-2.5	-11	8.3	+ 6.6	+ 49	-3.8
Taoujgalt	-8.4	-54	13.2	-1.9	-13	1.7	+ 6.5	+ 41	-11.5
Trab Labied	-9.1	-57	15.7	-2.8	-28	-5.3	+ 6.3	+ 29	-21
Argium	-7.1	-46	10.7	-1.0	-10	-1.9	+ 6.1	+ 36	-12.6

6.2.4 Isotopic characterization of extreme rain events

An extreme rain event occurred in the Drâa valley between March 31 and April 01, 2002. It has been the heaviest storm for the last 25 years in this region with a maximum of 77 mm in 24 hours, which represents more than half of the average annual sum for the Middle Drâa catchment. Such an event is of primordial importance regarding the recharge of the aquifers due to the aridity of the climat. In order to understand the origin of such exceptional rain events, various cases of important precipitation events have been studied in the Drâa valley (Sept 1988, Sept 1990, August-Sept 1999) by KNIPPERTZ et al. (2003). All cases reveal similar tropical-extra tropical interactions (Fig. 6.5). The moisture is transported northward to the east of a mid- to upper-level subtropical trough, which extends deep into the Tropics (KNIPPERTZ et al. 2003). Most of the transport occurs above the dry Saharan planetary boundary layer. The High Atlas Mountains create an orographic lifting responsible for the rainfalls (KNIPPERTZ et al. 2003).

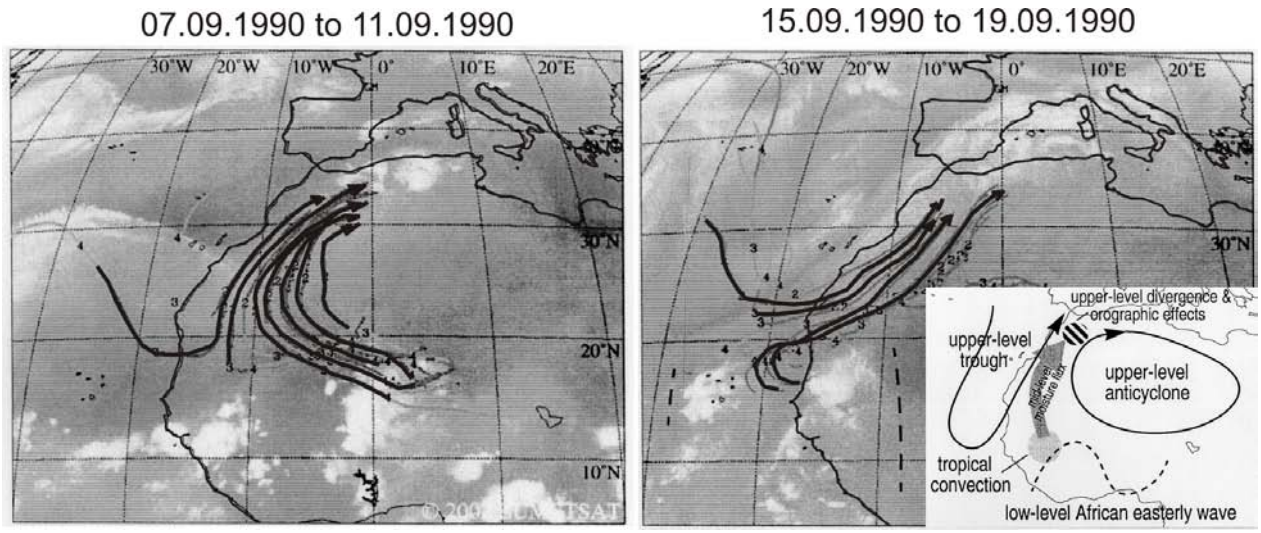

Fig. 6.5: Four-days trajectories over the southern margin of the Atlas Mountains for two cases of extreme precipitations (07.09.1990 to 11.09.1990 and 15.09.1990 to 19.09.1990) (after KNIPPERTZ et al. 2003) and schematic picture of a typical situation of a tropical-extra tropical interactions over west Africa (KNIPPERTZ et al. 2003).

Hence the isotope signatures of extreme rain events are expected to give hints on the air mass movement, selected important rain events were sampled during the time of investigation. Samples of the precipitation of April 01, 2002 (66 mm in two days at the Trab Labied station) are only available for Ouarzazate and only for a few hours. Although the resulting signature does not characterise the whole event, it is still interesting to note a distinct depletion of heavy isotopes in this sample ($\delta^{18}O$ = -10.5 ‰ and $\delta^{2}H$ = -75 ‰; d-excess = 8.9) compared to the weighted mean values at the other IMPETUS meteorological stations (Fig. 6.3).

On December 13, 2002, the IMPETUS meteorological stations recorded 40 mm of precipitation at Tizi Tounza and 24 mm at Trab Labied. This event was completely recorded. Strong isotopic depletions are observed:

- Tizi Tounza station: $\delta^{18}O$ = -15.4 ‰ and $\delta^{2}H$ = -108 ‰ (d-excess = 15.1).
- Trab Labied station: $\delta^{18}O$ = -15.4 ‰ and $\delta^{2}H$ = -107 ‰ (d-excess = 13.1).

Besides this local event, an extreme rain event was monitored over the whole catchment between October 21 and 23, 2003, with isotopic signatures between -21.4 and -2.5 ‰ for $\delta^{18}O$ and -161 ‰ and -21.4 ‰ for $\delta^{2}H$ (Fig. 6.6). Changes in the isotopic composition due to the amount of precipitation (Paragraph 3.3.1.7) were clearly proved for this extreme event (Tab. 6.2).

Tab. 6.2: Amount effect observed during the rain event occurring between October 21 and 23, 2003.

Station	Datum	P (mm)	$\delta^{18}0$	$\delta^{2}H$	d-excess
TRB (1,383 m)	21.10.03	16	-4.9	-24	14.9
	22.10.03	43	-12.3	-85	13.1
	23.10.03	11	-21.4	-161	10.2
ARG (1,020 m)	21.10.03	10	-6.7	-36	16.4
	22.10.03	37	-15.2	-111	10.9
	23.10.03	18	-17.6	-129	11.0

The rain collected over the whole catchment during October 23 is more depleted in heavy isotopes than the rain of October 21. For example, at Trab Labied station the $\delta^{18}O$ values vary from -4.9 ‰ the first day (21.10.03: 16 mm) over -12.3 ‰ the second day (22.10.03: 43 mm) to -

21.4 ‰ the third day (23.10.03: 11 mm) (Fig. 6.6). Although, this extreme rain event shows clear depletion in heavy isotopes, the regression line of the rain samples with an excess value of 10.63 is close to the LMWL, which proves the same origin of the vapour masses than for the other rains (Fig. 6.6).

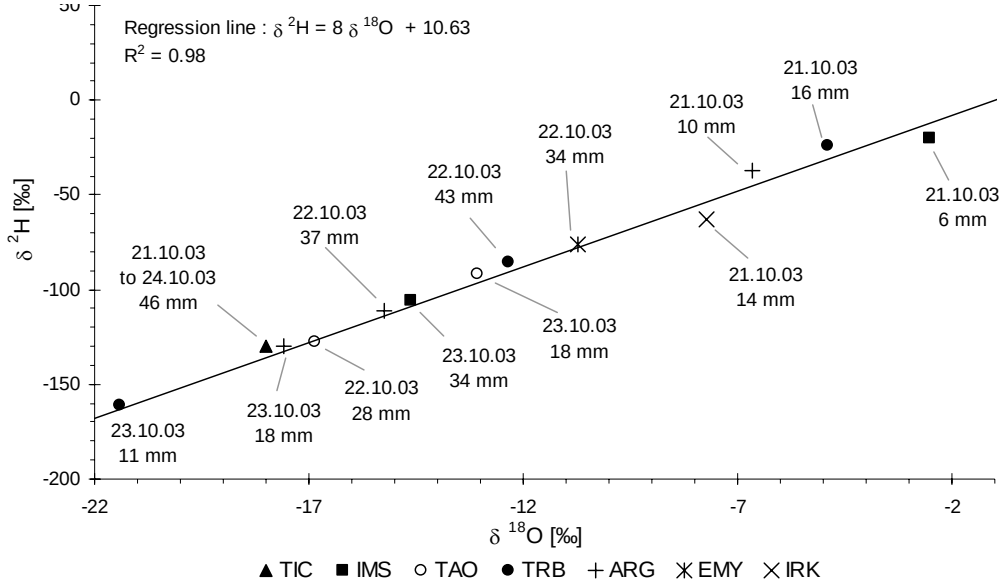

Fig. 6.6: Isotopic contents of precipitation during the extreme event in the Upper and Middle Drâa catchment between October 21 and 24, 2003. The regression line ($\delta^2H = 8\ \delta^{18}O + 10.63$) is close to the LMWL; TIC = Tichki, IMS = Imeskar, TAO = Taoujgalt, TRB = Trab Labied, ARG = Argium, EMY = El Miyit and IRK = Iriki (localisation see Fig. 2.2).

6.2.5 Isotopic characterization of snow

The snow cover of the High Atlas plays an important role in the recharge processes in high altitudes. SCHULZ (2006) showed that the snow represents about 50 % of the total precipitation at the Tichki station (3,260 m) (compare Fig. 5.2). In order to assess the influence of snow on the groundwater recharge, sampling of snow was carried out at different periods, altitudes and depths for an isotopic characterization (Fig. 6.7).

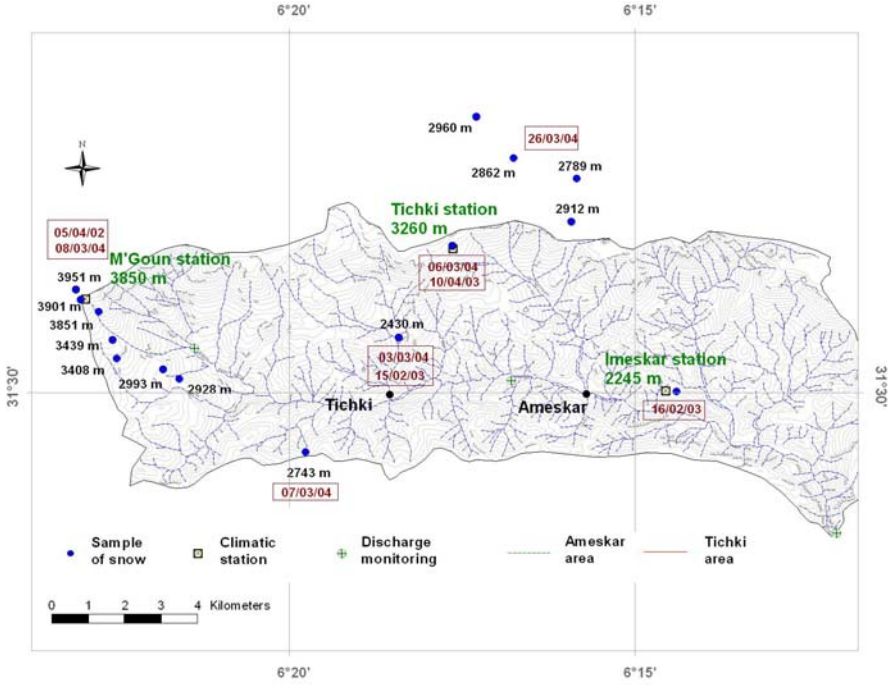

Fig. 6.7: Sampling of snow in the Assif-n'Ait-Ahmed catchment at different periods, altitudes and depths.

At all, 34 samples of snow were collected. Melt water was also sampled at one natural puddle. The mean value of these samples shows strong depletion of heavy isotopes in comparison with the rain: $\delta^{18}O$ = -10.3 ‰, $\delta^{2}H$ = -70 ‰ and d-excess= 12.2. Hence, the processes involved in the isotopic composition of the snow pack are multiple during the formation of snow, accumulation, ablation and phase changes during the melting, only a general description can be given.

The isotopic composition of the collected snow is close to the LMWL. Most of the samples have $\delta^{18}O$ values between -12.3 ‰ and -4.9 ‰ (Fig. 6.8-A). In contrast the fresh snow of the extreme event occurring between October 21 to 24, 2003 shows strong depletion in heavy isotopes due to the amount effect: $\delta^{18}O$ = - 25.1 ‰ and $\delta\ ^{2}H$ = -184 ‰ (Fig. 6.8-A). No altitude effect on the isotopic contents of snow is observed (Fig. 6.8-B). Its isotopic signature is more controlled by variations in the isotopic content of the individual precipitation event. For example, the snow from the precipitation event of October 2003 has similar isotopic signatures even though they were collected at two different altitudes (2,800 and 3,500 m).

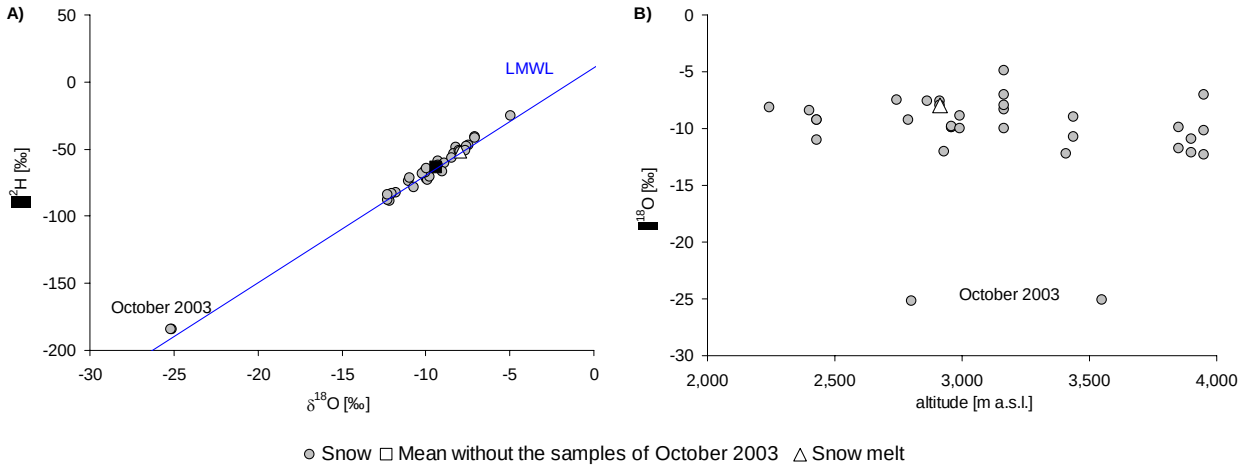

Fig. 6.8: Isotopic contents of snow in the Assif-n'Ait-Ahmed catchment (A) and snow $\delta^{18}O$ versus altitude (B); sampling of fresh snow of the precipitation event occurring between 21 to 24 October 2003 shows strong depletion in heavy isotope.

Although fractionation occurs during snow melt, which is multiple due to refreezing or sublimation processes, it is assumed in accordance to literature (e.g. LAWRENCE 1987, GIBSON et al. 1993) that the isotopic content of snowmelt is almost similar to the snow from which it melts. The sample of melt water confirms this having a similar isotopic signature as the snow sampled at the same altitude and at the same day: $\delta^{18}O$ = -8.0 and $\delta^{2}H$ = -51 (d-excess = 12.3) (Fig. 6.8-A and B).

Following a snow fall event on March 2, 2004 a detailed snow sampling campaign was carried out in the Assif-n'Ait-Ahmed catchment between March 4 and 8. The isotopic contents of snow was analysed at 5 different places: Tizi Tounza station (TZT 2,960 m), Tichki station (TIC 3,260 m) and various altitudes on the M'Goun (3,439 m, 3,091 m, 3,951 m) (Fig. 6.9). At each sampling point the total depth of snow was collected. Each sample is the integration over several decimetres of snow.

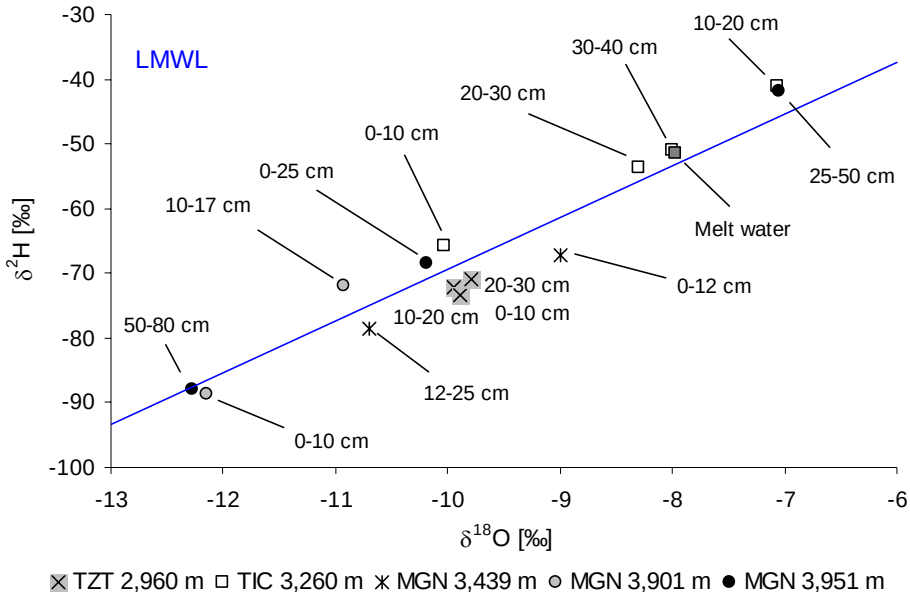

Fig. 6.9: Sampling campaign carried out between 4th and 8th March 2004 (last snowfall: 2nd March) at different altitudes and depths of snow (0 corresponds to the surface of snow); TZT = Tizi Tounza, TIC = Tichki and MG = M'Goun.

Snow packs show significant variations in their isotopic signature depending on the depth (Fig. 6.9). These variations seem to reveal the different origin of the snow formed during different precipitation events rather than fractionation occurring during the melt processes. Nevertheless, a correlation between the isotopic content of the snow and the temperature in the snow pack sampled at MGN 3,951 m (Fig. 6.10) exists but could not be interpreted due to the lack of information about the formation of this snow pack.

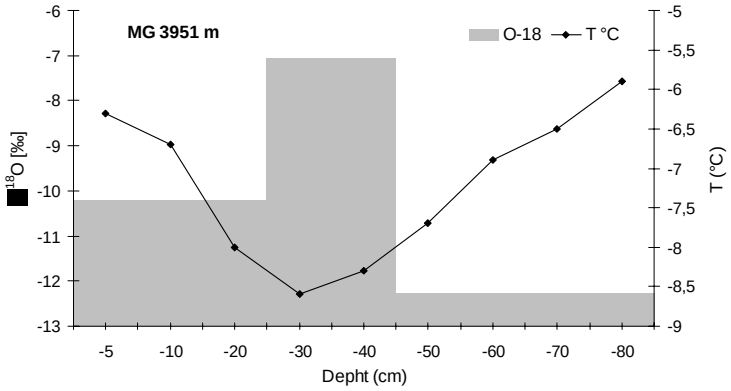

Fig. 6.10: Isotopic composition of the snow at the M'Goun (3951 m), δ18O [‰] and Temperature (°C) versus depth of snow.

6.2.6 Local altitude gradient of $\delta^{18}O$ for precipitation

The comparison of $\delta^{18}O$ data in rainfall with the altitude defines a gradient for the IMPETUS stations. For each station, the weighted mean in regard to the precipitation amount of the rain $\delta^{18}O$ is calculated. In order to take into account the influence of snow, a correction was done for the stations of M'Goun (3,850 m), Tichki (3,260 m) and Imeskar (2,240 m) (Tab. 6.3). Here, the proportion of snow in the total precipitation was calculated according to SCHULZ (2006) (compare Fig. 5.2) with the mean value of $\delta^{18}O$ of the 34 snow samples (Fig. 6.2). Using the weighted $\delta^{18}O$ mean values of precipitation sampled at all stations (Tab. 6.3) a local altitude gradient of $\delta^{18}O$ in precipitation of the Upper and Middle Drâa catchment of **0.20 ‰ per 100 m** is found (Fig. 6.11).

Tab. 6.3: Weighted $\delta^{18}O$ of precipitation at 8 IMPETUS station along the altitude gradient in the Upper and Middle Drâa catchment. The values of three upper stations (MGN, TIC and IMS) are corrected with the mean value of $\delta^{18}O$ of 34 samples of snow ($\delta^{18}O$ = -10.3 ‰).

Stations	Altitudes m a. s.l.	Type of precipitation (Number of sample)	Rain weighted $\delta^{18}O$ [‰]	Rain weighted $\delta^{18}O$ [‰] corrected with snow
M'Goun(MGN)	3,850	Rain 14 % (30) + snow 86 %	-5.9	-9.7
Tichki (TIC)	3,260	Rain 50 % (16) + snow 50 %	-3.6	-6.9
Imeskar (IMS)	2,200	Rain 75 % (26) + snow 25 %	-6.4	-7.0
Taoujgalt (TAO)	1,900	Rain (35)	-5.7	-5.7
Trab Labied (TRB)	1,383	Rain (19)	-5.0	-5.0
Argium (ARG)	1,020	Rain (23)	-4.6	-4.6
Bouskour (BSK)	1,420	Rain (25)	-3.2	-3.2
Iriki (IRK)	445	Rain (4)	-1.6	-1.6

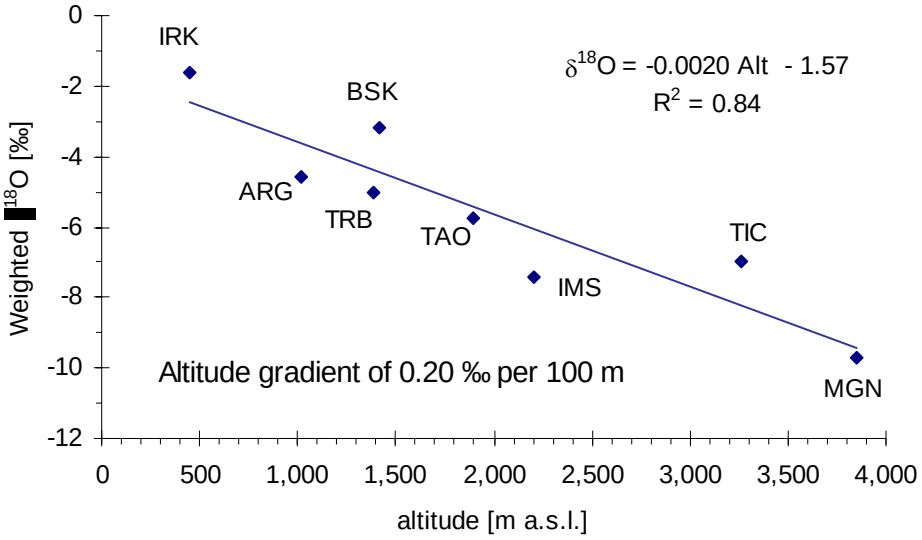

Fig. 6.11: Gradient of $\delta^{18}O$ [‰] versus altitude (m a .s.l.) of precipitation in the Upper and Middle Drâa catchment : 0.2 $\delta^{18}O$ per 100 m (MGN : M'Goun, TIC : Tichki, IMS: Imeskar, TAO : Taoujgalt, TRB : Trab Labied, BSK : Bouskour, ARG : Argium and IRK : Iriki).

Although the precipitation of the extreme event of October 2003 shows strong depletion in heavy isotope (see above), the resulting altitude gradient is with 0.29 ‰ per 100 m close to the local altitude gradient (Fig. 6.12).

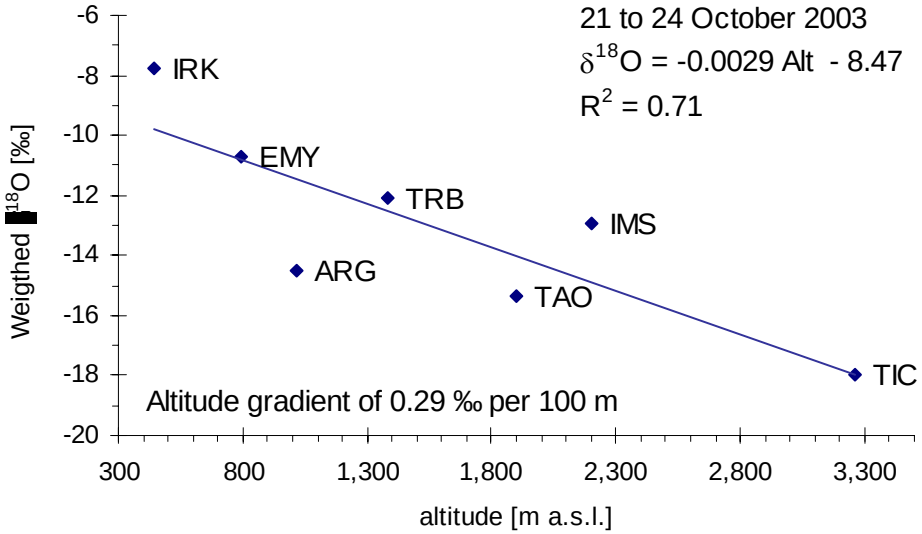

Fig. 6.12: Altitude gradient of $\delta^{18}O$ [‰] of precipitation versus altitude (m a.s.l.) of the extreme rain event between 21 to 24 October 2004.

6.2.7 Relation between $\delta^{18}O$ and groundwater mean recharge altitude

From the precipitation data set, the local $\delta^{18}O$ altitude gradient of the Upper and Middle Drâa catchment is defined as being 0.2 ‰ per 100 m (Fig. 6.11). This gradient can be used to estimate the mean recharge altitude of aquifers (FONTES 1976). But, beforehand it is necessary to verify this gradient for groundwater and to define the precise relationship between the $\delta^{18}O$ value of springs and the mean altitude of the recharge area. With the Digital Elevation Model (DEM), an estimation of the mean altitude of the catchment (corresponding to the recharge area) of six springs located in the High Atlas draining small sub-catchments (< 4 km^2) was delimited (Tab. 6.4 and Fig. 6.13). The spring 175 (150 km^2) is used to prove the relation within a bigger catchment.

Tab. 6.4: Mean altitude of recharge of 7 springs estimated with the Digital Elevation Model and $\delta^{18}O$ of the groundwater (location of springs: see Fig. 6.13).

Sample name	Altitude of springs m a.s.l.	Area (km^2)	Mean altitude estimated with the DEM (m. a.s.l.)	$\delta^{18}0$ [‰]
AFL	2,385	3	3,500	-9.88
147	2,810	2.7	3,360	-9.81
133	2,770	3 .5	3,350	-9.67
28	2535	3	3,100	-9.14
21	2,250	1.2	2,907	-9.02
74	2,308	3.4	2,600	-8.09
175	1,770	150	2,700	-8.38

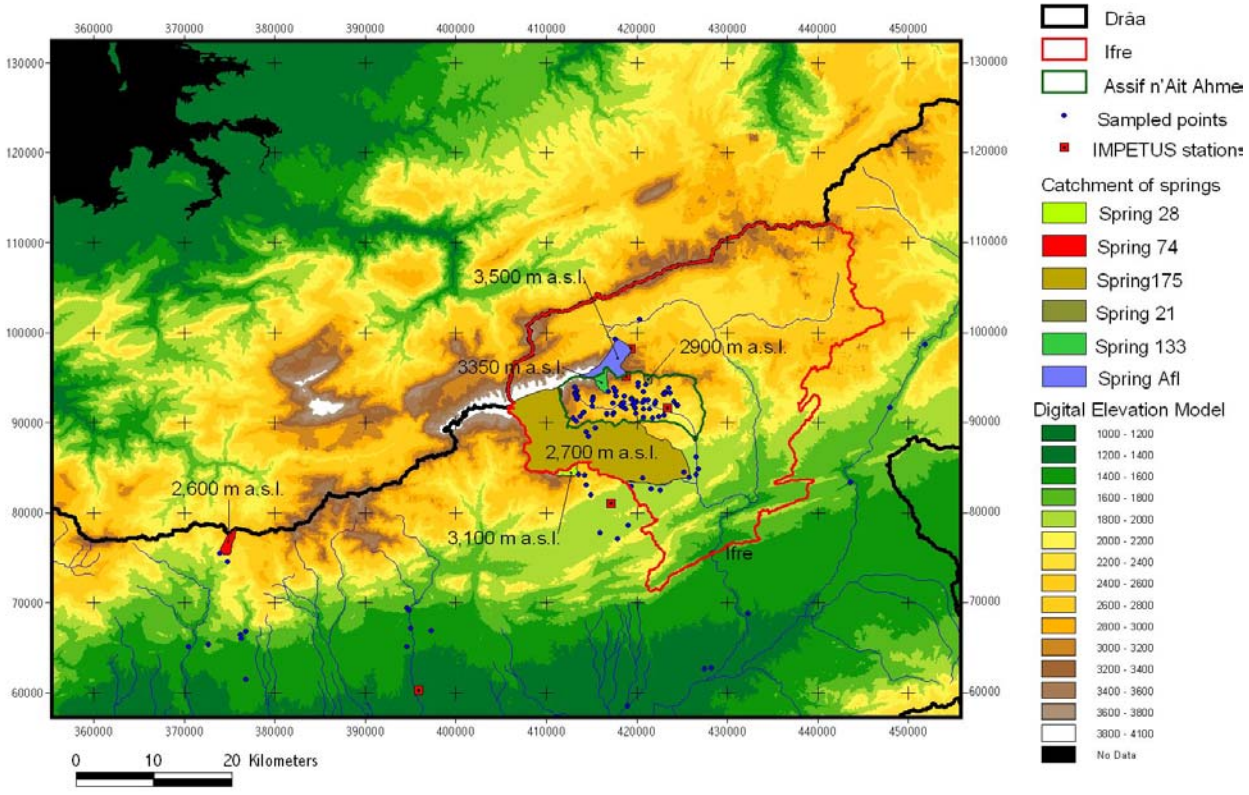

Fig. 6.13: Estimation of the mean altitude of the recharge area of 7 springs with the Digital Elevation Model (DEM).

The mean altitudes of the recharge areas calculated with the DEM of these seven springs are plotted according to the $\delta^{18}O$ values of groundwater (Fig. 6.14). The linear regression of these points gives a relation as **$\delta^{18}O$ = - 0.002 · "mean altitude of the recharge area"-3.0** (R^2=0.97).

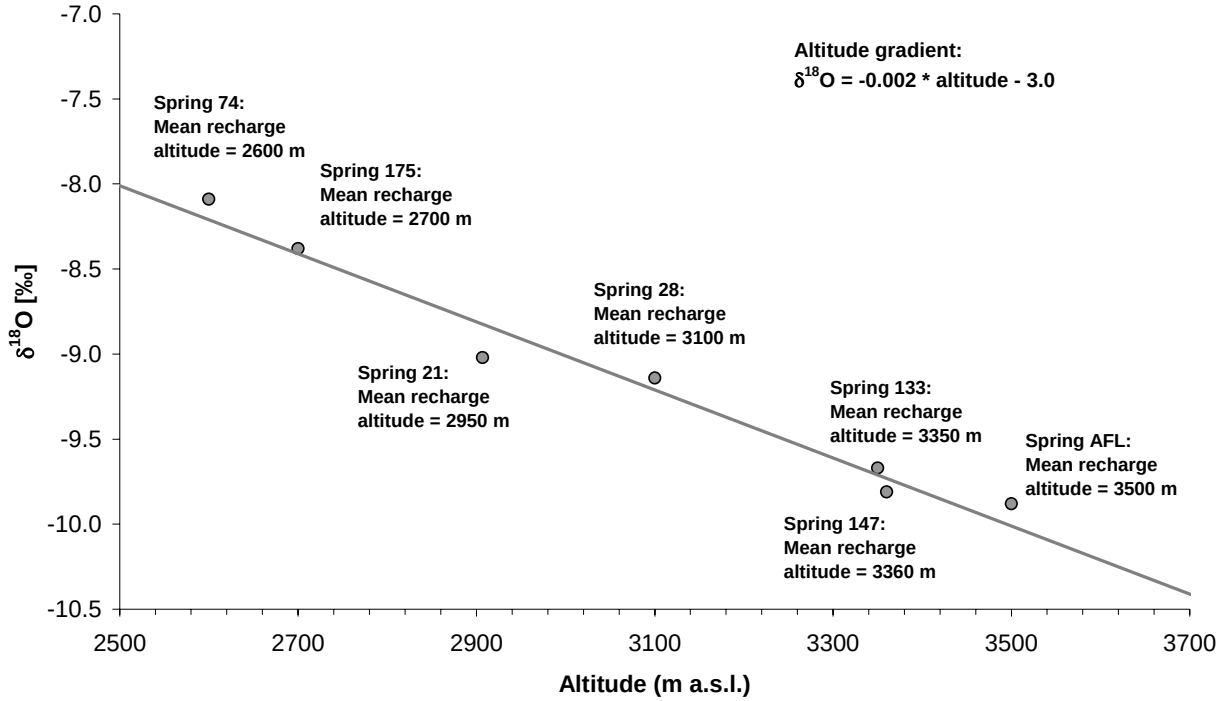

Fig. 6.14: Relation between the recharge altitude of springs calculated with the DEM and the mean $\delta^{18}O$ value of groundwater: $\delta^{18}O$ = -0.002 · "mean altitude of the recharge area" -3.0..

Hence the gradient of 0.2 $\delta^{18}O$ per 100 m determined from the precipitation data is the same as the relation $\delta^{18}O$ versus "Altitude" found using the DEM this equation allows to estimate the mean altitude of recharge of the groundwater in the Upper Drâa catchment. Due to the analytic precision, the error is about +/- 50 m.

EL OUALI et al. (1999) determined a local altitude gradient for the Errachidia basin located east of the Upper Drâa catchment which is with **$\delta^{18}O$ = -0.0027 · "altitude"-4.18** (R^2=0.85) close to the local altitude gradient found for the Upper Drâa catchment.

6.3 The radionuclide tritium (^3H) as a time marker

The "age" of groundwater has important implications for water resource management. Young groundwater reveals aquifers continuously renewed and potentially sustainable in regard to their exploitation. The recharge of the various aquifers of the Upper Drâa catchment is therefore assessed by the estimation of the mean transit time of the groundwater, which can be estimated from the decay of the radionuclide tritium (^3H) (Paragraph 3.3.2).

6.3.1 Tritium in precipitation as an input function

From a global network established by the IAEA (www.iaea.org/ programs/ri/gnip/ gnipmain.htm), the annual mean of tritium in precipitation at Tunis is used as input function (Fig. 6.15). The choice of using the tritium values in precipitation at Tunis (Tunisia) is motivated by the fact that this data set is the only one in North Africa with an almost complete record from 1968 up till now. Additional it clearly reflects the peak due to the nuclear weapon test in 1963/64.

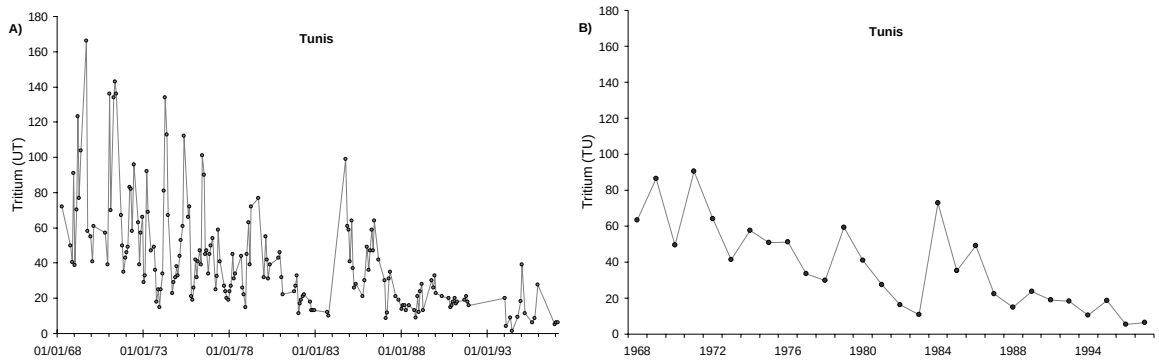

Fig. 6.15: Tritium content in precipitation at Tunis (Tunisia): data set available (A) and annual mean values (B) (Source: www.iaea.org/ programs/ri/gnip/ gnipmain.htm).

6.3.2 Interpretation of the tritium data of the groundwater

During autumn 2002 (IMP5) 50 samples of groundwater were collected in the Upper Drâa catchment for tritium analyses. Results of the analyses show ^{3}H values of groundwater ranging between 0.7 TU (precision of the measurement) and 10.2 TU. The mean residence time estimation of the groundwater from the tritium data is calculated using lumped parameter approaches (BoXmodelV3) (Paragraph 3.4.1). Due to the radioactive decay of the tritium, this method allows the estimation of mean residence time between few to 50 years (ZUBER & MALOSZEWSKI 2000).

Unconfined aquifer

In order to isotopically characterise unconfined aquifers an exponential model (EM) (ZUBER 1986, MALOSZEWSKI & ZUBER 1993, ZUBER & MALOSZEWSKI 2000) is used to describe (Fig. 6.16-A, B, C, D, E and F). Taking into account the range of tritium values observed in the groundwater of the Upper Drâa catchment (between 0.7 and 10.2 TU), three representative tritium values are discussed exemplarily for the interpretation: 10 TU, 6 TU and 3 TU sampled 2002. The model uses the tritium composition of precipitation at Tunis as input function (Paragraph 6.3.1). According to the results of the exponential model:

- A value of tritium equal to 10 TU observed corresponds to a residence time equal to 8 years or more than 50 years (Fig. 6.16-A). The calculated tritium concentration for a residence time (τ) equal to 8 years shows a good agreement with the observed concentration (10 TU) of groundwater in the year of sampling (Fig. 6.16-B).
- A value of tritium equal to 6 TU observed corresponds to a residence time < 2 years or more than 50 years (Fig. 6.16-C). The calculated tritium concentration for a residence time (τ) equal to 2 years shows a good agreement with the observed concentration (6 TU) of groundwater in the year of sampling (Fig. 6.16-D).
- A value of tritium equal to 3 TU observed corresponds to a residence time higher than 50 years (Fig. 6.16-E). The calculated tritium concentration for a residence time (τ) equal to 50 years shows that there is no intersection with the observed concentration (3 TU) at the year of sampling (2002) due to the limit of the method which cannot dated groundwater older than 50 years (Fig. 6.16-B).

An exponential model (EM) does not take into account the dispersion processes, which might change the estimated mean residence time. Therefore, a dispersion model (DM) is tested. The

concentration of tritium is calculated for three different dispersion parameters (Pd = 0.1, 0.4 and 0.8) (Fig. 6.16-G and H). The resulting estimations of the mean residence time are similar for groundwater showing tritium values below 10 TU (Fig. 6.16-G). Consequently, according to the observed values of tritium concentration in the groundwater of the Upper Drâa catchment (< 10 TU), the dispersion effect in the interpretation of the groundwater dating is considered as negligible.

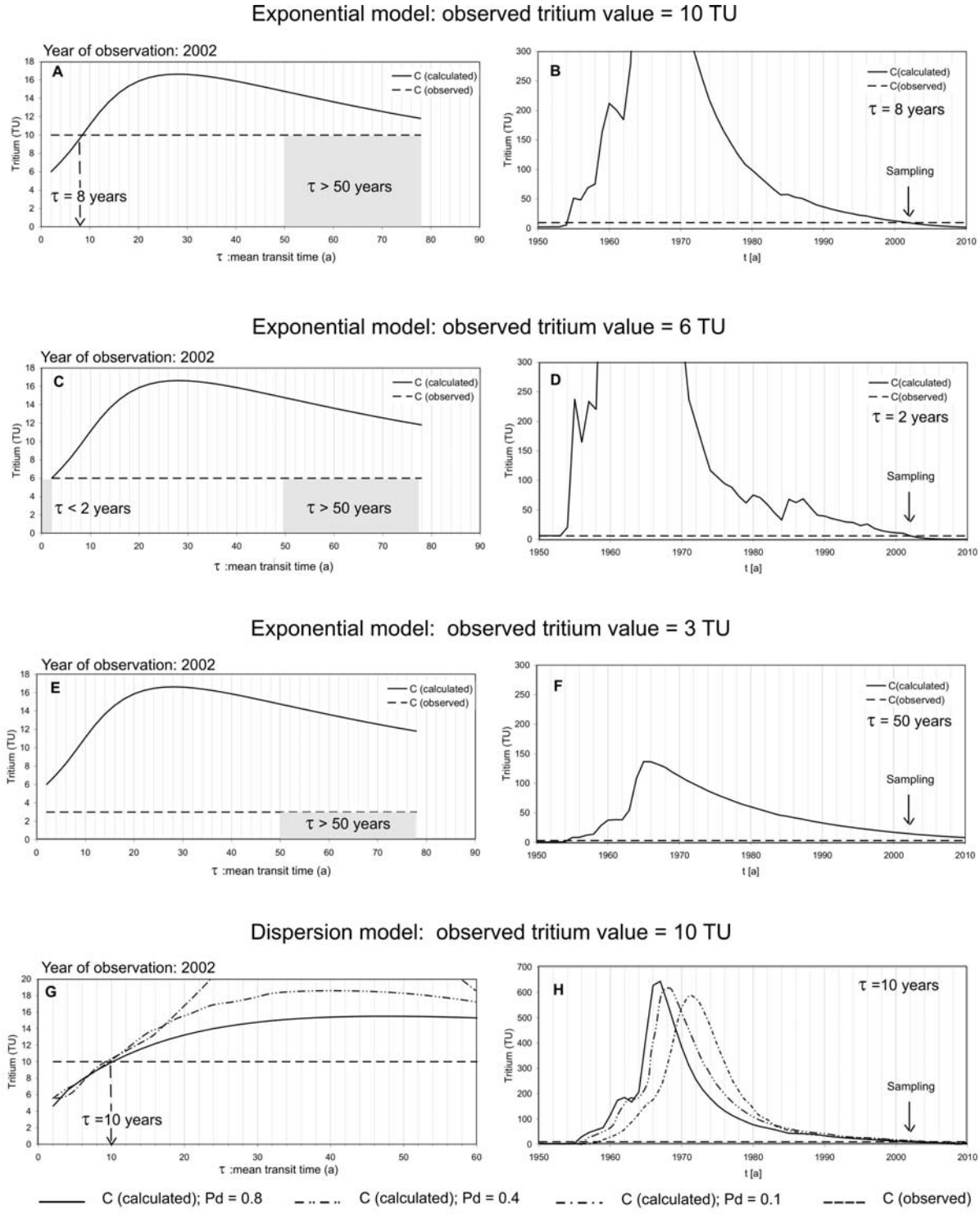

Fig. 6.16: Results of exponential and dispersion models with the tritium content in precipitation at Tunis as input function. The results are described for three tritium values. The mean residence time graphs (A, C, E, G) show the calculated concentration of ^{3}H as a function of "τ" (mean residence time) for 2002. The output graphs (B, D, F, and H) show the calculated ^{3}H concentration as a function of time t for a given parameter "τ". Graphs G and H give the results of dispersion model for three dispersion parameters (Pd = 0.8, 0.4 and 0.1) compared to a tritium value of 10 TU; (BoxmodelV3).

For the interpretation of the tritium data of the groundwater of unconfined aquifers in the Upper Drâa catchment the exponential model was applied based on the following results:

- Tritium values between 0 TU and 3 TU reveal a mean residence time of the groundwater greater than 50 years.
- Tritium values between 3 TU and 4 TU can not be clearly interpreted.
- Tritium values between 4 TU and 7 TU reveal a mean residence time between 0 to 4 years or more than 50 years.
- The Tritium values between 7 TU and 10 TU reveals a mean residence time between 4 to 8 years or older than 50 years.

The mean values of tritium in the precipitations observed at the end 1990's at Tunis averaging 6 TU (Fig. 6.15), the assumption of recent groundwater for groundwater tritium values between 4 TU and 10 TU is privileged. In this case, interpretations of tritium values have to take into account the hydrogeological framework of the considered aquifer.

Confined aquifer

Interpretation of the mean residence time of groundwater from a confined aquifer is done with a piston flow model (Fig. 6.17). Thus, groundwater showing tritium values below 2.5 TU in 2002, has a mean transit time higher than 45 years.

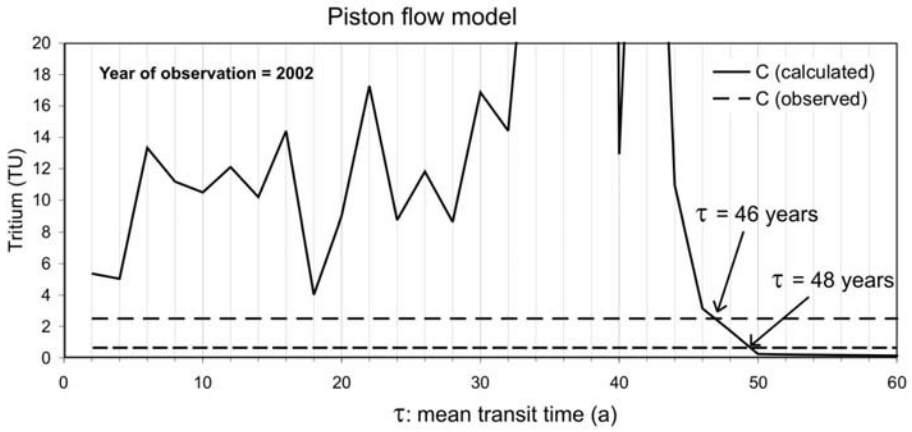

Fig. 6.17: Results of piston flow model using tritium content in precipitation at Tunis (Tunisia) as input function. The mean transit times of groundwater sampled in 2002 showing either a tritium value equal to 0.7 TU or 2.5 TU are estimated; (BoxmodelV3).

6.4 Conclusion

Based on isotopic analyses of rain samples collected at 10 IMPETUS meteorological stations between summer 2002 and autumn 2004 along a gradient of aridity and altitude, a local meteoric water line (LMWL) is defined for the middle and upper Drâa catchment such as:

$$\delta^2H = 8\ \delta^{18}O + 10.6\ (R^2=0.92)$$

The isotopic composition of rain shows high ranges of $\delta^{18}O$ (from -21.4 to 4.3 ‰) and δ^2H (from -161 to 28 ‰). Seasonal variations are observed with a clear enrichment in heavy isotopes during the dry season (May to September) compared to humid season (October to April) due to more recycled water condensed at warmer temperatures for the summer rain. The isotopic characterization of extreme rain events reveals a clear depletion of heavy isotopes due to the

“amount effect”. The isotopic characterization of these extreme rain events is important to understand the local recharge of the Basin of Ouarzazate.

The isotopic composition of the snow cover in the High Atlas was identified for different periods, altitudes and depth. But, the complex processes which are involved in the fractionation of the snow during its formation and its melting have not been clearly elucidated. The mean values of the isotopic ratios observed from 34 snow samples are: $\delta^{18}O$ = -10.3 ‰, $\delta^{2}H$ = -70 ‰ with a d-excess of 12.2.

Based on weighted mean $\delta^{18}O$ of the rain and taking into account the influence of the snow, a local altitude gradient for the precipitation in the High Atlas is defined, which averages 0.20 ‰ per 100 meter. Validated with the estimation of the mean altitude of the recharge area of seven springs of the High Atlas with the DEM, the following relationship is defined for groundwater:

$$\delta^{18}O = -0.002 \cdot \text{”altitude”} - 3.0 \quad (R^2 = 0.97)$$

The radionuclide tritium is used as time marker to estimate mean residence time of young groundwater (until 50 years) applying lumped parameter approaches. While, an exponential model is used to interpret tritium data in unconfined aquifers, a piston flow model was used for confined aquifers. Hence no long-term Moroccan tritium data are available the annual mean of tritium in precipitation at Tunis (Tunisia) is used as input function.

7 HYDROGEOLOGY OF THE JBEL SAGRHO AND OF THE HIGH ATLAS

7.1 Introduction

Knowledge of the aquifer systems prevailing in the Upper Drâa catchment is primordial to estimate the groundwater resources. In this chapter, the hydrogeological descriptions of the aquifer systems including a hydrogeochemical characterization of the groundwater of the Jbel Saghro (Anti Atlas) and of the High Atlas are presented. In the High Atlas, conceptual hydrogeological models of the Assif-n'Ait-Ahmed and Ifre catchments are proposed.

7.2 The Jbel Saghro

In order to characterize the groundwater geochemistry in the Jbel Saghro, three wells were investigated close to the mine of Bouskour: 80, 81 and 82 (compare Fig. 3.2). In this area Precambrian rocks are prevailing with alkaline granites, sub-alkaline granodiorites, acid dykes and the volcano-detritic series of Ouarzazate (Paragraph 4.3.1 and compare Fig. 4.8-A). Although highly fractured no prolific aquifer is observed in the Precambrian formations of the Jbel Saghro due to the low infiltration capacity of the rocks and to the scarcity of the local precipitation (annual mean value of precipitation at the IMPETUS station of Bouskour for the years 2002 to 2004 is 142 mm/a). The main groundwater storage is developed within small alluvial aquifers along the wadis, where the investigated wells are localised. The alluvial aquifers are made up of pebbles, sand and clays resulting of erosion and weathering of the Precambrian formations.

7.2.1 Hydrogeochemical characterization of the groundwater

The groundwater sampled in the Jbel Saghro (Bouskour test-site) reveal different hydrogeochemical characteristics (Tab. 7.1 and Fig. 7.1). Well 80 can be classified as a groundwater of the Ca-Mg-Na-HCO_3-SO_4 type, well 81 as Ca-Mg-Na-SO_4-HCO_3-Cl type and well 82 as Ca-Mg-HCO_3 type, which reflects the local variability of the alluvial aquifers. Well 81 shows clearly an effect of leaching of evaporitic minerals such as halite and gypsum with higher values of Na^+ (109.9 mg/l), Cl^- (182.1 mg/l) and SO_4^{2-} (424 mg/l) (Tab. 7.1).

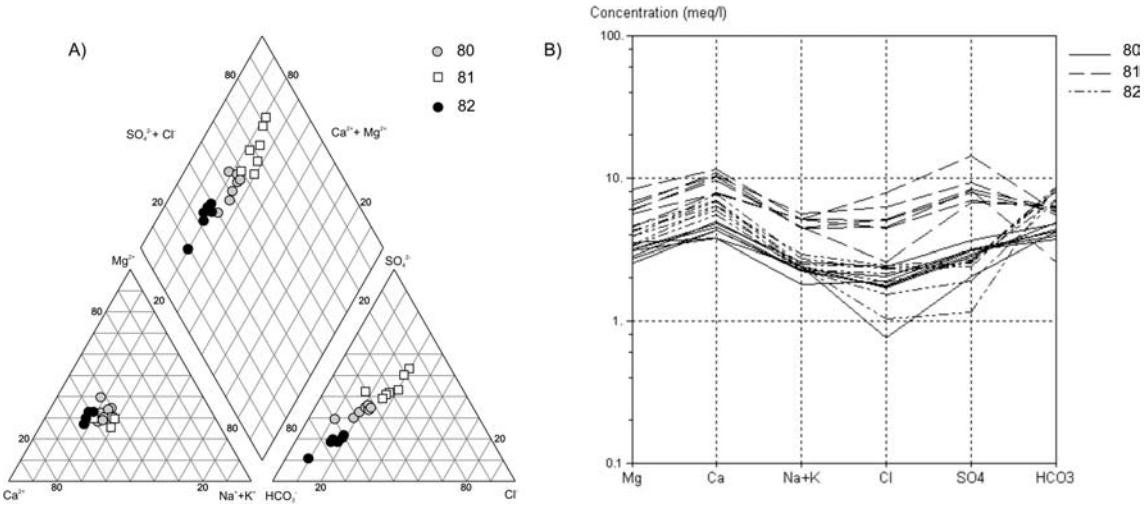

Fig. 7.1: Hydrogeochemical characteristic of the groundwater sampled in the Jbel Saghro (Bouskour test-site): Piper (A) and Schoeller (B) diagrams.

The values of SiO_2 (between 8.6 and 11.7 mg/l) and Mg^{2+} (36.8 to 76.0 mg/l) reveal that the groundwater is relatively evolved, which can be proved by the saturation indexes (Fig. 7.2).

Tab. 7.1: Hydrochemical characteristics (mean values) of the wells sampled in the Jbel Saghro (Bouskour)

wells	Ca^{2+} (mg/l)	Mg^{2+} (mg/l)	Na^{+} (mg/l)	K^{+} (mg/l)	SiO_2 (mg/l)	Fe_{total} (µg/l)	Mn^{2+} (µg/l)	Sr^{2+} (mg/l)	HCO_3^{-} (mg/l)	Cl^{-} (mg/l)	NO_3^{-} (mg/l)	SO_4^{2-} (mg/l)
80	87.1	36.8	49.4	5.7	8.6	14	22	1.1	262.5	62.6	14.3	143.6
81	195.5	76.0	109.9	5.3	11.1	18	4	2.2	336.9	182.1	35.0	424.1
82	131.3	47.9	54.3	5.7	11.7	15	30	1.3	494.4	69.6	10.2	109.3

The groundwater of the wells from the Bouskour test-site is under-saturated in regard to gypsum ($-0.81 < SI_{gypsum} < -1.77$) and in equilibrium to over-saturated in regard to calcite ($-0.16 < SI_{calcite} < 0.78$) (Fig. 7.2-A). While the groundwater is in equilibrium to over-saturated in regard to dolomite ($-0.43 < SI_{dolomite} < 1.38$), it is in equilibrium to slightly oversaturated in regard to quartz ($-0.02 < SI_{quartz} < 0.42$) (Fig. 7.2-B). Thus the groundwater in the area of Bouskour shows evolved groundwater particularly in regard to quartz, which reveals groundwater passage within magmatic material of Precambrian age as debris in the alluvium or within the Precambrian rocks.

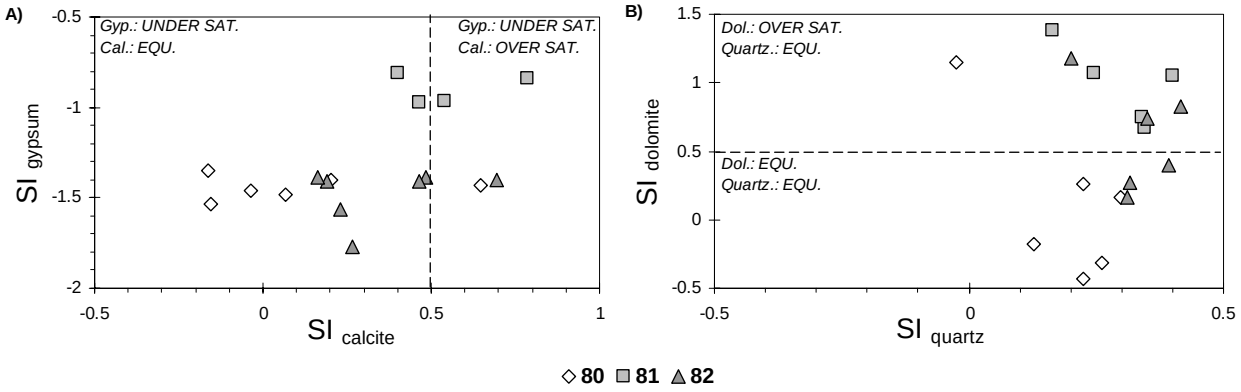

Fig. 7.2: Saturation indexes (SI) of the groundwater in the Jbel Saghro (Bouskour test site): SI_{gypsum} versus $SI_{calcite}$ (A) and $SI_{dolomite}$ versus SI_{quartz} (B).

7.2.2 Isotopic characterization

Isotopic analyses ($\delta^{18}O$ and $\delta^{2}H$) have been carried out for each campaign. The isotopic composition of the wells 80, 81 and 82 ranges between $-7.3 ‰ < \delta^{18}O < -5.5‰$ and $-49 ‰ < \delta^{2}H < -38‰$ (Fig. 7.3). The mean values of the stables isotopes of these wells are:

- well 80: $\delta^{18}O$ = -5.9 ‰, $\delta^{2}H$ = -39.5 ‰ and d-excess value = 8.0
- well 81: $\delta^{18}O$ = -6.6 ‰, $\delta^{2}H$ = -44.4 ‰ and d-excess value = 8.1
- well 82: $\delta^{18}O$ = -7.0 ‰, $\delta^{2}H$ = -46.4 ‰ and d-excess value = 9.6

Although the samples plot slightly below the Local Meteoric Water Line the mean d-excess values between 8.0 and 9.6 reveal distinct evaporation effect.

Tritium analyses are performed for well 80 on the 02.10.2002. With a value of 5.6 TU and according to the interpretation for unconfined aquifer (Chapter 6) well 80 shows young groundwater (< 4 years). Due to the fact that an age dating is only available for a single sample it is difficult to generalise to the other wells of the Jbel Saghro. Hence, the low saturation indexes of calcite ($SI_{calcite}$ = -0.15) and dolomite ($SI_{dolomite}$ = -0.31) of this sample might reveal a dilution with recent rain water (due to missing data the amount of precipitation is unknown for this period at the Bouskour station).

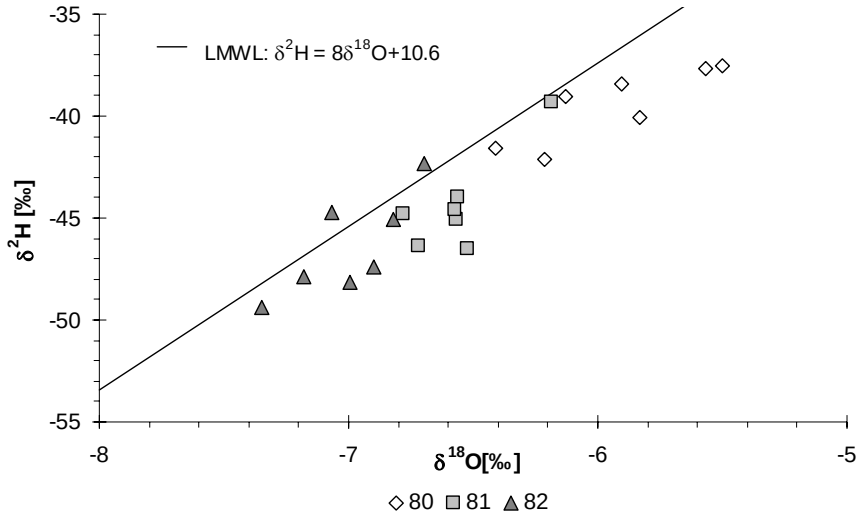

Fig. 7.3: Isotopic composition of the groundwater in the Jbel Saghro (Bouskour test-site).

7.3 The High Atlas

In order to describe the aquifer systems prevailing in the north of the Upper Drâa catchment, in the High Atlas mountains and to understand the relations between these aquifers and the Basin of Ouarzazate (Chapter 8), investigations have been carried out at two different scales, in the Assif-n'Ait-Ahmed catchment (110 km^2) and in the Ifre catchment (1,240 km^2). The properties of the aquifer systems are known from precise geological mapping. Based on hydrogeochemical analyses, the various types of groundwater are classified with statistical methods. The geochemical processes occurring along the groundwater flow paths are identified. To complete the understanding of the groundwater origin, the mean recharge altitudes of the aquifers as well as the mean residence times of the groundwater are evaluated from the isotopic composition of groundwater (^2H, ^{18}O, ^3H). As results, hydrogeological conceptual models of the catchments of Assif-n'Ait-Ahmed and Ifre are presented. In order to complete the characterization of the groundwater from the High Atlas aquifers, two springs in the Cambrian and Precambrian schists of the Skoura mole and two wells in the Dades canyon were sampled.

7.3.1 The Assif-n'Ait-Ahmed catchment

7.3.1.1 Hydrogeological overview

The Assif-n'Ait-Ahmed catchment is developed in an anticline of a west-east axis where the overthrusted massive Liassic limestones and dolomites of the "Toundoute Nappe" (Paragraph 4.4.2) overlie the Triassic sediments. The Triassic series crop out along the lower slopes in a tectonic window (Fig. 7.4 and compare Fig. 4.22). In this catchment, 67 springs were sampled for hydrogeochemical and isotopic analysis. The springs are mostly located at the contact between the Liassic formations and the Triassic clays as a "boundary spring" type or along faults within the Triassic basalt. Discharges of springs were monitored during each campaign. Low groundwater outflows with average discharge values around 1 l/s and maxima about 10 l/s are observed. Two springs (123 and 137) located in the bottom of the valley and in the middle of the catchment show the highest discharge (Fig. 7.4).

Precise geological mapping together with detailed lithological descriptions (OSTERHOLT 2002, HOFMANN 2002, BELL 2005, BUDEWIG *in progress* and this work) allow a hydrogeological classification of the various formations (Tab. 7.2). The two main geological formations of the

catchment are the Jurassic carbonates (Toundoute nappe and Agoulzi Formation) and the Triassic formations (Ait Aadel and Tafilalt formations).

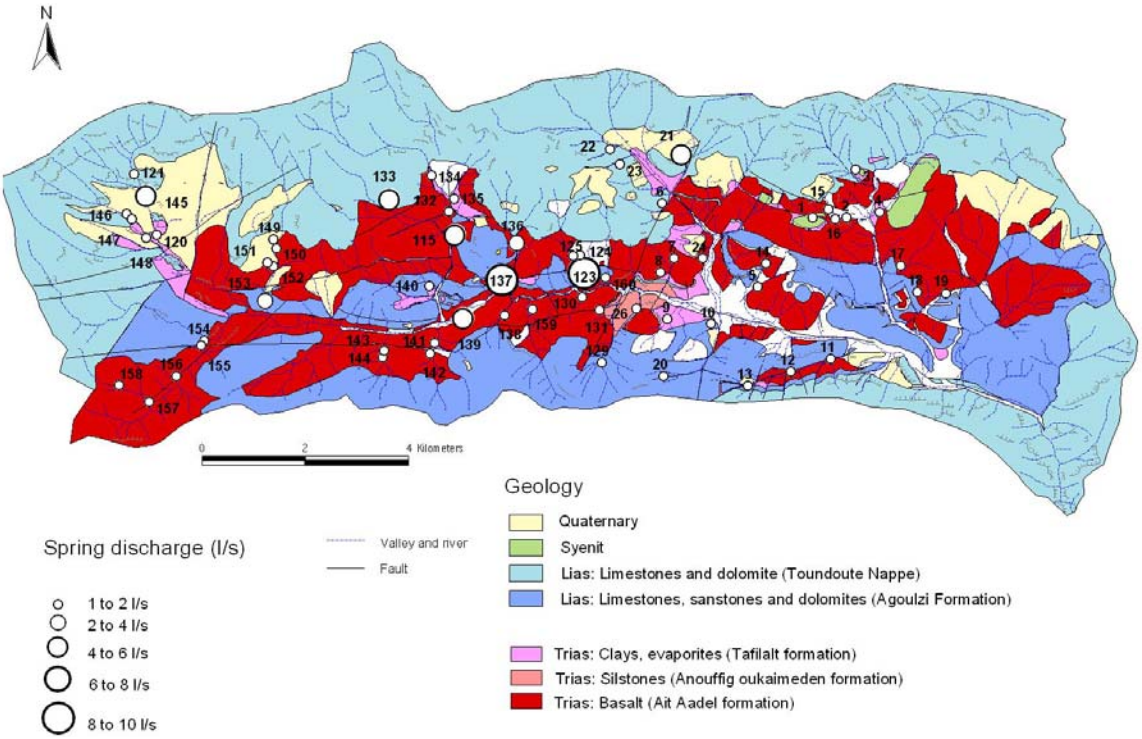

Fig. 7.4: Geological map of the Assif-n'Ait-Ahmed catchment (after OSTERHOLT 2002, HOFMANN 2002, BELL 2005, BUDEWIG in *progress* & this work), the numbers denote the sampled springs, the size of the circles show their discharge.

Tab. 7.2: Hydrogeological classification and hydrodynamic characteristics of the various geological formations in the Assif-n'Ait-Ahmed catchment.

Formations / Hydrogeological classification	Lithology	Aquifer volume [10^6 m^3]	Efficient porosity [%]	Potential ground-water volume [10^6 m^3]	K [m/s]	Discharge springs [10^6 m^3/a]
Quaternary / porous aquifer	breccias	120	1 - 5	1.2 - 6	10^{-3} to 10^{-2}	0.14
Lias (Toundoute nappe) / fractured to karstified aquifer	limestone, dolomite	17,800	1 - 2	178 - 356	10^{-6} to 10^{-3}	1.02
Lias (Agoulzi formation) / fractured aquifer	sandstone, limestone, dolomite	1,200	1 - 2	12 - 24	10^{-6} to 10^{-3}	0.62
Trias (Tafilalt formation) / aquitarde	clay	-	-	-	$<10^{-9}$	-
Trias (Ait-Aadel formation) / fractured aquifer	doloritic basalt	5,300	0.1 - 3	5 - 154	10^{-11} to 10^{-7}	0.46

The **Jurassic carbonates** (limestones and dolomite) cover approximately 60 % of the catchment with a maximal thickness of 400 m. Some karstic features (dolines and poljes) are observed within this formation in the south of the catchment. The Jurassic limestones and dolomites are clearly the most important aquifers. They are characterized by a significant primary porosity. The total volume of these formations can be estimated (Tab. 7.2) taking into account an efficient porosity between 1 to 5 % typical for carbonates formations (CASTANY 1963). Thus, a potential volume of groundwater was calculated of 0.19 to 0.38 km^3. Based on discharge measurements of springs draining the carbonates, a total outflow is estimated of about 1.64 million m^3/a (Tab. 7.2). The numbers given are rough estimations due to the fact that the unsaturated zone, which is generally deep in mountainous areas had to be neglected

because of the lack of appropriate data. Moreover, deep groundwater flow systems often extend beyond the boundaries of small catchments and losses occurring into underlying aquifers had to be neglected.

The **Triassic formations** cover approximately 24% of the catchment area and consist mainly of basalt (Ait Aadel formation) overlaid by clays (Tafilalt formation) which contain evaporitic minerals (Fig. 7.4). The thickness of this formation is between 150 m and 300 m. With an efficient porosity between 0.1 % and 3 % (HOFMANN 2002) the permeability of the Triassic rocks is low. But the basalt in the Assif-n'Ait-Ahmed catchment is locally densely fractured which increases the permeability at a small scale. Due to the presence of the overlying clays of the Tafilalt Formation which fill also faults and fractures in the basalt, the Triassic formations can be considered as a hydrogeological boundary of the Jurassic aquifer, and therefore as its aquitard.

7.3.1.2 Hydrogeochemical characterization of the groundwater

The groundwater of the 67 springs collected in the Assif-n'Ait-Ahmed catchment shows basic pH ranging between 7.12 and 8.42, which is typical for carbonate aquifers (Fig. 7.5). As expected from the geological setting, the groundwater samples exhibit a high variability in respect to the chemical composition, which reflects the groundwater passage within the Jurassic carbonate aquifer more or less affected by the leaching of evaporitic minerals of the Trias.

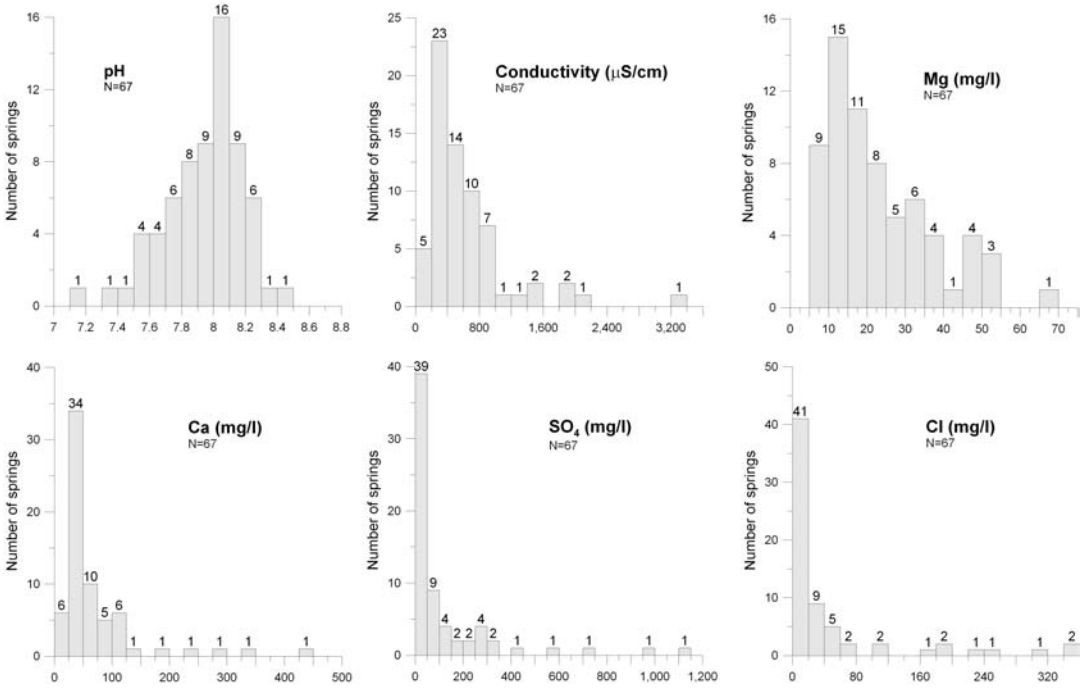

Fig. 7.5: Histograms of the mean values of electric conductivity, pH and some ions majors (Ca^{2+}, Mg^{2+}, Cl^- and SO_4^{2-}) for 67 springs values (N = number of springs) collected in the Assif-n'Ait-Ahmed catchment.

During the period of investigation, the groundwater of the Assif-n'Ait-Ahmed catchment shows very low variations in the hydrochemical contents, e.g. in the electric conductivities (EC) as a representative of the whole mineralization (Fig. 7.6-A) or in selected chemical parameter (Fig. 7.7). Springs with mean conductivities below 1,000 µS/cm show standard deviations ranging between 3 and 30 µS/cm, while springs with a mean conductivities between 1,000 µS/cm and 3,164 µS/cm show standard deviations between 7 and 235 µS/cm (Fig. 7.6-A). Although the air temperature in the Assif-n'Ait-Ahmed catchment shows high variations during the year (from -4°C to 25.5°C in 2003 with a mean value about 13.5°C at Imeskar station), groundwater shows

only low temperature deviations (standard deviation SD < 2°C) (Fig. 7.6-B). Even the two springs with higher discharges (123 and 137, Fig. 7.6 B) show a very constant temperature (SD < 0.5 °C) close to the annual mean value of the air temperature. Hence well developed karst aquifers are usually characterised by high variations in discharge, temperature and chemistry (BAKALOWICZ et al. 1995, CAPPY 2001) the low variability in the hydrochemical parameters in the groundwater of the Assif-n'Ait-Ahmed catchment proves an only slight degree of maturation of the karst aquifer in the Liassic carbonates.

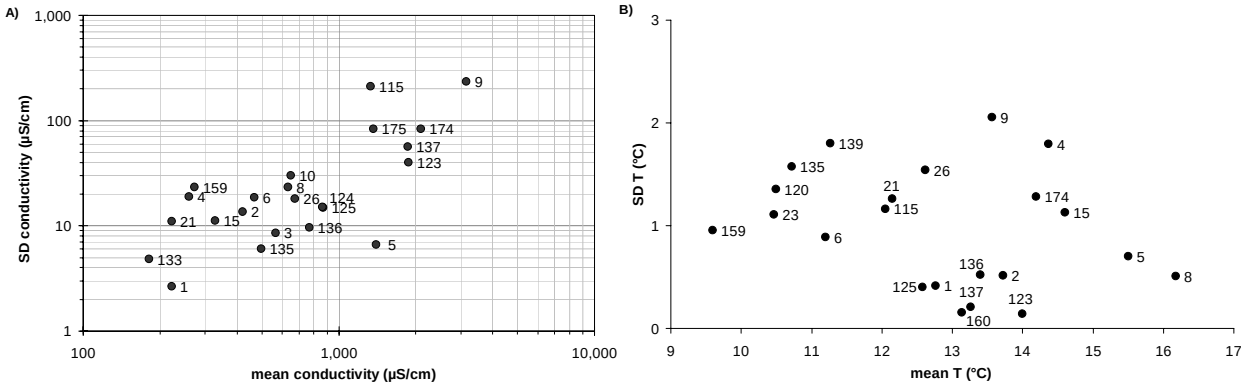

Fig. 7.6: Standard deviation (SD) versus mean values of conductivity (A) and mean values of T (°C) (B) of groundwater in the Assif-n'Ait-Ahmed catchment; Only springs with complete data series are selected.

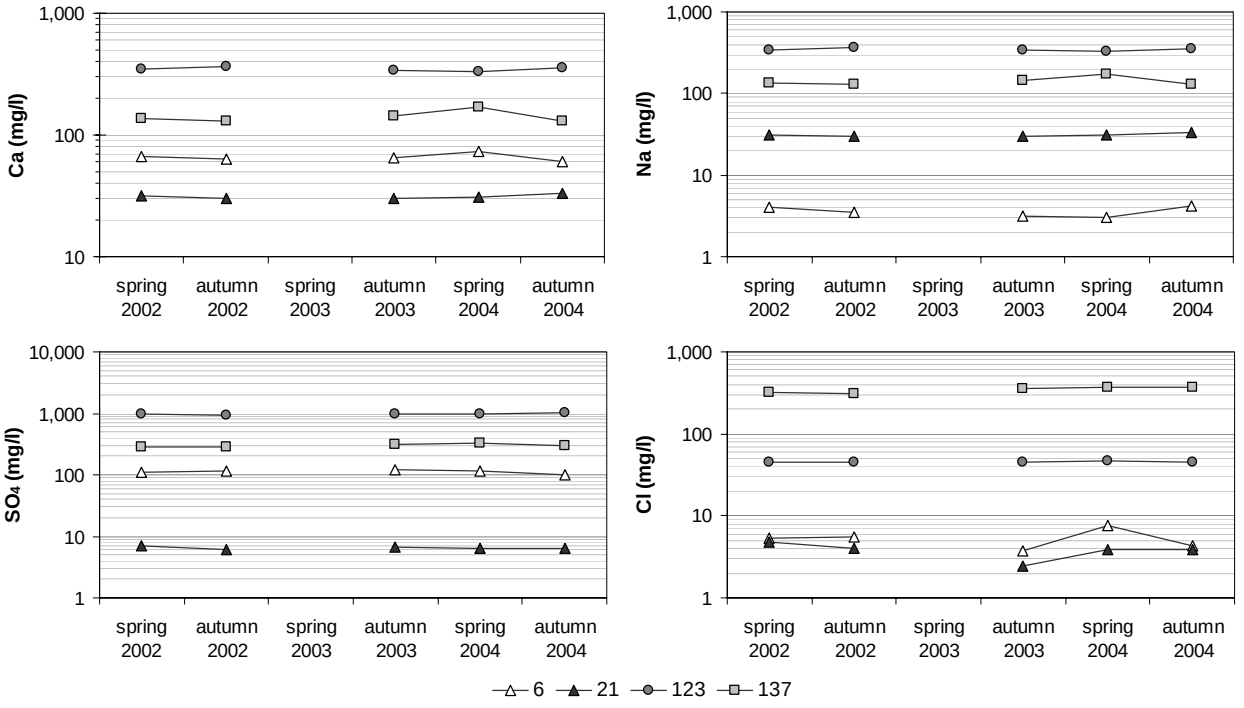

Fig. 7.7: Seasonal variations of Ca^{2+}, Na^{+}, SO_4^{2-} and Cl^{-} concentrations for 4 springs with high discharges but different chemical characteristics..

7.3.1.3 Hierarchical Cluster Analysis (HCA)

Hierarchical cluster analysis (HCA) is used to group groundwater samples into hydrochemical groups (Fig. 7.8). The classifying of 123 groundwater samples is done on the basis of two physico-chemical parameters (T, pH) and the concentrations of 12 elements. As the electric conductivity (EC) is a parameter strongly dependent on ion concentrations which are already included in the HCA, it was excluded from the statistical analyses.

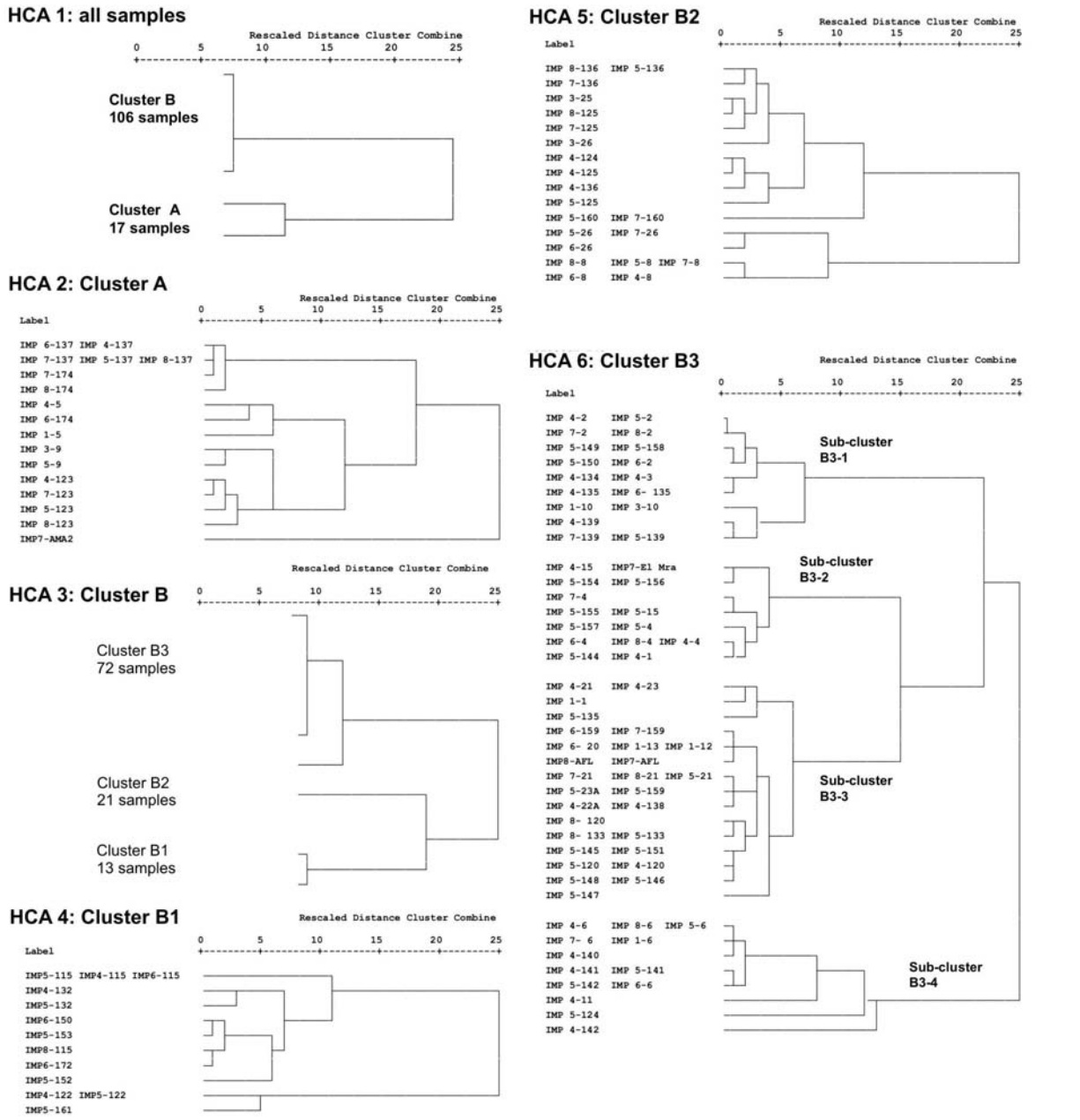

Fig. 7.8: Series of dendrograms of the Hierarchical Cluster Analyses (HCA) of groundwater from the Assif-n'Ait-Ahmed catchment.

The first clustering results in two major clusters A and B (Fig. 7.8: HCA 1). Cluster A representing only 17 samples is well separated from cluster B. The following separate clustering of the A and B (Fig. 7.8: HCA 2 and HCA 3) gives additional sub-clusters for B with B1 (13 samples), B2 (21 samples) and B3 (72 samples). Further clustering of B1, B2 and B3 (Fig. 7.8: HCA 4, HCA 5 and HCA 6) finally results in four distinctive sub-clusters: B3-1 (17 samples), B3-2 (14 samples, B3-3 (28 samples) and B3-4 (13 samples).

Cluster A is distinguished from cluster B by both higher mean concentrations of Na^+ (190.1 mg/l) and Cl^- (288.2 mg/l) revealing leaching of halite, and of SO_4^{2-} (648.7 mg/l), Ca^{2+} (251.5 mg/l) and Sr^{2+} (6.1 mg/l) revealing dissolution of gypsum (Tab. 7.3, Fig. 7.9). Cluster B is clearly less affected by leaching of evaporitic minerals (Tab. 7.3). As a result of the dissolution of evaporitic minerals, the samples of cluster A show significantly higher mean conductivities (2,186 µS/cm) than cluster B (528 µS/cm) (Tab. 7.3).

Tab. 7.3: Mean value (mean) and standard deviation (SD) of the variables for the cluster A and B and the sub-clusters B1, B2 and B3, defined by Hierarchical Cluster Analyse; EC = Electric conductivity.

Parameter	All samples (n = 123)		A (n = 17)		B (n = 106)		B1 (n = 13)		B2 (n = 21)		B3 (n = 72)	
	mean	SD	mean	SD	mean	SD	mean	SD	mean	SD	mean	SD
T (°C)	12 .6	2.3	14.4	1.9	12.3	2.2	13.0	2.8	13.7	1.6	11.8	2.0
pH	8.0	0.3	7.6	0.3	8.0	0.2	8.0	0.2	7.9	0.2	8.0	0.2
Ca^{2+} (mg/l)	83.6	87.7	251.5	119.3	54.8	29.1	61.2	19.3	100.7	15.8	40.2	16.6
Mg^{2+} (mg/l)	23.9	15.3	48.8	12.5	19.5	8.9	19.3	5.3	32.5	5.4	15.7	6.4
Na^{+} (mg/l)	51.8	95.9	190.1	204.6	30.0	43.4	133.0	42.4	23.8	10.9	13.3	14.8
K^{+} (mg/l)	1.7	1.5	3.1	2.8	1.4	1.1	1.9	0.6	1.3	0.7	1.4	1.3
Sr^{2+} (mg/l)	1.6	2.4	6.1	3.3	0.8	1.0	0.8	0.7	2.4	1.0	0.4	0.4
SiO_2 (mg/l)	3 .8	2.2	4.8	3.1	3.5	1.9	3.7	0.9	4.6	2.0	3.2	2.0
Fe_{tot} (µg/l)	12	13.5	10	6.1	12	15	8	7.2	11	9.6	13	17.2
Mn^{2+} (µg/l)	2	3.8	2	2.4	2	4	4	10.8	1	1.5	2	2.0
HCO_3^- (mg/l)	149.3	46.3	191.2	48.5	142.4	28.5	138.9	29.6	160.6	24.8	137.7	27.5
Cl^- (mg/l)	80.5	144.7	288.2	300.9	47.4	73.1	221.0	72.7	30.8	11.6	20.8	25.6
NO_3^- (mg/l)	6.8	15.5	1.9	2.7	5.9	3.3	6.1	2.7	4.3	2.1	6.3	3.5
SO_4^{2-} (mg/l)	168.5	262.6	648.7	361.2	86.5	97.0	67.6	56.8	254.4	44.5	40.9	48.1
EC (µS/cm) (*1)	764	724	2186	964	528	310	1089	267	769	118	358	138

(*1) *Electric conductivity (EC.) was not taken into account in the Hierarchical Cluster Analyse*

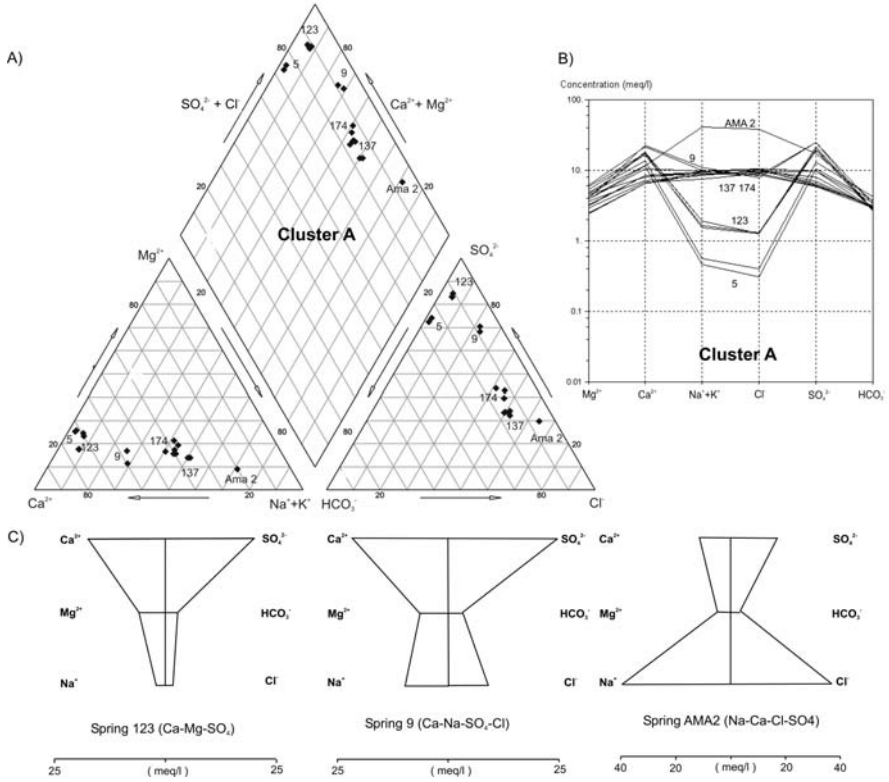

Fig. 7.9: Chemical composition of the cluster A defined by Hierarchical Cluster Analyses: Piper (A), Schoeller (B) and Stiff (C) diagrams.

The chemical composition of the samples of cluster A (Fig. 7.9-A, B and C) reveal groundwater from Ca-Mg-SO_4 type (springs 5 and 123) to Na-Ca-Cl-SO_4 type (spring Ama 2). Although the spring Ama 2 is not directly located in the Assif-n'Ait-Ahmed catchment (Fig. 7.13), this sample is included into the statistical analysis because its outflow is characterised by direct halite dissolution. Thus, Ama 2 is clearly representative for a groundwater composition strongly influenced by halite dissolution, while spring 123 is more representative for gypsum dissolution.

In order to characterize the groundwater of the cluster B (106 samples), the clusters B1, B2 and B3 are considered (Fig. 7.8: HCA 4, HCA 5 and HCA 6):

- Cluster B1 (EC = 1,089 µS/cm) is distinguished from the others by higher Na^+ (133 mg/l) and Cl^- (221 mg/l) values and a relative low value of SO_4^{2-} (67.6 mg/l) (Tab. 7.3). The groundwater of cluster B1 is of Na-Ca-Cl-HCO_3 type (Fig. 7.10), thus showing clear influence of halite dissolution.
- Cluster B2 (EC = 769 µS/cm) shows higher values of SO_4^{2-} (254.4 mg/l), Ca^{2+} (100.7 mg/l) and Sr^{2+} (2.4 mg/l) and relative low values of Na^+ (23.8 mg/l) and Cl^- (30.8 mg/l) (Tab. 7.3). The groundwater of the cluster B2 is of Ca-Mg-SO_4-HCO_3 type (Fig. 7.10) and influenced by gypsum dissolution.
- Cluster B3 (EC = 358 µS/cm) represents lower mineralised groundwater in regard to SO_4^{2-} (40.9 mg/l), Ca^{2+} (40.2 mg/l), Sr^{2+} (0.4 mg/l), Na^+ (13.3 mg/l) and Cl^- (20.8 mg/l) (Tab. 7.3).

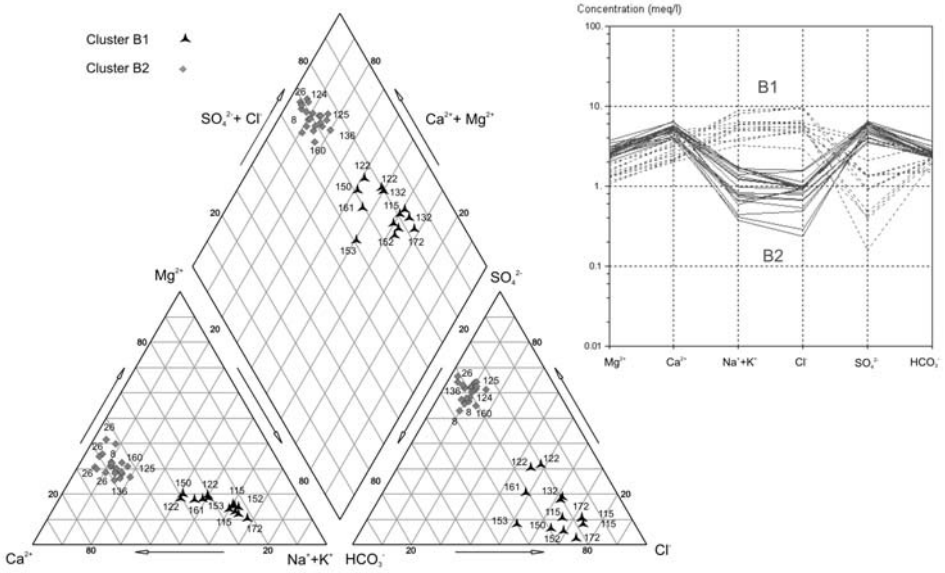

Fig. 7.10: Piper and Schoeller diagrams of the sub-clusters B1 and B2.

For a detailed description of the 72 samples of the cluster B3 the sub-clusters B3-1, B3-2 and B3-3 are considered (Fig. 7.8: HCA 6):

- Cluster B3-1 (EC = 484 µS/cm) is distinguished from the others by higher values of Na^+ (36.2 mg/l) and Cl^- (61.2 mg/l) (Tab. 7.4). Therefore, the groundwater of cluster B3-1 is slightly influenced by halite dissolution and shows a water type ranging between Ca-Mg-Na-Cl and Ca-Na-Cl-HCO_3 (Fig. 7.11).
- Cluster B3-2 (EC = 281 µS/cm) shows low mineralised groundwater of Ca-Mg-HCO_3 and Mg-Ca-HCO_3 types (Fig. 7.11). It is distinguished from the others by higher values of SiO_2 (6.4 mg/l) (Tab. 7.4). This is a clear indication that the aquifer drained by the groundwater of cluster B3-2 is characterized by an underground passage within the basalt.
- Cluster B3-3 (EC = 257 µS/cm) shows low mineralised groundwater of Ca-Mg-HCO_3 and Mg-Ca-HCO_3 types (Fig. 7.11) and is distinguished from the others by lower values

of SiO_2 (1.7 mg/l) (Tab. 7.4). Cluster B3-3 is clearly representative of the carbonate aquifer.

- Cluster B3-4 (EC = 492 µS/cm) is distinguished from the others by higher values of SO_4^{2-} (111.2 mg/l), Ca^{2+} (65.1 mg/l), Sr^{2+} (1.0 mg/l) and NO_3^- (19.7 mg/l) (Tab. 7.4). The groundwater of cluster B3-4 is slightly influenced by gypsum dissolution and shows a Ca-Mg-HCO_3-SO_4 type (Fig. 7.11). The higher concentration of NO_3^- observed at some wells reflects local pollution from cattle breeding activity.

Tab. 7.4: Means values of variables for the sub-clusters B3-1, B3-2, B3-3 and B3-4 defined with HCA.

Parameter	B 3-1 (N: 17)		B 3-2 (N: 14)		B 3-3 (N: 28)		B 3-4: (N: 13)	
	Mean	SD	Mean	SD	Mean	SD	Mean	SD
T (°C)	12.3	1.7	13.7	1.5	10.4	1.8	11.8	1.0
ph	8.0	0.2	8.0	0.2	8.1	0.2	8.0	0.2
Ca^{2+} (mg/l)	44.4	17.3	29.7	6.2	31.3	6.1	65.1	9.6
Mg^{2+} (mg/l)	15.8	4.4	13.8	4.7	12.0	4.2	25.4	4.1
Na^+ (mg/l)	36.2	8.9	8.4	2.8	4.8	6.3	6.9	10.0
K^+ (mg/l)	1.2	0.5	1.7	1.30	1.2	1.0	1.8	2.2
Sr^{2+} (mg/l)	0.25	0.1	0.2	0.13	0.2	0.2	1.0	0.8
SiO_2 (mg/l)	3.0	1.0	6.4	1.6	1.7	0.5	3.0	1.0
Fe^{2+} (µg/l)	8	7	14	15	10	11	26	30
Mn^{2+} (µg/l)	1	1	2	1	2	2	3	2
HCO_3^- (mg/l)	143.6	29.5	135.9	24.0	123.8	19.1	161.7	27.1
Cl^- (mg/l)	61.2	16.5	10.5	5.0	7.6	12.8	7.8	9.3
NO_3^- (mg/l)	6.8	1.8	4.6	2.0	7.1	4.7	19.7	50.7
SO_4^{2-} (mg/l)	38.5	35.7	19.1	15.6	20.6	19.0	111.2	63.6
EC (µS/cm) (*1)	484	100	281	45	257	70	492	118

(*1) *Electric conductivity (EC.) was not taken into account in the Hierarchical Cluster Analyse*

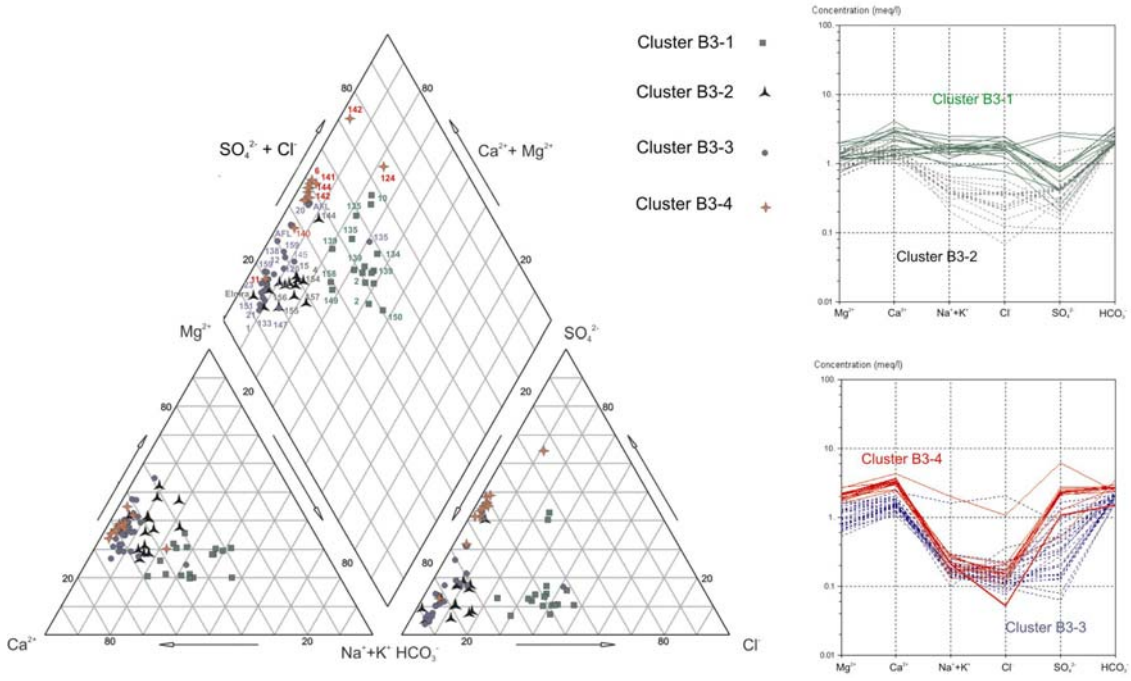

Fig. 7.11: Piper and Schoeller diagrams of the sub-clusters B3-1, B3-2, B3-3 and B3-4.

The results of the HCA reflect the chemical evolution along the flow paths from the low mineralised carbonate groundwater to saline groundwater after leaching of evaporitic minerals of the Triassic formations (Fig. 7.12). Cluster B3-3 and B3-2 reveal lower mineralised groundwater

of Ca-Mg-HCO_3 and Mg-Ca-HCO_3 types which are the groundwater facies of the Jurassic limestone and dolomite aquifer (Fig. 7.12). Cluster B3-2 shows higher concentrations of SiO_2 which reveals a groundwater passage within the Triassic basalt without any dissolution of evaporitic minerals. The other clusters reflect the chemical evolution of the groundwater of the Jurassic aquifer in more or less contact with the evaporitic minerals of the Triassic clays. While clusters B3-1 (Ca-Mg-Na-Cl and Ca-Na-Cl-HCO_3 types) and B1 (Na-Ca-Cl-HCO_3 type) show typical groundwater facies after halite dissolution, the clusters B3-4 (Ca-Mg-HCO_3-SO_4) and B2 (Ca-Mg-SO_4-HCO_3) reveal the influence of gypsum. Cluster A groups the groundwater with the highest electric conductivity (EC) due to important dissolution of gypsum and/or halite.

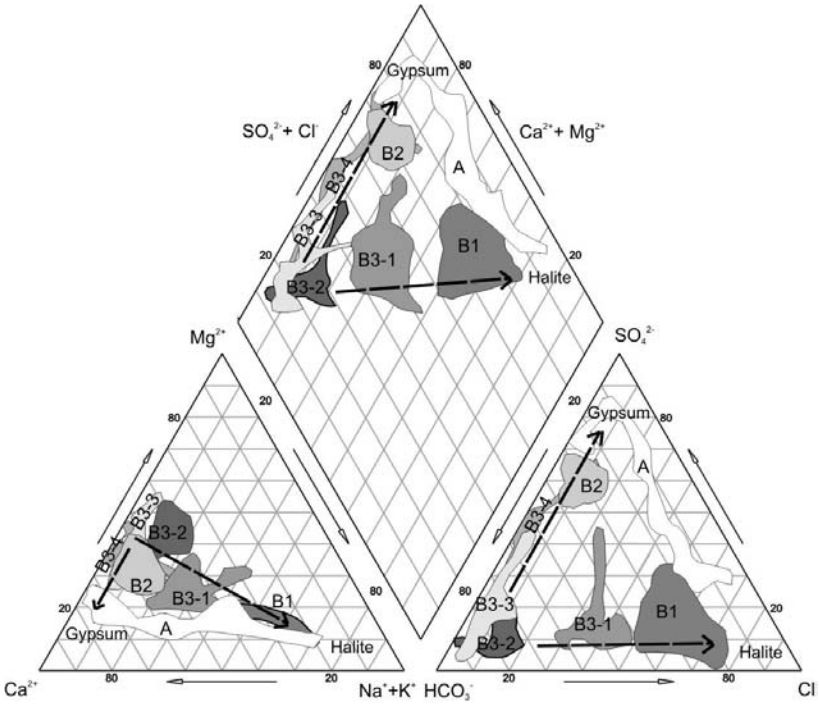

Fig. 7.12: Piper diagram showing the clusters and sub-clusters resulting of the Hierarchical Cluster Analyse applied to the groundwater of the Assif-n'Ait-Ahmed catchment; A represents the Ca-SO_4 and Ca-Cl-SO_4 groundwater, B1 is the Na-Ca-Cl-HCO_3, B2 is the Ca-Mg-SO_4-HCO_3, B3-1 is the Ca-Mg-Na-Cl and Ca-Na-Cl-HCO_3 groundwater, B3-2 and B3-3 are Ca-Mg-HCO_3 and Mg-Ca-HCO_3 groundwater and B3-4 is the Ca-Mg-HCO_3-SO_4 groundwater. Arrows represent the chemical evolution of groundwater along the flow paths.

The relationship of the statistically defined clusters of water samples to the geographic location is tested by plotting the various clusters on the geological map (Fig. 7.13). These results are compared with the chemical composition of the groundwater (Pie diagram) collected during autumn 2003 (Fig. 7.14). The springs of the cluster B3-3 showing low mineralised groundwater (Ca-Mg-HCO_3 and Mg-Ca-HCO_3 water types) are located at high altitude in the carbonates of the Toundoute nappe (spring 21 and 133) (Fig. 7.13). This group has a significant magnesium component due to the presence of dolomites (Fig. 7.14). Cluster B3-2 grouping low mineralised groundwater (Ca-Mg-HCO_3 and Mg-Ca-HCO_3 water types) is located within the Triassic basalt (springs 15, 155, 156 and 157) (Fig. 7.13) which confirms the higher SiO_2 concentration (mean value = 6.4 mg/l). The springs of clusters A, B1, B2, B3-1 and B3-2 are in contact with the Triassic clays which confirm the leaching of evaporitic minerals increasing the total mineralization. The springs 123 and 137 having the highest discharge (Fig. 7.4) are located in the centre of the catchment and belong to cluster A (Fig. 7.13). Some low developed karstic features e.g. outflow of the water through small karst channels and travertine precipitation are observed.

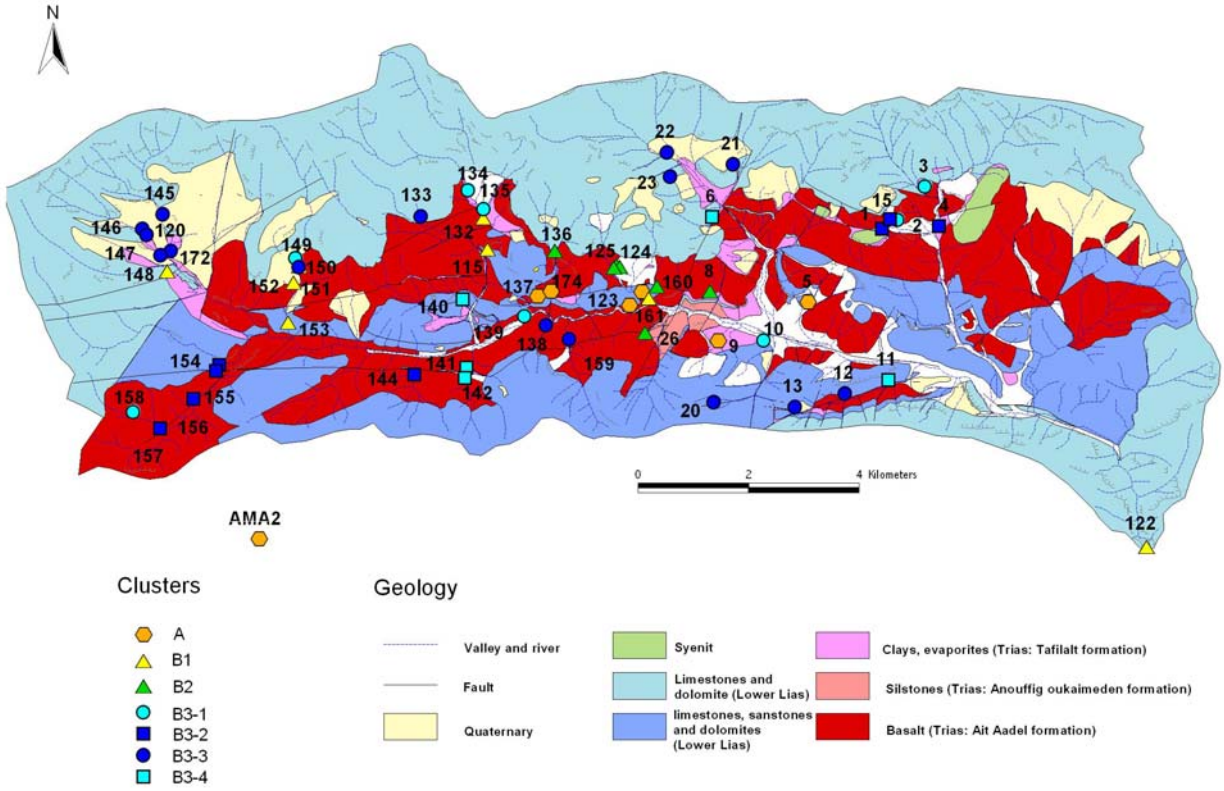

Fig. 7.13: Results of the HCA plotted on the geological map of the Assif-n'Ait-Ahmed catchment; cluster A: high mineralised groundwater influenced by gypsum and halite, B1 and B3-1: groundwater influenced by halite, B2 and B3-4: groundwater influenced by gypsum, B3-2: low mineralised groundwater showing passage in the Triassic basalt and B3-3 low mineralised groundwater from the Liassic carbonates. Numbers are the spring references. 122 is surface water.

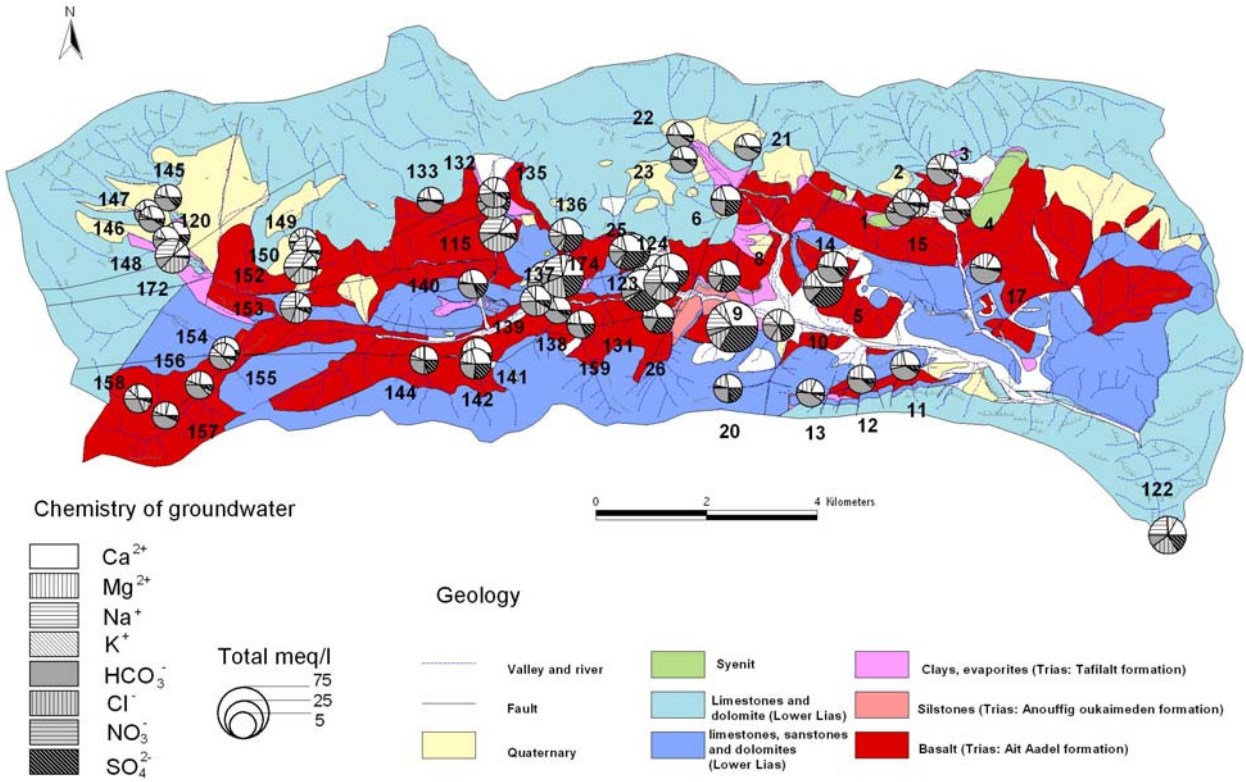

Fig. 7.14: Chemical composition (pie diagram) of the groundwater in the Assif-n'Ait-Ahmed catchment (autumn 2003); size of the circles represent the total mineralization (meq/l) (modified after BELL 2005). Numbers are the spring references.

7.3.1.4 Principal Component Analyse

In order to understand the correlation between the variables, a “Principal Component Analyse” (PCA) was performed. The entire data set of 123 samples and 13 variables (pH, T, 8 major ions and SiO_2, Mn^{2+} and Fe^{2+}) is used. For a better interpretation, the component loading matrix is rotated with the “varimax rotation” method. This procedure gives a new rotated matrix in which each component is better described by the variables. The three first components of the initial PCA explain 61.7 % of the total variance (Tab. 7.5, Fig. 7.15). Hence in the rotated matrix those components explain 61 % of the total variance, no loss of information occurred.

Tab. 7.5: Results of the Principal Component Analyse with percent and cumulative percent of variance explained by the various factors before and after rotation.

	Principal Component Analyse		Principal Component Analyse: rotated [*1]	
Component	Variance %	Cumulated variance %	Variance %	Cumulated variance %
1	35.5	35.5	25.1	25.1
2	16.1	51.6	21.6	46.7
3	10.1	61.7	14.3	61.0

[*1] Rotation method: Varimax with Kaiser normalising

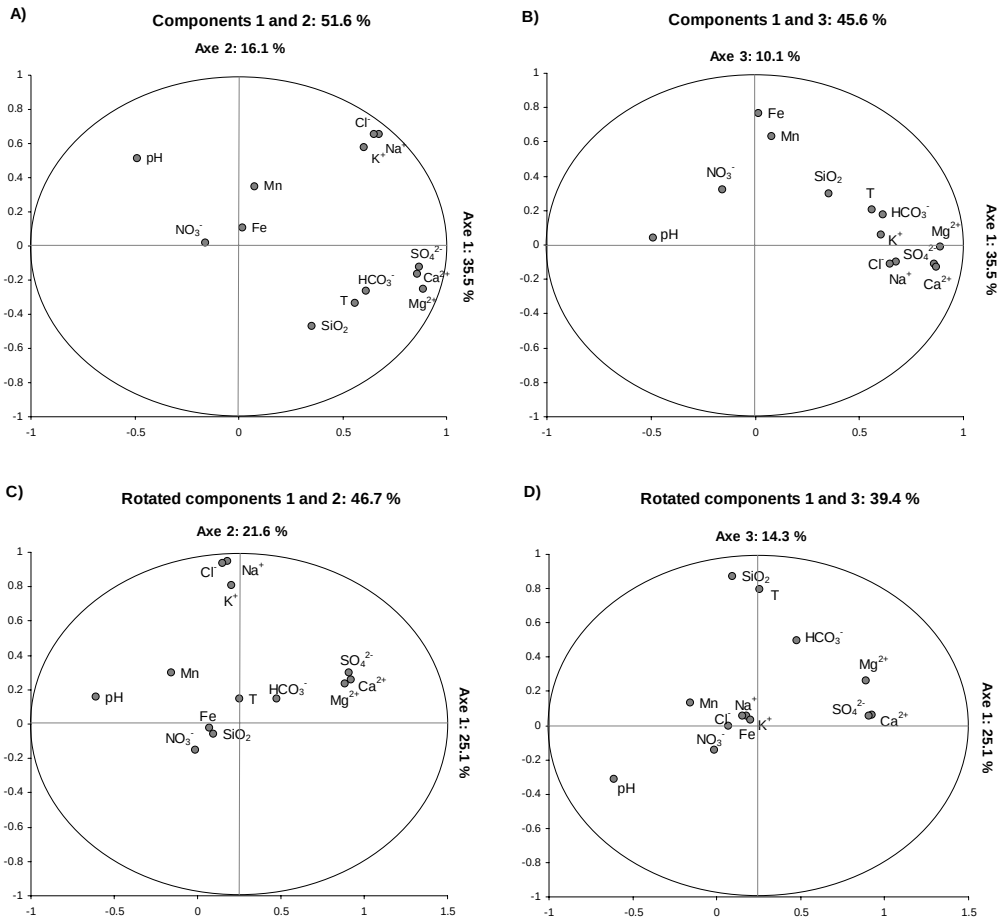

Fig. 7.15: Results of the Principal Component Analyse before (A and B) and after rotation (C and D).

The initial PCA results in 3 components (Fig. 7.15-A and B):

- Component 1 (axis 1) accounts for 35.5 % of the total variance. The concentrations of Ca^{2+}, Mg^{2+} and SO_4^{2-} have a strong loading with 0.86, 0.89 and 0.87. Thus, Component 1 reflects the dissolution of gypsum which is correlated with the concentration of Mg^{2+}.
- Component 2 (axis 2: 16.1%) is not well described by the variables.

- Component 3 (axis 3: 10.1 %) reflects a low correlation between Fe^{2+} (0.77) and Mn^{2+} (0.63).

After rotation the components are better described by the variables (Fig. 7.15-C and D):

- The component 1 (axe 1: 35.5 %) reflects both the strong correlation already observed between Ca^{2+} (0.92), SO_4^{2-} (0.91) and Mg^{2+} (0.89) and an anti-correlation with pH (-0.61).
- The component 2 (axe 2: 21.6 %) describes the correlation of Na^+ (0.94), Cl^- (0.93) and K^+ (0.80). Thus it reflects the dissolution of both halite (NaCl) and sylvite (KCl).
- The component 3 (axe 3: 14.3 %) is clearly described by the content of SiO_2 (0.87) which is correlated with the temperature (0.80).

No correlation is observed between the dissolution of gypsum and halite, because they are described with two different independent components (1 and 2). The absence of this correlation reveals the sedimentological variation of facies types typical for the paleo-geographical setting during the sedimentation of the Triassic clays (BELL 2005). With the third component an additional dissolution process is addressed. SiO_2 (0.87) in groundwater results from the hydrolyse of silicate minerals. Only the Triassic series offer enough silicates for significant SiO_2 values with either an underground passage within the Triassic clays or the Triassic basalts. Hence SiO_2 is not correlated to Na^+, Cl^- and SO_4^{2-} characterising the Triassic clays due to the leaching of either halite/sylvite or gypsum, no relation between the SiO_2 content and a passage in the Triassic clays exist. Thus elevated SiO_2 concentrations are representative of an underground passage within the basalt. The correlation between SiO_2 and temperature can be related to the residence time. Due to the high altitude of the catchment and to the snowmelt during springtime, the temperature of the recharge is relatively low (≈ 10 °C). But in the basalt aquifer with longer residence times due to its low permeability, groundwater temperature equilibrates with the annual mean temperature prevailing in the catchment of around 13.5 °C (measured at Imeskar station).

7.3.1.5 Saturation Index

In order to define the degree of evolution of the groundwater in the Assif-n'Ait-Ahmed catchment, saturation indexes (SI) are calculated. The ranges of the saturation indexes observed are:

$$-0.35 < SI_{calcite} < 0.94,\ -0.97 < SI_{dolomite} < 2.31,\ -3.41 < SI_{gypsum} < -0.20 \text{ and } -0.76 < SI_{quartz} < 0.32.$$

Some groundwater of cluster A are in equilibrium in respect to gypsum ($-0.5 < SI_{gypsum} < 0$) (Fig. 7.16-A). Under natural conditions, saturation of gypsum is rarely reached. Saturation occurs only in strongly evaporated solutions due to the high dissolution rate of gypsum controlled by simple diffusion. The dissolution of gypsum adding Ca^{2+} in the solution increases the calcite saturation, which explains the observed correlation between the $SI_{calcite}$ and the SI_{gypsum} of the mean values of the clusters defined by HCA (Fig. 7.16-B). In respect to the saturation indexes of calcite and dolomite (Fig. 7.17-A) clusters B1, B3-1, B3-2 and B3-3 are in equilibrium with calcite and dolomite, while clusters B3-4, B2 and A revealing gypsum dissolution are slightly saturated. Although, all samples are close to the equilibrium in regard to quartz, a distinct trend can be observed (Fig. 7.17-B, C, and D). While cluster B3-3 representative of the calcareous Jurassic aquifer is slightly under-saturated, the cluster B3-2 is slightly over-saturated

revealing an additional groundwater passage within basalt. The samples of clusters A, B1 and B2 show negative and positive SI_{quartz} depending on the influence of an underground passage in the basalt.

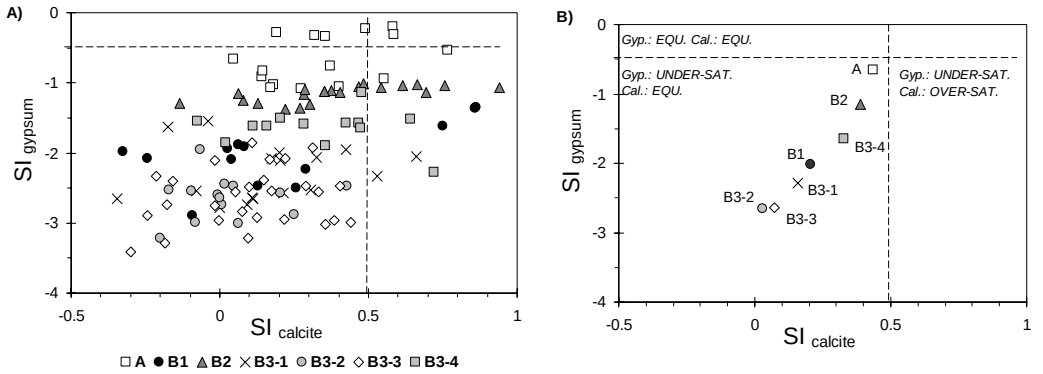

Fig. 7.16: Saturation indexes ($SI_{calcite}$ versus SI_{gypsum}) in groundwater from the Assif-n'Ait-Ahmed catchment: samples (A) and mean values of clusters defined by HCA (B); Gyp. = gypsum, Cal. = calcite, EQU. = equilibrium, UNDER-SAT. = under-saturation and OVER-SAT. = over-saturation.

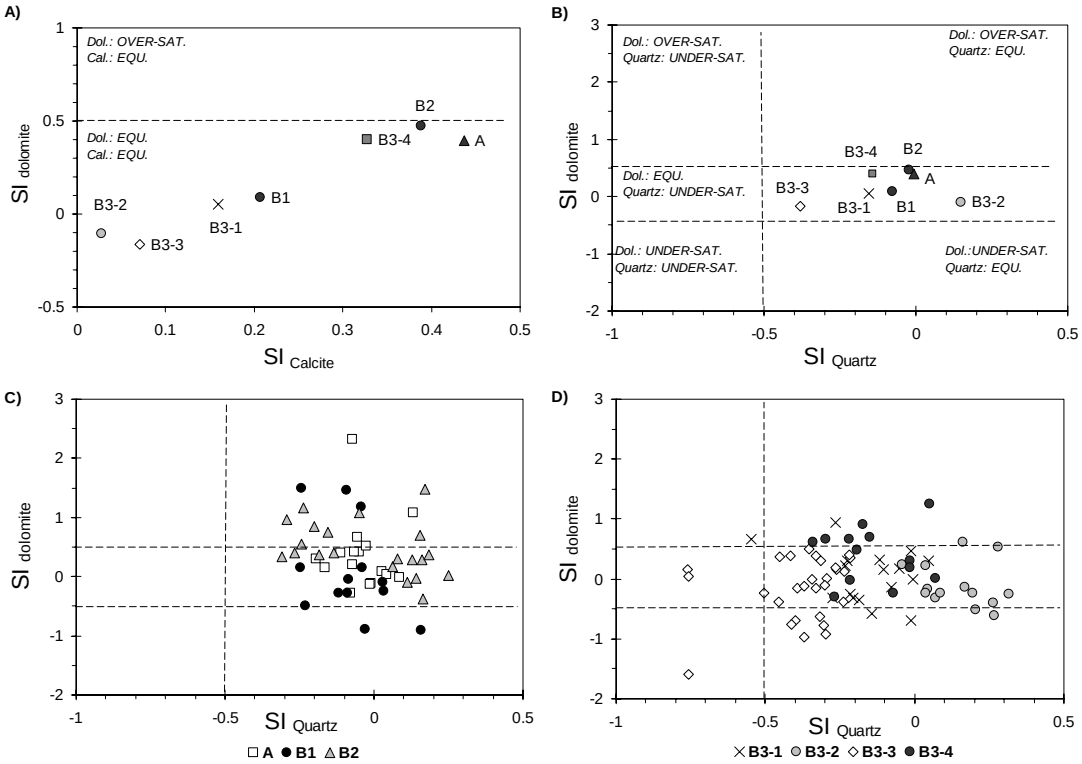

Fig. 7.17: Saturation indexes (SI) of calcite, dolomite and quartz for the various clusters defined by HCA for the groundwater of the Assif-n'Ait-Ahmed catchment: Mean values: A) $SI_{dolomite}$ versus $SI_{calcite}$, B) $SI_{dolomite}$ versus SI_{quartz} ; $SI_{dolomite}$ versus SI_{quartz} of clusters A, B1, B2, B3.1, B3.2, B3.3, B3.4 C) and D); Dol. = dolomite, Cal. = calcite, EQU. = equilibrium, UNDER-SAT. = under-saturation and OVER-SAT. = over-saturation.

The mean values of SI_{quartz} are plotted to the geological map (Fig. 7.18). Springs with $-0.76 < SI_Q < -0.3$ are characteristic of groundwater of the Jurassic carbonates without contact to the Triassic sediments e.g. springs 21 and 133. Springs with $-0.3 < SI_Q < 0$ reveal influence of the Triassic sediments but without important residence time in the basalt e.g. the two biggest springs of the catchment (123 and 137). Springs with $0 < SI_Q < 0.33$ correspond to groundwater from the basalt. They have very low discharges which emphasizes the hypothesis of basalt acting as the aquitard of the Jurassic aquifer.

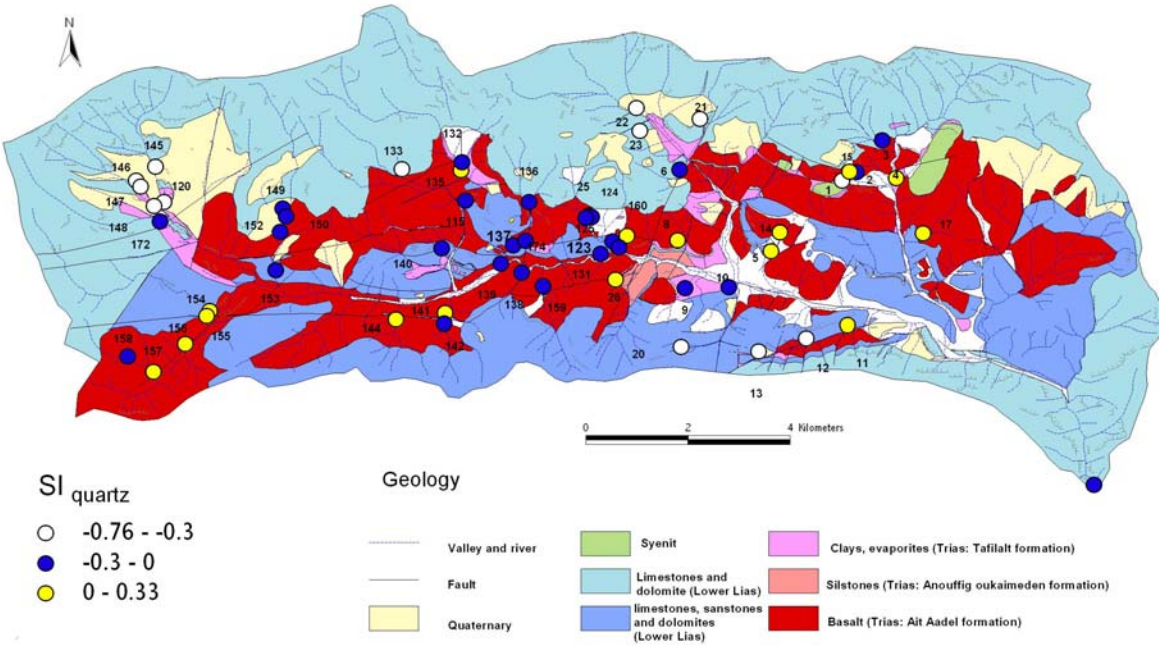

Fig. 7.18: Mean saturation index of quartz plotted on the geological map of the Assif-n'Ait-Ahmed catchment. Numbers are the spring references.

7.3.1.6 Important process during the underground passage

According to given hydrochemical results an effect of dedolomitization exists along the flow path of the groundwater. In general, dedolomitization occurs in aquifers containing limestones and dolomites in combination with gypsiferous layers (APPELO & POSTMA 1999). Dissolution of anhydrite or gypsum takes place according to:

$$CaSO_4 \longrightarrow Ca^{2+} + SO_4^{2-}$$

Groundwater in presence of gypsum is in equilibrium with calcite and dolomite. Increasing Ca^{2+} concentrations due to gypsum dissolution cause the precipitation of calcite to precipitate and thus the decrease of the CO_3^{2-} concentration during calcite precipitation. This provokes the dissolution of dolomite and thus an increase of the Mg^{2+} concentration:

$$Ca^{2+} + CaMg(CO_3)_2 \longleftrightarrow 2CaCO_3 + Mg^{2+}$$

As a result the dissolution of gypsum induces the transformation of dolomite to calcite in the rocks and produces waters with elevated Mg^{2+}, Ca^{2+} and SO_4^{2-} concentrations (PCA proved a correlation between these elements). The precipitation of the carbonate phases also generates protons, providing a possible explanation for the observed anti-correlation between the pH and the $Mg^{2+}$and SO_4^{2-} concentration:

$$Ca^{2+} + HCO_3^- = CaCO_3 + H^+$$

7.3.1.7 Stable Isotopes

Isotopic analyses ($\delta^{18}O$ and $\delta^{2}H$) were carried out on the groundwater of the catchment during each campaign. The mean values of the isotopic composition of springs of the Assif-n'Ait-Ahmed catchment range between -65 ‰ and -55 ‰ for $\delta^{18}O$ and -9.8 ‰ and -8.3 ‰ for $\delta^{2}H$ (Fig. 7.19) With a calculated mean d-excess of 13.3 the groundwater samples plot slightly above the Local Meteoric Water Line (LMWL) (Fig. 7.19). To explain this difference, it has to be remained that

the LMWL is defined for the whole Middle and Upper Drâa catchment (Chapter 6) and reflects evaporation effects occurring during the rainfalls prevailing in the southern part of the catchment.

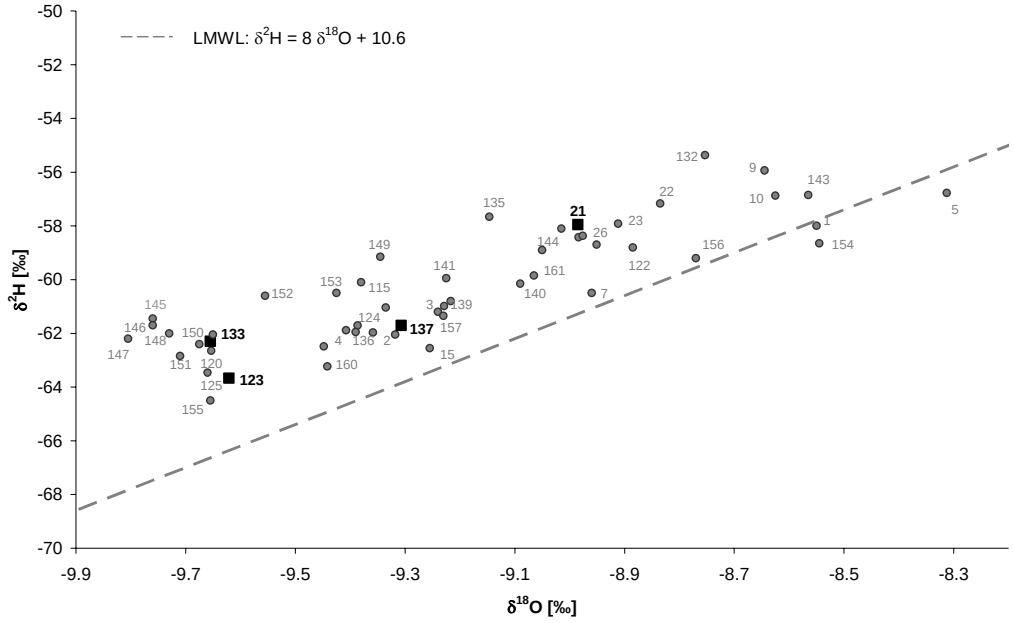

Fig. 7.19: Isotopic composition of the groundwater of the Assif-n'Ait-Ahmed catchment (mean values), and Local Meteoric Water Line (LMWL); the springs with the highest discharges are marked in black squares: 123, 137, 21 and 133.

Although the isotopic signature of the precipitation shows high variability e.g. $\delta^{18}O$ from -14.6 to -0.2 ‰ in time (compare Fig. 6.3-A), the groundwater signatures in the Assif-n'Ait-Ahmed catchment show no significant seasonal variations during the period of investigation (Fig. 7.20). With few exceptions the seasonal variations are below the error of measurement ($\delta^{18}O$ error = 0.1 ‰).

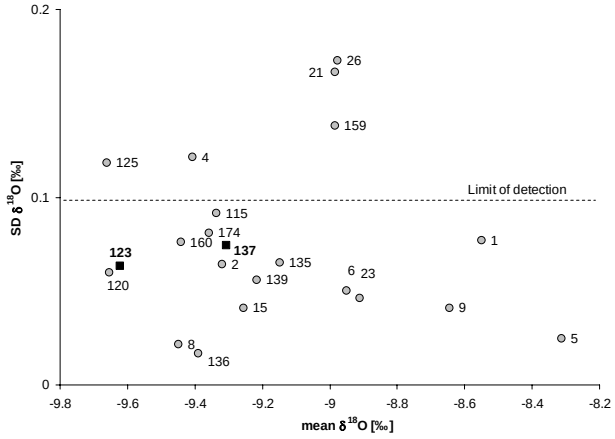

Fig. 7.20: $\delta^{18}O$ Standard Deviation (SD) versus $\delta^{18}O$ mean values of the groundwater in the Assif-n'Ait-Ahmed catchment.

While the springs 123 (2,250 m; $\delta^{18}O$ = -9.6 ‰) and 137 (2,300 m; $\delta^{18}O$ = -9.3 ‰) are located in the valley in contact with the Triassic series, the springs 21 (2,550 m; $\delta^{18}O$ = -9.0 ‰) and 133 (2,750 m; $\delta^{18}O$ = -9.7 ‰) are located at higher altitude and drain only the carbonates of the Liassic formations. There is no correlation between the altitude of the springs and the isotopic composition of groundwater (Fig. 7.21). But the isotopic signature of spring 123 shows great similarities to spring 133 located 500 m above. Hence no isotopic seasonal variation are observed at these springs and taking into account the "altitude effect" (Paragraph 3.3.1.7) spring 123 and 133 have comparable mean altitudes of recharge.

Using the relation $\delta^{18}O$ = -0.002 · "mean altitude of the recharge area " -3.0 (Chapter 6) approved in the Assif-n'Ait-Ahmed catchment for the springs 21, 133 and 147 with the DEM, the mean recharge altitude of aquifers in the Upper Drâa catchment can be estimated (Fig.7.22).

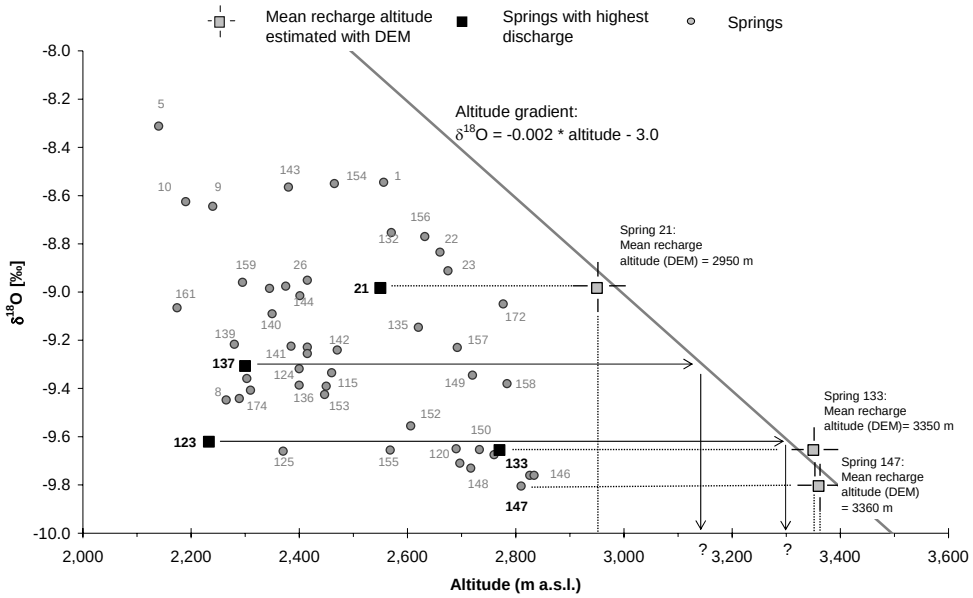

Fig. 7.21: Estimation of the recharge altitude of springs in the Assif-n'Ait-Ahmed catchment; $\delta^{18}O$ versus altitude of springs and altitude gradient based on the isotopic composition of precipitation (0.2 $\delta^{18}O$ per 100 m) and the mean altitude of the recharge area of the springs 21 (2,950 m), 133 (3,350 m) and 147 (3,360 m) calculated from the DEM.

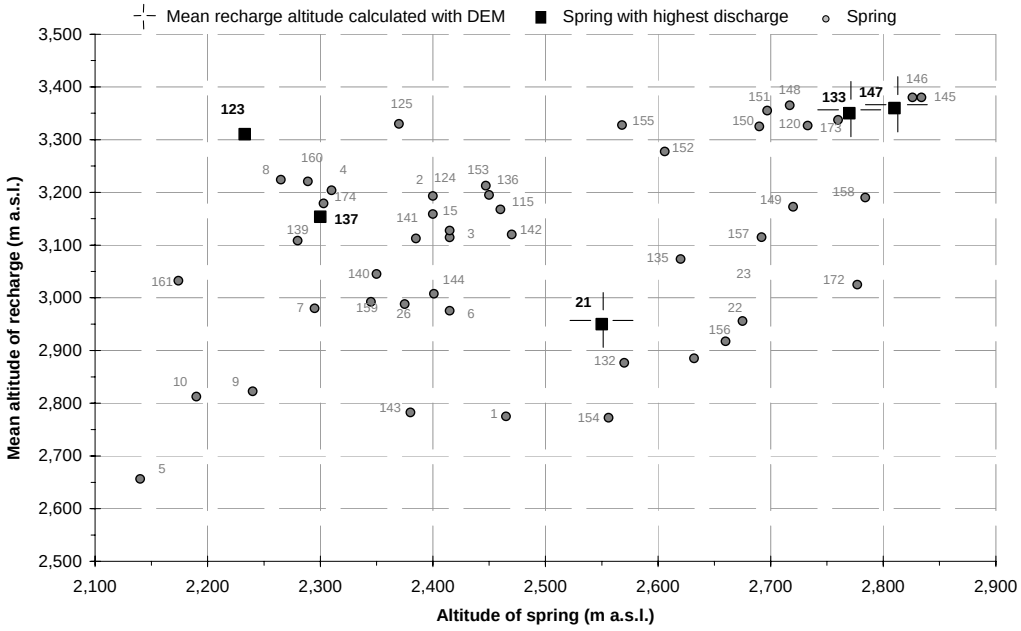

Fig. 7.22: "Mean altitude of the recharge area" versus "altitude of the spring" in the Assif-n'Ait-Ahmed catchment calculated from the relation: $\delta^{18}O$ = -0.002 · " mean altitude of the recharge area" -3.0. The altitude of the recharge area of the springs 147, 133 and 21 was defined from the DEM.

Plotting the mean recharge altitudes as indicative arrows which do not reflect the real mixing processes of the groundwater in the catchment map (Fig. 7.23) reveals unexpected high altitudes of the recharge areas particularly for the springs 123 and 137 with 3,360 m and 3,200 m respectively. Besides the fact that the amount of precipitation increases with the altitude, the varying infiltration capacities of the various geological units explain these results. In fact, the Triassic series (clays and basalt) cropping out at the lower slopes of the valley generate

important runoff during rain events and almost no significant recharge. Consequently, the carbonates with their higher infiltration rates, which form the upper slopes of the catchment are considered as the main recharge area.

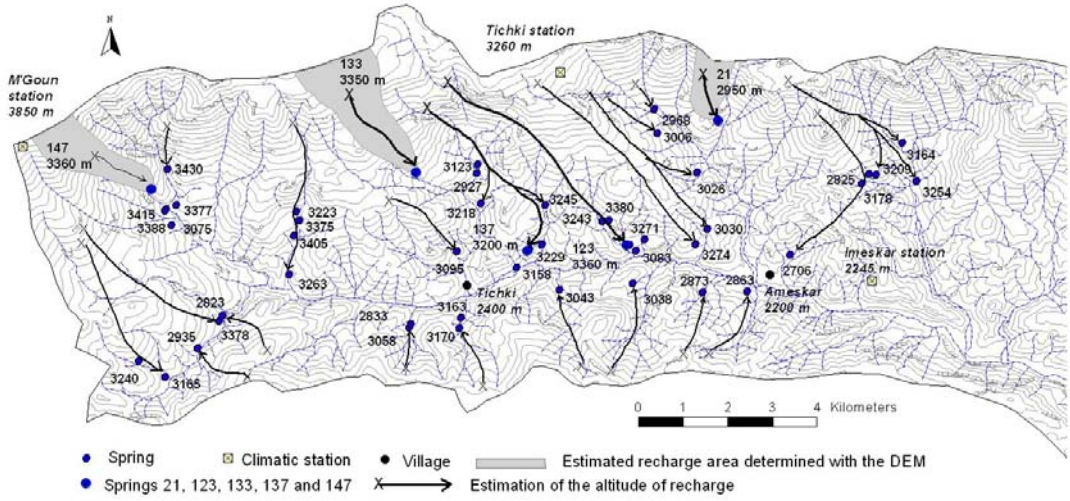

Fig. 7.23: Estimated mean recharge altitude of the springs (number in m a.s.l.) and representation of these recharge altitudes as indicative arrows; the altitude of the recharge area of the springs 147, 133 and 21 was defined from the DEM.

7.3.1.8 Tritium

Tritium analyses were carried out in five selected springs in the Assif-n-Ait-Ahmed in autumn 2002: (2, 4, 123, 133 and 137; locations see Fig. 7.36). In accordance to the interpretation used for unconfined aquifer (Chapter 6), the springs 123 (^{3}H = 6.7 TU) and 137 (^{3}H = 4.9 TU) show recent groundwater (< 4 years). This proves a rapid transit due to the karstification in the recharge area of these springs, which show the highest discharges. Springs 133 (^{3}H = 10.2 TU) and 2 (^{3}H = 7.1 TU) show mean transit times between 4 and 8 years revealing a less mature karst aquifer in their recharge area. Spring 4 shows a low value of tritium (^{3}H = 0.7 TU) revealing a mean residence time of more than 50 years. This is in good accordance to the hydrogeochemical results. Spring 4 is representative of groundwater from basalt (Fig. 7.13: cluster B3-2) and reveals an evolved groundwater. Proved by saturation indexes in regard to quarz between 0.05 and 0.28 (Fig. 7.18), which is clearly elevated, a high residence time was already postulated.

7.3.1.9 Hydrogeological conceptual model of the Assif-n'Ait-Ahmed catchment

Based on the geological investigations and on the hydrochemical and isotopical interpretations a conceptual hydrogeological model of the Assif-n'Ait-Ahmed catchment is elucidated (Fig. 7.24). Two main types of springs can be distinguished:

- Low mineralized springs (21 and 133) draining the limestones and dolomites of the Liassic aquifer located at high altitudes (above 2,400 m) with mean residence times between 4 and 8 years.
- Springs located in the valley (between 2,200 and 2,300 m) draining the Liassic aquifer, but chemically influenced by the Triassic formations (123 and 137). Their high discharges, their short mean residence times (< 4 years) and high mean altitudes of their recharge areas between 3,200 m and 3,360 m prove a rapid transit due to pronounced karstification.

Along the flow paths the groundwater evolves from Ca-Mg-HCO_3 type to Ca-SO_4-Mg or Na-Ca-Cl-SO_4 at the contact to the Triassic formations which act as an aquitard (mean residence time > 50 years). The leaching of evaporate minerals increase considerably the mineralization of the groundwater and generates both a dedolomitization process within the Agoulzi Formation and a precipitation of travertine at the outlet of the most developed springs.

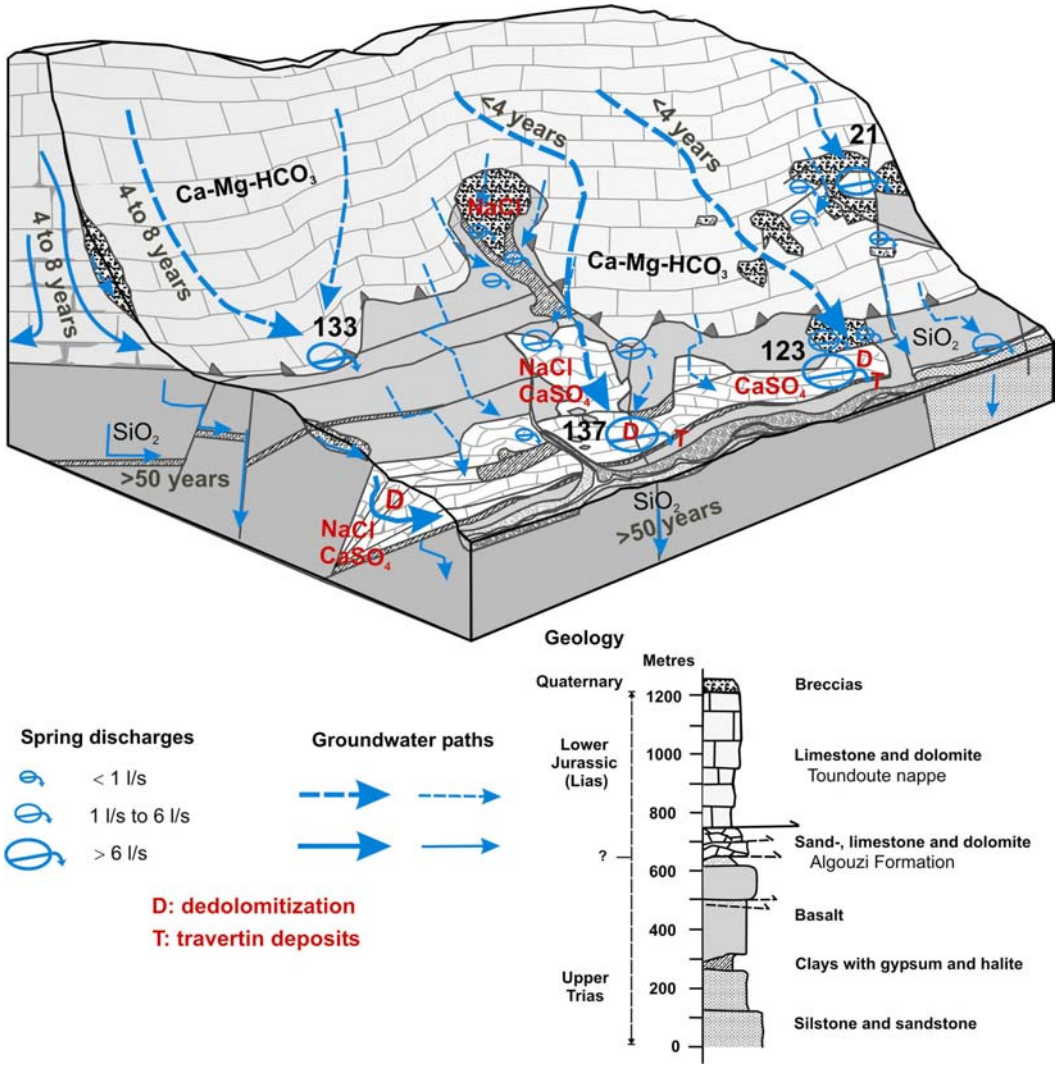

Fig. 7.24: Conceptual hydrogeological model of the Assif-n'Ait-Ahmed catchment based on geological and hydrogeochemical and isotopical interpretation including the determining chemical processes and the mean residence times (spring 21: Ca-Mg-HCO_3, 240 µs/cm; spring 133: Ca-Mg-HCO_3, 180 µs/cm; spring 123: Ca-SO_4-Mg; 1,900 µs/cm; and spring 137:Na-Ca-Cl-SO_4, 1,850 µs/cm;).

7.3.2 The Ifre catchment

7.3.2.1 Hydrogeological overview

The Ifre catchment is located between the Mio-Pliocene basins of Ait Kandoula and Seddrat and stretches from the carbonate heights in north to the Eocene-Cretaceous formations of the "Southern Atlasic Marginal Zone" in south (compare Fig. 3.2). The Assif-n'Ait-Ahmed catchment (Paragraph 7.3.1) is one of the sub-catchments of this 1,240 km^2 sized catchment area (Fig. 7.25).

Comparable to the Assif-n'Ait-Ahmed catchment, Jurassic carbonates form the major part of the Ifre catchment (Fig. 7.25). Due to the change of the paleogeography during the Jurassic (Paragraph 4.3.3), those carbonates show important facies variations. The Lotharagian (L1),

forming the main aquifer of the Toundoute Nappe the Assif-n'Ait-Ahmed catchment (Paragraph 7.3.1), consist of series of massive limestones and dolomites which form the most prolific aquifer with an extension of about 305 km^2 (ca. 24% of the catchment). The Domerian (L 2-3) covering 300 km^2 (ca. 24 %) of the catchment consists of limestones alternating with marls with no karstic features. The Toarcian-Aalenian (L 4-5) and the Aalenian-Bajocian (J 1-2) build of marls do not have groundwater storage and show low permeability. The Triassic formations crop out in the west of the Ifre catchment. The investigations in the Assif-n'Ait-Ahmed catchment proved that these formations act as the aquitard of the Jurassic aquifer. In the middle of the catchment in the Ait Kandoula basin, the formations of the Quaternary (alluvial cones, terraces and other recent deposits), Pliocene (conglomerates and gravel) and Mio-Pliocene (conglomerates, lacustrine limestones and pink sandy-clay) overlay the Jurassic carbonates of the Toundoute Nappe (compare Fig. 4.21). The aquifers developed in these overlaying formations are limited and closely connected to the wadis. In the matrix of the conglomerates, high content of clay was observed, which can locally strongly reduce the permeability. On the contrary, some lacustrine limestones within the overlaying formations show local groundwater storage. The southern part of the catchment is formed by the "Southern Atlas Marginal Zone" (SAMZ). The SAMZ is a compressional deformation zone with a frontal tectonic repetition of the Upper Cretaceous-Eocene sequence (Paragraph 4.4.2: compare Fig. 4.21 and 4.23). Due to the presence of marls in these formations (Paragraph 4.3.4: compare Fig. 4.14 and 4.15), the SAMZ is considered as a hydrogeological barrier between the High Atlas and the Basin of Ouarzazate.

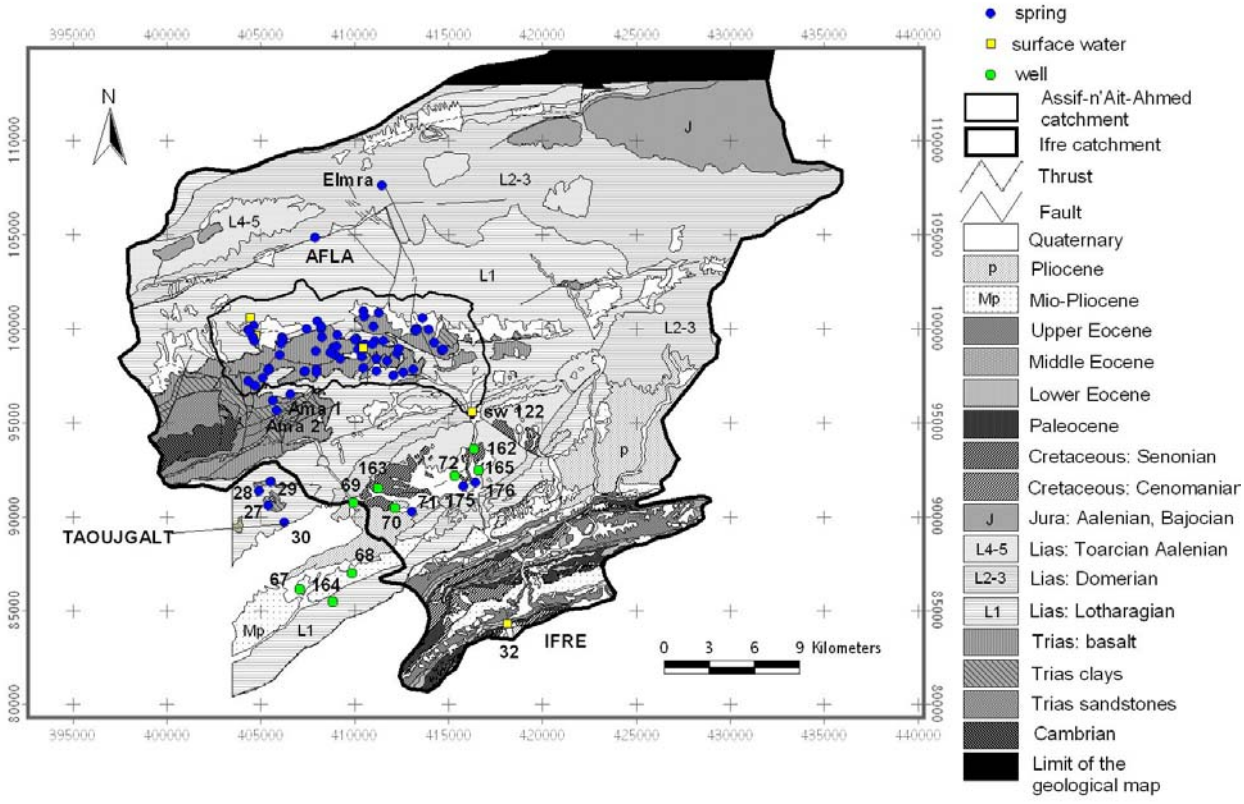

Fig. 7.25: Location of the groundwater samples (indicated by the numbers) on the geological map of the Ifre catchment (after Geological map 1/200 000: Jbel Saghro-Dades, CHOUBERT et al. 1980).

Due to the difficult accessibility, sampling was limited to the western part of the catchment (Fig. 7.25) with 11 springs, 10 wells and 1 surface water in addition to the samples of the Assif-n'Ait-Ahmed catchment. In the north, the spring AFLA is the main spring of the M'Goun River (30 l/s). This spring, which shows karstic characteristics (dissolution features), is located along an

important fault between the massif carbonates of the Lotharagian and the marly limestones of the Domerian. The IMPETUS test site Taoujgalt is represented by 4 springs (27, 28, 29 and 30). The springs 175 (15 l/s) and 176 (10 l/s) drain the Domerian calcareous and the Quaternary formations.

For a detailed description of the alluvial aquifer between the villages of Taoujgalt and Alemdoun, electric conductivity (EC) and precise water level measurements with a differential GPS of 40 wells was carried out in autumn 2003 (IMP 6) (Fig. 7.26-A and B). The alluvial aquifer is mainly developed in Quaternary formations overlaying the Cretaceous and Jurassic series.

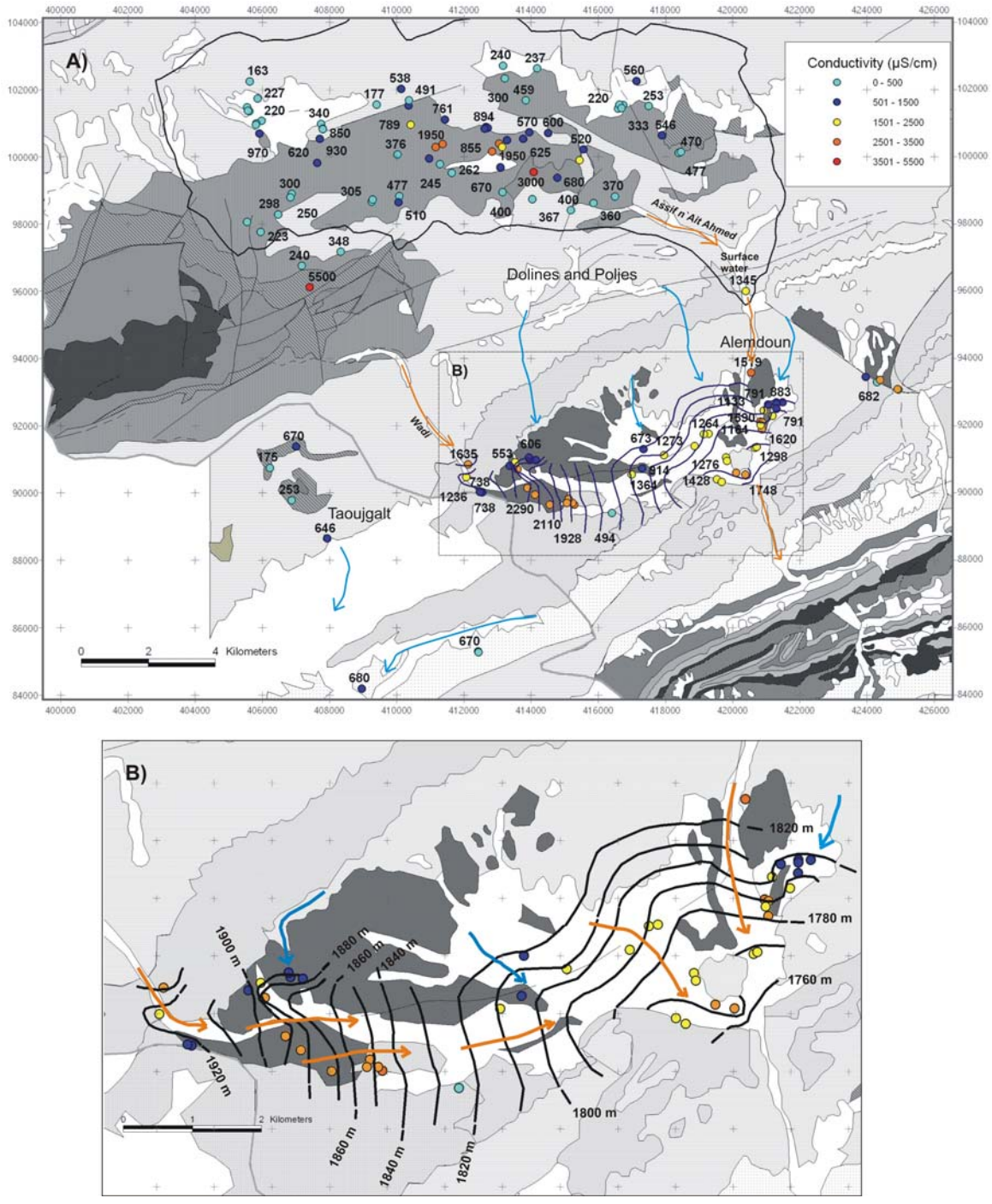

Fig. 7.26: A) Distribution of the electric conductivity (number) in the south-western part of the Ifre catchment; B) water table (autumn 2003) of the basin between Taoujgalt and Alemdoun: orange arrows: groundwater recharge from the Wadis showing higher mineralization; blue arrows: lateral groundwater recharge from the low mineralised carbonate aquifers (geological map after geological map 1/200,000 Jbel Saghro-Dades, SAADI et al. 1977).

The alluvial aquifer shows high spatial variability of electric conductivities between 494 µS/cm and 2,290 µS/cm (Fig. 7.26-A). Two main origins of groundwater of the alluvial aquifer can be distinguished:

- Groundwater from the Liassic carbonates by lateral affluxes with relative low electric conductivities (EC from 494 to 800 µS/cm) (Fig. 7.26: blue arrows). Poljes and dolines overhanging the basin prove the existence of a prevailing underground drainage of the limestone plateau. Due to the lack of further information the estimation of the proportion of water recharging the alluvial aquifer and infiltrating deeper into the carbonates of the Toundoute Nappe is not possible.
- Groundwater recharged by riverbed infiltration from the wadis with electric conductivities around 1,400 µS/cm (Fig. 7.26: orange arrows).

The high electric conductivity observed at some wells (EC up to 2,290 µS/cm) is due to the leaching of evaporitic minerals present in the underlying Cretaceous formations.

In respect to seasonal fluctuations of the groundwater levels within the alluvial aquifer great difference are observed (Fig. 7.27). While the wells 68 and 72 show only slight variations between the dry and wet seasons, the wells 69 and 70 located close to the main wadis show differences up to 10 meters (70). This enhances the idea of the heterogeneity of the aquifer system with very dynamic parts in direct connection to the wadis, and parts recharged by the Liassic limestones showing low seasonal variations of the groundwater table.

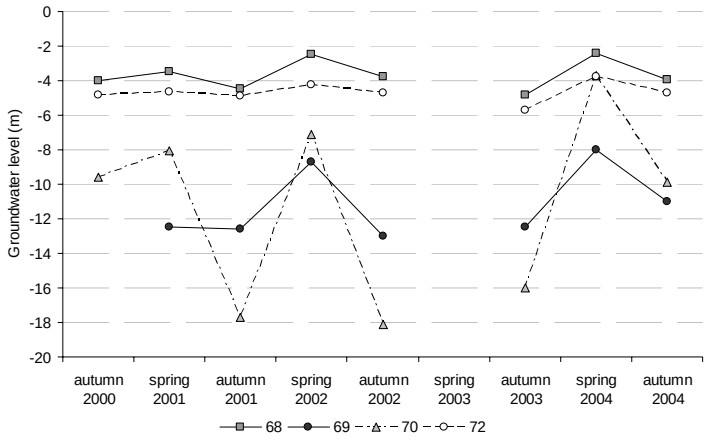

Fig. 7.27: Seasonal variation of the groundwater level for four wells (68, 69, 70 and 72) located in the Ifre catchment (autumn = dry season).

7.3.2.2 Hierarchical Cluster Analyses

A Hierarchical Cluster Analyse (HCA) was carried out on 18 observation points including selected points of the Assif-n'Ait-Ahmed catchment. Clustering results in three well defined groups (Fig. 7.28-A). As observed in the Assif-n'Ait-Ahmed catchment (Fig. 7.12), groundwater samples lay between three distinctive end members (Figure 7.28-B): groundwater of Liassic carbonates (spring Elmra), groundwater affected by leaching of gypsum (spring 123) and groundwater affected by leaching of halite (Ama 2). Consequently, the classifying of the groundwater reflects the leaching of evaporitic minerals with increasing concentrations of Ca^{2+}, SO_4^{2-}, Na^+, Cl^-, K^+ and Sr^{2+} (Tab. 7.6).

Clusters 1 and 2 show similar groundwater facies of Ca-Mg-HCO_3-Cl/SO_4 type revealing a groundwater passage in the Liassic aquifer (Fig. 7.28-B and C). While cluster 1 groups the

lowest mineralised groundwater, cluster 2 is slightly more mineralized due to the influence of gypsum leaching (Tab. 7.6 and Fig. 7.28-C). Moreover, cluster 2 is distinguished from the others by a higher value of SiO_2 (6.1 mg/l) revealing a groundwater passage within the Triassic formations (Paragraph 7.3.1) and a higher mean value of NO_3^- (36.3 mg/l) which results clearly from local anthropogenic pollution. The more mineralised groundwater of cluster 3 shows elevated values of Ca^{2+} (132.8 mg/l), SO_4^{2-} (197.5 mg/l) and Cl^- (211.8 mg/l) due to dissolution of gypsum and halite and belongs to the Ca-Na-Mg-Cl groundwater facies (Fig. 7.28-B and C).

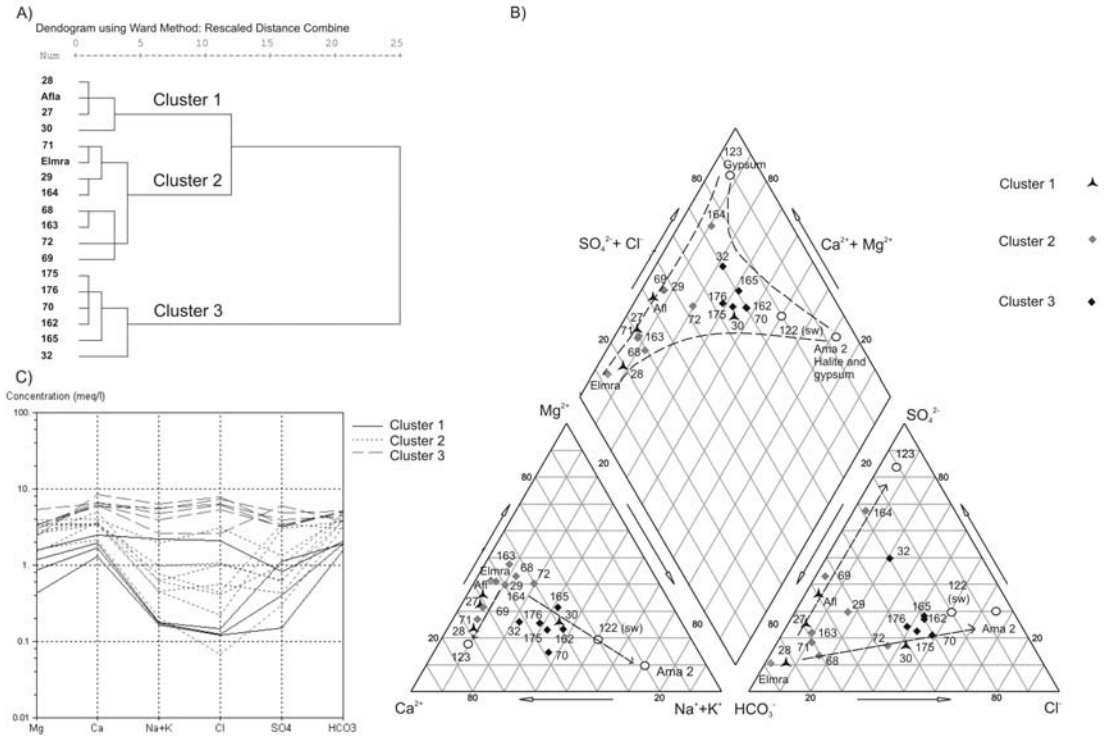

Fig. 7.28: Groundwater chemistry of the Ifre catchment based on mean values; HCA (A), Piper diagram (arrows show the evolution of the groundwater from the carbonate (Elmra) to the chloride (Ama 2) or sulphate facies (123) due to the leaching of evaporitic minerals (sw: surface water) (B) and Schoeller diagram (C).

Tab. 7.6: Mean values of variables for the clusters of groundwater defined by HCA in the Ifre catchment.

Parameter	Cluster 1 (N: 4)		Cluster 2 (N: 8)		Cluster 3 (N: 6)	
	mean	SD	mean	SD	mean	SD
T (°C)	13.6	6.0	16.1	1.8	15.4	2.2
ph	8.13	0.08	7.74	0.16	7.70	0.29
Ca^{2+} (mg/l)	37.2	10.0	71.5	15.5	132.8	18.1
Mg^{2+} (mg/l)	12.3	5.9	33.1	10.6	42.39	11.9
Na^+ (mg/l)	14.8	22.8	16.4	12.2	108.9	31.2
K^+ (mg/l)	1.4	0.9	1.6	0.48	2.6	0.37
Sr^{2+} (mg/l)	0.2	0.1	1.3	1.4	2.2	0.5
SiO_2 (mg/l)	2.1	0.4	6.1	1.5	5.2	0.9
Fe^{2+} (µg/l)	15	7	9	3	17	9
Mn^{2+} (µg/l)	3	4	2	1	5	4
HCO_3^- (mg/l)	113.7	12.6	243.6	44.3	288.9	34.2
Cl^- (mg/l)	22.2	35.1	30.4	33.9	211.8	66.9
NO_3^- (mg/l)	19.5	20.0	36.3	32.4	8.9	4.8
SO_4^{2-} (mg/l)	30.2	21.2	64.9	58.6	197.5	55.1
EC (µS/cm) (*1)	346	205	634	176	1428	232

(*1) *Electric conductivity (EC.) was not taken into account in the Hierarchical Cluster Analyse*

The springs of Taoujgalt (27, 28, 29, 30) and the wells 68, 69, 71, 72, 163 and 164 show the typical lower mineralised groundwater of the Liassic aquifer (clusters 1 and 2) (Fig. 7.29). Their significant Mg^{2+} component (Fig. 7.30) results from a passage within dolomite. Cluster 3 reveals the chemistry of the subsurface flow in the alluvial aquifer (Fig. 7.29) proved by the fact that the wells (70, 162, 165) and the springs close to the village of Alemdoun (175, 176) have substantial similarity in the chemistry to the surface water (point 122) at the outlet of the Assif-n'Ait-Ahmed catchment (Fig. 7.30, Fig. 7.28-B). Moreover, well 70 has a direct hydraulic connection to a wadi as already proved with its hydrodynamic reaction (Fig. 7.27).

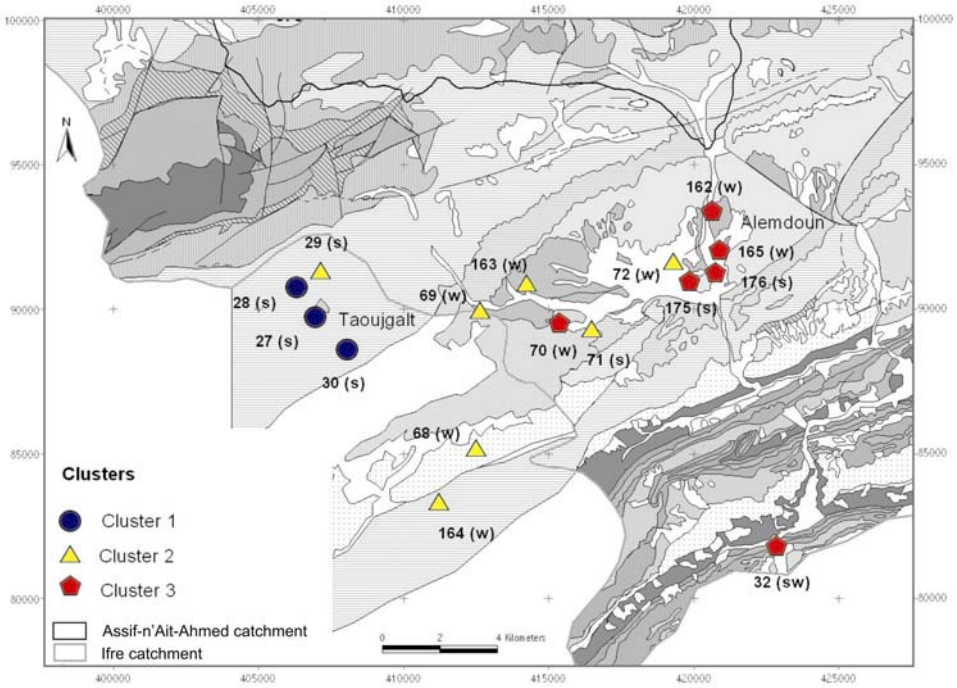

Fig. 7.29: Distribution of the clusters defined with HCA in the Ifre catchment: cluster 1 and 2 group groundwater from the Liassic carbonates and cluster 3 reflects the recharge by the wadis; s = spring, w = well, sw = surface water. Numbers are the sampled point references

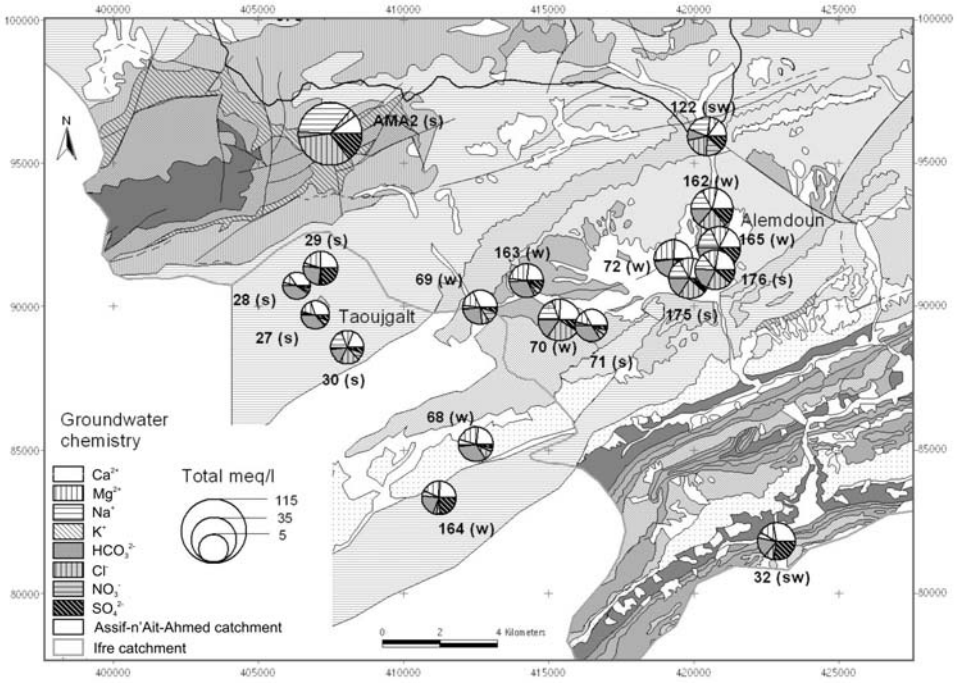

Fig. 7.30: Pie diagrams of the groundwater chemistry in the Ifre catchment (autumn 2003); s = spring, w = well, sw = surface water. Numbers are the sampled point references

7.3.2.3 Principal Component Analyse

Principal Component Analyse (PCA) are applied to the mean values of 12 variables at 18 observed points (Fig. 7.31-A and B). The components were rotated. The three first components explain 86.6 % of the total variation which reveals a good structure of the data:

- Component 1 (axe 1) accounts for 41.2 % of the total variance with strong loadings for Ca^{2+}, SO_4^{2-}, Na^+ and Cl^-. Thus, this component reflects the dissolution of gypsum and halite.
- Component 2 (axe 2) accounts for 34.5 % and describes the correlation of SiO_2, $(CO_2)_{aq}$ and partly Mg^{2+} and HCO_3^- anti-correlated with pH. Thus it reflects the higher transit time of groundwater in contact with basalt and dolomite revealing.
- Component 3 (axe 3) accounts for 10.9% and reveals the impact of local pollution by the nitrates.

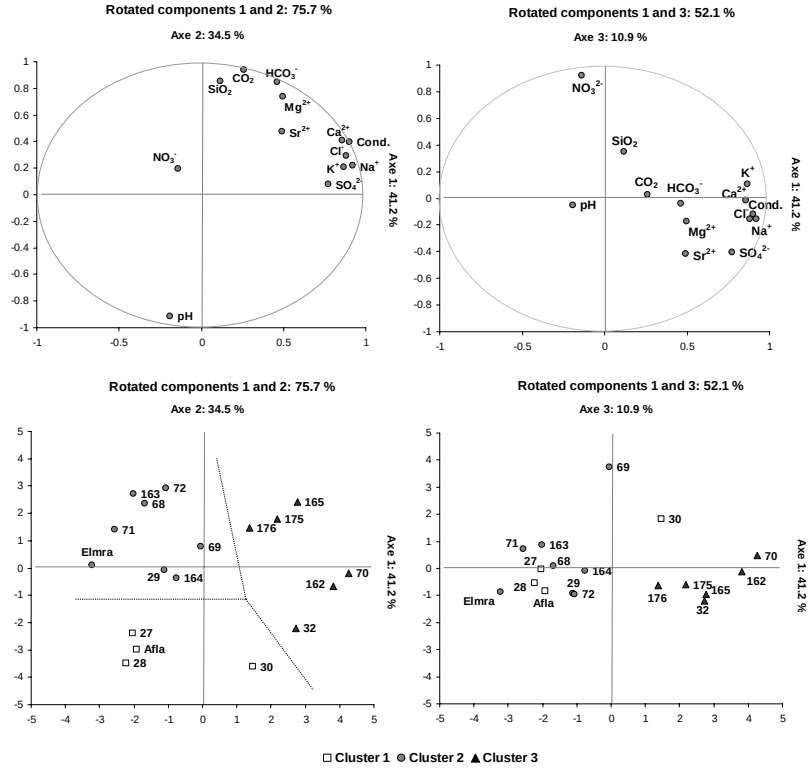

Fig. 7.31: Principal Component Analyses (PCA) in the Ifre catchment, results of the rotated components for the variables and samples (the clusters are defined by HCA).

The PCA confirms the results of the Hierarchical Cluster Analyse e.g. Well 70 (cluster 3) showing strong influences of evaporitic minerals plots close to component 1 or the elevated nitrate concentrations of well 69 (cluster 2) result in a plotting close to component 3 (Fig. 7.31-C and D).

7.3.2.4 Saturation Index

Saturation indexes (SI) of calcite, dolomite, gypsum and quartz are calculated for the mean values and used to define the degree of evolution of the groundwater in the Ifre catchment (Fig. 7.32, Tab 7.7). While cluster 1 and 2 show equilibrium in regard to calcite ($SI_{calcite\ (1)}$ = 0.12; $SI_{calcite\ (2)}$ = 0.29), cluster 3 is slightly over-saturated ($SI_{calcite\ (3)}$ = 0.50). In regard to dolomite, cluster 1 is in equilibrium to slightly under-saturated ($SI_{dolomite\ (1)}$ = -0.11) and therefore well distinguished from clusters 2 and 3 ($SI_{dolomite\ (2)}$ = 0.45; $SI_{dolomite\ (3)}$ = 0.59). In regard to quartz,

cluster 1 shows lower values ($SI_{quartz\ (1)}$ = -0.31) than the other two clusters 2 ($SI_{quartz\ (2)}$ = 0.08; $SI_{quartz\ (3)}$ = 0.05). Additionally, cluster 3 is more saturated in regard to gypsum (-1.24). Taking into consideration that the dissolution of gypsum increases the general saturation of the solution, it is assumed that cluster 2 being less influenced by leaching of gypsum reveals the more evolved groundwater with higher residence time.

Tab. 7.7: Mean values of the saturation indexes (SI) in regard to calcite, dolomite, gypsum and quartz of the clusters defined by Hierarchical Cluster Analyse in the Ifre catchment.

Cluster	$SI_{calcite}$	$SI_{dolomite}$	SI_{gypsum}	SI_{quartz}
1	0.12	-0.11	-2.52	-0.31
2	0.29	0.45	-2.02	0.08
3	0.50	0.59	-1.24	0.05

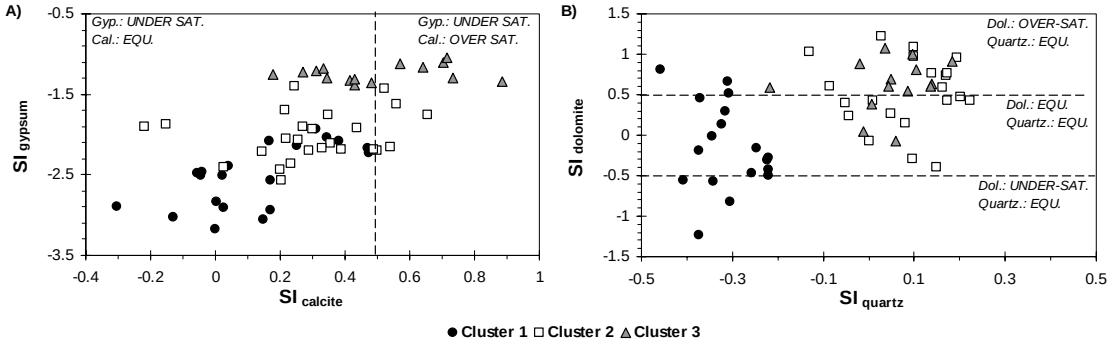

Fig. 7.32: Saturation index (SI) of the groundwater in the Ifre catchment: SI_{gypsum} versus $SI_{calcite}$ (A); $SI_{dolomite}$ versus SI_{quartz} (B); Gyp. = gypsum, Cal. = calcite, Dol. = dolomite, EQU. = equilibrium, UNDER-SAT. = under saturation and OVER-SAT. = over saturation.

7.3.2.5 Stable isotopes

The isotopic composition of springs, wells and surface water of the Ifre catchment sampled during each campaign is characterized by a significant variation of $\delta^{18}O$ contents between -9.9‰ and -7.5 ‰ and -66 ‰ and -54 ‰, for $\delta^{2}H$ respectively (Fig. 7.33). Groundwater plots close to the Local Meteoric Water Line (LMWL). Only spring 71 (having a very low discharge) and the wells 67 and 68 show evaporation effects. The isotopic signature of the surface water at the outlet of the Ifre catchment (Fig. 7.25, n°. 32) is of a similar type as the signatures prevailing in the Assif-n'Ait-Ahmed catchment and do not show any evaporation effects (Fig. 7.33).

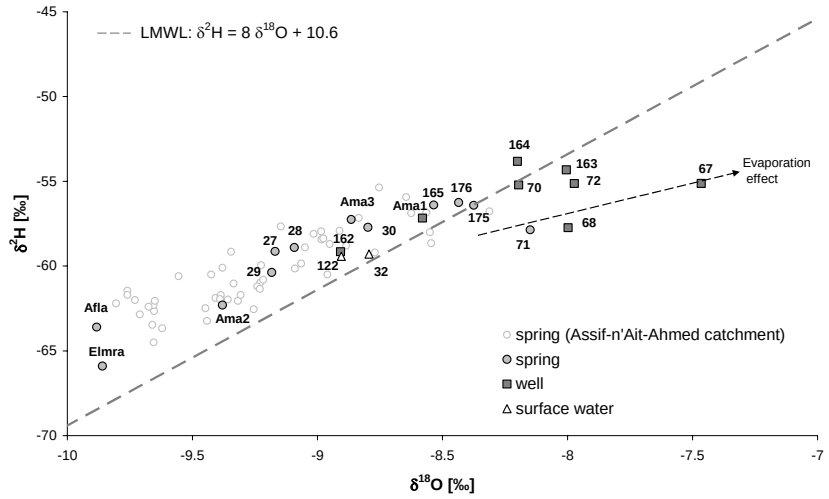

Fig. 7.33: Isotopic composition of the groundwater of the Ifre catchment (mean values) and LMWL.

Applying the calculated relation between altitude and oxygene-18 which was validated with the DEM (Paragraph 6.2.7: $\delta^{18}O$ = -0.002 · "mean altitude of the recharge area" -3.0) the mean

altitude of the recharge areas of the springs and wells are estimated (Fig. 7.34). Due to the observed evaporation effect well 67 was excluded from this interpretation. The springs Afla (2,385 m) and Elmra (2,236 m) draining the Liassic carbonates in the north have the highest mean recharge altitude about 3,450 m (Fig. 7.35). Although, the springs of Taoujgalt (27, 28 and 29) are located at different altitudes (between 2,215 and 2,535 m), they show a similar mean altitude of recharge of 3,050 m (Fig. 7.35), thus proving the Liassic carbonates as recharge area. The groundwater of the alluvial aquifer between Taoujgalt and Alemdoun (70, 71, 162, 163, 165, 175 and 176) situated between 1,768 m to 1,908 m show mean altitudes of recharge between 2,400 m and 3,000 m (Fig. 7.35). In general, the estimations prove a mean altitude of the recharge areas up to 1,100 m above the sampling point in the Ifre catchment. The isotopic signature of the surface water at the Ifre station (32) reflects a mean altitude of the recharge area of 2,900 m (Fig. 7.35) corresponding to the Liassic carbonates of the Lotharagian-Domerian (cropping out between 1,700 and 4,100 m of altitude with a mean of 2,750 m). Hence, the results of YOUBI (1990) giving a proportion of 75 % of base flow in the M'Goun River at Ifre station (Paragraph 5.3.4) is evidenced with the isotopic signatures.

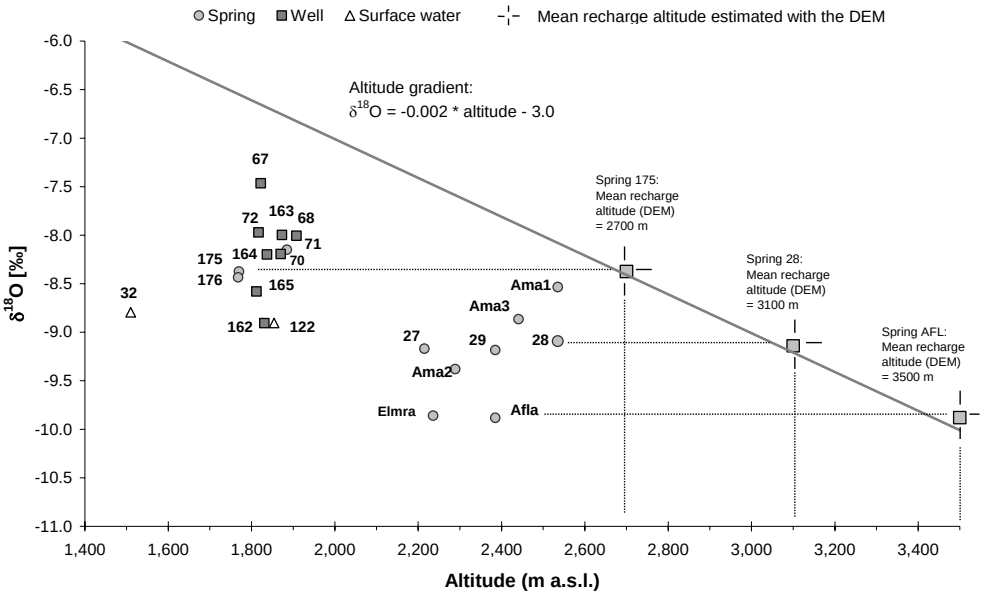

Fig. 7.34: Estimation of the mean recharge altitudes of the observation points in the Ifre catchment according to the relation $\delta^{18}O = -0.002 \cdot$ "mean altitude of the recharge area" – 3.0 (Chapter 6).

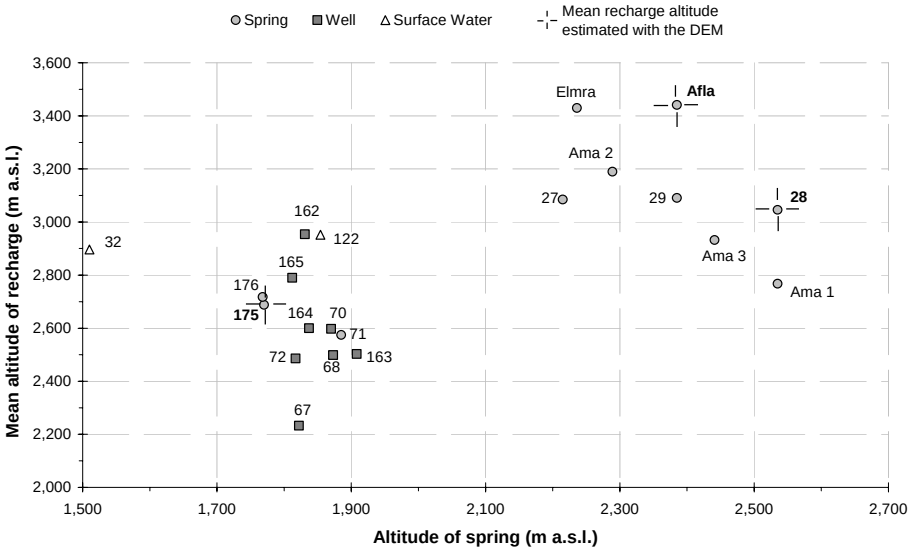

Fig. 7.35: "Mean altitude of the recharge area" versus "altitude of the spring" in the Ifre catchment.

7.3.2.6 Tritium

In the Ifre catchment, 2 springs at Taoujgalt (27 and 28), 5 wells (70, 72, 162, 163 and 165) and the surface water at Ifre (32) were sampled for tritium analyses and interpreted (Chapter 6) in order to complete the results of the Assif-n'Ait-Ahmed catchment (Fig. 7.36). Results and interpretations of tritium analyses considering the case of unconfined aquifer are compared according to the 3 clusters (Paragraph 7.3.2.2):

- Cluster 1: low mineralized groundwater from the Liassic aquifer. Given by the relative high values of tritium of the representative springs 27 (8.0 TU) and 28 (9.1 TU) mean residence times between 4 to 8 years are calculated.
- Cluster 2: low mineralized groundwater from the Liassic aquifer but with relative high content of SiO_2 (6.1 mg/l; and slightly over-saturation in regard to quartz, see Tab. 7.6 and 7.7) revealing higher mean residence times and an underground passage within basalt. The representative wells 72 (4.5 TU) and 163 (3.6 TU) show relative low contents of tritium. Interpretation of those values is only possible by the combination of both the hydrogeochemical and the isotopic data (Fig. 7.37). The water of the two wells is the result of a mixing between recent groundwater from the Liassic carbonates (8 TU to 10 TU) and older groundwater from the Triassic formations (e.g. spring 4 in the Assif-n'Ait-Ahmed with 0.7 TU) (Fig. 7.37).
- Cluster 3: mineralized groundwater of the alluvial aquifer. The representative wells 70 (6.7 TU), 162 (6.2 TU) and 165 (5.5 TU) reveal recent groundwater with a mean residence time below 4 years.

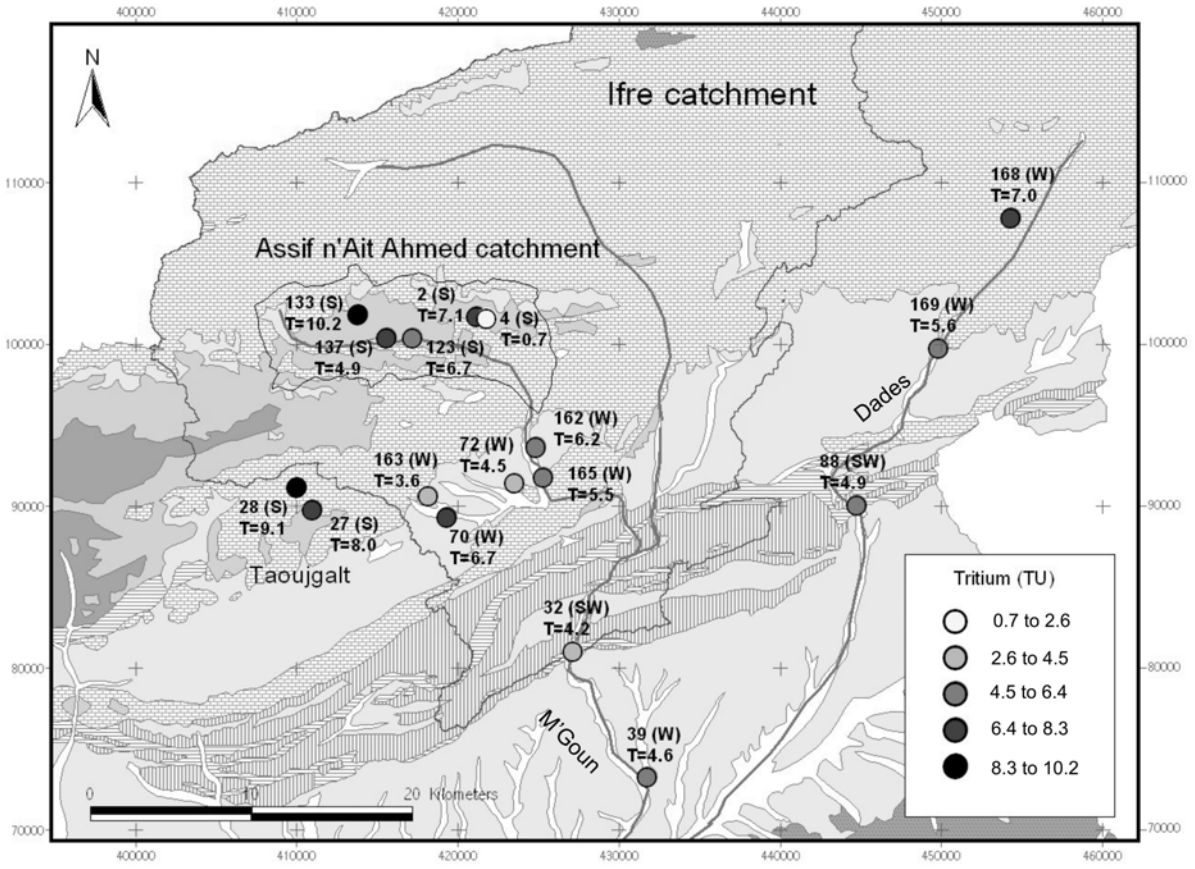

Fig. 7.36: Tritium values (TU) of groundwater and surface water in the Ifre catchment and at the Dades canyon (W = well, S = spring and SW = surface water).

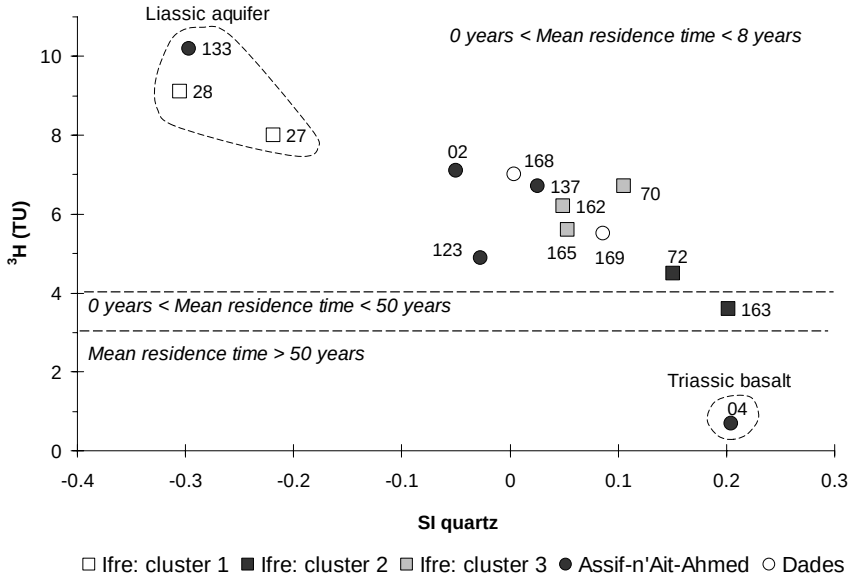

Fig. 7.37: ^{3}H versus SI_{quartz} (IMP5) of the groundwater of High Atlas: Ifre catchment (clusters defined by HCA), Assif-n'Ait-Ahmed catchment and samples from the Dades valley.

7.3.3 Skoura mole and Dades canyon

In order to complete the characterization of the groundwater from the High Atlas aquifers, two springs in the Cambrian and Precambrian schists of the Skoura mole (73 and 74) and two wells (168 and 169) and the Dades Wadi (88) were sampled in the Dades canyon (Fig. 3.2).

The Ca-Mg-HCO_3 type groundwater of the Precambrian rocks of the Skoura Mole is low mineralized with electric conductivities between 300 and 500 µS/cm (Fig. 7.38) in comparison to the groundwater from the Dades canyon draining the Lower Jurassic aquifer (EC = 700 to 1,100 µS/cm). The groundwater water type in the Dades canyon ranges between Ca-Mg-Na-HCO_3 and Ca-Mg-HCO_3-SO_4 revealing leaching of evaporitic minerals as observed in the Ifre catchment (Fig. 7.38).

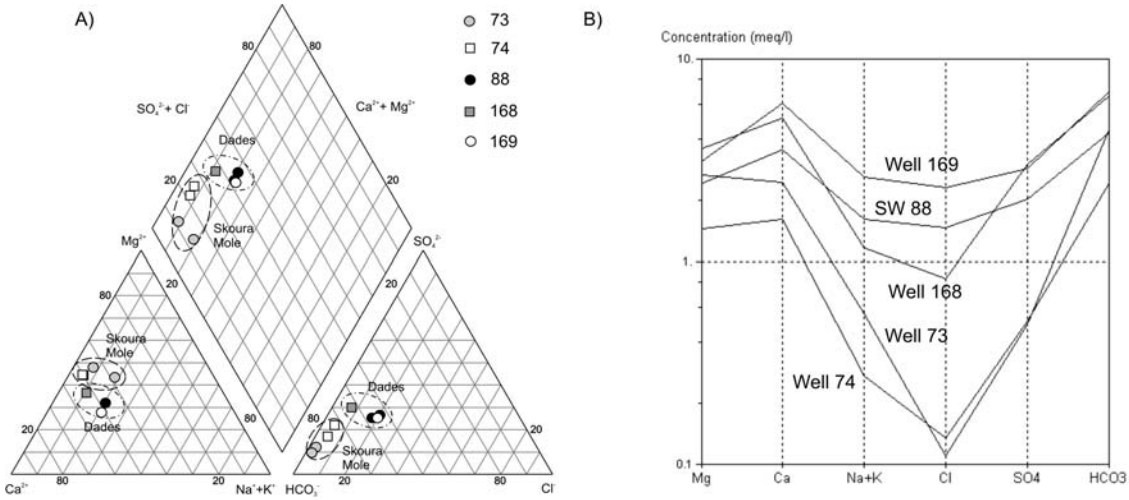

Fig. 7.38: Hydrogeochemical characteristic of the groundwater sampled in the Skoura Mole and in the Dades Valley: Piper (A) and Schoeller (B) diagrams.

In respect to the stable isotopes the sampled water plot around the Local Water Meteoric Water Line (Fig. 7.39 and Tab. 7.8). While the groundwater samples of the Skoura Mole with d-exess values of 10.4 and 12.8 are close to the LWML, the samples from the Dades valley shows slight evaporation effects (d-exess = 8.3 and 9.4).

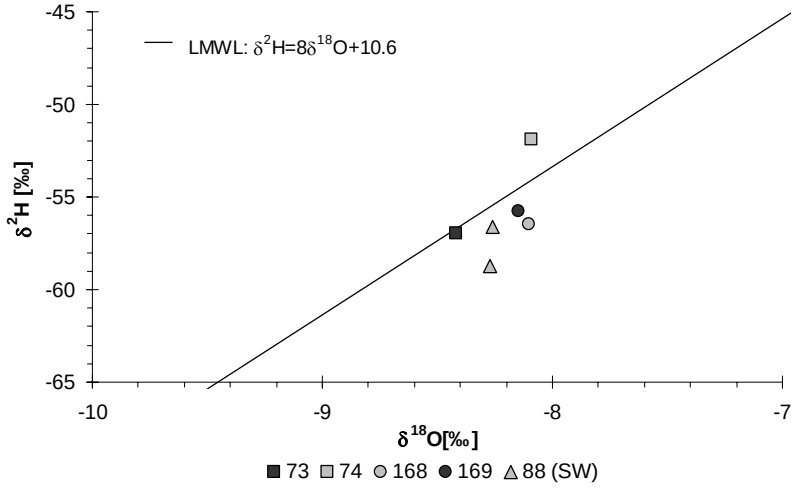

Fig. 7.39: Isotopic composition of the groundwater in the Precambrian Skoura Mole (73 and 74) and in the Dades valley (168 and 169), and of the Dades Wadi (88); SW= surface water.

The evaluation of the mean altitude of the recharge area of these wells is carried out with the same method already described for the Assif-n'Ait-Ahmed and Ifre catchments (Tab. 7.8). The calculated mean recharge altitude of the observation points ranges between 2,575 m to 2,700 m.

Tab. 7.8: Isotopes composition of the groundwater sampled in the Skoura Mole and in the Dades Valley.

Nr	Place	Type of water	$\delta^{18}O$ [‰]	$\delta^{2}H$ [‰]	Excess	Altitude of the sampling point (m a.s.l.)	Estimated altitude of the recharge (m a.s.l.)
73	Skoura mole	well	-8.4	-57	10.4	2110	2700 m
74	Skoura mole	well	-8.1	-52	12.8	2300	2575 m
168	Dades canyon	well	-8.1	-56	8.3	1760	2575 m
169	Dades canyon	well	-8.1	-56	9.4	1700	2575 m
88	Dades canyon	surface water	-8.3	-58	8.5	1550	2650 m

In the Dades valley, the mean residence time is between 0 to 4 years at well 169 (^{3}H = 5.6 TU) and between 4 to 8 years at well 168 (^{3}H = 7.0 TU). These evaluations are done with the interpretations described in chapter 6 for unconfined aquifer.

7.3.4 Hydrogeological conceptual model of the High Atlas aquifer system

A conceptual model of the aquifer systems of the High Atlas (Fig. 7.40) is elucidated based on detailed investigations of both the Assif-n'Ait-Ahmed and the Ifre catchment.

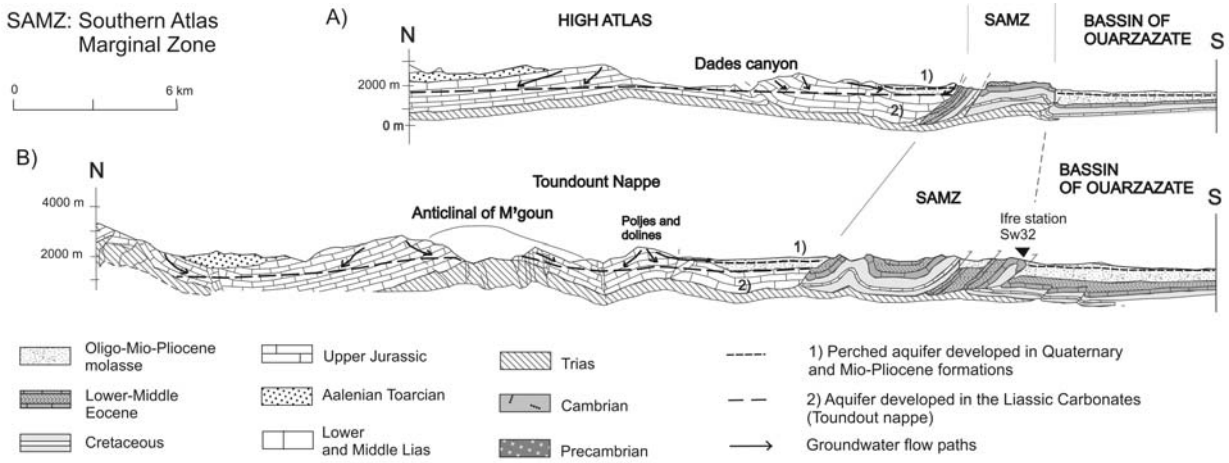

Fig. 7.40: Hydrogeological conceptual model of the High Atlas aquifers: the Southern Atlas Marginal Zone (SAMZ) acts as a hydrogeological barrier between the karst aquifers of the High Atlas and the Basin of Ouarzazate (profiles after JOSSEN & FILALI 1988); localisation Fig. 4.19 and 4.20.

The Lower Liassic series (Lotharagian-Domerian) represent the main fissured and partly karstified aquifer. The Triassic rocks act as the aquitard. Due to its geological characteristics the Southern Atlas Marginal Zone (SAMZ) acts as a hydrogeological barrier between the aquifers of the High Atlas and the Basin of Ouarzazate. Therefore a direct contribution of the Liassic aquifer to the recharge of the Basin of Ouarzazate (Chapter 8) seems unrealistic except the possibility of a lateral groundwater flow in the region of Toundoute.

The presence of evaporitic minerals such as gypsum, halite and sylvite in the Triassic formations and also in the Cretaceous and Eocene series increase the mineralization of the groundwater and can generate processes of dedolomitization as described in the Assif-n'Ait-Ahmed catchment.

The Liassic aquifer is overlaid by Quaternary to Mio-Pliocene formations where perched aquifers are developed. These shallow or alluvial aquifers are strongly linked with the wadis. Besides direct recharge by precipitation the recharge of those perched aquifers can be distinguished into three components:

- The most important component of the recharge occurs through wadis characterized by an elevated mineralization due to the leaching of evaporitic minerals at the contact with the Triassic and Cretaceous rocks. The groundwater recharged by this component show a mean residence time below 4 years.
- The second component of the recharge originates from the Liassic carbonates which shows low mineralized groundwater with mean residence times between 4 and 8 years.
- The third component considers groundwater from the Liassic carbonates influenced by an underground passage within or at the contact to the Triassic aquitard, which is proved by higher SiO_2 contents. The mean residence time of this groundwater, results of the mixing of groundwater from the Liassic aquifer (between 4 and 8 years) and of groundwater from Triassic formations (> 50 years: defined in the Assif-n'Ait-Ahmed catchment).

7.3.5 Comparison of the Anti Atlas (Jbel Saghro) and the High Atlas

While the aquifer system in the Jbel Saghro (Anti Atlas) shows simple hydrogeological features with alluvial aquifers overlying low permeable rocks of Precambrian, the folded and faulted carbonates of High Atlas show a more complex hydrogeological setting.

In the Assif-n'Ait-Ahmed catchment (110 km^2), the Liassic carbonates of the Toundoute nappe represent the most important aquifer in this catchment with a potential groundwater volume ranging between 0.19 and 0.38 km^3. The Triassic formations underlying the Liassic aquifer act as an aquitard. The leaching of evaporitic minerals within the Triassic clays increases the mineralization of the groundwater. Processes of dedolomitization linked with gypsum dissolution are identified explaining the observed correlation between Mg^{2+} and SO_4^{2-} in the groundwater. While, the mean residence time of groundwater from the Liassic carbonates ranges between few years to 8 years according to the karstification, the groundwater from Triassic formations show clearly a mean residence time above 50 years. The groundwater of the Assif-n'Ait-Ahmed shows high mean altitude of recharge area between 2,650 m to 3,400 m according to the isotopic signature.

Almost 50% of the Ifre catchment (1,240 km^2) is covered by Liassic carbonates (305 km^2 of massive limestones and dolomites of Lotharagian and 300 km^2 of limestones alternating with marls of Domerian). These formations represent the main groundwater storage of the Upper Drâa catchment. The south-western part of the Ifre catchment is investigated in regard to the geology, the hydrogeochemistry of groundwater and the hydrodynamic with the setting of a precise piezometric map. The investigations reveal two types of aquifers: the Liassic carbonates of the Toundoute nappe and the overlaying Quaternary-Mio-Pliocene formations where an alluvial aquifer is developed. The alluvial aquifer is recharged in one hand by riverbed infiltration of wadis characterized by high mineralised groundwater with mean residence time below 4 years, and in another hand by lateral groundwater flows from the Liassic aquifer (mean residence time between 4 and 8 years). Mixing between groundwater from Liassic formations and Triassic formations is observed in the alluvial aquifer. The groundwater of the Ifre catchment shows high mean altitude of recharge area between 2,200 m to 3,450 m according to the isotopic signature.

From a geological point of view, the Southern Atlas Marginal Zone acts as a hydrogeological barrier between the High Atlas and the Basin of Ouarzazate. The drainage of the aquifer of the High Atlas occurs mainly by the alluvial aquifers, which recharge the Basin of Ouarzazate. The sink of the Liassic aquifer is not known.

Compared to the High Atlas, the groundwater sampled in the Jbel Saghro appears to be more evolved (mean $SI_{dolomite}$ = 0.52, mean SI_{quartz} = 0.27) (Tab. 7.9), although the only sample for tritium analyse shows recent groundwater (< 4 years). In the High Atlas, an evolution of the saturation of the groundwater can be observed between the Assif-n'Ait-Ahmed and the Ifre catchments (Tab. 7.9) reflecting the general groundwater flow direction.

Tab. 7.9: Comparison of the calculated mean saturation indexes of calcite, dolomite, gypsum and quartz in the Anti Atlas (Jbel Saghro) and in the High Atlas.

		Anti Atlas	High Atlas			
Place		**Jbel Saghro** 3 points 20 samples	**Assif-n'Ait-Ahmed** 63 points 156 samples	**Ifre** 15 points 60 samples	**Skoura Mole** 2 points 4 samples	**Dades** 2 points 2 samples
$SI_{calcite}$	min	-0.16	-0.35	-0.3	-0.58	0.12
	max	0.78	0.94	0.88	0.18	0.16
	mean	**0.32**	**0.19**	**0.29**	**-0.20**	**0.14**
	SD	0.28	0.32	0.25	-	-
$SI_{dolomite}$	min	-0.43	-0.97	-1.23	-1.18	-0.05
	max	1.39	2.31	1.22	0.44	0.17
	mean	**0.52**	**0.10**	**0.30**	**-0.40**	**0.06**
	SD	0.54	0.62	0.55	-	-
SI_{gypsum}	min	-0.81	-3.41	-3.18	-2.43	-1.39
	max	-1.77	-0.20	-1.04	-2.28	-1.36
	mean	**-1.33**	**-1.91**	**-1.99**	**-2.35**	**-1.38**
	SD	0.27	0.83	0.57	-	-
SI_{quartz}	min	-0.02	-0.76	-0.46	-0.80	0.00
	max	0.42	0.32	0.22	0.18	0.05
	mean	**0.27**	**-0.11**	**-0.06**	**-0.31**	**0.03**
	SD	0.11	0.24	0.20	-	-

In regard to the isotopic signature, the groundwater in High Atlas (mean $\delta^{18}O_{Ifre}$= -8.6‰) is clearly more depleted in heavy isotopes than the groundwater in the Jbel Saghro (mean $\delta^{18}O_{Jbel\ Saghro}$ = -6.5‰) (Tab. 7.10). This difference reflects a combination of the altitude effect during the recharge by precipitation in the High Atlas and the evaporation effect occurring in the alluvial aquifers of the Anti Atlas.

Tab. 7.10: Comparison of the stable isotopes of the Anti Atlas (Jbel Saghro) and the High Atlas.

		Anti Atlas	**High Atlas**			
Place		**Jbel Saghro** 3 points 20 samples	**Assif-n'Ait-Ahmed** 63 points 187 samples	**Ifre** 15 points 73 samples	**Skoura Mole** 2 points 2 samples	**Dades** 2 points 2 samples
$\delta^{18}O$ [‰]	min	-7.3	-10.8	-9.9	-8.1	-8.1
	max	-5.5	-7.6	-6.6	-8.4	-8.1
	mean	**-6.5**	**-9.1**	**-8.6**	**-8.3**	**-8.1**
	SD	0.5	0.5	0.6	-	-
$\delta^{2}H$ [‰]	min	-49	-71	-66	-52	-56
	max	-38	-53	-49	-57	-56
	mean	**-43**	**-60**	**-58**	**-54**	**-56**
	SD	4	3	2	-	-
d-excess	min	5.7	5.7	3.4	12.8	8.3
	max	11.8	16.6	16.0	10.4	9.4
	mean	**8.6**	**12.8**	**10.8**	**11.6**	**8.9**
	SD	1.6	1.8	2.8	-	-

8 HYDROGEOLOGY OF THE BASIN OF OUARZAZATE

8.1 Introduction

The population of the Upper Drâa catchment is concentrated in the Basin of Ouarzazate, mainly in the city of Ouarzazate but also in smaller towns such as Skoura, Kelaa M'Gouna or Boumalne. Agriculture in the various palm-groves and tourism are the main economic activities, which require an efficient and sustainable freshwater resource management. Therefore, a profound knowledge about the aquifer system in the Basin of Ouarzazate is of primordial importance. This chapter gives a hydrodynamic description of the various aquifers based on the given lithology. During the investigations wells (35 with 2 artesian), springs (4) and surface water (7 wadis) were sampled regularly in the basin (Fig. 8.1). A hydrogeochemical characterization of the groundwater is performed using statistical methods such as Hierarchical Cluster Analyses (HCA) and Principal Component Analyses (PCA). The various processes affecting the groundwater chemistry (e.g. mixing) are accessed taking into account the seasonal variations and the interaction between surface water and groundwater. Saturation indices calculated in respect to selected minerals reveal the evolution of the groundwater, which reflects the geochemical type of the aquifer and the transit time. Additional, environmental isotopes (^{3}H, ^{2}H and ^{18}O) are used to identify both the recharge areas and the transit times.

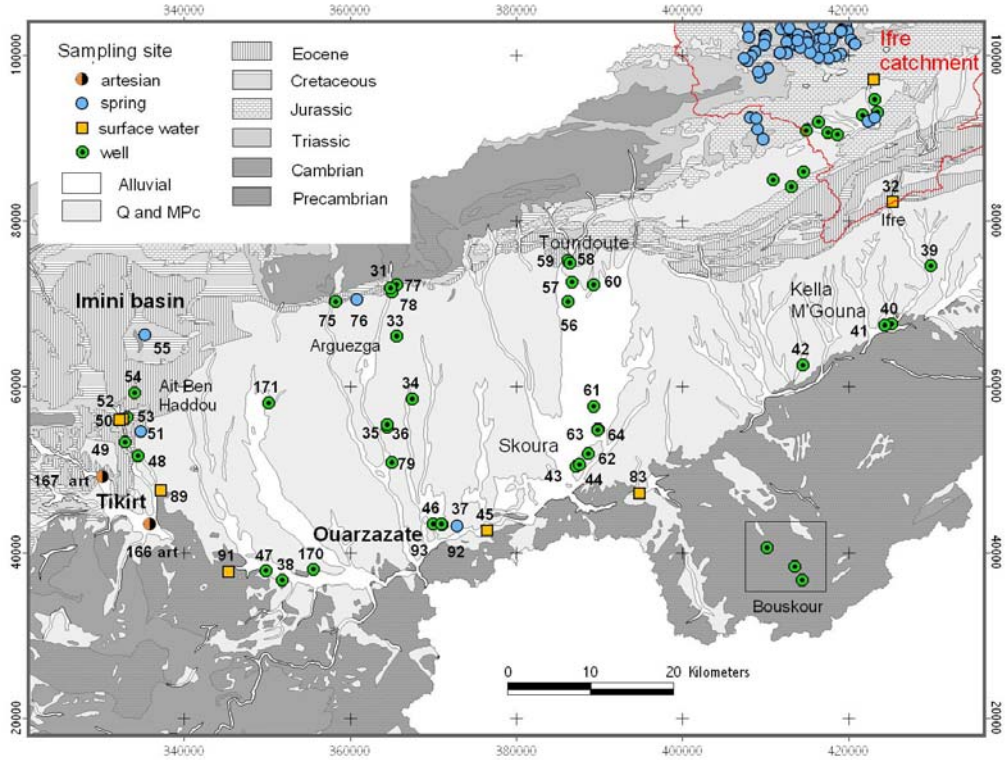

Fig. 8.1: Localisation of the sampling sites in the Basin of Ouarzazate (Q= Quaternary and MPc= Mio-Pliocene).

8.2 Hydrogeological overview

The Basin of Ouarzazate is an asymmetrical synclinal with a Tertiary and Quaternary continental infilling (Chapter 4). Two main types of aquifers can be distinguished. While shallow aquifers are developed in the Quaternary and the superficial Mio-Pliocene deposits, deeper aquifers exist in the Mio-Pliocene, Eocene and Cretaceous formations.

8.2.1 Shallow aquifers

Shallow aquifers are developed in Quaternary formations and in reworked Mio-Pliocene deposits made of conglomerates and sandstones. These formations generally overlay Mio-Pliocene marls and clays. The shallow aquifers, which are merged as alluvial aquifers in the context of this thesis, are more or less in hydraulic connection to the wadis. Within the Basin of Ouarzazate three main alluvial aquifer systems are developed, one along the Dades and M'Goun Wadis in the north-east, a second stretching between Toundoute and Skoura and a third around Ouarzazate with a surface area averaging 80 km^2. In general, the alluvial aquifers show a high variability within the catchment in regard to both thickness (generally between 0 and 25 m, but up to 40 m near Toundoute) and lithology (Tab. 8.1and Fig. 8.2) and thus a high heterogeneity in permeability. KHALIL & RACHACH (1986) calculated a mean transmissivity value of 5.2 ·10^{-2} m^2/s and a storage coefficient around 9 % in the Ouarzazate alluvial aquifer. In some cases the alluvial aquifers of the M'Goun and Dades wadis extend to the terraces and pediment covers and might have local hydraulic connections to the underlying Mio-Pliocene formations (MINISTÈRE DE L'ÉQUIPEMENT et al. 2002).

Tab. 8.1: Lithology of the alluvial aquifer at 8 boreholes of the Basin of Ouarzazate (localisation Fig. 8.2); data from DRH.

Well	Depth	Lithology
664/55	25 m	clayey silt, pebble and conglomerates
736/55	25 m	clayey silt and conglomerates
741/55	4 m	clayey silt with pebbles and gravel
887/54	25 m	clayey silt, clays and gravel
773/63	10 m	clayey silt
738/63	18 m	Conglomerates. with clayey matrix
1004/63	10 m	Sand, marls, gravel

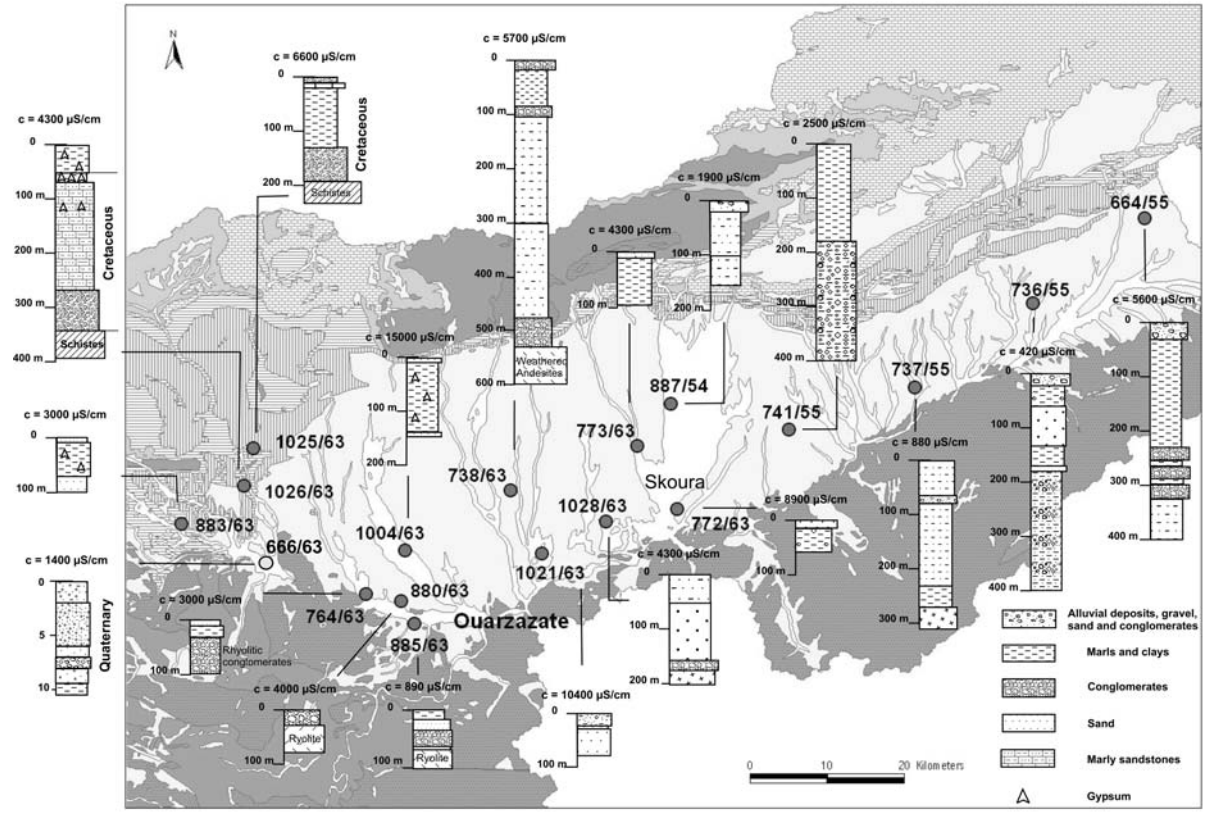

Fig. 8.2: Lithology at selected boreholes in the Basin of Ouarzazate; data from DRH.

The separated alluvial aquifer systems in the Basin of Ouarzazate form the main prolific groundwater resources of the Basin of Ouarzazate.

8.2.2 Semi-deep aquifer of the Mio-Pliocene

The Mio-Pliocene formations show a high variability of facies and thickness due to there deposition in a pro-grading alluvial fan system (Paragraph 4.3) (Tab. 8.2). They consist of marls, clays, siltstones, sandstones, lenses of sand, conglomerates and primary gypsum. Although these formations are generally clayey and consequently have low permeability, some local aquifer exists. Pumping test performed by the DRH proved a wide range of transmissivities and productivities (Tab. 8.2). Conglomerates often possess a clayey matrix resulting in low productivities and reduced transmissivities (e.g. borehole 664/55).

Tab. 8.2: Depth, water temperature, electric conductivity (EC), transmissivities calculated for the drawdown (T_d) and the recovery (T_r)) and lithology of 4 deep boreholes compared to a typical alluvial profile (666/63) in the Basin of Ouarzazate (localisation Fig. 8.2); data from DRH.

IRE	Depth (m)	T (°C)	EC (µS/cm)	Q (l/s)	T_d (m^2/s)	T_r (m^2/s)	Lithology
666/63	10	18	1,400	25	0.02	0.64	clayey silt, sand, gravel and pebble
664/55	400	22.9	5,610	2	$6 \cdot 10^{-6}$	$5 \cdot 10^{-6}$	0 - 24 m: clayey silt and conglomerates 24 - 236 m: marls 236 - 312 m: conglomerates (clayey matrix) alternating with marls 312 - 400 m: sandy marls
737/55	284	22.4	880	10	$0.4 \cdot 10^{-3}$	$0.4 \cdot 10^{-3}$	0 - 67 m: marls 67 - 80 m : pebble, gravel and sand 80 - 225 m: marls with sand and gravel 225 – 274 m: marls 274 - 284 m: granite
736/55	400	22.2	420	20	$1.3 \cdot 10^{-3}$	$0.8 \cdot 10^{-3}$	0 - 25 m: clayey silt with gravel, sand and gravel 25 - 66 m: clays and marls 66 - 125 m: sand and gravel 125 - 136 m: sandstones 136 - 170 m: marls with sand and gravel 170 - 402 m: marls alternating with conglomerates
741/55	400	29.6	2,500	4	$4.5 \cdot 10^{-5}$	$3.4 \cdot 10^{-5}$	0-4 m: clayey silt with pebble and gravel 4-188 m: marls 188-400 m: conglomerates (marly matrix)

Between Ouarzazate and Skoura, an important deeper aquifer is developed within the Mio-Pliocene sand and conglomerates (Fig. 8.2) with both a high storage capacity and a potential high productivity. Consequently, the Mio-Pliocene formations might represent potential groundwater resources in spite of their high heterogeneity. But an exploitation of such aquifers has to take into account the quality (e.g. high mineralization) and the renewability of the groundwater.

8.2.3 Eocene and Cretaceous aquifers

While in the Imini basin, the Eocene carbonates (20 to 30 m of thickness) crop out over 330 km^2 forming small and unproductive perched aquifers which are drained by boundary springs (Fig. 8.3), in the Basin of Ouarzazate these formations are covered by a considerable thickness of the Mio-Pliocene series (compare Fig. 4.20). Consequently, these formations do not represent exploitable groundwater resources.

Conglomerates, sandstones and sand of the Infracenomanian and limestones and dolomites of the Cenomano-Turonian form a prolific confined aquifer in the eastern part of the Basin of

Ouarzazate (Fig. 8.3), which is drained by artesian wells (e.g. 166-art and 167-art). The 50 m thick aquitard is given by overlaying Senonian marls and/or Mio-Pliocene clays (MINISTÈRE DE L'ÉQUIPEMENT et al., 2002). Transmissivities vary between 0.2 $\cdot 10^{-3}$ to 6.6 $\cdot 10^{-3}$ m^2/s (KHALIL & RACHACH 1986). The groundwater flow direction is from north to south (KHALIL & RACHACH 1986) with a direct recharge in the out crop area of the Cretaceous series in the north (compare Fig. 4.20 profile F).

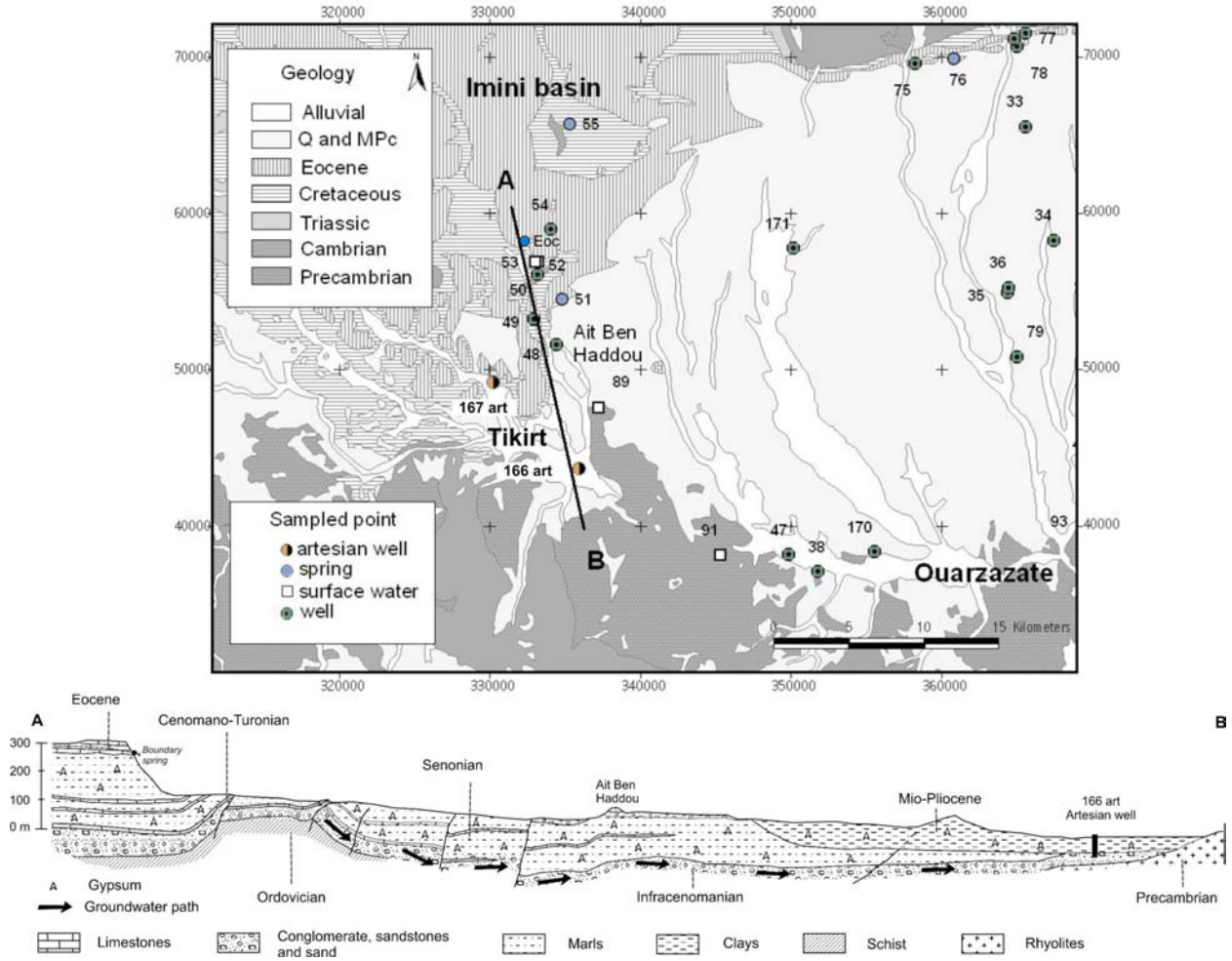

Fig. 8.3: Profile and location map in the western part of the Basin of Ouarzazate showing the confined Infracenomanian aquifer and the perched aquifer developed in the Eocene carbonates (Profile after JOSSEN & FILALI 1988; modified).

8.3 Groundwater table

A regional map of groundwater table contour lines of the alluvial aquifers is defined from data of the Direction Régionale de l'Hydraulique (DRH) completed by own observations (Fig. 8.4). The interpolation of the groundwater level is based on the Kriging extrapolation method and on hydrogeological interpretations. The hydrogeological limit of the northern range of the Basin of Ouarzazate is given by the impermeable rocks of the Skoura Mole (Precambrian to Ordovician schist and quartzite) and by the Southern Atlas Marginal Zone "SAMZ" (Fig. 8.4), which acts as a hydrogeological barrier between the carbonated aquifers of the High Atlas and the Basin of Ouarzazate. Hence, it is considered that the recharge of the basin occurs mainly by riverbed infiltration along the wadis. The southern range of the Basin of Ouarzazate is delimited by the impermeable Precambrian and Cambrian rocks of the Jbel Saghro.

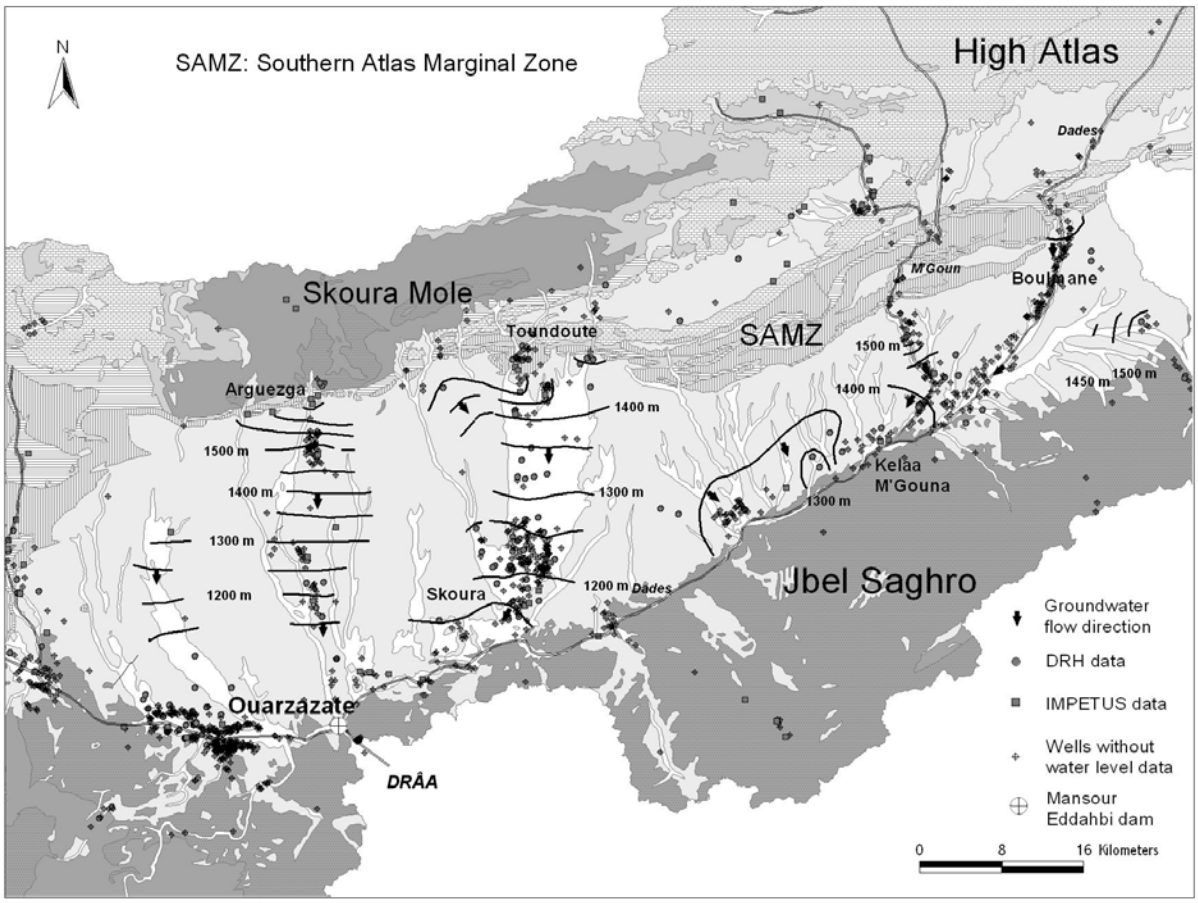

Fig. 8.4: Groundwater level contours of the shallow aquifers in the Basin of Ouarzazate; arrows represent the groundwater flow directions; data from DRH.

The groundwater level map (Fig. 8.4) shows the separated alluvial aquifers of the Basin of Ouarzazate. The general groundwater flow direction is from north and north-east toward south-west, converging in Ouarzazate. South-west of Kelaa M'Gouna, the alluvial aquifer shows a south-eastward groundwater flow direction due to the drainage of the Dades. The Anti-Atlas does not contribute efficiently to the recharge of the basin by lateral afflux. A strong gradient of the water table exists from the northern range to the middle of the basin (1/100) following the superficial slope. In the southern part of the basin, groundwater ponds towards the Precambrian rocks. Thus, the hydraulic gradient is less steep. The Drâa River with the Mansour Eddahbi reservoir represents the only superficial outflow of the basin.

The seasonal variation of the groundwater levels in the alluvial aquifers are more or less accentuated depending on the storage capacity of the aquifers and on the degree of an interaction with the surface water of the wadis (Fig. 8.5). The wells 623/54 and 626/54 (C) located in the northern range of the basin show the highest seasonal variations (up to 4 meters for well 626/54). Hence, the aquifer in this area does not have efficient recharge during the dry season. Contrarily, the well 521/63 (E) between Ouarzazate and Skoura shows low variations (standard deviation = 0.30 m) which could be the proof of a hydraulic connection with the semi-deep aquifer of the sandy Mio-Pliocene formations (Paragraph 8.2.2). The different response of the alluvial aquifers was emphasised during the drought between 1982 and 1987, when precipitation in Ouarzazate was down to 18.7 mm/a (1982-83) and 18.5 mm/a (1983-84). The drought ended in 1987 with a yearly precipitation of 227 mm (1987-88). Several wells (612/63 and 630/63 (B) nearby Ouarzazate; 189/63 and 181/63 (D) in the west of Skoura; 212/63 and

171/63 (E) in the Skoura area and 421/55 and 492/55 (F) in Kelaa M'Gouna) show clear decreasing of water levels during the drought (e.g. more that 6 m in well 612/63). Contrarily, the wells 104/63 and 113/63 (A) west of Ouarzazate as well as the well 521/63 (E) near Skoura and the well 431/55 (F) in the north-east of the basin, did not show any influences of the drought proving that at these wells the groundwater storage or the recharge is enough to face the lack of precipitation.

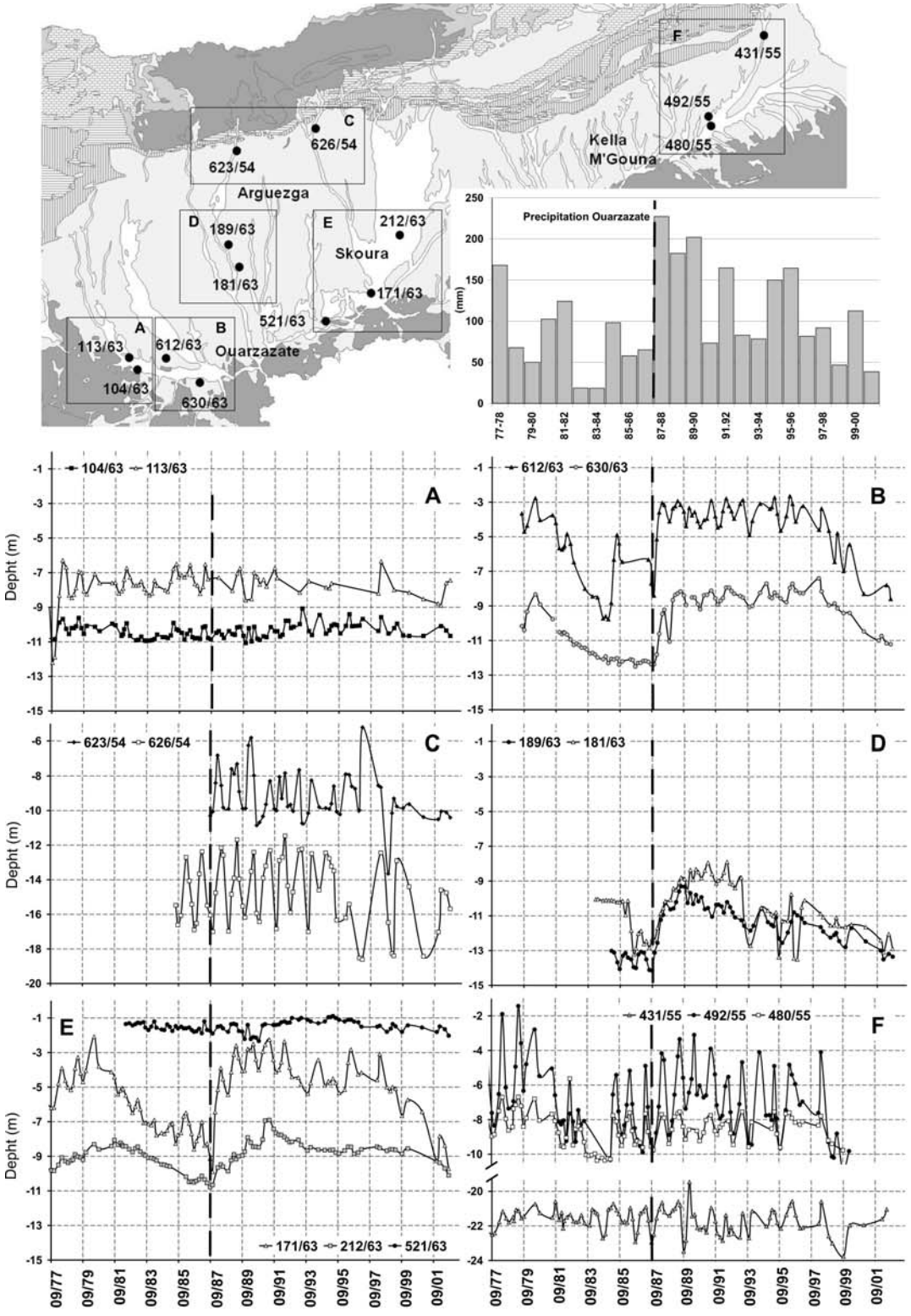

Fig. 8.5: Groundwater water fluctuations of 14 wells in the Basin of Ouarzazate compared to the precipitation (annual mean) for 1977 to 2001 (dashed line: end of the drought in 1987); data from DRH.

8.4 Hydrogeochemical characterization of the groundwater

8.4.1 Regional variability of the mineralization

The mineralization of the various groundwater systems in the Basin of Ouarzazate shows a high variability as expected from the given lithological heterogeneity of the basin filling. The specific electric conductivity (EC) considered as a measure for the total mineralization shows that groundwater of the shallow aquifer systems (borehole < 40 m depth) ranges from low mineralized (570 µS/cm) in the north-eastern part of the basin to high mineralized (7,080 µS/cm) nearby Ouarzazate (Fig. 8.6). In the north-eastern of the basin, groundwater is mainly recharged by riverbed infiltration along wadis. Hence the mineralization of the wadis is comparable low with conductivities between 700 µS/cm (Dades) and 1,100 µS/cm (M'Goun). The locally high mineralization of the groundwater of the alluvial aquifer of Ouarzazate (3,000 to 7,080 µS/cm) results from intensive leaching of evaporitic minerals within the aquifer.

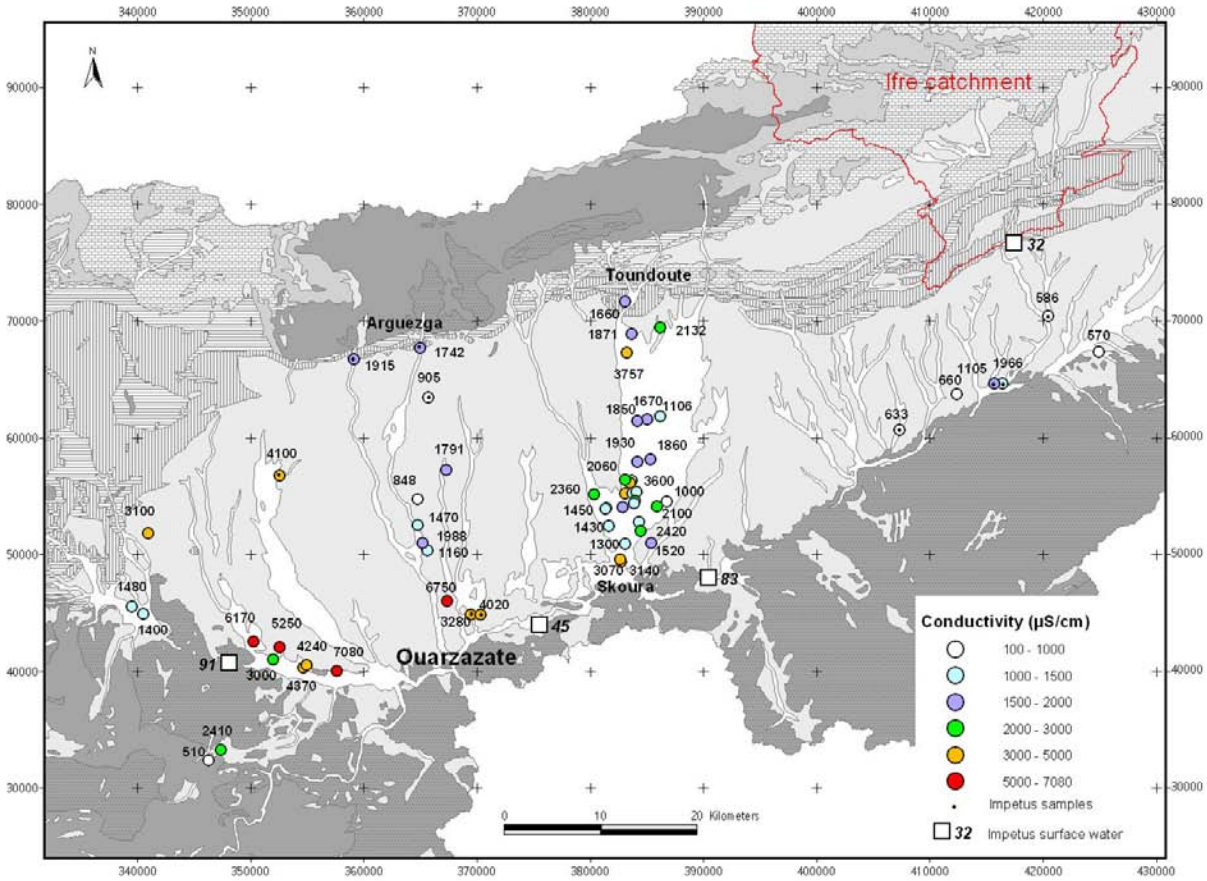

Fig. 8.6: Mineralization of the groundwater of the alluvial aquifers (boreholes with depths < 40 m) displayed by electric conductivity (own and DRH data).

The variability of the mineralization within the deeper aquifer systems (boreholes with depths from 50 to 250 m) in the Basin of Ouarzazate is even greater than in the shallow system with conductivities ranging from 420 µS/cm in the north-eastern part of the basin to 15,050 µS/cm in the western part (Fig. 8.7). As for the shallow aquifer the high conductivities observed in deep aquifer results from the leaching of evaporitic minerals present in the Mio-Pliocene and Senonian formations. A borehole near Toundoute drilled in the gypsum containing Eocene and Cretaceous formation proves this assumption with an extreme value of 27,240 µS/cm. Comparable to the shallow wells, the north-eastern part of the basin shows lower mineralized water ranging between 400 and 1,000 µS/cm (except two boreholes with 5,610 µS/cm).

Although groundwater in the south-western part of the Basin of Ouarzazate shows general higher salinities, relative low mineralised groundwater is observed at Ouarzazate city (from 730 to 910 µS/cm), which reveals a separated aquifer obviously recharged by surface water from the Anti-Atlas.

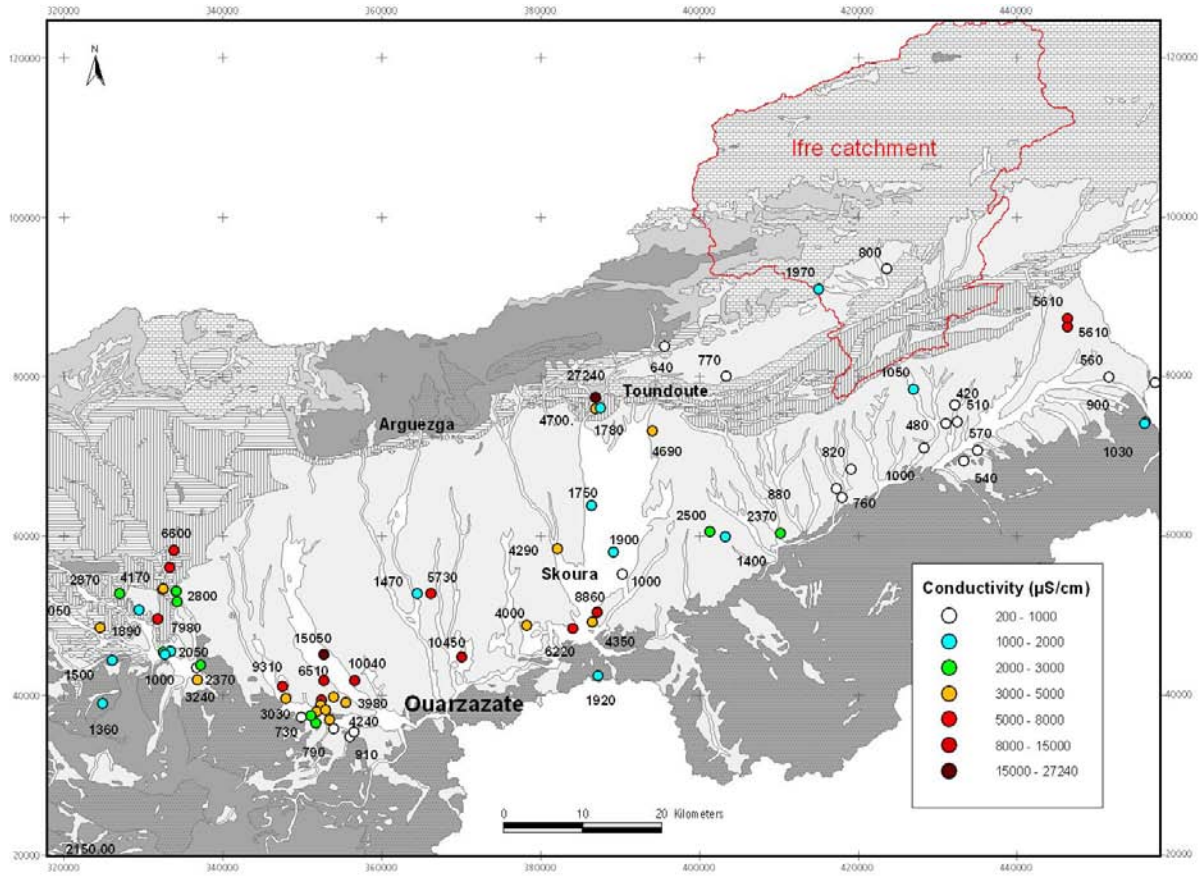

Fig. 8.7: Mineralization of the groundwater of the deeper aquifers (boreholes with depths between 40 and 250 m) displayed by electric conductivity (DRH data).

According to the mineralization of the groundwater, the aquifers in the north-eastern part of the Basin of Ouarzazate show good quality compared to the south-western aquifers, which are more affected by leaching of evaporitic minerals. The alluvial aquifer of Ouarzazate and the semi-deep aquifer developed in the Mio-Pliocene sand between Skoura and Ouarzazate show high mineralised groundwater, which limits its exploitation for drinking water supply.

8.4.2 Hierarchical Cluster Analysis

Hierarchical cluster analysis (HCA) is used to group groundwater samples into hydrochemical clusters (Fig. 8.8). The classification of 108 groundwater samples (IMP5 to IMP8) is based on 13 parameters (pH and 12 elements). As the electric conductivity is a parameter strongly dependent on ion concentrations which are already included in the HCA, it was excluded from the statistical analyses.

The first clustering results in two major clusters. Cluster 1 with 75 samples is well separated from cluster 2 (Fig. 8.8-A). The following clustering of the cluster 1 and 2 give additional sub-clusters for cluster 1 (1-1: 56 samples; 1-2: 19 samples) (Fig. 8.8-B) and for cluster 2 (2-1: 18 samples and 2-2: 14 samples) (Fig. 8.8-C). These sub-clusters are not well structured and do not allow further clustering.

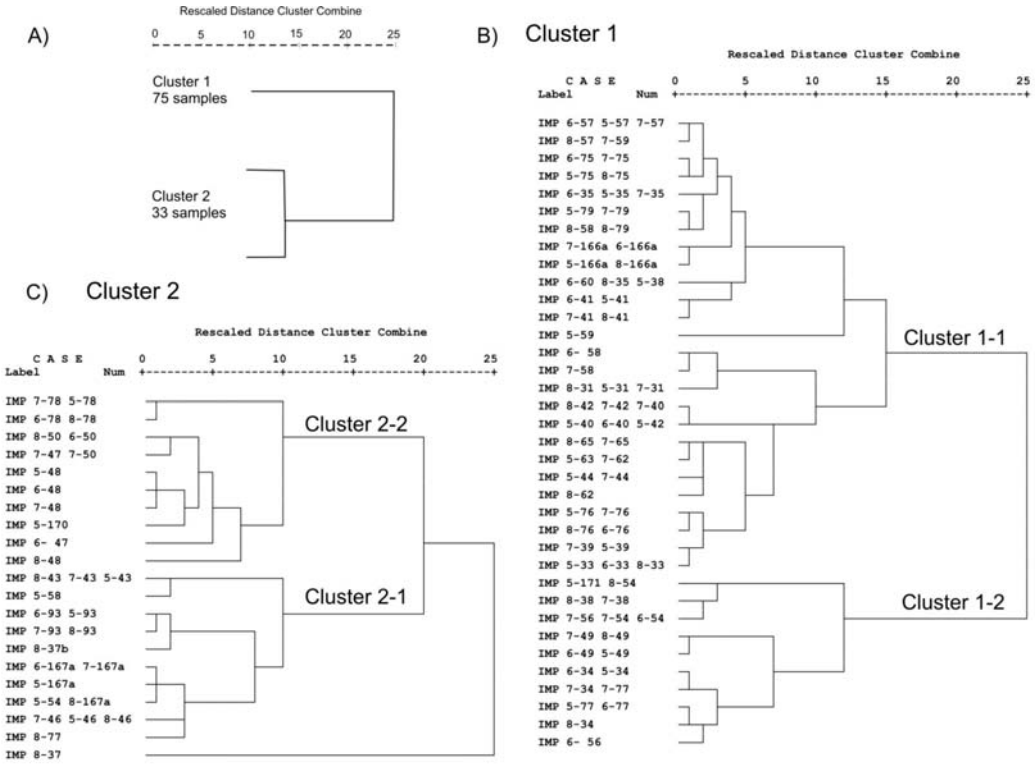

Fig. 8.8: Dendrogram of Hierarchical Cluster Analyse (HCA) for 108 groundwater samples (IMP5 to IMP8) from the Basin of Ouarzazate based on pH, Ca^{2+}, Mg^{2+}, Na^{+}, K+, SiO_2, Fe_{Total}, Mn^{2+}, HCO_3^{2-}, Cl^{-}, NO_3^{-}, SO_4^{2-} and Sr^{2+}.

The geochemistry of the groundwater in the Basin of Ouarzazate is mainly affected by the dissolution of gypsum and halite, which involves principally Ca^{2+}, SO_4^{2-}, Cl^{-}, Na^{+} and Sr^{2+}. Consequently, the groundwater samples are grouped according to their concentration reflecting the degree of leaching of evaporitic minerals: clusters 1-1 (1,400 µS/cm) and 1-2 (2,229 µS/cm), 2-1 (3,329 µS/cm) and 2-2 (5,310 µS/cm) (Tab. 8.3 and Fig. 8.9-A).

Tab. 8.3: Mean value (mean) and standard deviation (SD) of the variables for the cluster 1 and 2 and the sub-clusters 1-1, 1-2, 2-1 and 2-2 defined by (HCA); EC = electric conductivity in µS/cm.

Parameter	Cluster 1 (N: 75)		Cluster 1-1 (N: 56)		Cluster 1-2 (N: 19)		Cluster 2 (N: 33)		Cluster 2-1 (N: 18)		Cluster 2-2 (N: 14)	
	mean	SD	mean	SD	mean	SD	mean	SD	mean	SD	mean	SD
pH	7.57	0.29	7.55	0.3	7.62	0.2	7.3	0.4	7.2	0.3	7.4	0.3
Ca^{2+} (mg/l)	167	82	131	54	274	51	443	123	377	105	531	91
Mg^{2+} (mg/l)	65	25	56	21	92	17	131	44	103	31	163	33
Na^{+} (mg/l)	120	91	109	70	149	131	424	363	291	158	528	432
K^{+} (mg/l)	7	5	6	3	11	7	13	16	10	6	11	4
Sr^{2+} (mg/l)	4.3	3.0	3.3	2.3	7.0	3.3	13.1	7.3	12.9	6.2	13.6	8.9
SiO_2 (mg/l)	9.5	2.9	9.6	3.2	9.1	1.8	13.1	4.0	14.3	2.8	10.8	3.5
Fe_{Total} (µg/l)	20	81	23	94	13	6	12	11	12	9	10	9
Mn^{2+} (µg/l)	4	5	3	4	6	7	15	24	19	28	9	19
HCO_3^{-} (mg/l)	271	98	292	101	211	55	294	360	349	155	224	112
Cl^{-} (mg/l)	167	146	148	109	221	216	653	578	450	290	832	724
SO_4^{2-} (mg/l)	439	297	303	178	840	196	1,318	449	1,054	363	1,675	294
NO_3^{2-} (mg/l)	21	38	24	43	13	7	30	33	9	12	59	32
EC (*1)	1,610	670	1,400	534	2,229	661	4,339	2,063	3,329	807	5,310	2,364

(*1) *Electric conductivity (EC.) was not taken into account in the Hierarchical Cluster Analyse*

Cluster 2-1 is distinguished from the other clusters by higher HCO_3^{2-} (349.0 mg/l) and SiO_2 (14.3 mg/l) concentrations and lower pH (7.2) (Tab. 8.3 and Fig. 8.9-B). This cluster groups

groundwater with enhanced impact of CO_2 coming up through the faults of the basement. In some cases, the input of CO_2 is accompanied by an inflow of groundwater from the quartzitic and magmatic Precambrian rocks, which leads to elevated SiO_2 values. Cluster 2-2 shows higher value of NO_3^{2-} (59.0 mg/l) due to local pollution observed at some wells (Tab. 8.3).

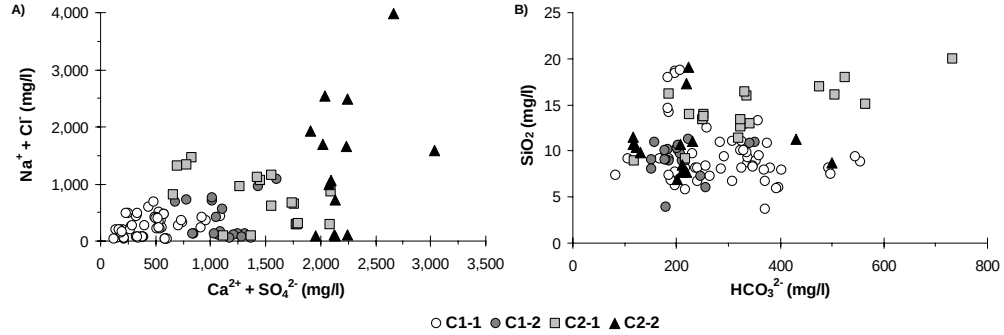

Fig. 8.9: [$Na^+ + Cl^-$] versus [$Ca^{2+} + SO_4^{2-}$] (A) and [SiO_2] versus [HCO_3^{2-}] (B) of the clusters 1-1, 1-2, 2-1 and 2-2.

Groundwater of cluster 1-1 reveals a high diversity of water types from Ca-Na-Mg-HCO_3 (5-166 art) to Ca-Mg-SO_4-Cl (7-58) and Na-Ca-Cl-SO_4 (8-62) (Fig. 8.10-A), which reflects the leaching of gypsum and/or halite.

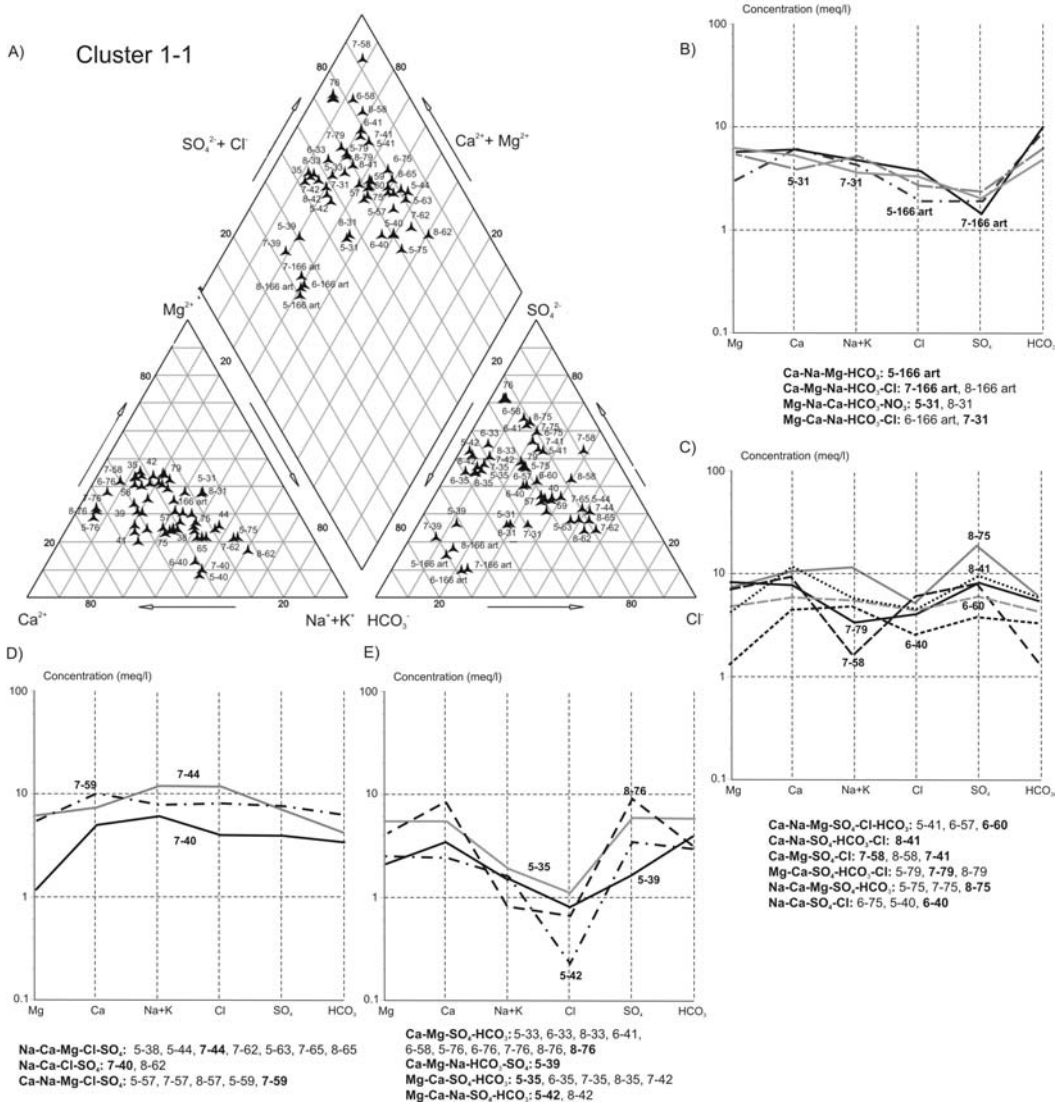

Fig. 8.10: Hydrochemical composition of the cluster 1-1: Piper diagram (A) and Schoeller diagrams of selected samples representative of each water type in (B, C, D and E).

Samples of this cluster can be further distinguished between groundwater with lower concentrations of SO_4^{2-} (wells: 31 and 166 art) (Fig. 8.10-B), groundwater with high concentrations of both SO_4^{2-} and Cl^- (wells: 38, 40, 41, 44, 57, 58, 59, 60, 62, 63, 65, 75 and 79) (Fig. 8.10-C and D) and groundwater with lower concentration of Cl^- (wells: 33, 35, 39, 41, 42, 58 and 76) (Fig. 8.10-E).

Samples of the cluster 1-2 can be distinguished in two groundwater types, groundwater with Ca-Mg-SO_4 type (wells: 77, 34 and 49) and groundwater with Na-Cl-SO_4 or Ca-Na-SO_4/Cl water types (wells: 38, 54, 56 and 171) (8.11-A and B).

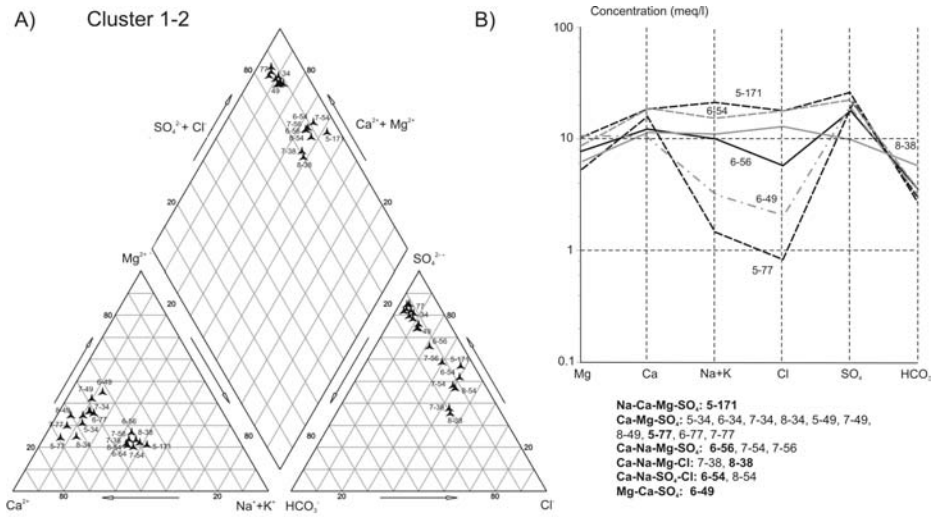

Fig. 8.11: Hydrochemical composition of the cluster 1-2: Piper diagram (A) and selected samples representative of each water type in Schoeller diagram (B).

Groundwater of cluster 2-1 varies between Ca-Mg-SO_4 water type (wells 54, 58, 77 and 167art) (Fig. 8.12-B) and Na-Ca-Cl-SO_4 water type (wells 37b 43, 93 and 46) (Fig. 8.12-C). The sample 8-37b reveals a higher content of HCO_3^{2-} (Fig. 8.12-B), which is due to the presence of CO_2 gaseous in the well.

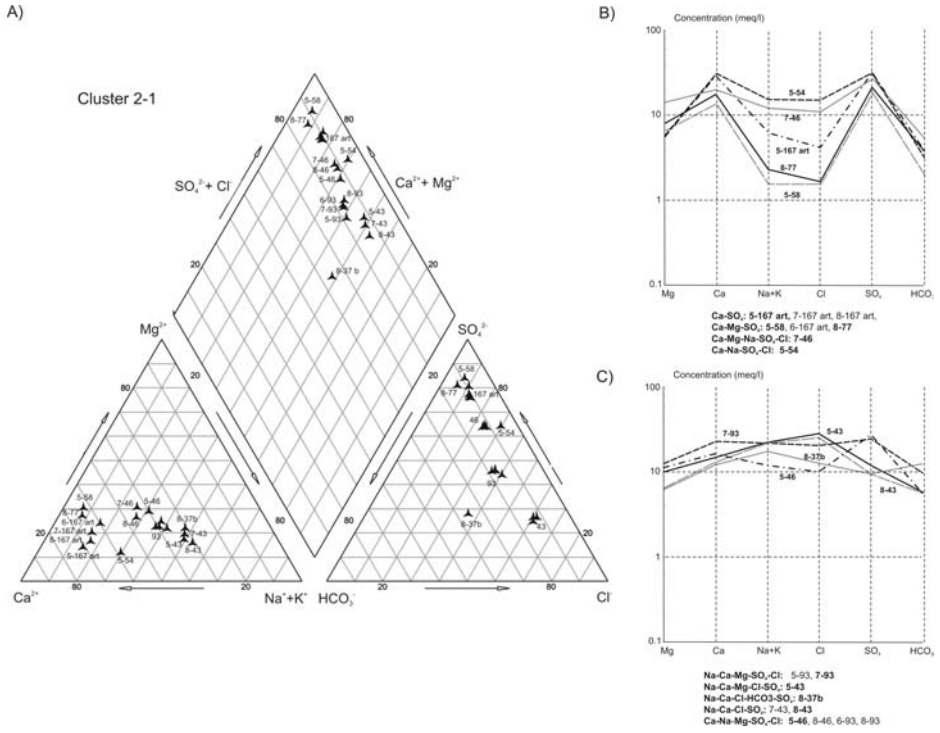

Fig. 8.12: Hydrochemical composition of the cluster 2-1: Piper diagram (A) and selected samples representative of each water type in Schoeller diagrams (B and C).

Cluster 2-2 groups groundwater samples from Ca-Mg-SO_4 (well 78) to Na-Ca-Cl-SO_4 type (well 48) (Fig. 8.13-A and B).

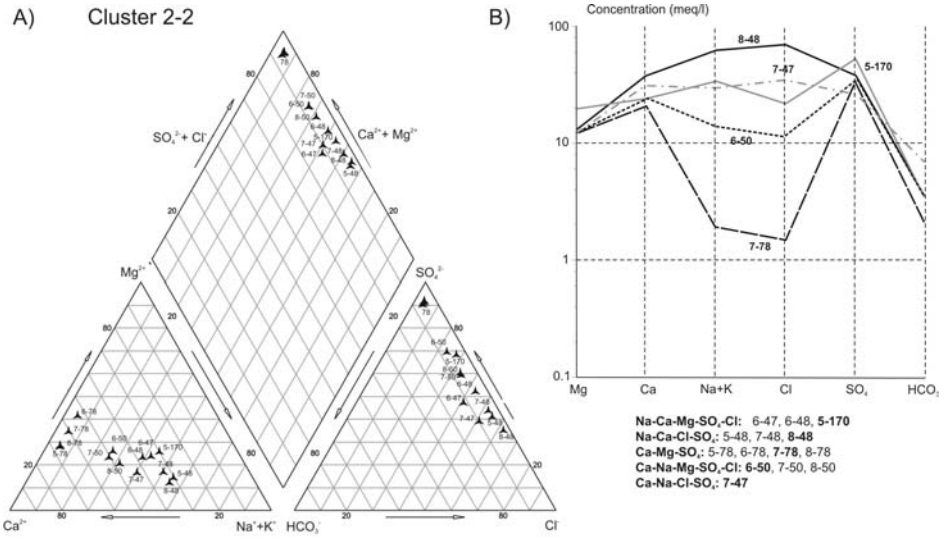

Fig. 8.13: Hydrochemical composition of the cluster 2-2: Piper diagram (A) and selected samples representative of each water type in Schoeller diagram (B).

The relationship of the statistically defined clusters of water samples to the geographic location is tested by plotting the various clusters on the geological map (Fig. 8.14) The clusters cannot be related to a specific domain of the Basin of Ouarzazate as already proved with the specific electric conductivity (Paragraph 8.4.1).

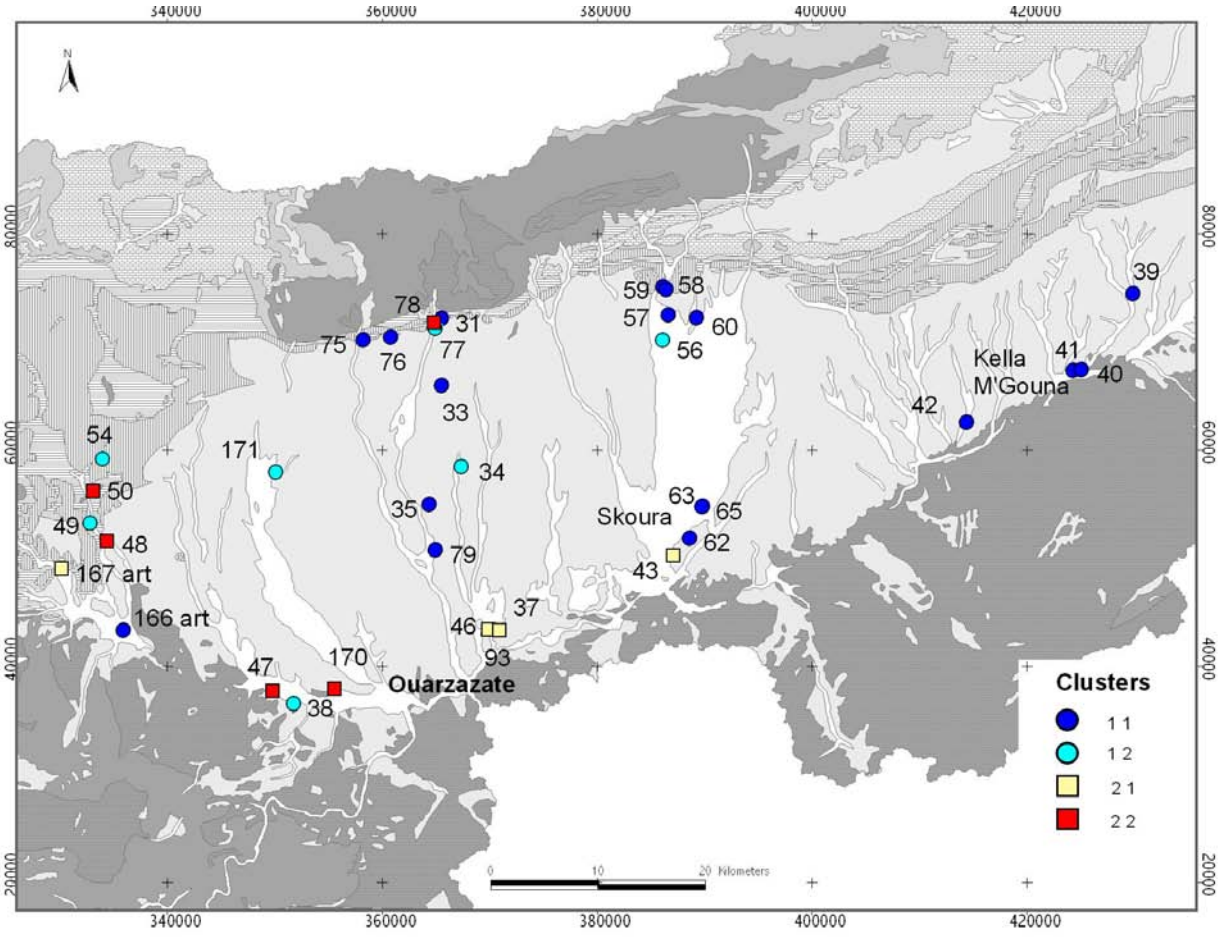

Fig. 8.14: Clusters defined with Hierarchical Cluster Analyse plotted to the geological map of the Basin of Ouarzazate.

8.4.3 Principal Component Analysis

The correlation between the various variables is described by a Principal Component Analyse (PCA) applied to 108 groundwater samples from the Basin of Ouarzazate (IMP5 to IMP8) considering 13 variables (Fig. 8.15). After rotation the three first components explain 63.9 % of the total variation:

- Component 1 (axis 1) accounts for 32.5% of the total variance and reflects a strong correlation between Ca^{2+} (0.95), SO_4^{2-} (0.93), Sr^{2+} (0.84) due to the dissolution of gypsum and Mg^{2+} (0.82). The correlation between Mg^{2+} and the dissolution of gypsum reflects obviously a dedolomitization effect although this chemical process is not proved in the Basin of Ouarzazate. Component 1 reflects also the correlation between Cl^- (0.68) and Na^+ (0.66) due to the dissolution of halite, although it is not strongly related to the gypsum dissolution.
- Component 2 (axis 2) accounts for 22.3% of the total variance and reflects an anti-correlation between HCO_3^{2-} (0.95) and pH (-0.68). This component describes the input of CO_2 from the Precambrian crystalline rocks, which increases the HCO_3^{2-} content in the groundwater and then decreases the pH. A correlation HCO_3^{2-} and K^+ (0.85) is observed which is difficult to explain due to the various possible origins of K^+ (organic, leaching of sylvite or alteration of feldspar by leaching of clays or magmatic rocks).
- Component 3 (axis 3) accounts for 9.1 % of the total variance and reflects the domestic pollution by nitrates (NO_3^- = 0.86).

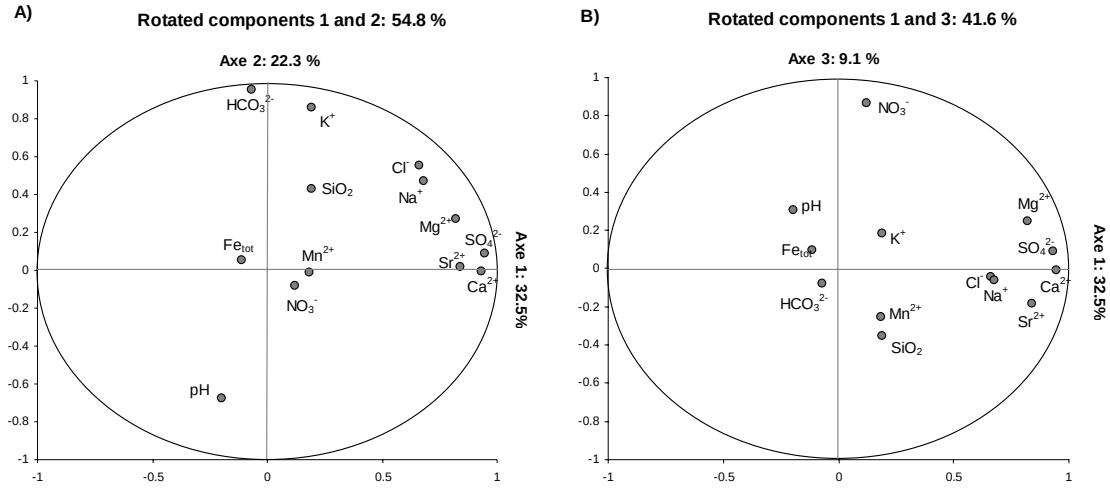

Fig. 8-15: Principal Component Analyses of the groundwater samples (IMP5 to 8) in the Basin of Ouarzazate after rotation.

8.4.4 Surface water chemistry

The recharge of the aquifer system in the Basin of Ouarzazate occurs mainly through the various wadis. Therefore, the hydrochemical characterization of the surface water is primordial to understand the recharge processes (Fig. 8.16 and Tab. 8.4). In the eastern part of the basin, the Dades Wadi shows the lowest mineralization at Ait Mouted station (88: 703 to 769 µS/cm) with a typical Ca-Mg-HCO_3 water facies from the Liassic dolomite environment which prevails in the Dades Valley. The M'Goun Wadi drains water slightly more mineralised (32: 1,020 to 1,319 µS/cm) at Ifre station with Ca-Na-SO_4-Cl facies. Downstream at Tinouar station (45), the

mineralization of the Dades increases (2,010 to 2,270 µS/cm) and the facies of the water changes to Ca-Na-Mg-SO_4-Cl due to the drainage of more mineralized groundwater.

Tab. 8.4: Electric conductivity (EC) (µS/cm) and type of the surface water of the Basin of Ouarzazate.

River / Sample-Nr	$Q_{mean\ annual}$ (10^6 m^3)	Observed EC (µS/cm)	Type of water
Assif-n'Ait-Ahmed / 122	-	1,330 - 1,345	Na-Ca-Cl-SO_4
M'Goun / 32	136	1,020 - 1,319	Ca-Na-SO_4-Cl
Dades / 88	116	703 - 769	Ca-Mg-HCO_3
Dades / 83	-	1,691 - 1,994	Ca-Na-Mg-SO_4-Cl
Dades / 45	243	2,010 - 2,270	Ca-Na-Mg-SO_4-Cl
Mellah (Western tributary) / 53	-	14,740 - 17,630	Na-Ca-Cl
Mellah (Eastern tributary) / 52	-	3,020 - 4,730	Na-Ca-SO_4-Cl
Mellah / 89	48	6,430 - 10,780	Na-Ca-Cl-SO_4
Ouarzazate / 91	121	2,570 - 3,480	Na-Ca-Cl-SO_4

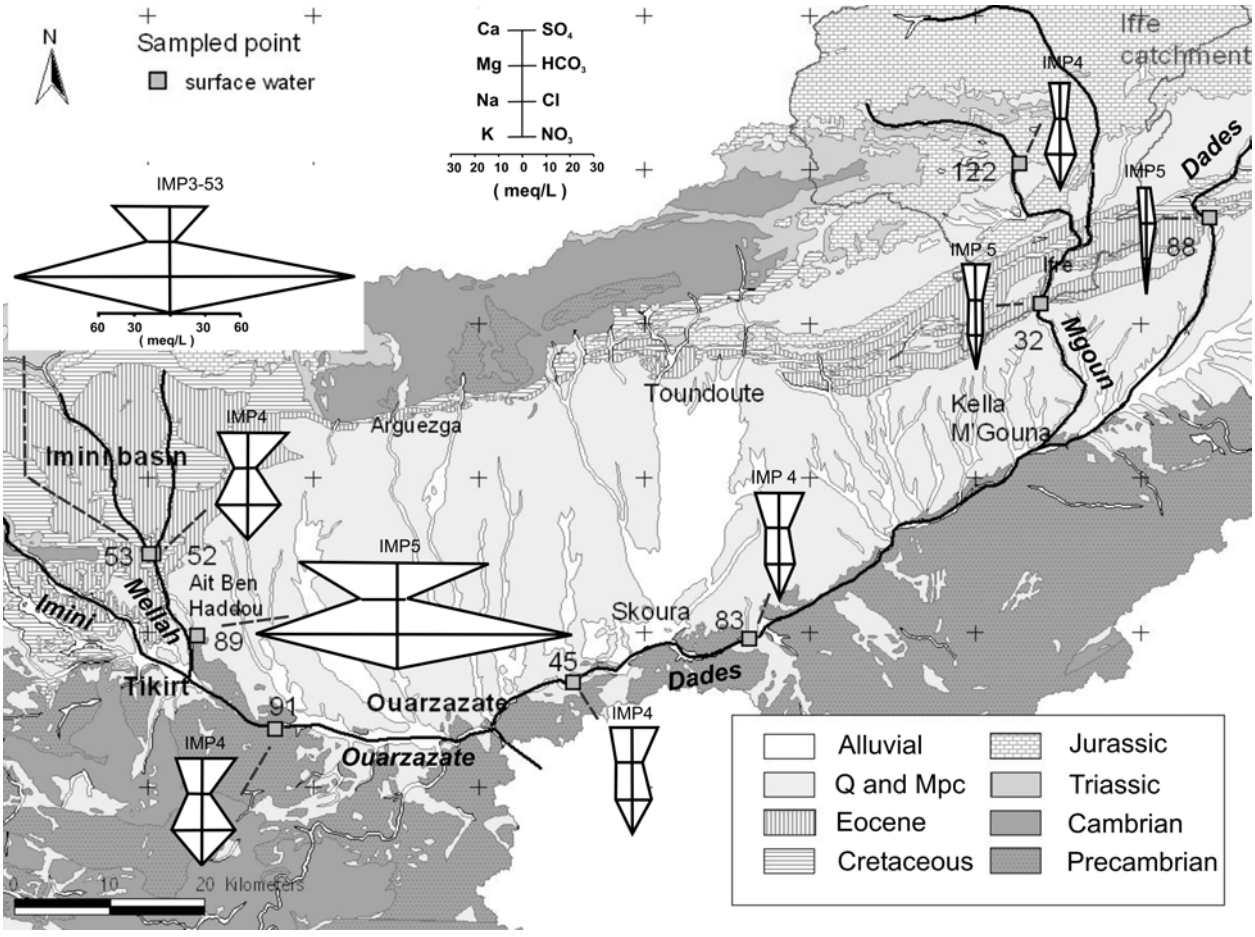

Fig. 8.16: Chemistry of the surface water in the Basin of Ouarzazate (Stiff diagrams).

In the western part of the Basin of Ouarzazate, the two tributaries (52 and 53) of the Mellah Wadi (89) (Fig. 8.16) show extreme differences in their chemistry. While brackish water is observed at the point 53 (14,740 to 17,630 µS/cm) with Na-Ca-Cl type due to the leaching of halite northwest of the catchment, the surface water at the point 52 is clearly less mineralized (3,020 to 4,730 µS/cm) with a Na-Ca-SO_4-Cl water type. Downstream at point 89, mixing of the tributaries result in high conductivities between 6,430 and 10,780 µS/cm with a Na-Ca-Cl-SO_4 type. An enrichment of SO_4^{2-} is observed at the point 89 in comparison to 52 and 53 (Fig. 8.16), due to drainage of the alluvial aquifer showing groundwater with elevated sulphate content.

8.4.5 Hydrogeochemistry of the groundwater in the Basin of Ouarzazate

Due to the high heterogeneity of the various aquifer systems in the Basin of Ouarzazate the eastern and the western part of the basin are considered separately.

Eastern Part of the Basin of Ouarzazate

As already showed by the distribution of the electric conductivity (EC) (Paragraph 8.4.1), relative low mineralized groundwater characterizes the eastern part of the basin (wells 39, 40, 41 and 42) (Fig. 8.17). The recharge of the groundwater occurs mainly by riverbed infiltration along the Dades and M'Goun Wadis. But it can also occur along minor wadis which are active during extreme rain events, as proved by groundwater at the well 39 (Ca-Mg-HCO_3) which shows clear different chemical composition than the M'Goun Wadi (32: Ca-Na-SO_4-Cl) (Fig. 8.17). The high difference in their groundwater chemistry of well 40 and 41 in spite of their close geographic proximity proves the extreme heterogeneity of the aquifers (Fig. 8.17). While groundwater at the well 41 shows higher concentration of Ca^{2+} and SO_4^{2-} due to a local leaching of gypsum (Fig. 8.18-A), well 40 reveals low mineralised groundwater of Na-Ca-Cl-SO_4 to Na-Ca-SO_4-Cl facies. Another particularities of the groundwater at the well 40 is a very low concentration of Mg^{2+} (9.8 to 18.0 mg/l: Fig. 8.18-B) compared to the mean value of groundwater observed in the Basin of Ouarzazate (80 mg/l). Its elevated SiO_2 content (15.1 to 18.6 mg/l) reveals a relatively long transit time of the groundwater within a silicate aquifer such as sandstone or magmatic rocks. Thus the hydrochemistry of the groundwater of well 40 shows clear indications of a hydraulic contact to a semi-deep aquifer of Mio-Pliocene age.

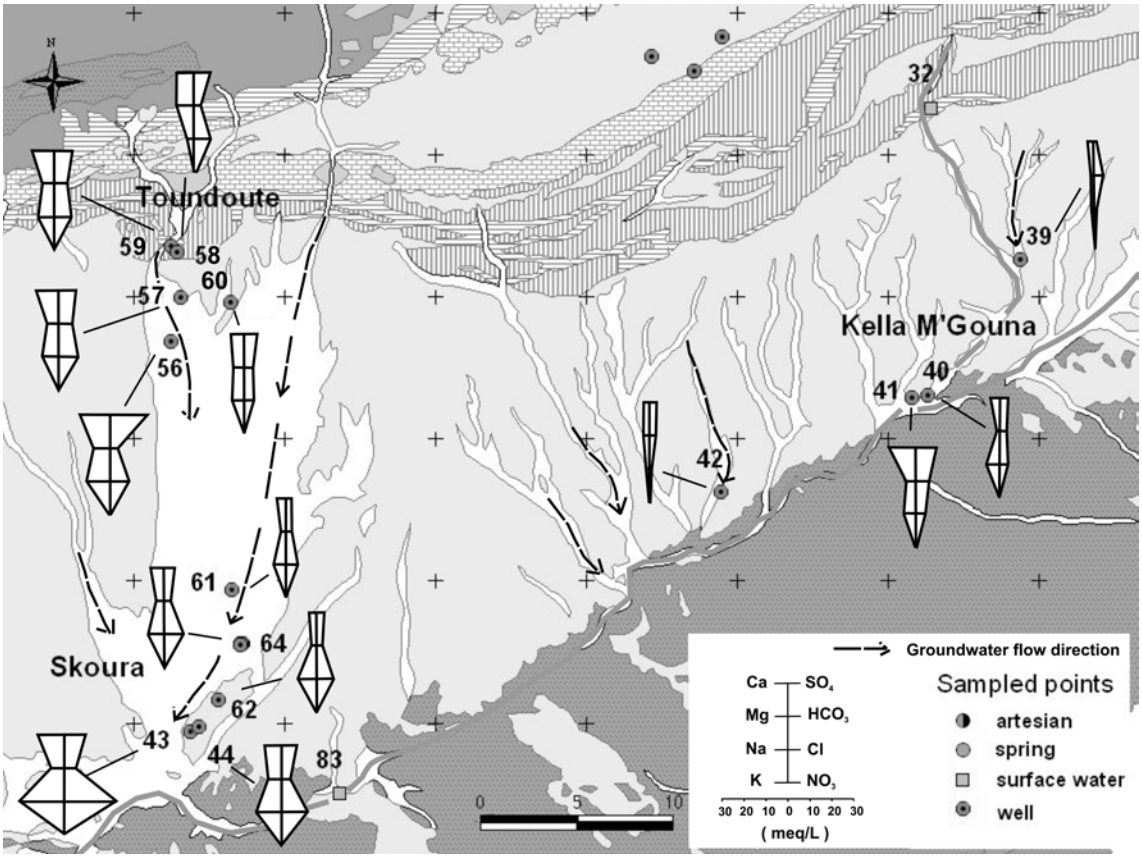

Fig. 8.17: Chemistry of groundwater in the eastern part of the Basin of Ouarzazate during base flow conditions (IMP 5: autumn 2002).

Groundwater between Toundoute and Skoura show high differences in regard to the water chemistry (Fig. 8.17). While the groundwater shows elevated sulphate contents at Toundoute (Fig. 8.19-A), the groundwater evolution tends to enhanced chloride contents at Skoura toward the well 43 (Fig. 8.19-B). The low content of sulphate at wells 61, 62 and 64 proves a recharge by riverbed infiltration along a wadi located at the east of Toundoute with lower mineralised water (Fig. 8.17). The elevated content of Na^+ and Cl^- of well 43 results from the leaching of halite, which is locally described in the Mio-Pliocene formations. In general, the high chemical variability at this well reflects mixing processes between the sulphate rich groundwater from the north and the local chloride rich groundwater (Fig. 8-19-B).

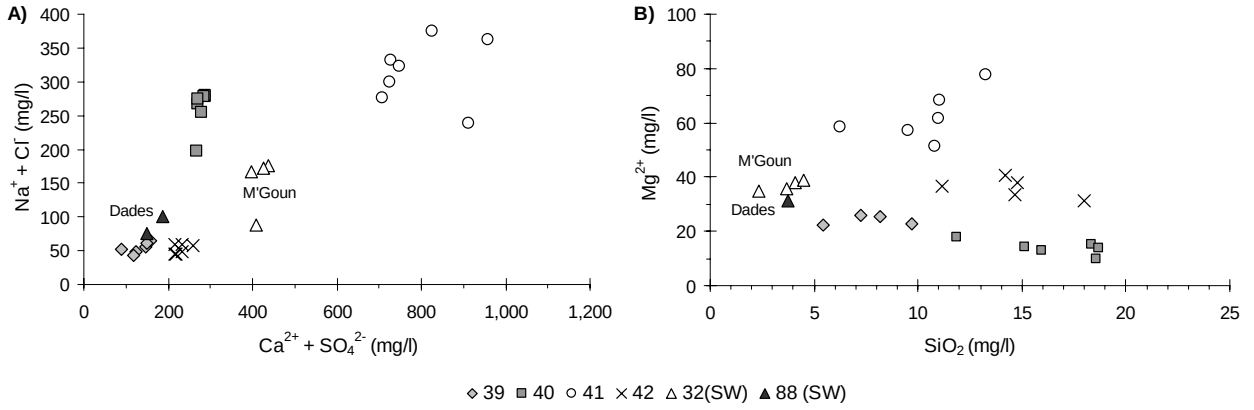

Fig. 8.18: Diagrams $[Na^+ + Cl^-]$ versus $[Ca^{2+} + SO_4^{2-}]$ (A) and Mg^{2+} versus SiO_2 of the groundwater in the area of Kelaa M'Gouna; SW = surface water (M'Goun and Dades Wadis); localisation Fig. 8.17.

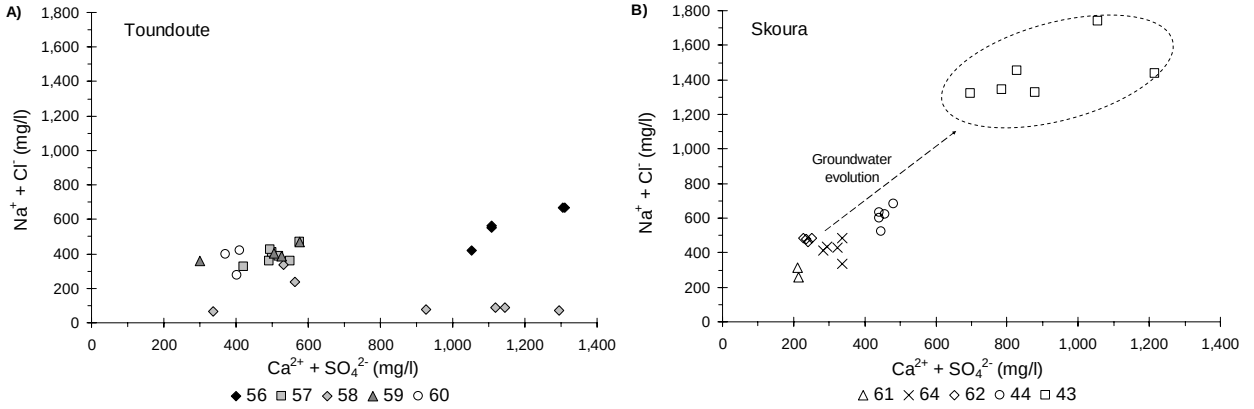

Fig. 8.19: Diagram $[Na^+ + Cl^-]$ versus $[Ca^{2+} + SO_4^{2-}]$ showing the chemistry of the groundwater at Toundoute (56, 57, 58, 59 and 60) (A) and the groundwater evolution at Skoura (43, 44, 61, 62 and 64) (B); localisation Fig. 8.17.

Seasonal variation

No clear seasonal variations between springtime and autumn are observed in the eastern part of the Basin of Ouarzazate (Fig. 8.20). Moreover, no general correlation between the variation of the groundwater level and the chemistry is possible. While at well 39 the groundwater chemistry is stable (Standard Deviation (SD): EC = 30 µS/cm, SO_4^{2-} = 19 mg/l and Cl^- = 6 mg/l) in spite of a high level changes (SD = 2.1 m), well 41 shows significant variations (SD: EC = 152 µS/cm, SO_4^{2-} = 80 mg/l and Cl^- = 37 mg/l) related to small water level changes (SD = 1.3 m) (Fig. 8.20-A, C, E and G).

As proved by the principal component analyses, the leaching of halite and gypsum are not well related along the groundwater flow path due to high changes of sedimentological facies within the geological formations. Also at some wells (40, 41 and 58) the seasonal variation between

SO_4^{2-} and Cl^- are not correlated which proves a different groundwater flow path between base flow conditions and humid periods.

Only well 43 shows a clear correlation between a significant draw down of the water table (from -18.10 m to -22.40 m) and a continuous decreasing of the mineralization between autumn 2000 and autumn 2004, with a decrease of the conductivity from 6,280 to 3,720 µS/cm. Hence the overall decrease is mainly due to sulphate (from 883 to 451 mg/l) and chloride (from 1,561 to 844 mg/l), an admixture of low mineralized surface water from the adjacent wadi might be possible by an excessive pumping for irrigation, which leads to a change of the hydrodynamic behaviour of the aquifer.

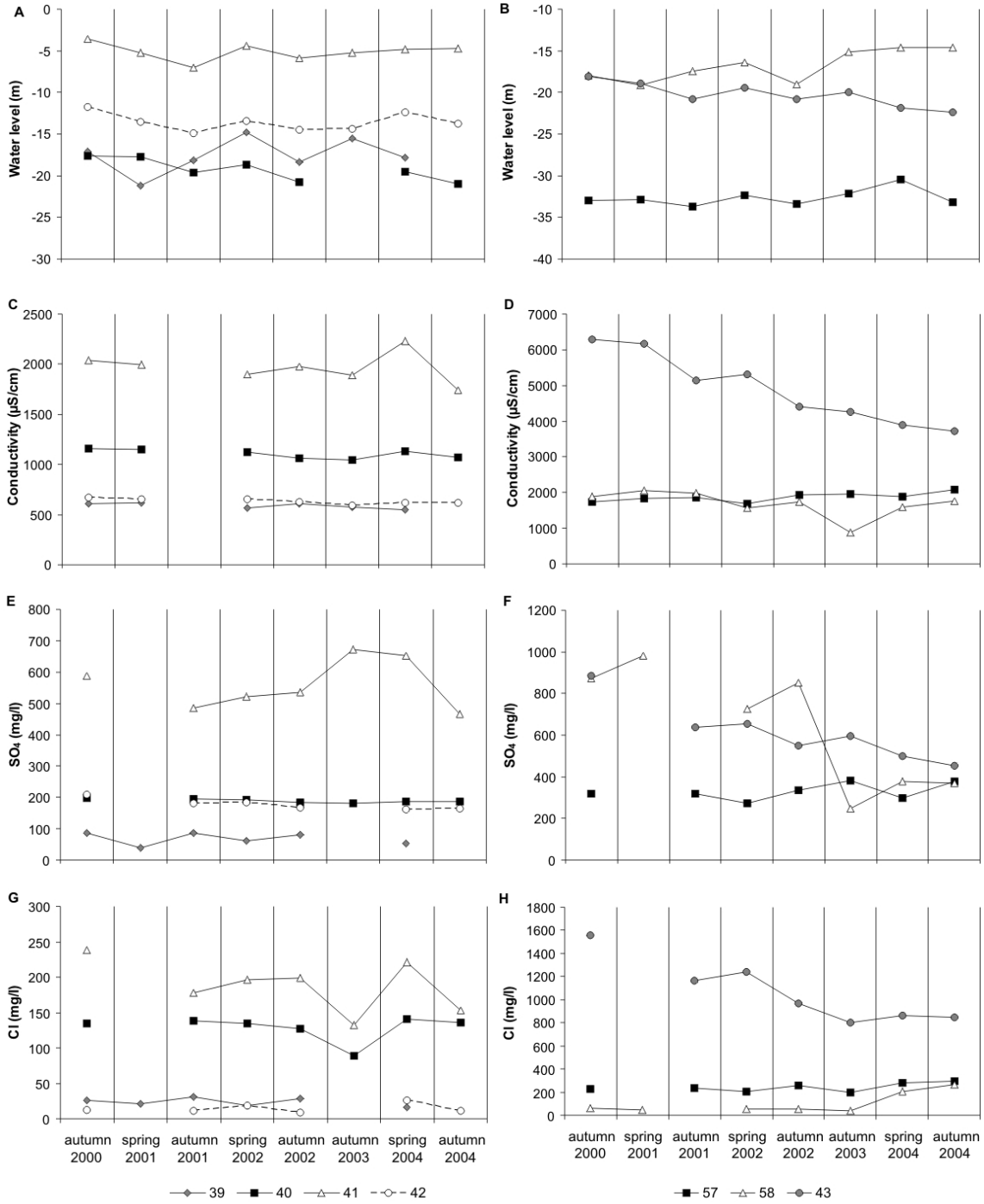

Fig. 8.20: Variation of the water level, the conductivity and the SO_4^{2-} and Cl^- concentrations of selected wells in the eastern part of the Basin of Ouarzazate during the period of investigation: autumn 2000 (IMP1), to autumn 2004 (IMP8); localisation Fig. 8.17.

Western part of the Basin of Ouarzazate

Between Arguezga and Ouarzazate (31, 77, 78, 76, 75, 33, 34, 35, 36 and 79) the groundwater shows a broad range of groundwater types (Fig. 8.21). The comparison between [Na^+ and Cl^-] and [Ca^{2+} + SO_4^{2-}] of the groundwater in this area (Fig. 8.22-A) reveals strong differences in the groundwater chemistry, which are difficult to correlate with the general groundwater flow direction. In general, the groundwater chemistry reveals a strongly inhomogeneous aquifer system consisting of several small alluvial aquifers along the various wadis. Local pollutions of domestic origin are proved by higher nitrate contents clearly correlated to elevated Cl^- concentrations (wells 78 and 31) (Fig. 8.22-B).

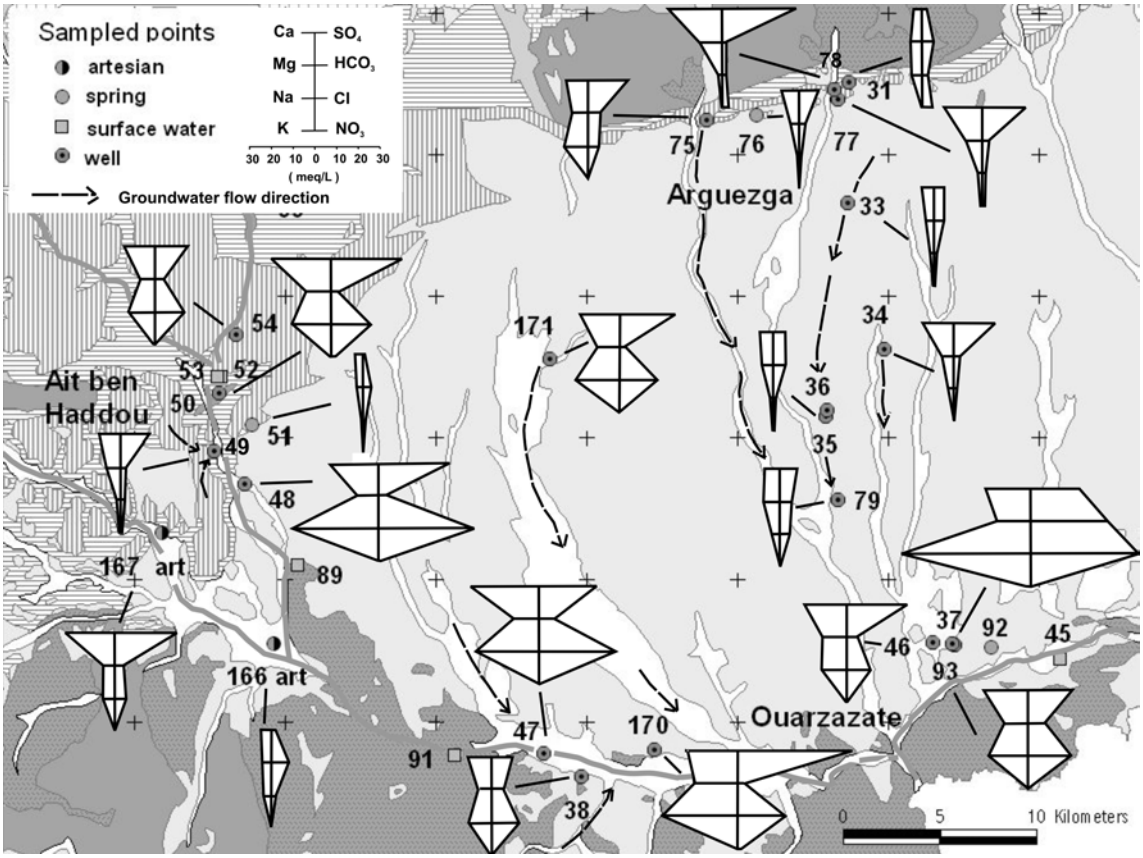

Fig. 8.21: Hydrochemical characterization of the groundwater in the western part of the Basin of Ouarzazate during base flow conditions (IMP 5: autumn 2002).

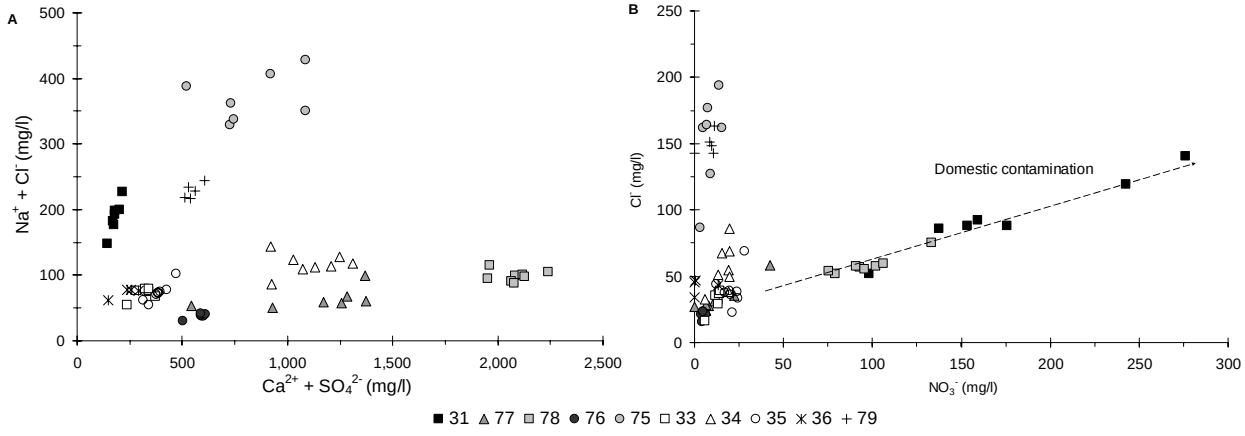

Fig. 8.22: Diagrams [Na^+ + Cl^-] versus [Ca^{2+} + SO_4^{2-}] (A) and Cl^- versus NO_3^- (B) of the groundwater between Arguezga and Ouarzazate (localisation Fig. 8.21).

In the east of Ouarzazate city, the small spring 92 and the wells 37 and 93 are clearly influenced by CO_2 gas coming up along faults of the Precambrian (Fig. 8.23). Hydrogeologically this region is characterized by two superposed aquifers separated by clays (at 6 meters of depth). While a shallow aquifer is developed in Quaternary and Mio-Pliocene sediments, a confined aquifer exists in the underlying Mio-Pliocene formations.

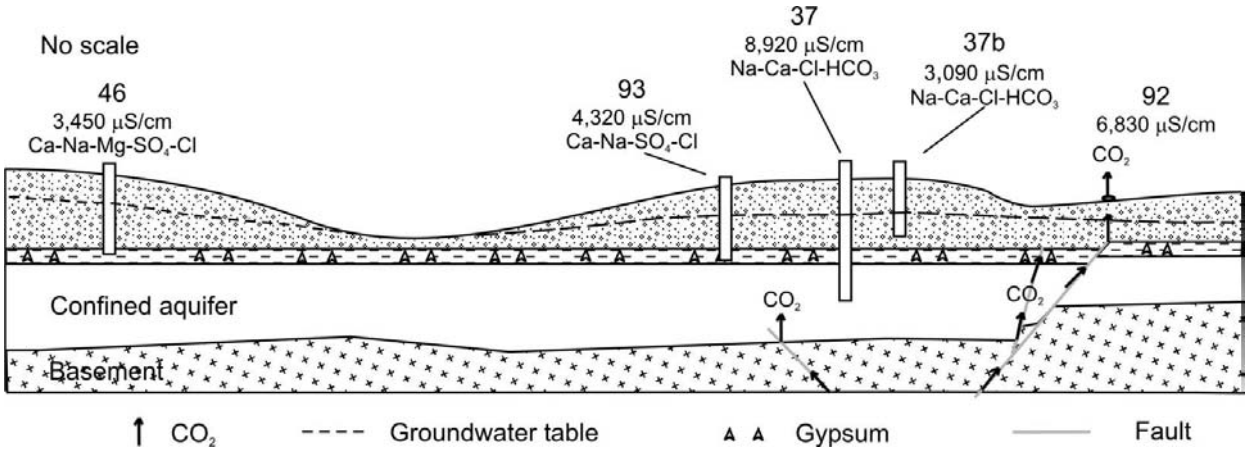

Fig. 8.23: Schematic profile showing the geological framework of the wells affected by the input of gas.

The confined aquifer (well 37) is characterized by high mineralised groundwater (up to 8,920 µS/cm) (Fig. 8.24-A) due to high contents of Na^+ and Cl^- (2,533 mg/l < $[Na^+ + Cl^-]$ < 3,157 mg/l) (Fig. 8.24-C) strongly correlated with K^+. This clearly proves the influence of halite and sylvite leaching (Fig. 8.24-D). Low pH (6.03 to 6.21) (Fig. 8.24-A) related with elevated HCO_3^- content (2,183 mg/l) reveals the presence of CO_2 gas. The groundwater shows also high SiO_2 content (24 mg/l) (Fig. 8.24-B), which proves groundwater passage within the crystalline Precambrian rocks with a relative high residence time. Consequently, groundwater affluxes occurred from the fractured Precambrian obviously related to the rising up of CO_2 gas. Well 93 is influenced by comparable effects (Fig. 8.23), but from the elevated Ca^{2+} and SO_4^2 contents (1,263 to 1,559 mg/l) (Fig. 8.24-C) a clear overprint by a flow path within the underlying clayey aquitard can be recognized.

The shallow aquifer (well 46), when it is not influenced by leakage from the confined aquifer shows less mineralised groundwater (3,450 µS/cm) with lower concentration of Na^+ and Cl^- (540 mg/l < $[Na^+ + Cl^-]$ < 641 mg/l) and SiO_2 (8.7 to 13.4 mg/l) (Fig. 8.24-A, B and C). The pH values are higher (7.35 to 7.62) and the HCO_3^- content are lower (320 to 378 mg/l) (Fig. 8.24-A and B), which prove the absence of CO_2 gas. Well 46, contrarily to well 37b, shows high values of Ca^{2+} and SO_4^{2-} (1,257 mg/l < $[Ca^{2+} + SO_4^{2-}]$ < 1,759 mg/l) due to the leaching of gypsum present within the clayey aquitard (Fig. 8.24-C).

An intense degassing of CO_2 occurs at the spring 92, although no discharge of water was observed during the period of investigation. At this point, stagnant water present at the outflow has been analysed showing a high mineralization (6,610 µS/cm), low pH (6.29) (Fig. 8.24-A), high contents of HCO_3^{2-} (2,470 mg/l) (Fig. 8.24-B) and K^+ (138 mg/l) (Fig. 8.24-D). The very high concentration of K^+ at this spring can be explained by presence of plants and algae which assimilate and concentrate the K^+ in the small pool where the samples have been taken.

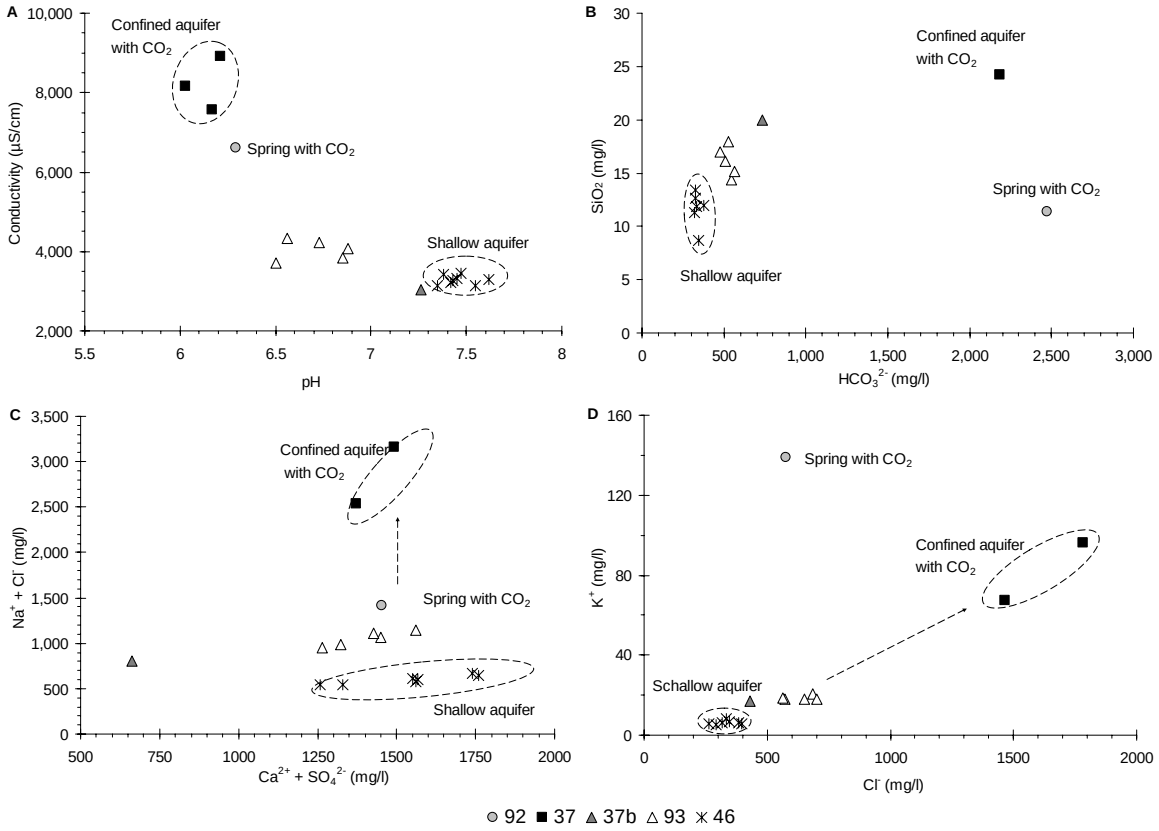

Fig. 8.24: Groundwater from shallow and confined aquifers with an influx of CO_2 gas nearby Ouarzazate, Conductivity versus pH (A), SiO_2 versus HCO_3^{2-} (B), $[Na^+ + Cl^-]$ versus $[Ca^{2+} + SO_4^{2-}$ (C) and K^+ versus Na^+ (D) (localisation Fig. 8.21).

In the area of Ouarzazate, the wells 38 and 47 and the surface water (91) show similar ratios $[Na^+ + Cl^-] : [Ca^{2+} + SO_4^{2-}]$ (Fig. 8.25-A). Consequently, hydraulic connection exists between these wells and the Ouarzazate Wadi. But the groundwater of the well 38 is mixed with lower saline water from the Anti-Atlas which explains the increasing of the SiO_2 content (Fig. 8.25-B).

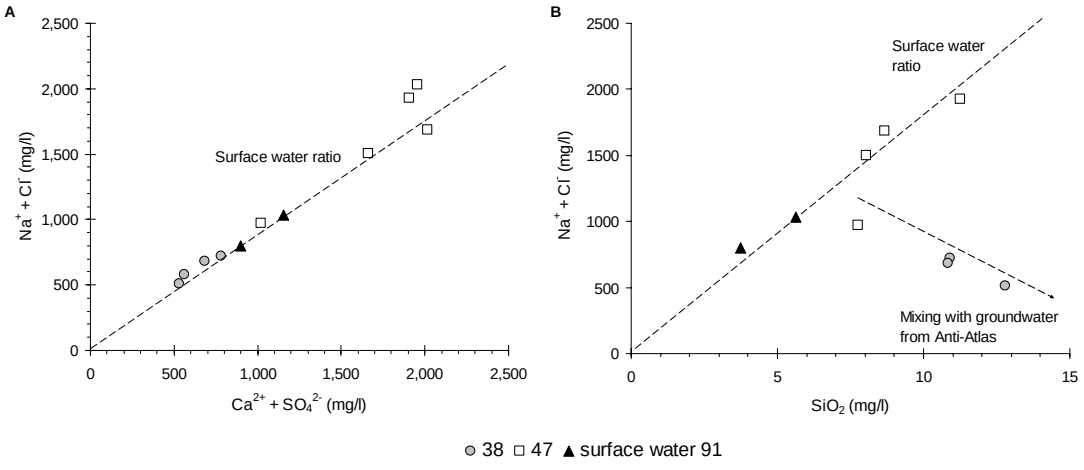

Fig. 8.25: Diagrams $[Na^+ + Cl^-]$ versus $[Ca^{2+} + SO_4^{2-}]$ (A) and $[Na^+ + Cl^-]$ versus SiO_2 (B) of the groundwater nearby Ouarzazate (localisation Fig. 8.21).

At Ait Ben Haddou, the wells located in the alluvial aquifer show hydraulic connection with the Wadi Mellah (Na-Ca-Cl water type) as proved by almost similar hydrochemical signatures (Fig. 8.21). The hydraulic connection is clear with groundwater of the alluvial aquifer influenced by the surface water with Na^+ and Cl^- contents (> 700 mg/l), and surface water (89) influenced by the more sulphated groundwater due to the leaching of gypsum of the Senonian (Fig. 8.26-A).

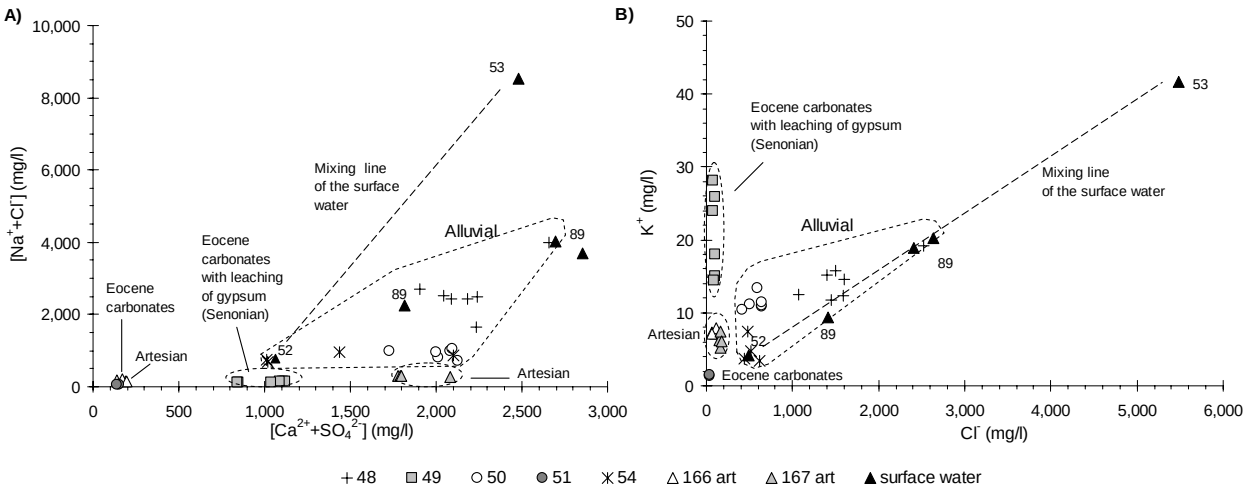

Fig. 8.26: Diagrams [$Na^+ + Cl^-$] versus [$Ca^{2+} + SO_4^{2-}$] (A) and K^+ versus Cl^- (B) of the groundwater and surface water at Ait Ben Haddou (localisation Fig. 8.21). Hence the surface waters 52 and 53 are two tributaries of the surface water 89, a mixing line is defined.

The perched aquifer of Eocene which is not connected to an alluvial aquifer (compare Fig. 8.3) shows low mineralized groundwater (621 µS/cm) of Ca-Mg-HCO_3 type (spring 51: Fig. 8.21). Both Na^+ and Cl^- contents and Ca^{2+} and SO_4^{2-} contents are lower than in the alluvial aquifers (Fig. 8.26-A). But the mineralization of the groundwater from the Eocene aquifers increases at the contact with the underlying Senonian due to the leaching of gypsum present in the marls (839 mg/l < $[Ca^{2+} + SO_4^{2-}]_{49}$ < 1,122 mg/l).

Two different origins of K^+ in groundwater have to be distinguished. While in the alluvial aquifer, K^+ is provided by the infiltration of surface water which show high K^+ content (53) correlated with Cl^- and thus proving the leaching of sylvite (Fig. 8.26-B), groundwater from the perched Eocene aquifer show high content of K^+ up to 28 mg/l after contact with the Senonian sediments (well 49) but without any correlation with Cl^- (Fig. 8.26-B). A geogene origin is assumed due to the absence of organic pollution. The weathering of clay minerals from the Senonian marls with unaltered feldspar or mica particles ($KAlSi_3O_8$ and $KAlSi_2O_6$) seem to be the source of potassium.

The confined aquifer of the Infracenomanian (compare Fig. 8.3) shows a well differentiated groundwater chemistry proving the heterogeneity of this aquifer (Fig. 8.21). While the artesian well 167art shows higher conductivity (2,470 to 2,910 µS/cm) with sulphate rich groundwater (Ca-Mg-SO_4), well 166art (1,018 to 1,200 µS/cm) shows a clear carbonate facies (Ca-Mg-HCO_3). Both artesian wells show low contents of Na^+ and Cl^- (153 to 302 mg/l) proving that no infiltration from the surface water of the Mellah Wadi or from the associated alluvial aquifer occurs. The higher values of Ca^{2+} and SO_4^{2-} observed at well 167art (Fig. 8.26-A) result from the dissolution of gypsum present in the Senonian formations.

Seasonal variations

Between Arguezga and Ouarzazate (Fig. 8.27-A, C, E and G), only well 77 shows clear seasonal hydrochemical variations with lower mineralization during springtime (due to lower SO_4^{2-} contents). This well is in hydraulic connection to a wadi, which drains the Precambrian rocks of the Skoura Mole. Thus, a dilution of the groundwater by the infiltration of lower mineralized surface water occurs during the humid periods, although no direct correlation exists with the variation of the water level (which shows low variation: SD = 0.87 m).

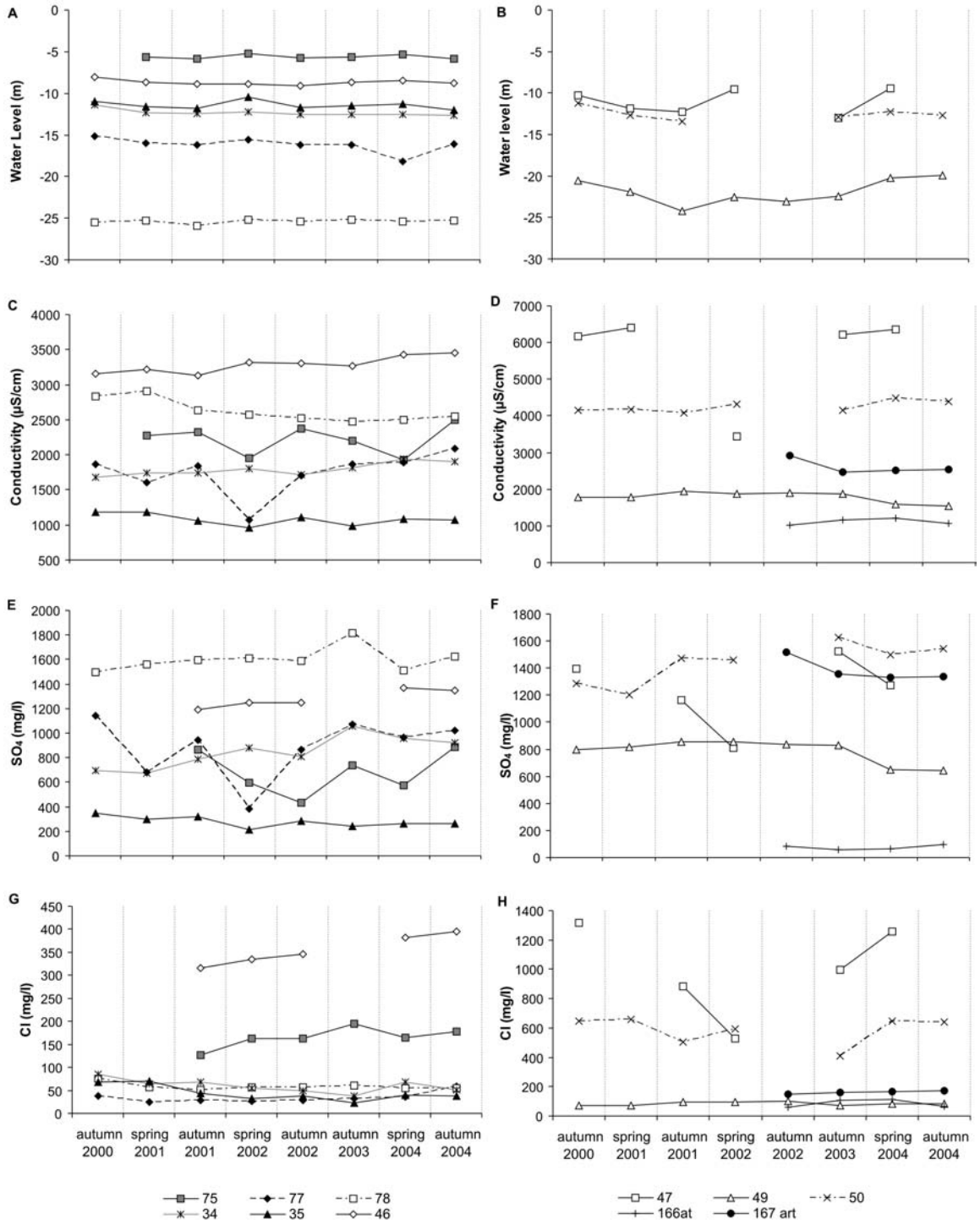

Fig. 8.27: Variation of the water level, the conductivity and the SO_4^{2-} and Cl^- concentrations of selected wells in the eastern part of the Basin of Ouarzazate during the period of investigation from autumn 2000 to autumn 2004 (IMP8); Localisation Fig. 8.21.

Well 47 near Ouarzazate reveals very high variations of the chemistry (SD: EC = 1,273 µS/cm) due to its hydraulic connection to the adjacent wadi. The mineralization during spring 2002 was particularly depleted (3,450 µS/cm), certainly related to a flood in the Ouarzazate Wadi.

The Eocene aquifer (well 49) shows correlated variations between the mineralization and the water level, although the aquifer is not connected to the Mellah Wadi or an alluvial aquifer. The correlation observed reflects the effect of dilution within the aquifer after recharge by precipitation without mixing processes with other groundwater types.

8.4.6 Saturation Index

Surface waters of the western part of the basin, where Triassic and Cretaceous formations with evaporitic minerals crop out, are in equilibrium or slightly under-saturated in regard to gypsum (Fig. 8.28-A), while in the eastern part surface waters draining the Liassic limestones of the High Atlas are clearly under-saturated (Fig. 8.28-B). In regard to quartz, the surface waters are in equilibrium to slightly under-saturated, which proves the importance of the base flow component in the discharge of the wadis (Fig. 8.28-E and F). The under-saturation in regard to the CO_2 reflects the degassing occurring in water in direct contact with the air ($-3.13 < SI_{CO_2} < -2.59$). In consequence of this degassing and according to the reactions of the dissolution of carbonates (Chapter 3, Eq. 20), the surface water becomes widely oversaturated in regard to calcite and dolomite ($0.94 < SI_{calcite} < 1.18$ and $1.60 < SI_{dolomite} < 2.11$) (Fig. 8.28-C and D).

The eastern part of the basin shows under-saturated groundwater in regard to gypsum (-1.84 to -0.48) as observed for the surface water in this area, which recharges the alluvial aquifer by riverbed infiltration (Fig. 8.28-A and Fig. 8.29). The wells localised at the southern border of the basin (40, 41 and 42: Kelaa M'Gouna; 43 and 44: Skoura) show higher SI_{quartz} (> 0.3) (Fig. 8.28-F and Fig. 8.30). Thus revealing a longer residence time in the Mio-Pliocene sand. But affluxes of groundwater coming up from the underlying fractured Precambrian rocks are also possible. Comparable to the described hydrochemical evaluation of the groundwater of well 40 the higher quartz saturation (SI_{quartz} = 0.46) and lower dolomite saturation ($SI_{dolomite}$ = 0.10) proves a hydraulic connection of the alluvial aquifer to the semi-deep Mio-Pliocene aquifer (Fig. 8.28-F and D).

The groundwater in the western part of the basin shows higher saturation in regard to gypsum (up to -0.13) due to the leaching of evaporitic minerals within the Triassic and Cretaceous formations. Groundwater of well 31 at the northern range of the basin close to the Precambrian and Cambrian rocks of the Skoura Mole (Fig. 8.21) is in equilibrium with quartz (0.18) and shows the highest saturation index in regard to dolomite (1.36) although this well is broadly under-saturated with gypsum (-1.69) (Fig. 8.28-A and C). These characteristics reveal groundwater with a long residence time.

Wells affected by CO_2 gas are clearly distinguishable with groundwater equilibrated in regard to this gas (wells 92 and 37: Fig. 8.28-E). The relative low values of $SI_{calcite}$ (0.08) and $SI_{dolomite}$ (0.03) at well 37 (Fig. 8.28-C) are due to the presence of CO_2 gas which lowers the pH and then increases the capacity of dissolution of carbonates (Chapter 3, Eq. 20), which results in a decreasing of the carbonate saturation. Well 93 shows the same characteristics proving the presence of gas at this well. Moreover, groundwater with presence of CO_2 gas shows clear over-saturation of quartz (SI_{quartz}: 37 = 0.63 and 93 = 0.46), which reveals groundwater affluxes from the fractured Precambrian rocks related to the rising up of CO_2 gas as already proved by the chemistry.

The groundwater from the perched aquifer of the Eocene carbonates (51) is over-saturated with dolomite (0.85), in equilibrium with quartz (0.20) and under-saturated with gypsum (-1.75) which proves a relative long residence time (Fig. 8.28-A, C and E).

The heterogeneity of the confined aquifer of Infracenomanian already showed with the chemistry is confirmed with high differences of saturation indexes observed at the wells 166art and 167art (Fig. 8.29 and Fig. 8.30). While the groundwater of well 166art is under-saturated in regard to

gypsum (-1.74), over-saturated with dolomite (0.60) and in equilibrium with quartz (0.17), the groundwater of well 167art is clearly affected by a dissolution of gypsum (-0.16) but shows lower saturation of dolomite (0.36) and higher saturation of quartz (0.39) (Fig. 8.28-A, C and E). Consequently, the origin of the groundwater of these artesian wells are different, with well 167art showing a clear leaching of evaporitic minerals of the Senonian formations and longer residence times within the sandy aquifer of Infracenomanian.

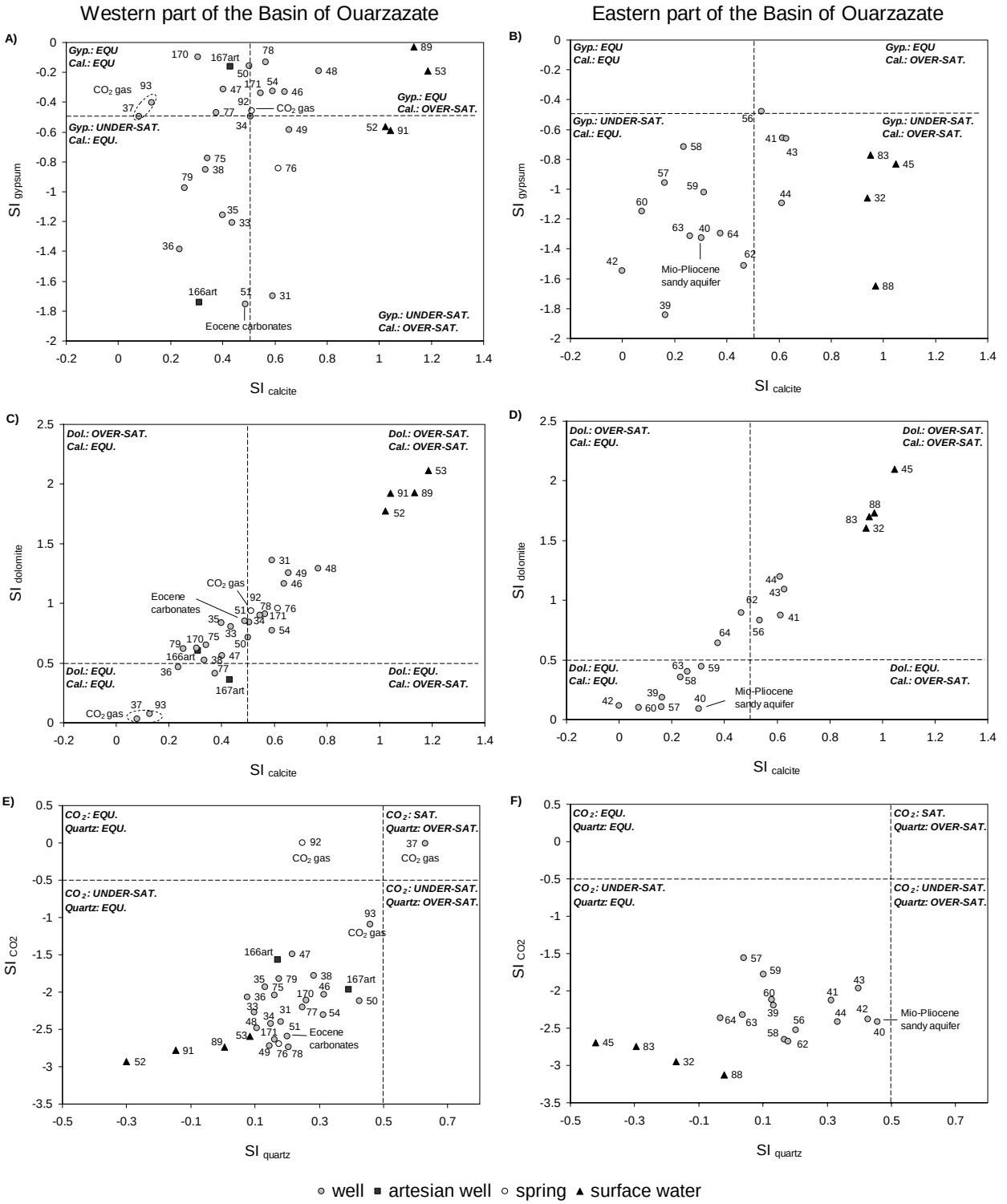

Fig. 8.28: Saturation indexes (SI) of surface water and groundwater of the western (A, C and E) and eastern (B, D and F) parts of the Basin of Ouarzazate (localisation see Fig. 8.17 and 8.22) based on mean values: SI $_{gypsum}$ versus SI $_{calcite}$ (A and B), SI $_{dolomite}$ versus SI $_{calcite}$ (C and D) and SI $_{CO2}$ versus SI $_{quartz}$ (E and F).

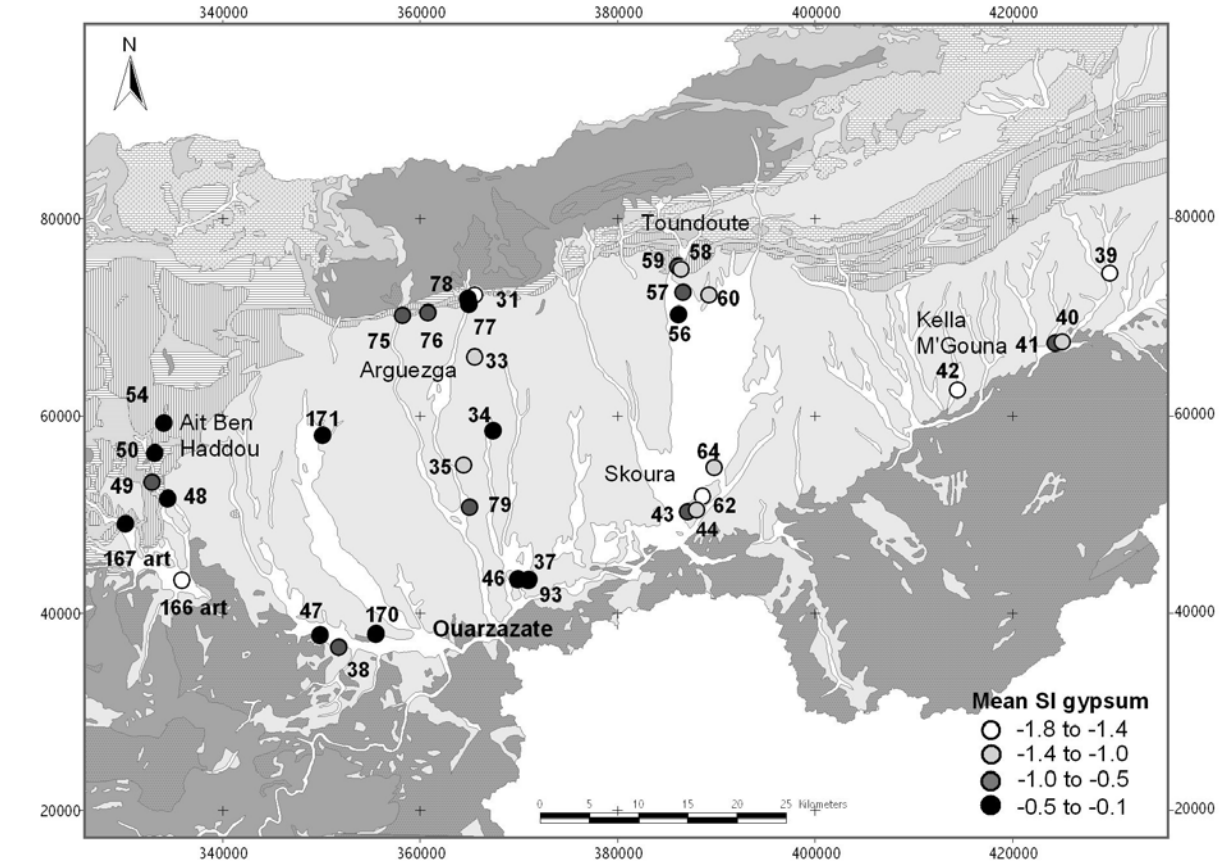

Fig. 8.29: Mean values of SI_{gypsum} of the groundwater in the Basin of Ouarzazate.

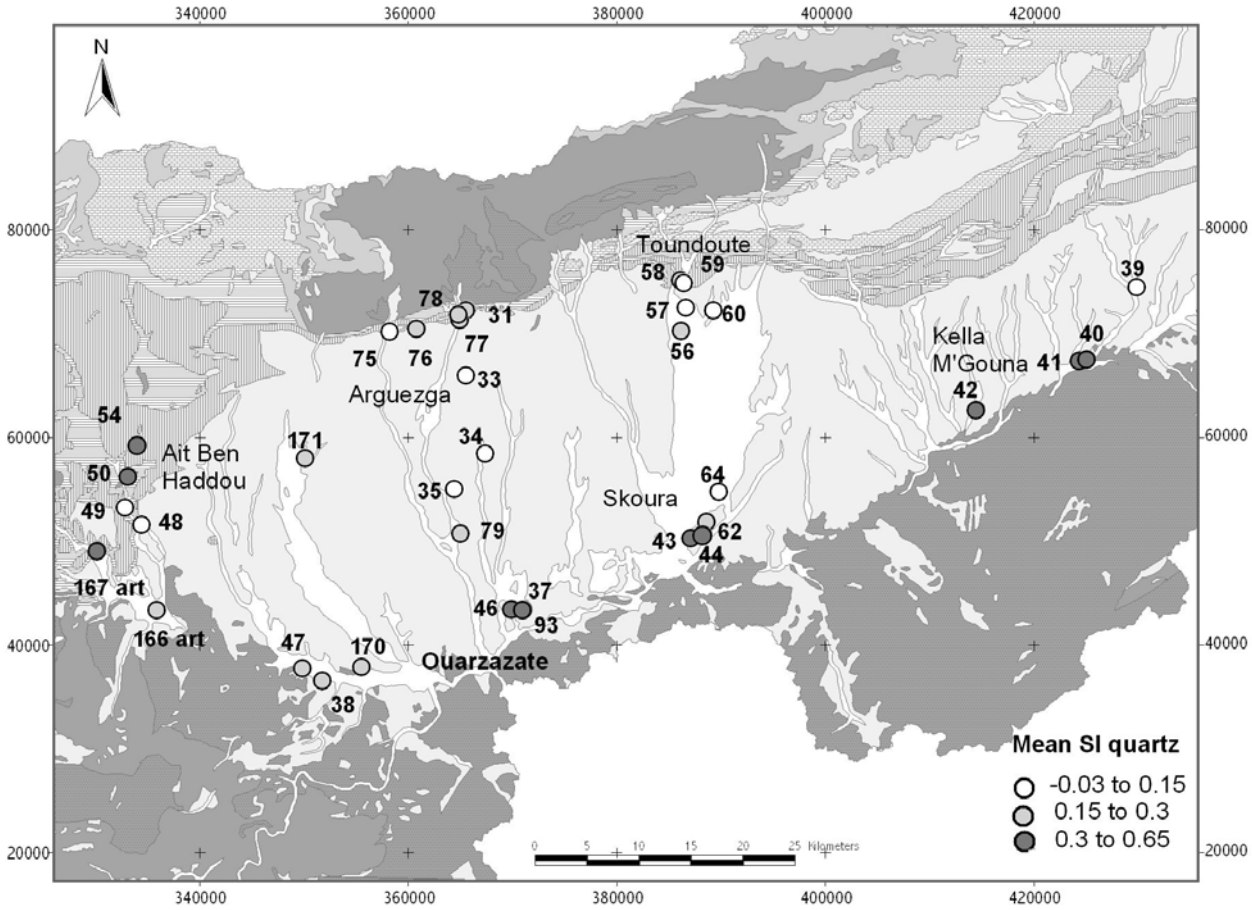

Fig. 8.30: Mean values of SI_{quartz} of the groundwater in the Basin of Ouarzazate.

8.5 Stable Isotopes

8.5.1 Isotopic composition of the groundwater

All groundwater samples of the Basin of Ouarzazate plot close to the Local Meteoric Water Line (LMWL) except for those in connection with evaporated surface water (Fig. 8.31). Comparing those signatures with the isotopic composition of groundwater of the Jbel Saghro (AA = Anti Atlas) and of the Ifre catchment (HA = High Atlas) the groundwater of most of the investigated wells reveals a recharge by water from the High Atlas and shows little influences from the evaporated groundwater of the Anti-Atlas

The isotopic composition of the surface water shows significant differences within the Basin of Ouarzazate. In the eastern part, the Dades (88) and M'Goun (32) Wadis draining the High Atlas do not show any evaporation effect (88_{mean}: d-excess = 9.5 and 32_{mean}: d-excess = 10.8) (Fig. 8.31-A and Fig. 8.32). Downstream, the evaporation portion in the Dades Wadi increases with d-excess equal to 3.1 nearby Skoura (83) and up to 1.1 in the east of Ouarzazate town (45) (Fig. 8.31-B and D). In the western part of the basin nearby Ait Ben Haddou, the eastern tributary (52) of the Mellah Wadi does not show strong evaporation with d-excess equal to 9.9, while the western tributary and the Mellah Wadi downstream are clearly evaporated (53_{mean}: d-excess = 1.9 and 89_{mean}: d-excess = 3.8) (Fig. 8.31-E).

In the eastern part of the basin, the groundwater at the wells 39, 41 and 42 (nearby Kelaa M'Gouna) are clearly recharged by groundwater from High Atlas without evaporation effect (-8.6 ‰ < $\delta^{18}O$ < -7.8 ‰ and -57 ‰ < $\delta^{2}H$ < -52 ‰) (Fig. 33-A and Fig. 8.32). The groundwater of well 40, hydraulically connected to a semi-deep aquifer of Mio-Pliocene, reveals a distinctive isotopic signature (Fig. 33-A) by slightly plotting below the LMWL. Additional the groundwater isotopic signature doesn't show significant variations by time. But the particularity of this groundwater is a strong depletion in heavy isotopes of both ^{18}O and ^{2}H and a d-excess value lower than the LMWL (40_{mean}: $\delta^{18}O$ = -9.4 ‰, $\delta^{2}H$ = -67 ‰ and d-excess = 8.0). The groundwater of this well is the most depleted in heavy isotopes observed in the whole Upper Drâa catchment. Consequently, the origin of this groundwater is clearly distinguishable from the other groundwater. Thus, the riverbed infiltration from the wadis, which is proved as the main recharge mechanism for the alluvial aquifers in the basin, is not effectual for the groundwater of well 40.

Between Toundoute and Skoura, the groundwater from the wells 43, 44, 57, 59, 60, 61, 62 and 64 has almost identical isotopic compositions (-8.7 ‰ < $\delta^{18}O$ < -8.0 ‰ and -58 ‰ < $\delta^{2}H$ < -54 ‰), which reflect the same origin from the High Atlas without evaporation effect (Figure 8.33-B and Fig. 8.32). In opposite, wells 56 and 58 show evaporated groundwater (Figure 8.33-B). But this evaporation of groundwater is not natural and occurs directly within these wells due to the shallowness of the groundwater (56) and to the broad dimension of the well (58). Moreover, well 58 is located in an irrigated area which might increase the evaporation effect.

In the Arguezga area (Fig. 8.31-C and Fig. 8.32), the groundwater does not show any evaporation effect and is clearly recharged by groundwater from the High Atlas (-8.9 ‰ < $\delta^{18}O$ < -7.8 ‰ and -61 ‰ < $\delta^{2}H$ < -53 ‰).

Nearby Ouarzazate city (Fig. 8.31-D and Fig. 8.32), the wells 38 and 47 show high evaporation due to their hydraulic connection with the Ouarzazate Wadi (91). Contrarily, no evaporation effect is observed at the wells 37, 37b, 46 and 93 localised at the east of Ouarzazate where CO_2

gas and a confined aquifer are observed (Fig. 8.23). While wells 37b, 46 and 93 have similar isotopic contents revealing a recharge from the High Atlas (-8.9 ‰ < $\delta^{18}O$ < -8.4‰ and -62 ‰ < $\delta^{2}H$ < -59 ‰), well 37 draining a confined aquifer shows groundwater clearly more depleted in heavy isotopes (37 $_{mean}$: $\delta^{18}O$ = -9.2 ‰, $\delta^{2}H$ = -64 ‰ and excess = 9.4). This depletion is due to afflux of deep groundwater up-coming together with CO_2 gas.

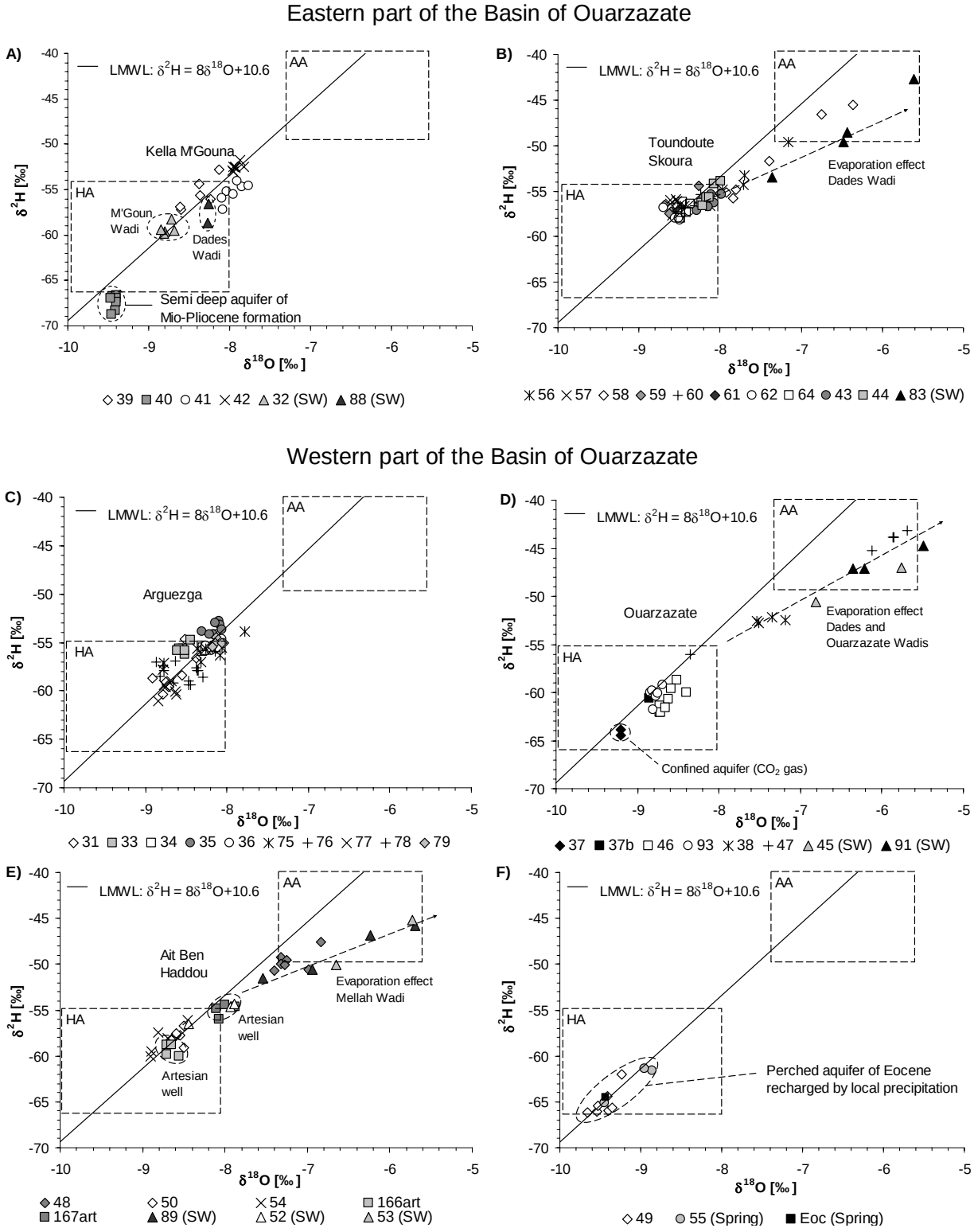

Fig. 8.31: Isotopic composition of groundwater and surface water (SW) of the Basin of Ouarzazate: Kelaa M'Gouna (A), Toundoute-Skoura (B), Arguezga (C), Ouarzazate (D) and Ait Ben Haddou (E and F) (localisation see Fig. 8.32). The groundwater of the Basin of Ouarzazate is compared to the Local Meteoric Water Line (LMWL) and to the isotopic composition of groundwater observed in the Ifre catchment (HA = High Atlas) and at Bouskour test-site (AA = Anti Atlas).

Wells 50 and 54 located within the alluvial aquifer of the Mellah Wadi in the area of Ait Ben Haddou (Fig. 8.31-E and Fig. 8.32), have groundwater plotting close to the LMWL with a similar isotope signature than groundwater from the High Atlas (-8.9 ‰ < $\delta^{18}O$ < -8.5‰; -60 ‰ < $\delta^{2}H$ < -57 ‰). These wells are in hydraulic connection with the eastern tributary (52) of the Mellah Wadi. In opposition, well 48 located downstream shows strong evaporation due to its connection with the evaporated surface water of the Mellah Wadi (91).

In comparison to the isotopic composition of the groundwater observed in the Mellah Wadi's alluvial aquifer, the groundwater of the perched aquifer of Eocene (well 49 and boundary springs 55 and Eoc) displays a clear depletion in heavy isotope (-9.6 ‰ < $\delta^{18}O$ < -8.9‰ and -66 ‰ < $\delta^{2}H$ < -61 ‰) (Fig. 8.31-E).

The already mentioned different origins of the groundwater of the artesian wells of the confined aquifer of Infracenomanian (south of Ait Ben Haddou) is clearly emphasised by clearly distinguishable isotopic signatures (Fig. 8.31-E and Fig. 8.32). Although, both plot close to the LMWL, groundwater at well 166art is clearly recharged in High Atlas ($\delta^{18}O$ = -8.7‰, $\delta^{2}H$ = -59 ‰ and d-excess = 9.9). The groundwater at well 167art is more depleted in heavy isotope ($\delta^{18}O$ = -8.0‰, $\delta^{2}H$ = -55 ‰ and d-excess = 9.2). This depletion might be the result from an influx of water from a shallow aquifer. Although, the hydrogeochemical interpretations (Paragraph 8.4.5) excluded infiltration of the chloride rich groundwater of the Mellah Wadi's alluvial aquifer into the confined aquifer, it is still possible that leakage occurs from the Imini Wadi's alluvial aquifer located more in the west.

As mentioned before, the following wells show particularly depletion in heavy isotope (Fig. 8.32):

- Well 40 in hydraulic connection with a semi-deep aquifer of Mio-Pliocene at Kelaa M'Gouna (40_{mean}: $\delta^{18}O$ = -9.4 ‰, $\delta^{2}H$ = -67 ‰ and d-excess = 8.0).
- Well 37 at Ouarzazate where CO_2 gas and afflux of groundwater from the Precambrian rocks is proved (37_{mean}: $\delta^{18}O$ = -9.2 ‰, $\delta^{2}H$ = -64 ‰ and d-excess = 9.4).
- Groundwater from the Eocene perched aquifer at Ait Ben Haddou (49_{mean}: $\delta^{18}O$ = -9.4 ‰, $\delta^{2}H$ = -65 ‰ and d-excess = 10.5)

Different interpretations explain the strong depletion in heavy isotopes observed at these wells:

- As observed at well 40 and 37, the groundwater is in connection with deeper aquifers with long residence times proved by the SI_{quartz} (Fig. 8.28-E and F). Its recharge area could be located in the High Atlas or Anti Atlas Mountains but due to temporal changes of the isotopic composition in rain, the groundwater shows isotopic signature different from the actual recharge area. Consequently, fossil groundwater might exist, for example within sand lenses of the Mio-Pliocene formations or within the fractured Precambrian rocks.
- In the case of the perched aquifer of the Eocene carbonates, which is not in hydraulic connection with the Mellah Wadi's alluvial aquifer, the recharge occurs only by local precipitation. Although the Basin of Ouarzazate shows clear arid conditions with a low mean yearly precipitation (100 mm/a), rare and short but intensive rain events can potentially recharge the aquifer system (Chapter 2). The isotopic characterization of these extreme events showed a high "amount effect" (Chapter 6) providing strongly

depleted rain water, which explains the depletion observed in the groundwater of the Eocene perched aquifer.

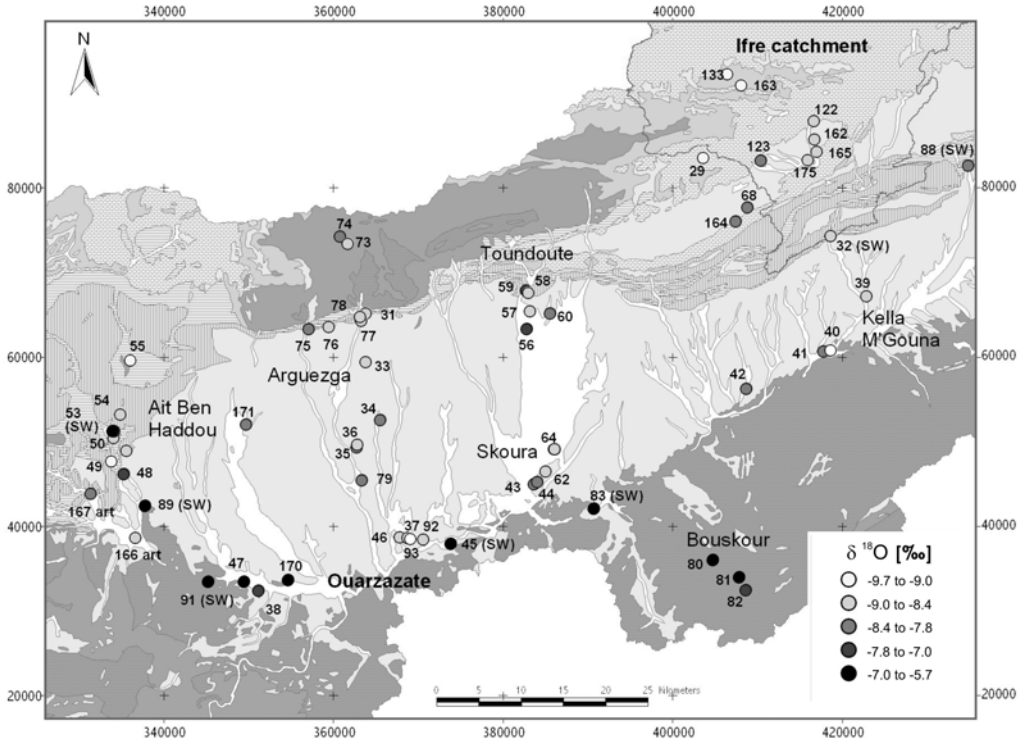

Fig. 8.32: $\delta^{18}O$ mean values of the groundwater and surface water (SW) of the Basin of Ouarzazate, Bouskour and selected groundwater of the Ifre catchment.

8.5.2 Estimation of the mean altitude of the groundwater recharge area

The estimation of the recharge altitude in the Basin of Ouarzazate is carried out using the relation: $\delta^{18}O$ = -0.002 · "altitude"-3.0 (Chapter 6) (Fig. 8.33-A). The wells showing some strong evaporation effects as well as the wells showing a particular depletion of heavy isotope (37, 40 and the groundwater of the perched aquifer of the Eocene) are excluded. The estimated mean recharge altitude of the Basin of Ouarzazate ranges between 2,400 m and 2,900 m (+/- 50 m) (Fig. 8.33-B). As the maximum elevation of the Basin of Ouarzazate is about 1,800 m the results clarify that there is no significant groundwater recharge within the basin. While the artesian well 166art has a mean recharge altitude of 2,800 m, the mean recharge altitude of the well 167art is around 2,500 m.

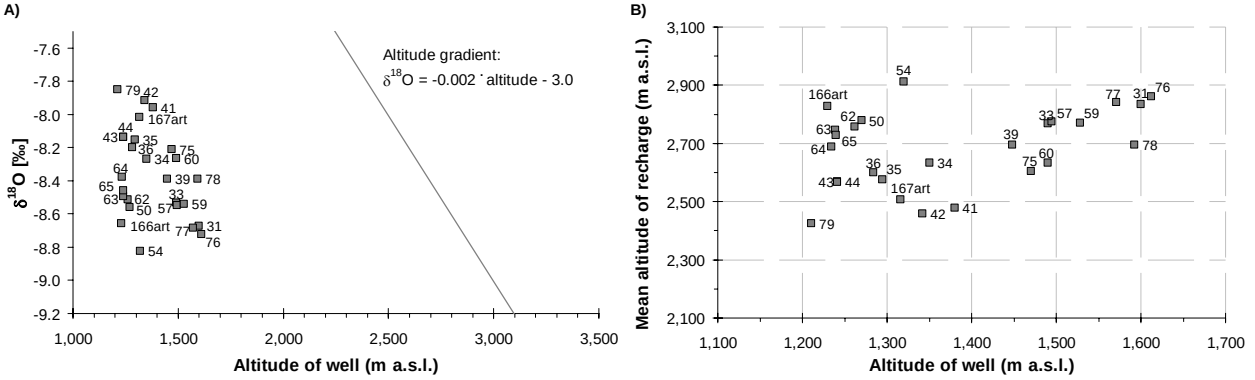

Fig. 8.33: Estimation of the recharge altitude of wells in the Basin of Ouarzazate according to the relation $\delta^{18}O$ = -0.002*altitude-3.0 defined for the High Atlas and based on the isotopic composition of precipitation (A) and "mean altitude of recharge" versus "altitude of the well" (B).

8.6 Tritium

Tritium values are available for 11 observation points in the eastern part (Fig. 8.34) and 19 observations points in the western part of the Basin of Ouarzazate (Fig 8.35) sampled in autumn 2002.

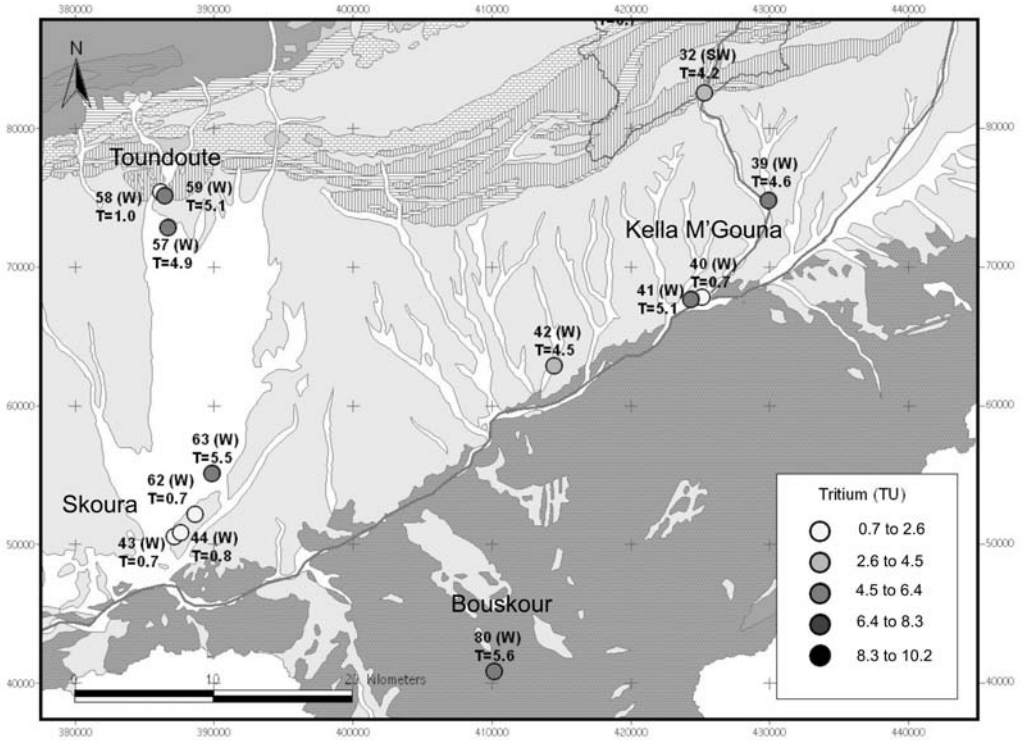

Fig. 8.34: Tritium values (TU) of groundwater and surface water in the eastern part of the Basin of Ouarzazate (W = well, S = spring and SW = surface water).

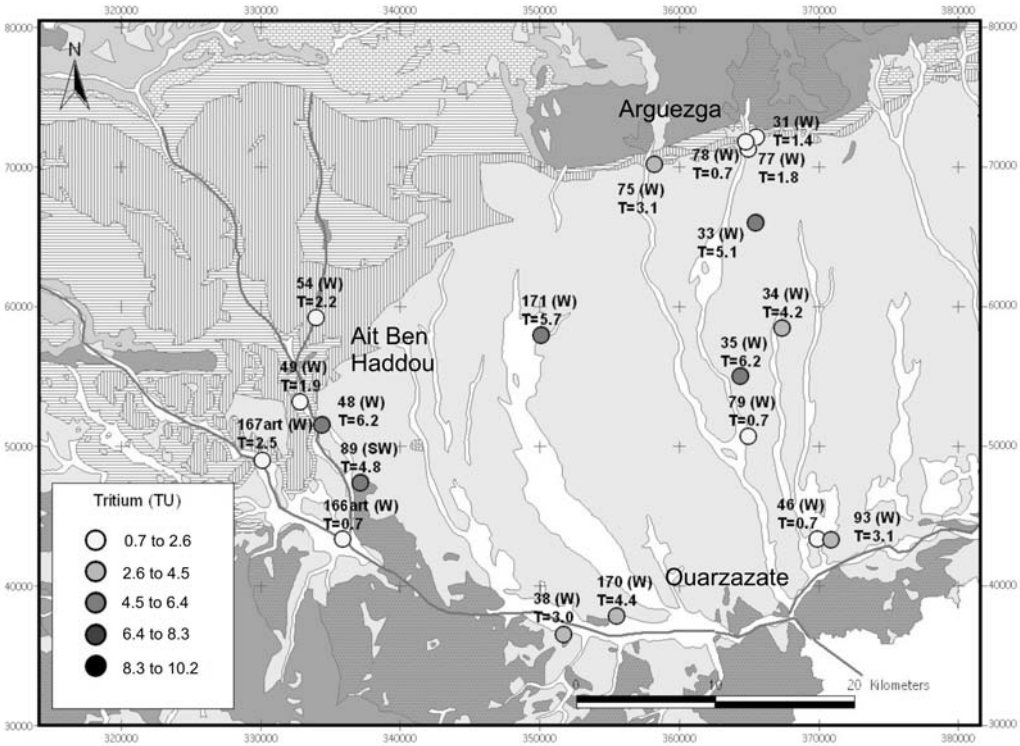

Fig. 8.35: Tritium values (TU) of groundwater and surface water in the western part of the Basin of Ouarzazate (W = well, S = spring and SW = surface water).

In accordance to the interpretation used for unconfined aquifer (Chapter 6), two distinctive types of groundwater in regard to the mean residence time can be observed in the eastern part of the basin (Fig. 8.36):

- Recent groundwater (< 4 years) with tritium values between 4 TU and 5.5 TU revealing a direct recharge from the wadis draining the High Atlas: wells 39, 41, 42 (Kelaa M'Gouna), 57, 59 (Toundoute) and 63 (Skoura).
- Groundwater with a mean residence time above 50 years with tritium values below 1.0 TU: wells 40 (Kelaa M'Gouna), 58 (Toundoute), 43, 44 and 62 (Skoura). As already shown by the chemistry, well 40 is connected with a semi-deep aquifer of Mio-Pliocene. The high residence time observed at this well proves that the recharge is not efficient as already assumed by the stable isotopic signature. Although, the stable isotopes of groundwater at the wells 43, 44 and 62 reveals a recharge from the High Atlas, the high residence time might reflect a groundwater passage within semi-deep aquifer of Mio-Pliocene. In contrarily, the high mean residence time observed at well 58 located at the northern range of the basin is related to a recharge from the low permeable Precambrian and Cambrian rocks cropping out in the High Atlas (Skoura Mole: compare Fig. 8.1).

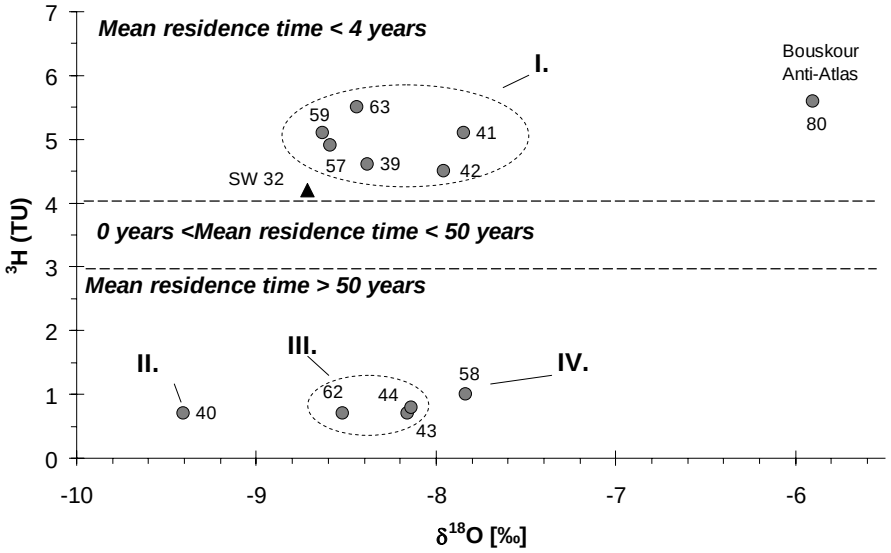

Fig. 8.36: ^{3}H versus δ^{18}O (IMP5) of the groundwater in the eastern part of the Basin of Ouarzazate (SW = surface water).

In the western part of the Basin of Ouarzazate (Fig. 8.35), three distinctive types of groundwater in regard to the mean residence time can be observed (Fig. 8.37):

- Recent groundwater with tritium values above 4TU revealing a direct recharge from the wadis draining the High Atlas: wells 33, 34, 35, 48, 170 and 171.
- Groundwater older than 50 years but with a possible admixture of young water showing tritium values between 1.0 TU and 3.1 TU: 31, 38, 49, 54, 75, 77, 93 and 167art.
- Groundwater older than 50 years with tritium values below 1.0 TU: 46, 78, 79 and 166art.

At Arguezga (Fig. 8.35 and Fig. 8.37), wells 31, 77 and 78 show a mean residence time older than 50 years, which proves a recharge from the low permeable fractured rocks of Precambrian and Cambrian localised in High Atlas (Skoura mole: compare Fig. 8.1). The tritium contents of 3 TU of the groundwater of well 38 at Ouarzazate city reflects a mixing between young and old groundwater. While the young component derives from the infiltration of surface water (Ouarzazate Wadi), the old component comes from the Precambrian rocks of the Anti Atlas as already proved by the hydrogeochemistry evaluations (compare Fig. 8.25).

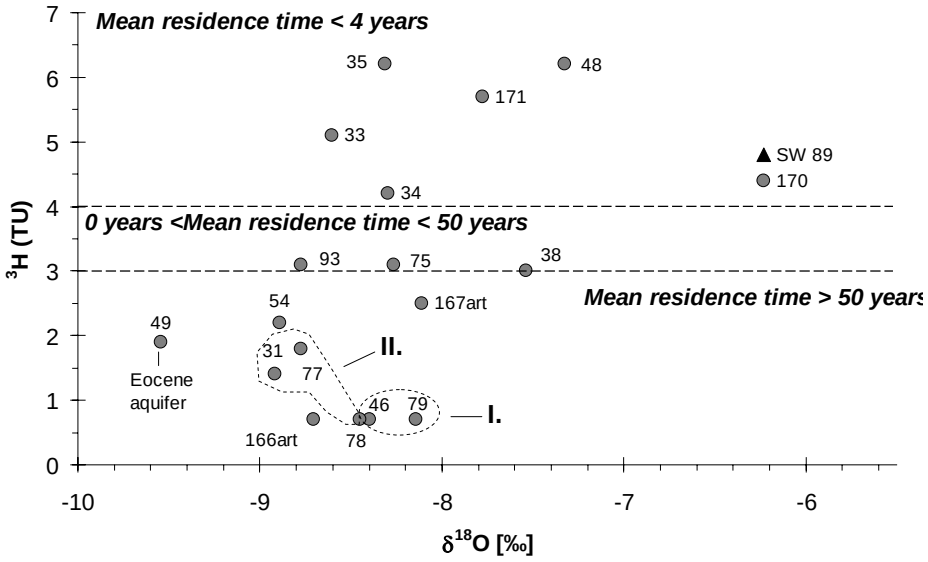

I. Recharge from High Atlas and groundwater passage within Mio-Plioc. semi-deep aquifer

II. Recharge from the low permeable Precambrian rocks of the Skoura Mole (High Atlas)

Fig. 8.37: ^{3}H versus δ^{18}O (IMP5) of the groundwater in the western part of the Basin of Ouarzazate (SW = surface water).

Although well 54 has hydraulic connections with the Mellah Wadi, groundwater shows low value of tritium during the sampling campaign (^{3}H = 2.2 TU) revealing groundwater older than 50 years (Fig. 8.35 and Fig. 8.37). Therefore, during the base flow conditions the groundwater at this well is mainly recharged by the surrounding Eocene rocks.

The artesian wells 166art (0.7 TU) and 167art (2.5 TU) have mean residence times around 50 years according to the piston flow approach (Chapter 6). The admixture of groundwater from the Imini Wadi's alluvial aquifer might explain the higher value of tritium observed at the well 167art (Fig. 8.35 and Fig. 8.37).

8.7 Dating of groundwater with ^{14}C

Carbon-14 and carbon-13 analyses are carried out in 10 selected locations (autumn 2002) in order to define whether old groundwater is mixed with younger groundwater or not (Fig. 8.38). Hence the interpretation of ^{14}C dating depends strongly on the dissolution of calcite, several models of correction are required based on chemical and isotopic balances taking into account isotopic and cation exchanges and dissolution effects (Paragraph 3.3.2.3).

Groundwater shows ^{13}C values ranging between -13.7 ‰ (57) and -7.0 ‰ (49), and a^{14}C values between 39.1 pmC (31) and 102.4 pmC (57) (Table 8.5). Well 57 has an a^{14}C equal to 102.4 pmC revealing the influence of the peak in the atmosphere due to the nuclear weapon tests in 1950's (compare Fig. 3.15). As already confirmed by the tritium value (4.9 TU), this well reveals young groundwater.

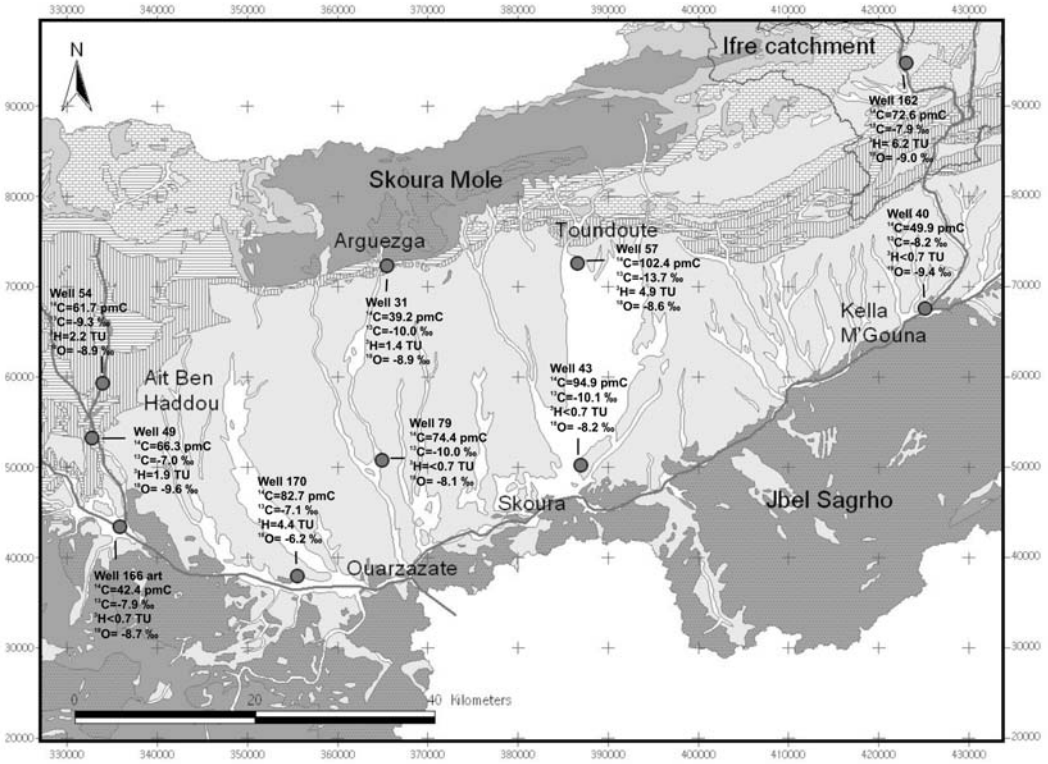

Fig. 8.38: Results of the ^{14}C, ^{13}C, ^{3}H and ^{18}O of ten wells in the Upper Drâa catchment.

Although the tritium data show recent groundwater at the wells 162 and 170, the $a^{14}C$ are lower than 100 pmC (162: $a^{14}C$ = 72.6 pmC and 170: $a^{14}C$ = 82.7 pmC). These values reflect the dissolution of calcite incorporating “dead” carbon (0 pmC) in the DIC of the groundwater, which has to be considered for the necessary correction of the input function (Paragraph 3.3.2.3):

- The model of Tamer is based on the chemical balance of the main forms of the Dissolved Inorganic Carbon (DIC).
- The model of Pearson is based on the isotopic balance using the ^{13}C values.
- The model of Mook takes into account the isotopic exchange between $CO_{2,soil}$ and DIC-carbonates.
- The model of Fontes-Garnier is based on matrix exchange taking into account the dissolution of Ca^{2+} and Mg^{2+} with a correction for evaporite dissolution and cation exchanges.

Based on the given chemistry data (Tab. 8.5) and the following assumptions apparent residence time of the groundwater were calculated (Tab. 8.6):

- Carbonates are of marine origin with $a^{14}C_{carb}$ = 0 pmC (dead carbon) and $\delta^{13}C_{carb}$ = 0 ‰.
- The $a^{14}C_{Soil}$ is considered as 100 pmC.
- Almost 100% of plants are of C3 cycle in the High Atlas Mountains (Taoujgalt test site), while in the Basin of Ouarzazate 70 % of plants are of C3 cycle, 25 % of CAM cycle and only 5 % of C4 (Trab Labied test site) (M. Finck: personal communication). Based on this information, the $\delta^{13}C_{soil}$ is estimated as -27 ‰ in the High Atlas and -24 ‰ in the Basin of Ouarzazate.
- The fractionation factors of ^{13}C between the carbonates species are considered at 20 °C: $\varepsilon^{13}C_{CO2/HCO3-}$ = -8.5 ‰ and $\varepsilon^{13}C_{CO2/CaCO3}$ = -11.1 ‰ (compare: Tab. 3.6).

Tab. 8.5: Chemical characteristics, ^{18}O, ^{2}H, ^{3}H, ^{13}C and ^{14}C of the groundwater sampled for ^{14}C dating in the Upper Drâa catchment (autumn 2002: IMP5); EC = electric conductivity.

Nr	31	40	43	49	54	57	79	162	166art	170
EC (µs/cm)	1,158	1,062	4,410	1,896	4,030	1,931	1,550	1,339	1,018	6,690
pH	7.94	7.55	7.29	7.71	7.55	7.01	7.12	7.82	7.34	7.31
Ca^{2+} (mol/l)	1.73	2.36	6.9	6.31	15.02	4.13	2.93	2.5	2.71	11.84
Mg^{2+} (mol/l)	2.34	0.4	4.81	4.35	2.85	2.37	3.59	1.47	1.33	9.89
Na^{+} (mol/l)	4.21	5.52	21.14	2.35	15.13	6.78	3.31	5.59	3.56	34.72
K^{+} (mol/l)	0.39	0.04	0.17	0.66	0.12	0.18	0.23	0.09	0.19	0.28
HCO_3^{-} (mol/l)	5.55	3.25	5.5	2.9	3.05	6.5	5.4	4.25	8.1	3.4
Cl^{-} (mol/l)	2.42	3.59	27.25	2.8	14.68	7.15	4.02	5.43	1.71	22.2
SO_4^{2-} (mol/l)	1.04	1.92	5.74	8.67	15.57	3.49	4.09	1.71	0.84	26.6
SiO_2 (mg/l)	8.8	18.6	15.9	10.0	16.2	6.0	10.0	4.8	8.1	10.7
$SI_{calcite}$	0.66	0.21	0.59	0.55	0.67	0.07	0.02	0.48	0.45	0.31
HCO_3^{-} (mg/l)	339	198	335	177	186	397	329	259	494	207
H_2CO_3 (mg/l)	2.6	4.4	18.5	5.3	9.7	31.2	17.6	10.6	26.4	13.2
^{18}O (‰)	-8.9	-9.4	-8.2	-9.5	-8.9	-8.6	-8.1	-9	-8.7	-6.2
^{2}H (‰)	-59	-67	-56	-66	-59	-58	-55	-59	-59	-47
^{3}H (TU)	1.4	< 0.7	< 0.7	1.9	2.2	4.9	< 0.7	6.2	< 0.7	4.4
^{13}C (‰)	-10	-8.2	-10.1	-7.0	-9.3	-13.7	-10	-7.9	-7.9	-7.1
$a^{14}C$ (pmC)	39.2	49.9	94.9	66.3	61.7	102.4	74.4	72.6	42.4	82.7

Tab. 8.6: Dating with ^{14}C using the Tamers, Pearson (Pears) and Mook corrections and using the Fontes-Garnier (F-G) model based on matrix exchange.

Nr	$\delta^{13}C_{soil}$	31	40	43	49	54	57	79	162	166 art	170
$a^{14}C$ (pmC)	-	39.2	49.9	94.9	66.3	61.7	102.4	74.4	72.6	42.4	82.7
$a^{14}C_{rech(Tamers)}$ (pmC)	-	50.4	51.1	52.6	51.4	52.5	53.6	52.5	51.9	52.5	53
Age $_{(Tamers)}$ (year)	**-**	**2,076**	**194**	**-4877**	**-2097**	**-1339**	**-5345**	**-2877**	**-2766**	**1772**	**-3679**
$a^{14}C_{rech(Pears)}$ (pmC)	-27‰	36.9	30.3	37.6	25.9	34.3	50.8	36.9	29.3	29.3	26.1
Age $_{(Pears)}$ (year)	-27‰	-502	-4136	-7657	-7752	-4847	-5794	-5784	-7504	-3067	-9521
$a^{14}C_{rech(Pears)}$ (pmC)	-24‰	41.5	34.0	42.3	29.2	38.6	57.2	41.6	33.0	32.9	29.4
Age $_{(Pears)}$ (year)	**-24‰**	**471**	**-3162**	**-6683**	**-6778**	**-3873**	**-4820**	**-4810**	**-6530**	**-2093**	**-8547**
K_{Mook}	-27‰	-8.28	-12.78	-9.22	-15.64	-11.13	-1.74	-9.56	-13.91	-14.28	-16.48
$a^{14}C_{rech(Mook)}$ (pmC)	-27‰	42.10	38.31	43.40	35.81	41.34	51.91	42.98	38.05	38.25	36.52
Age $_{(Mook)}$ (year)	**-27‰**	**591**	**-2186**	**-6470**	**-5093**	**-3311**	**-5617**	**-4537**	**-5341**	**-851**	**-6758**
K_{Mook}	-24‰	-5.20	-9.98	-6.04	-13.02	-8.11	2.06	-6.41	-11.12	-11.48	-13.80
$a^{14}C_{rech(Mook)}$ (pmC)	-24‰	45.18	41.11	46.57	38.43	44.37	55.71	46.13	40.84	41.05	39.19
Age $_{(Mook)}$ (year)	**-24‰**	**1,175**	**-1602**	**-5886**	**-4509**	**-2727**	**-5034**	**-3953**	**-4758**	**-267**	**-6174**
DIC carb (mol/l)	-27‰	4.12	1.84	3.01	2.1	2.58	2.92	2.19	2.39	4.23	1.53
DIC CO2 -exch (mol/l)	-27‰	1.05	-0.73	-0.73	-0.08	0.98	-0.47	-2.06	-1.04	-2.55	-1.66
q_{F-G}	-27‰	0.45	0.21	0.32	0.25	0.48	0.48	0.21	0.19	0.16	0.06
$a^{14}C_{rech\ (F-G)}$ (pmC)	-27‰	44.67	21.03	32.15	24.77	47.53	47.81	21.26	19.20	16.31	6.02
Age $_{(F-G)}$ (year)	**-27‰**	**1,080**	**-7146**	**-8949**	**-8139**	**-2157**	**-6297**	**-10356**	**-10999**	**-7900**	**-21659**
DIC CO2 -exch (mol/l)	-24‰	1.63	-0.57	-0.32	0.08	1.32	0.25	-1.80	-0.85	-2.25	-1.62
q_{F-G}	-24‰	0.55	0.26	0.40	0.31	0.59	0.59	0.26	0.24	0.20	0.07
$a^{14}C_{rech\ (F-G)}$ (pmC)	-24‰	55.06	25.92	39.63	30.54	58.58	58.93	26.21	23.66	20.10	7.42
Age $_{(F-G)}$ (year)	**-24‰**	**2,809**	**-5417**	**-7220**	**-6411**	**-429**	**-4568**	**-8627**	**-9270**	**-6171**	**-19930**

Calculated with $a^{14}C_{Soil}$ = 100 pmC, $\delta^{13}C_{carb}$ = 0 ‰, $a^{14}C_{carb}$ = 0 pmC, $\varepsilon^{13}C_{CO2/HCO3-}$ = -8.5 ‰ (20 °C) and $\varepsilon^{13}C_{CO2/CaCO3}$ = -11.1 ‰ (20 °C) (Tab. 3.6).

Only well 31 shows clearly a long residence time:

- Tamer: 2,076 years.
- Pearson: 471 years ($\delta^{13}C_{soil}$ = -24 ‰).
- Mook: 591 years ($\delta^{13}C_{soil}$ = -27 ‰) and 1,175 years ($\delta^{13}C_{soil}$ = -24 ‰).
- Fontes-Garnier: 1,080 years ($\delta^{13}C_{soil}$ = -27 ‰) and 2,809 years ($\delta^{13}C_{soil}$ = -24 ‰).

Well 31 is drilled in the quartzite of Precambrian which is a fractured aquifer with low permeability. The tritium value of 1.4 TU reveals a mixing with recent groundwater.

8.8 Conclusion

Alluvial aquifers

The various alluvial aquifers of the Basin of Ouarzazate provide the first groundwater resources for irrigation or domestic uses. These aquifers are developed in alluvial deposits (sand, gravel, pebble and conglomerates) with a thickness varying between few meters to 25 m and overlaying either the clayey Miocene formations or the Senonian marls (Tikirt area). The quality of the groundwater varies broadly within the basin. While low mineralised groundwater (conductivities around 500 µS/cm) is observed in the eastern part of the basin, some saline groundwater prevails at Ouarzazate (conductivities up to 7,000 µS/cm). Hence the isotopic composition of the groundwater does not reveal strong evaporation effects in the Basin of Ouarzazate, the high mineralization is only due to leaching of gypsum and halite present within the geological formations. High variability of the groundwater types are observed through the basin, which do not correspond directly to the general flow pattern. No clear seasonal variations between base flow conditions (autumn) and humid periods (spring) is observed. The hydrochemical variations depend mainly on the degree of hydraulic connection with the wadis. The groundwater level map and the isotopic composition of the groundwater prove that the recharge of the alluvial aquifers occurs mainly through wadis draining the High Atlas. This is emphasised by estimated mean altitudes of the groundwater recharge area between 2,400 m to 2,900 m. Hence the maximum elevation of the Basin of Ouarzazate averages 1,800 m, these results clarify that there is no significant groundwater recharge within the basin. The recharge is effective with a mean residence time below 10 years.

Semi-deep aquifer of Mio-Pliocene formation

Groundwater from a semi-deep aquifer within the Mio-Pliocene formation was identified at the well 40 nearby Kelaa M'Gouna. This groundwater reveals old (> 50 years) and relatively low mineralised groundwater (mean conductivity = 1,100 µS/cm) with a Na-Ca-Cl-SO_4 to Na-Ca-SO_4-Cl. facies. Its particular low contents of Mg^{2+} (9.8 mg/l < Mg^{2+} < 18.0 mg/l) excludes a long transit from the High Atlas where the dolomites are prevalent. The groundwater is also slightly oversaturated in regard to quartz (SI_{quartz} = 0.46), which proves the passage of groundwater within a silicate aquifer such as quartz sand, sandstones, quartzite or magmatic rocks with a relative high residence time. The stable isotopic composition of the groundwater of well 40 reveals the highest depletion in heavy isotope observed in the whole Drâa catchment (40_{mean}: $\delta^{18}O$ = -9.4 ‰, $\delta^{2}H$ = -67 ‰ and d-excess = 8.0). Consequently no current effective recharge occurs and the isotopic signature of the groundwater gives old groundwater although the carbon-14 analyse did not prove fossil groundwater.

The high variation with time of the hydrochemical composition of the groundwater of well 43 in near Skoura results from variable mixing processes of groundwater from the north (Toundoute) and a local saline groundwater of Na-Ca-Cl-SO_4 to Na-Ca-Mg-Cl-SO_4 type. The lithological description of the Mio-Pliocene formations show the existence of a semi-deep aquifer developed in sand and conglomerates between Skoura and Ouarzazate. Some hydraulic connections between this aquifer and the alluvial aquifer are possible. The high salinity due to high Na^+ and Cl^- contents (1,318 mg/l < $[Na^+ + Cl^-]_{43}$ < 1,739 mg/l) characterising the groundwater at well 43 reflects a groundwater passage within this semi-deep aquifer. The isotopic signature gives clear evidence of the recharge from the High Atlas. Both the tritium data and the saturation indexes reveal older and evolved groundwater.

Influence of CO_2 gas from the Precambrian rocks

Nearby Ouarzazate, groundwater chemistry is clearly influenced by affluxes CO_2 gas coming up along faults of the Precambrian (well 37 and spring 92). The proved anti-correlation between pH and HCO_3^{2-} (PCA) results from the dissolution of CO_2 in groundwater. The dissolution is connected to a production of free protons, which decrease the pH and increase the HCO_3^{2-} concentration according to the following equilibrium equation:

$$CO_{2(g)} + H_2O \xleftrightarrow{K_{co_2}} H_2CO_3 \xleftrightarrow{K1} H^+ + HCO_3^- \xleftrightarrow{K2} 2H^+ + CO_3^{2-}$$

The second observed effect resulting of the input of CO_2 gas is the increasing capacity for a dissolution of carbonates, thus decreasing their saturation indexes. Groundwater of the alluvial aquifers in contact to CO_2 gas was in perfect equilibrium in regard to calcite and dolomite (well 37: $SI_{calcite}$ = 0.08 and $SI_{dolomite}$ = 0.03). Additional the clear over-saturation in regard to quartz (SI_{quartz} = 0.63) in well 37 reveals the flow up of deep CO_2 gas rich groundwater from the Precambrian rocks with high residence times.

The perched Eocene aquifer (Tikirt area)

In the Tikirt area, the groundwater geochemistry of the perched aquifer developed in the Eocene carbonates (e.g. spring 51) shows low mineralization with no influences of leaching of evaporitic minerals. The strong depletion in heavy isotopes of the groundwater of the perched Eocene aquifer can not be related to a recharge from the High Atlas. This depletion is characteristic for the local precipitation recharge with strongly depleted precipitation due to the proved amount effect during extreme rain events in the Basin of Ouarzazate. The perched aquifer of Eocene shows groundwater older than 50 years which enhance the hypothesis that the local recharge is not efficient at the scale of the basin.

Confined Infracenomanian aquifer (Tikirt area)

The investigated at two artesian wells (166art and 167art) of the confined Infracenomanian aquifer in Tikirt area show clear differences in their geochemistry and isotopic composition (166art $_{mean}$: $\delta^{18}O$ = -8.7‰, δ^2H = -59 ‰ and excess = 9.9 and 167art $_{mean}$: $\delta^{18}O$ = -8.0‰, δ^2H = -55 ‰ and d-excess = 9.2), which reveals the inhomogeneous character of this aquifer. The lower contents of Na^+ and Cl^- in the groundwater of the Infracenomanian aquifer (153 mg/l < $[Na^+ + Cl^-]_{Infracenomanian}$ < 302 mg/l) in comparison to the alluvial aquifer of the Mellah Wadi (700 mg/l < $[Na^+ + Cl^-]_{Mellah\ alluvial\ aquifer}$ < 4,000 mg/l) proves that no infiltration occurs from the superficial aquifer into the confined aquifer. The estimation of the mean altitude of the recharge area for the well 166art is about 2,800 m (+/-50 m) while the well 167art shows a lower mean

altitude about 2,500 m (+/- 50 m). The lower recharge altitude of well 167art is due to an admixture of groundwater from the alluvial aquifer of the Imini Wadi. The confined aquifer shows groundwater equal or superior to 50 years according to the tritium data.

Precambrian rocks of the Skoura Mole in High Atlas

The groundwater from the Precambrian rocks of the Skoura Mole located in the north of the basin showing mean residence time older than 50 years according to tritium data. Carbon-14 proves the presence of old groundwater mixed with recent groundwater at the well 31 drilled in the quartzite of Precambrian in the northern range of the Basin of Ouarzazate. According the various models, the mean residence time at this well varies between approximately 500 (Pearson) to 2800 years (Fontes-Garnier).

9 GROUNDWATER MODELLING OF THE BASIN OF OUARZAZATE

9.1 Introduction

The simulation of the groundwater system prevailing in the Basin of Ouarzazate is performed using numerical groundwater modelling techniques. For that purpose, the groundwater model MODFLOW PMWIN5 (CHIANG et al. 1998, CHIANG & KINZELBACH 2000) was selected. The numerical model shall help to understand the general hydraulic system of the alluvial aquifer system. The design of the groundwater model and the calibration for steady state conditions are discussed in this chapter.

9.2 Model design

9.2.1 Localisation and overview of the model domain

The groundwater model attempts to describe the shallow aquifers of the Basin of Ouarzazate developed in quaternary deposits. The model is defined as a rectangle of 129.0 km by 78.5 km (Fig. 9.1 and Tab. 9.1). The altitude of the Basin of Ouarzazate ranges between 1,100 and 1,800 m a.s.l. with a mean altitude of 1,350 m a.s.l.. The area of the basin itself is estimated to be about 2,600 km^2.

Three main wadis flow in the Basin of Ouarzazate (Paragraph 2.4): the Ouarzazate Wadi at the west and the Dades and the M'Goun Wadis at the east (Fig. 9.1-A). Various wadis of second order flow from the High Atlas dominate in particular in the area of Toundoute. Besides the superficial runoff, the wadis are recharged by infiltration from the various alluvial aquifers. The geomorphology of the basin is strongly moulded by the various wadis. They cut the basin into shallow valleys (Fig. 9.1-B), which are filled with heterogeneous material of erosion. The landscape is slightly hilly with a southern topographic inclination.

Tab. 9.1: Coordinates (Lambert) and altitudes of the model area

Coordinates of the Grid	X (m): length	Y (m): width	Z (m): Altitude (m)
min	331,493.2	18,545.7	1,100 m
max	460,493.2	97,045.7	1,800 m

The shallow aquifer is complex and heterogeneous. It is located in the permeable material of the Quaternary, overlaying the clayey Mio-Pliocene formations. The knowledge of the geometry and lithology of the shallow aquifer is based on data from the Direction Régionale de Hydraulique (DRH). The data are scarce and inhomogeneous distributed over the basin (Fig. 9.2). The thickness of the alluvial aquifers and the properties of permeability are extrapolated from these data (Fig. 9.3 and 9.4). The thickness of the shallow aquifer varies between 0 to 40 m. The aquifers are developed in alluvial sediments consisting of silt, sand, gravel and pebble with a more or less clayey matrix and coarse and heterometric conglomerates. Few results of pumping tests are available (Paragraph 8.2).

9.2.2 Model geometry and boundary conditions

Mesh size

The aquifer system is simulated by a discretized domain consisting of an array of nodes and associated finite difference blocks (cells). The model consists of a mesh of cells of 516 columns (Y-direction) and 314 rows (X-direction). The cell size is 250 m of side (X- and Y-directions).

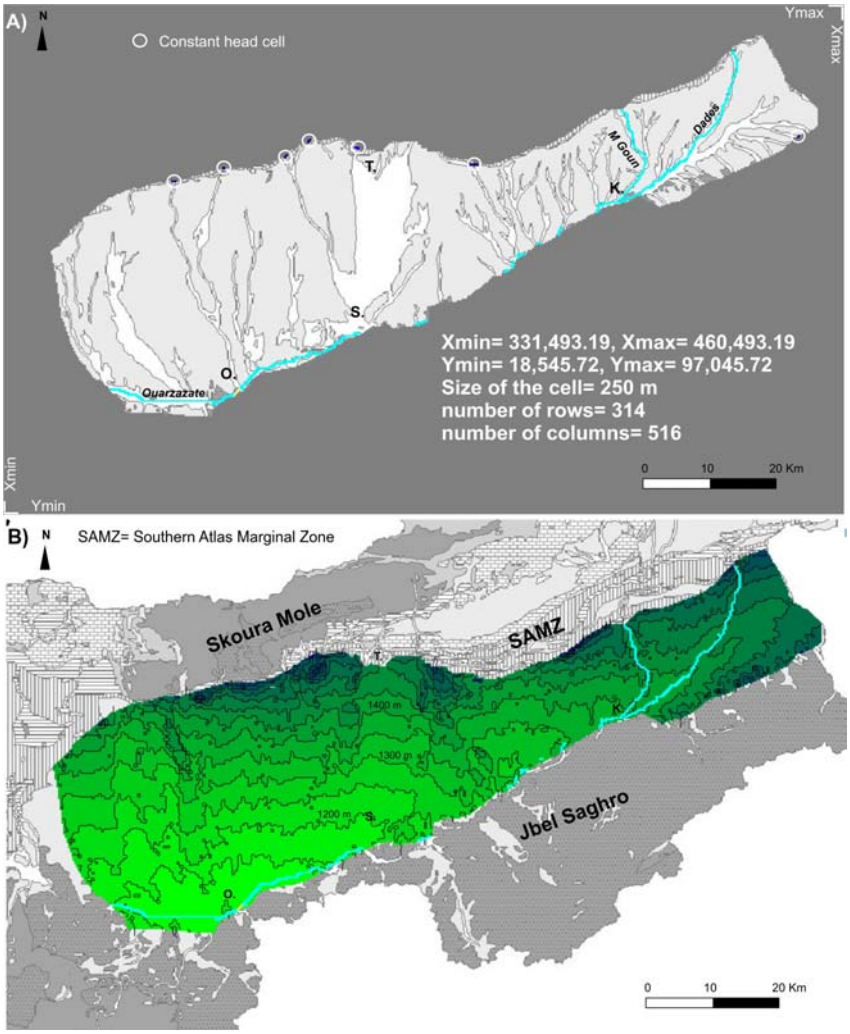

Fig. 9.1: **Model area and boundary conditions (grey = inactive cell), (A) and Digital Elevation Model used for the model (B); O. = Ouarzazate, S. = Skoura, T. = Toundoute and K. = Kelaa M'Gouna.**

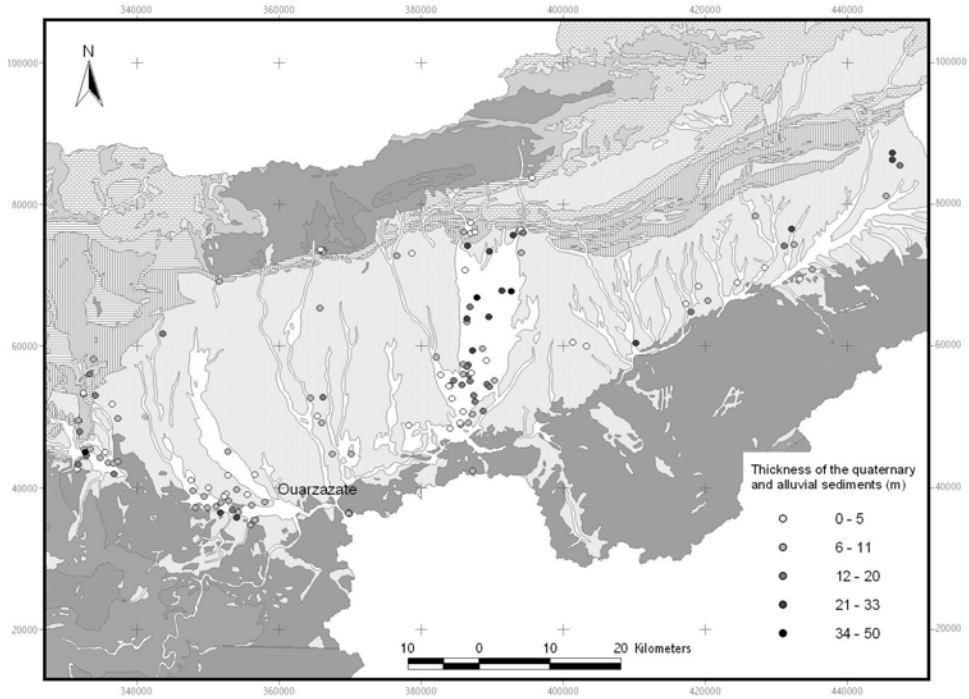

Fig. 9.2: **Localisation of wells and boreholes with available lithological data and thickness of the Quaternary and alluvial sediments (data from DRH).**

Layers

Vertically the model is built up by two layers. The upper layer represents the unconfined shallow alluvial aquifer and the lower layer the Mio-Pliocene formations. The top of the upper layer is the ground surface given by the Digital Elevation Model as the top grid. The bottom of the first layer corresponds to the maximum depth of the alluvial deposits. Thus, spatial variations of thickness of the alluvial aquifer were taken into account by means of interpolation of available data of lithology from bore logs using GIS ArcView (Kriging methods) (Fig. 9.2 and 9.3). The Mio-Pliocene formations are mainly clayey. Thus, their hydraulic conductivity is low and a leakage of the alluvial aquifer into those formations is negligible compared to the horizontal flow. But, it has to be remained that the lithological descriptions of the Mio-Pliocene formations show locally sandy parts (Paragraph 8.2) which are not taken into account due to the lack of detailed information. The Mio-Pliocene formations are considered as the aquitard of the alluvial aquifer. In order to avoid numerical problems resulting from the specific geometry of the model (ΔX = 129 km, ΔZ = 0.7 km) with a thickness of the modelled aquifer between 5 and 50 m, these clayey formations are simulated as a second layer. The thickness of this second layer was arbitrarily defined to constantly 40 m. This low permeable layer is described with a constant transmissivity and varying pressure situations between confined and unconfined.

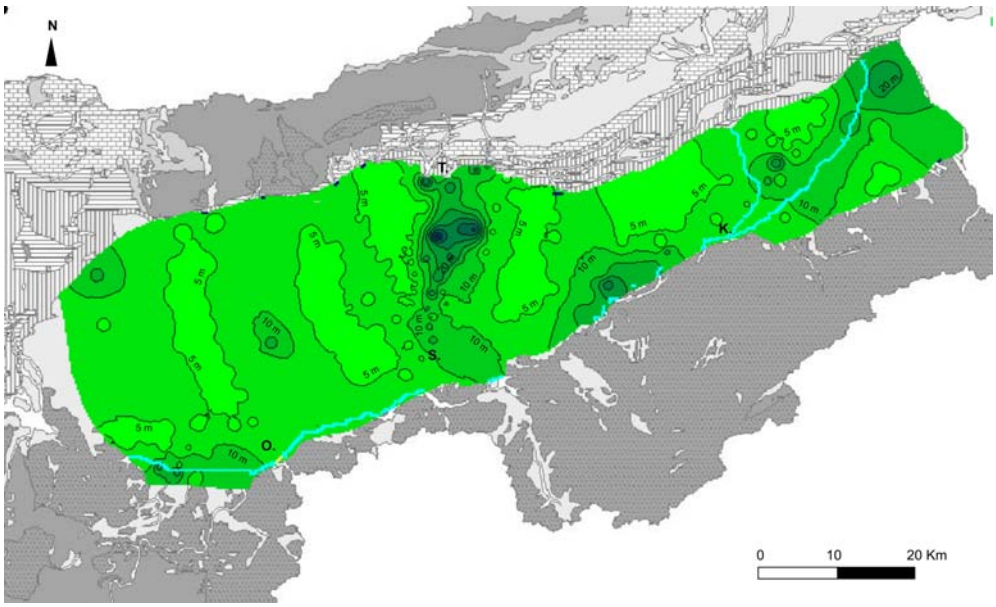

Fig. 9.3: Interpolated map (Kriging method) of the thickness of the shallow aquifer used for the model based on lithological descriptions of boreholes (see Fig. 9.2); O. = Ouarzazate, S. = Skoura, T. = Toundoute and K. = Kelaa M'Gouna.

Lateral boundaries

Due to the geological framework (Chapter 4), the recharge of the basin through lateral groundwater flows from the Skoura Mole, the Southern Atlas Marginal Zone and from the Precambrian rocks of the Jbel Saghro (Fig. 9.1-B) is negligible and therefore considered as no-flow boundaries (Fig. 9.1-A).

9.2.3 Model parameters

Units

All exploitation data is given in m^3/s, piezometric levels in meter above the sea level and time in second.

Hydraulic conductivity

It is necessary to determine the hydraulic parameters of the aquifers in the model to simulate the groundwater flow as realistic as possible. Based on interpretations of the lithological descriptions of boreholes available in the catchment added to information from the geological map (Ouarzazate 1/500,000), a map of the horizontal permeability of the shallow aquifer (layer 1) was created (Fig. 9.4). Although KHALIL & RACHACH (1986) give a K value of 3.47 $\cdot 10^{-3}$ m/s for the alluvial aquifer of Ouarzazate (Paragraph 8.2.1), it is considered that at a regional level a smaller K value is more representative for the shallow aquifers. The interpolated permeability map shows K values between 10^{-4} and 10^{-6} m/s (Fig. 9.4). The horizontal hydraulic conductivity of the second layer in the model is defined as 1 $\cdot 10^{-8}$ m/s. In order to take into account the vertical component of the groundwater flow, a vertical permeability is defined in the model. A ratio of horizontal (K_H) to vertical hydraulic conductivity (K_v) between 1 : 1 and 1000 : 1 is common in model application (CHIANG & KINZELBACH 2000). In this study, a ratio of 10 : 1 was chosen for both layers following SPITZ & Moreno (1996).

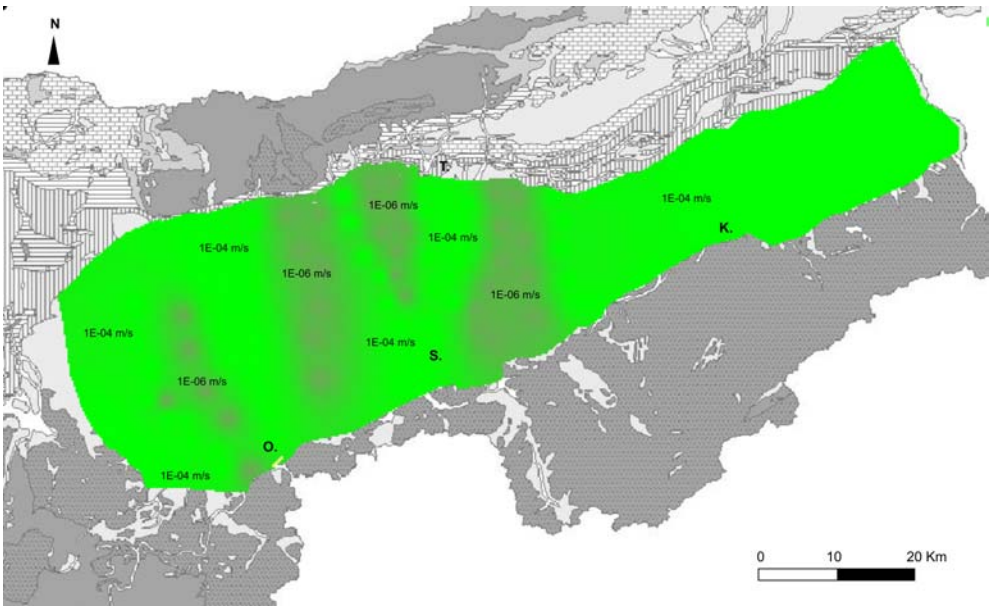

Fig. 9.4: Interpolated map (Kriging method) of the permeability (K values in m/s) of the shallow aquifer system. O. = Ouarzazate, S. = Skoura, T. = Toundoute and K. = Kelaa M'Gouna.

Precipitation and evapotranspiration

Due to the lack of information regarding the effective recharge by precipitation and the real evapotranspiration in the Basin of Ouarzazate, assumptions had to be done. Based on the results of the water budget calculated for Ifre catchment (Chapter 5), the recharge by precipitation is estimated to 10 % of the total precipitation. Therefore, taking into account an annual mean precipitation equal to 100 mm/a (Paragraph 2.3), a recharge of 10 mm/a (3.16 $\cdot 10^{-10}$ m/s) is applied to the top grid layer using the "recharge package" (Paragraph 3.4.2.3). The effect of plant transpiration and direct evaporation in removing water from the saturated groundwater zone is simulated with the "evapotranspiration" package. Evapotranspiration values are adjusted during the calibration phase with a maximum of 3,000 mm/a, which is the value of the potential evaporation in Ouarzazate (Piche and Bac method, Paragraph 2.3). An evapotranspiration extinction depth of 2 m is assigned.

9.2.4 Wadis and Rivers

Wadis with constant flow

The recharge of the alluvial aquifers occurs mainly through the wadis draining the High Atlas. Only the Ouarzazate, Dades and M'Goun Wadis present almost continual flow. The "River package" (Paragraph 3.4.2.3) is used to simulate the flow between the aquifer and the surface water for these wadis.

Wadis with rare surface flow

The "River package" is not suitable to simulate wadis with rare surface flow. Nevertheless, the role of those Wadis for the recharge of the alluvial aquifer is of primordial importance due to the existence of subsurface flow within the riverbed. In order to estimate the contribution of this groundwater recharge, three approaches were chosen to simulate the flow between the aquifer and those wadis: "constant head cells", the "River package" and the "Well package".

The "constant head cells" are used to simulate 6 small Wadis from the High Atlas and 1 from the Jbel Saghro (Fig. 9.1-A). To simulate the recharge of the alluvial aquifer between Toundoute and Skoura two models are tested. The first model (Model 1) uses a combination of "constant head cells" and "River package" (Fig. 9.5-A). The second model (Model 2) applying the "Well package" simulates the recharge at Toundoute with 26 injection wells (Fig. 9.5-B).

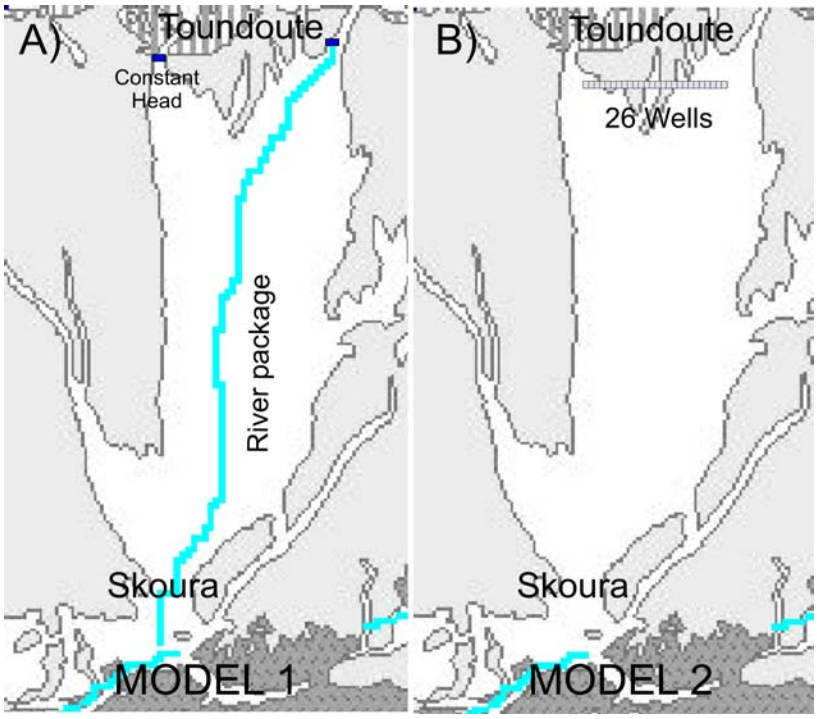

Fig. 9.5: Two approaches are tested to simulate the recharge by the wadi with rare surface flow of the alluvial aquifer between Toundoute and Skoura using the River package (A) and the Well package (B).

9.2.5 Major model assumptions

An overview of the various geological and hydrogeological assumptions for the model is presented in Table 9.2. The model is build up by two layers. Layer 1 represents the heterogeneous alluvial aquifer which is mainly recharged by the Wadis. Layer 2 represents the Mio-Pliocene formations considered as being homogeneous, with a constant thickness and very low permeability.

Tab. 9.2: Major model assumptions (K_H = horizontal permeability, K_V = vertical permeability).

Layer	Geological assumptions		Hydrogeological assumptions	
Layer 1: Alluvial aquifer unconfined	Heterogeneous porous medium	Thickness between 5 to 50 m	Recharge mainly by wadis Lateral groundwater recharge at the boundary is negligible Recharge by precipitation = 10 mm/a	Varying hydraulic conductivity (silt, sand, gravel, coarse conglomerates with clayey matrix): $K_H = 10^{-4}$ to 10^{-6} m/s $K_V = 10^{-5}$ to 10^{-7} m/s
Layer 2: Mio-Pliocene Unconfined-Confined (constant transmissivity)	Homogeneous porous medium	Constant thickness of 40 m	Leakage from the Alluvial aquifer is negligible	Very low hydraulic conductivity (considered as aquitard of the alluvial aquifer) $K_H = 10^{-8}$ m/s $K_V = 10^{-9}$ m/s

9.3 Results

The results of modelling are presented for steady state conditions for the two models. While Model 1 uses the combination "constant head cell" and "River package" to simulate the recharge between Toundoute and Skoura, the Model 2 uses the "Well package".

Based on several runs of both models, the value of evapotranspiration is adjusted in order to acquire a water budget in steady state close to zero. A real evapotranspiration rate of $1 \cdot 10^{-8}$ m/s equivalent to 316 mm/a is defined. This value is then fixed to the entire model domain.

Model 1

Hence Model 1 uses the River package to simulate the recharge by the wadi between Toundoute and Skoura (Fig. 9.5-A), a realistic value of the riverbed hydraulic conductance (C_{RIV}) has to be given. C_{RIV} strongly depends on the effective hydraulic conductivities of the river bed (K_{RIV}) (Paragraph 3.4.2.3; Eq. 42). C_{RIV} is calculated for a length of the river within a cell equal to 250 m, a width of the river equal to 50 m and a thickness of the riverbed equal to 2 m. The effective hydraulic conductivities of the riverbed (K_{RIV}) are classified according to the material characteristics (USDA NRCS, 1993) (Tab. 9.3). This classification ranges between very high loss rate (gravel and large sand) to low loss rate (consolidated bed material with high silt-clay content). Based on this classification, the respective K_{RIV} are chosen for the simulations (Tab. 9.4) and the C_{RIV} values are calculated ranging between $1.6 \cdot 10^{-4}$ m/s and $1.6 \cdot 10^{-7}$ m/s.

Tab. 9.3: Effective hydraulic conductivity (K_{RIV}) versus bed material characteristics (USDA NRCS 1993).

Category	Description	Bed material characteristics	Effective hydraulic conductivity (K_{RIV})
1	Very high loss rate	Very clean gravel and large sand	Greater than $3.53 \cdot 10^{-5}$
2	High loss rate	Clean sand and gravel	$1.41 \cdot 10^{-5}$ to $3.53 \cdot 10^{-5}$
3	Moderately high loss rate	Sand and gravel mixture with low silt-clay content	$7.06 \cdot 10^{-6}$ to $2.12 \cdot 10^{-5}$
4	Moderate loss rate	Sand and gravel mixture with high silt-clay content	$1.76 \cdot 10^{-6}$ to $7.06 \cdot 10^{-6}$
5	low to insignificant loss rate	Consolidated bed material with high silt-clay content	Below $1.76 \cdot 10^{-6}$

From the 6 simulations with the various C_{RIV} values (Tab. 9.4), the simulations 1 ($C_{RIV} = 1$) and 3 ($C_{RIV} = 0.05$) show very high discrepancy in regard to the water budget (Tab. 9.5), respectively

- 28.71 % and -12.06 %. Thus, they are excluded. The simulations 2 (C_{RIV} = 0.1), 4 (C_{RIV} = 0.02), 5 (C_{RIV} = 0.01) and 6 (C_{RIV} = 0.001) show low discrepancies in regard to the water budget. Although simulation 6 (C_{RIV}= 0.001) shows no discrepancy (0.00 %), this simulation have to be excluded because the calculated groundwater level does not reflect the reality (Figure 9.6). In fact, this simulation displays a dry aquifer between Toundoute and Skoura. Consequently, the simulations 2, 4 and 5 appear to be the most accurate simulations.

Tab. 9.4: Simulations with various C_{RIV} values calculated from various K_{RIV} (each river is represented within a cell with a length of 250 m, a width of 50 m and thickness of the riverbed of 2 m). The categories refer to the Tab. 9.3.

Simulation	Category	K_{RIV} (m/s)	C_{RIV} (m^2/s)
1	1	$1.6 \cdot 10^{-4}$	1
2	2	$1.6 \cdot 10^{-5}$	0.1
3	3	$8 \cdot 10^{-6}$	0.05
4	4	$3.2 \cdot 10^{-6}$	0.02
5	5	$1.6 \cdot 10^{-6}$	0.01
6	5	$1.6 \cdot 10^{-7}$	0.001

Tab. 9.5: Model 1: water budget of the whole model domain for 6 simulations taking into account various C_{RIV} values: flows are positive if they are entering the system.

Simulation	1	2	3	4	5	6
Conductance	C_{RIV} = 1 K = $1.6 \cdot 10^{-4}$ m/s Class 1	C_{RIV} = 0.1 K = $1.6 \cdot 10^{-5}$ m/s Class 2	C_{RIV} = 0.05 K = $8 \cdot 10^{-6}$ m/s Class 3	C_{RIV} = 0.02 K = $3.2 \cdot 10^{-6}$ m/s Class 4	C_{RIV} = 0.01 K = $1.6 \cdot 10^{-6}$ m/s Class 5	C_{RIV} = 0.001 K = $1.6 \cdot 10^{-7}$m/s Class 5
Constant Head (10^6 m^3/a)	3.55	3.56	3.50	3.56	3.56	3.46
Drains (10^6 m^3/a)	-0.15	-0.06	-0.19	-0.23	-0.20	0
Recharge (10^6 m^3/a)	4.59	4.92	4.90	4.86	4.81	2.35
Evapotranspiration (10^6 m^3/a)	-37.49	-38.63	-40.12	-36.05	-32.16	-15.95
River leakage (10^6 m^3/a)	-48.95	30.23	7.42	27.79	23.98	10.14
Water budget (10^6 m^3/a)	-78 .4574	0.0143	-24.4945	-0.0785	-0.0097	0.0001
Discrepancy	-28.71 %	0.01 %	-12.06 %	-0.06 %	-0.01 %	0.00 %

The total recharge of the alluvial aquifer system is the sum of recharge by precipitation and recharge by leakage from the wadis (riverbed infiltration). The recharge by precipitation is simulated with the “recharge package” while the recharge from the wadis is simulated with “constant head cells” and the “river package”. In regard to the “river leakage”, “IN” flow can be considered as the total riverbed infiltration (leakage from the wadis into the aquifer), while “OUT” flow is the total drainage of the aquifer by the wadis. Consequently, the effective recharge of the alluvial aquifers by the Wadis is the difference between the total riverbed infiltration and the total drainage of the aquifer by the wadis (“IN”-“OUT”: “river leakage”) (Tab. 9.6).

Tab. 9.6: Model 1: components of the recharge in m^3/a over the whole model domain for the simulations 2, 4 and 5; flows are considered "IN" if they are entering the groundwater system.

Simulation	2 : C_{RIV} = 0.1 (10^6 m^3/a)			4 : C_{RIV} = 0.02 (10^6 m^3/a)			5 : C_{RIV} = 0.01 (10^6 m^3/a)		
	IN	OUT	IN-OUT	IN	OUT	IN-OUT	IN	OUT	IN-OUT
Recharge (precipitation)	4.92	0.00	4.92	4.86	0.00	4.86	4.81	0.00	4.81
Constant head (Wadi)	3.63	0.07	3.56	3.63	0.07	3.56	3.63	0.07	3.56
River leakage (Wadi)	209.29	179.06	30.23	126.59	98.80	27.79	84.65	60.68	23.98
water budget discrepancy			0.01 %			0.06 %			0.01 %

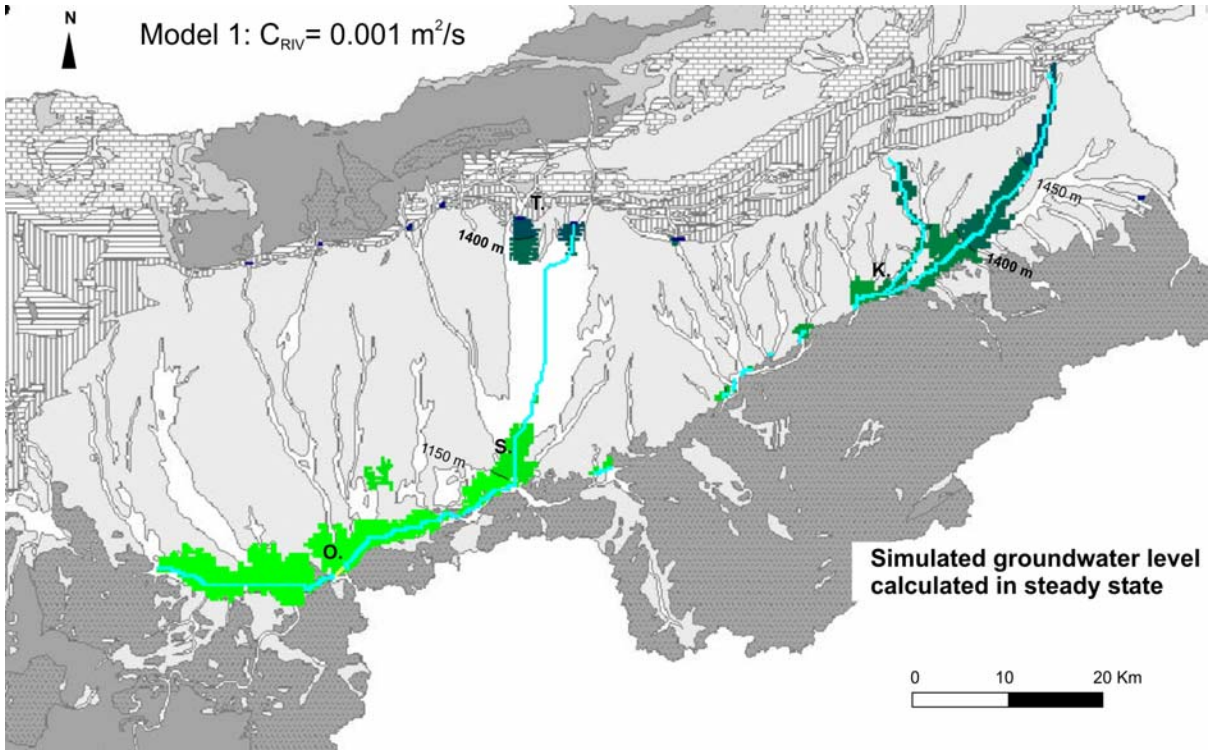

Fig. 9.6: Model 1: groundwater level calculated from the simulation 6 taking into account C_{RIV}=0.001 m^2/s (steady state); O. = Ouarzazate, S. = Skoura, T. = Toundoute and K. = Kelaa M'Gouna.

The simulation 2 seems to overestimate the total riverbed infiltration (209.29 $\cdot 10^6$ m^3/a) and the total drainage of the wadis (179.06 $\cdot 10^6$ m^3/a) in comparison to the discharge of wadis monitored at Mansour Eddahbi reservoir (378.00 $\cdot 10^6$ m^3/a: compare Tab. 2.1). The simulation 5 appears to be the most accurate (discrepancy = 0.01%) and the most realistic in respect to the recharge from the Wadis over the whole Basin of Ouarzazate (total riverbed infiltration = 84.65 $\cdot 10^6$ m^3/a and total wadis drainage = 60.68 $\cdot 10^6$ m^3/a). Therefore, only the simulation 5 is further considered for the model 1. The simulation 5 corresponds to a value of C_{RIV} = 0.01 m^2/s associated with a value of K_{RIV} = 1.6 $\cdot 10^{-6}$ m/s. This value of K_{RIV} corresponds to a "low loss rate" of the riverbed (Tab. 9.3). This low value of K_{RIV} can be explained by the high mud content of the surface-water during floods, the mud filling in pores and interstices of the coarse riverbed material after a flood event.

Simulation 5 (C_{RIV}= 0.01) proves a clear spatial separation of the shallow aquifer in three main alluvial aquifer systems: the aquifer of Ouarzazate (115 km^2), an aquifer extending between Toundoute and Skoura (236 km^2) and one along the Dades and the M'Goun Wadis (131 km^2) (Fig. 9.7). At a regional scale, the piezometric level calculated for these alluvial aquifers is in accordance to the measured data (compare Fig. 8.4) although some errors exist with the

presence of water above the ground level. These errors are partly due to the accuracy of the Digital Elevation Model (vertical resolution = +/- 15 m) and to the lack of precise data about aquifer proprieties. Although some wells in the north-western part of the model domain prove the presence of an aquifer (compare Fig. 8.4), the simulation results in dry cells. These wells are located in a network of wadis connected to local superficial aquifers, which cannot be represented in the given model scale.

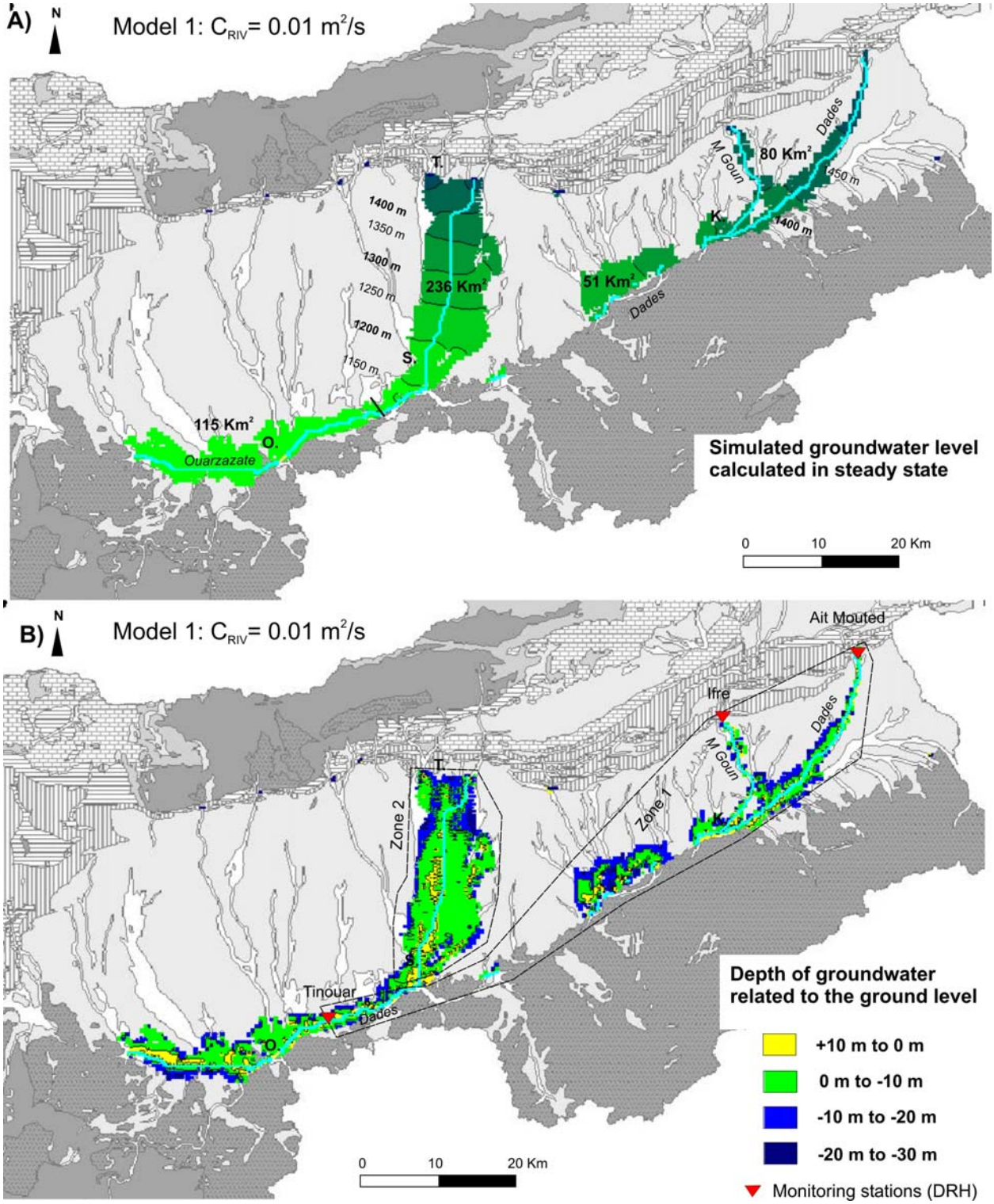

Fig. 9.7: **Model 1: results of the simulation with C_{RIV} = 0.01 m²/s (steady state); groundwater level and areas of the various alluvial aquifers (A) and depth of groundwater related to the ground level (B). Two zones are defined for the water budget (see Tab. 9.7); O. = Ouarzazate, S. = Skoura, T. = Toundoute and K. = Kelaa M'Gouna.**

It has to be noted that due to a problem of calculation, MODFLOW is unable to simulate the recharge by precipitation ("recharge package") for dry cells. Consequently, the recharge by precipitation is only applied to areas where an aquifer exists. But this error is negligible if we consider that the precipitation in the Basin of Ouarzazate is very low (≈ 100 mm/a) and that the areas with none aquifer (dry cells) correspond generally to zones with clayey soils. The infiltration in those areas is consequently very low and the runoff predominant.

The calculated recharge by precipitation resulting of the simulation 5 is equal to 4.81 $\cdot 10^6$ m^3/a (10 mm/a) (Tab. 9.6) respectively a recharge area of 481 km^2. This area is in good accordance to the total area of the alluvial aquifers calculated with ArcView (482 km^2) (Fig. 9.7-A).

Taking into account the whole Basin of Ouarzazate, the effective recharge of the alluvial aquifers by the wadis equals 27.54 $\cdot 10^6$ m^3/a (Tab. 9.6: constant head = 3.56 $\cdot 10^6$ m^3/a + river leakage = 23.98 $\cdot 10^6$ m^3/a). Consequently, as a result of the simulation 5, 15 % of the recharge of the alluvial aquifers at the scale of the Basin of Ouarzazate occurs by infiltration of precipitation, while 85 % by riverbed infiltration.

Two sub-regions are defined (Fig. 9.7-B), where the water budget is calculated for the simulation 5 (Tab. 9.7). Zone 1 includes the M'Goun and Dades Wadis from the northern range to the centre of the basin. Zone 2 considers the area between Toundoute and Skoura.

Tab. 9.7: Model 1: Water budget of the zone 1 and zone 2 (see Fig. 9.7 for location) for the simulation 5 (C_{RIV} = 0.01 m^2/s); flows are considered "IN" if they are entering the groundwater system.

Water budget of Zone 1 (Layer 1)	**IN (10^6 m^3/a)**	**OUT (10^6 m^3/a)**	**IN-OUT (10^6 m^3/a)**
Horizontal exchange	0.274	0.159	0.116
Exchange with Layer 2	0.027	0.023	0.004
Recharge	1.589	0.000	1.589
Evapotranspiration	0.000	11.983	-11.983
River leakage	**48.210**	**37.940**	**10.270**
Sum of zone 1	50.100	50.105	-0.005
Discrepancy of zone 1			-0.01 %
Water budget of Zone 2 (Layer 1)	**IN (10^6 m^3/a)**	**OUT (10^6 m^3/a)**	**IN-OUT (10^6 m^3/a)**
Constant head	3.427	0.000	3.427
Horizontal exchange	0.037	0.828	-0.791
Exchange with Layer 2	0.017	0.017	0.000
Recharge	2.084	0.000	2.084
Evapotranspiration	0.000	10.006	-10.006
River leakage	17.873	12.589	5.284
Sum of zone 2	23.438	23.440	-0.002
Discrepancy of zone 2			-0.01 %
Sum of the whole model domain	93.090	93.100	-0.010
Discrepancy of the whole model domain			-0.01 %

For zone 1, discharge values of the wadis are available from three DRH stations with mean values from 116 $\cdot 10^6$ m^3/a (Ait Mouted) over 136 $\cdot 10^6$ m^3/a (Ifre) to 243 $\cdot 10^6$ m^3/a (Tinouar). The comparison between the upstream (Ait Mouted and Ifre) and the downstream discharges (Tinouar) reveals a loss of water around 9 $\cdot 10^6$ m^3/a. This loss of water corresponds to the recharge of the aquifer, the irrigation and the evaporation effect. The water budget in zone 1 of the simulation 5 (Tab. 9.7) shows that the total riverbed infiltration recharging the aquifer system is equal to 48.2 $\cdot 10^6$ m^3/a ("IN" flow: "river leakage"), while the total drainage of the aquifer

equals 37.9 $\cdot 10^6$ m^3/a ("OUT" flow: "river leakage"). Thus, the total leakage represents almost 20% of the discharge monitored at Tinouar, while the total drainage represents approximately 16 %. The effective recharge of the alluvial aquifers from the Dades and M'Goun Wadis ("IN"-"OUT": "river leakage") in zone 1 is equal to 10.3 $\cdot 10^6$ m^3/a (Tab. 9.7). This value is in the same order than the loss of water observed for the M'Goun and Dades Wadis at the respective monitoring stations (9 $\cdot 10^6$ m^3/a).

In zone 2 the calculated total riverbed infiltration is about 17.87 $\cdot 10^6$ m^3/a and the "constant head cells" infiltrate 3.43 $\cdot 10^6$ m^3/a of water into the aquifer (Tab. 9.7). Consequently, it is estimated with model 1 (simulation 5) that a total of 21.3 $\cdot 10^6$ m^3/a of water enters the aquifer between Toundoute and Skoura by infiltration from the wadis.

Model 2

The second model uses the "Well package" to simulate the recharge from the wadi at Toundoute. Based on the results of the Model 1, a conductance (C_{RIV}) of the river equal to 0.01 m^2/s is applied to simulate the M'Goun and Dades Wadis. The Wadi at Toundoute shows rare surface flow, although subsurface flow recharging the aquifer exists. The catchment area in the High Atlas of this Wadi (up to Toundoute) is estimated with ArcView equal to 450 km^2. The specific discharges of the wadis ($Q_{specific}$) prevailing in the High Atlas range between 76 $\cdot 10^3$ $m^3/a/km^2$ (Dades at Ait Moutade) and 110 $\cdot 10^3$ $m^3/a/km^2$ (M'Goun at Ifre) (compare Tab. 2.1). Therefore, a maximum discharge (surface and sub-surface flows) of the wadi at Toundoute should be between 34.2 $\cdot 10^6$ m^3/a and 49.5 $\cdot 10^6$ m^3/a. These values are also considered as the maximum recharge of the aquifer at Toundoute, and then as the maximum recharge rate which should be simulated in form of injection wells.

Various values of the total rate injected in the wells (Q_W) are tested (Tab. 9.8 and Fig. 9.8). The discrepancies in regard to the water budget of these simulations are acceptable with values between -0.01% and -0.03% (Tab. 9.8). Simulation 2 and 3 with Q_W equal to 21.20 $\cdot 10^6$ m^3/a and 32.90 $\cdot 10^6$ m^3/a present considerable errors in the area of Toundoute with groundwater levels largely above the ground surface (Fig. 8-B and C). In this case, the evapotranspiration will be largely overestimated (Tab. 9.8). Simulation 1 with Q_W equal to 8.22 $\cdot 10^6$ m^3/a is more accurate (Fig. 8-A).

Tab. 9.8: Model 2: water budget resulting of simulations with various total discharge rate of the injection wells (Q_W): 8.22 $\cdot 10^6$ m^3/a, 21.20 $\cdot 10^6$ m^3/a and 32.90 $\cdot 10^6$ m^3/a.

Simulation	1	2	3
Q_W (10^6 m^3/s)	8.22	21.20	32.90
Constant head (10^6 m^3/s)	0.130	0.130	0.130
Recharge (10^6 m^3/s)	4.18	4.32	4.33
Evapotranspiration (10^6 m^3/s)	-29.13	-42.23	-53.93
River leakage (10^6 m^3/s)	16.58	16.58	16.58
Water budget (10^6 m^3/s)	-0.018	-0.008	-0.008
Discrepancy (%)	-0.03	-0.01	-0.01

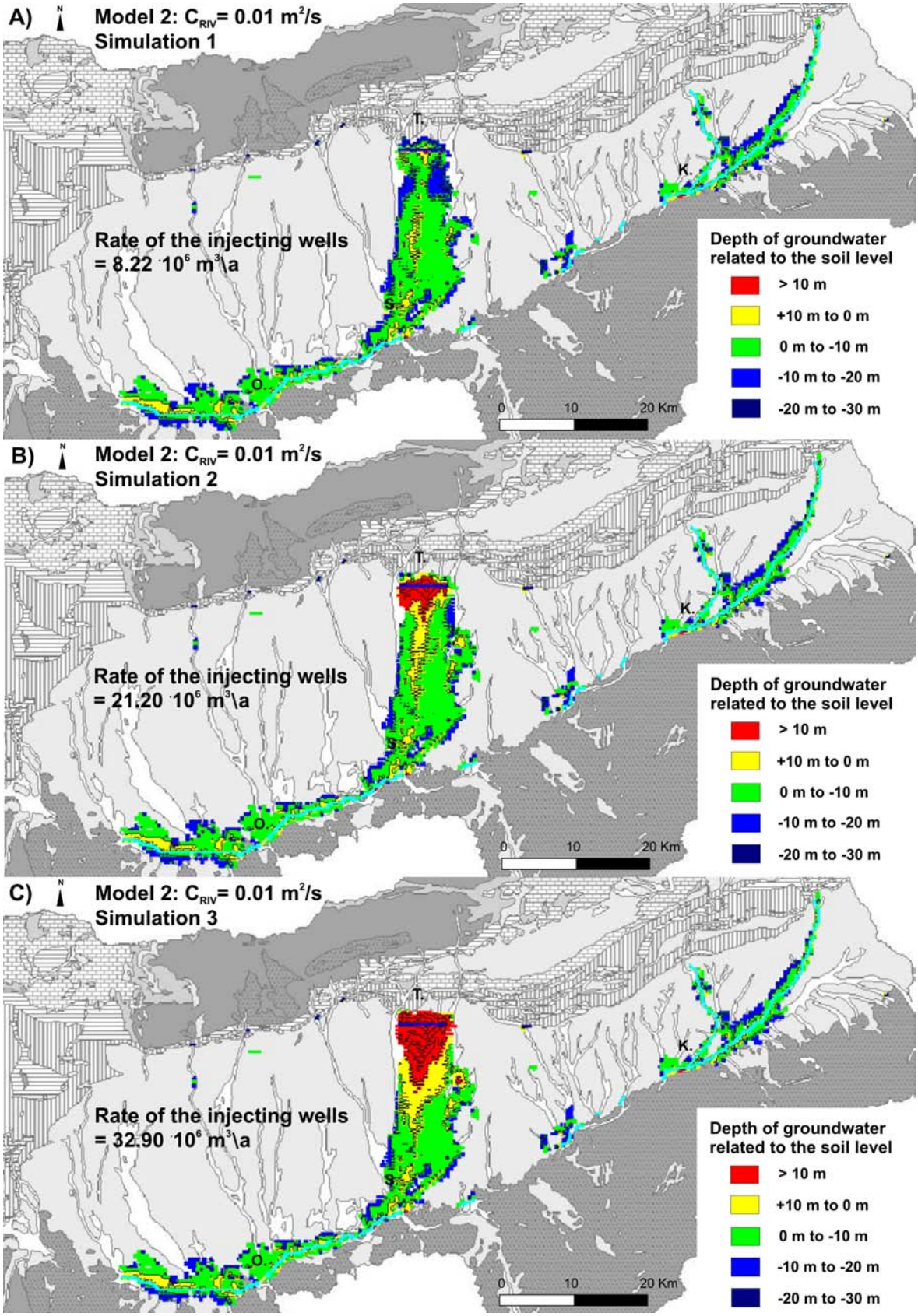

Fig. 9.8: **Model 2: depth of groundwater related to the ground level resulting of simulations with total discharge rate applied to the injection wells equal to 8.22 $\cdot 10^6$ m³/a (A), to 21.20 $\cdot 10^6$ m³/a (B) and to 32.90 $\cdot 10^6$ m³/a (C); O. = Ouarzazate, S. = Skoura, T. = Toundoute and K. = Kelaa M'Gouna.**

9.4 Conclusion of the modelling

The simulation of the alluvial aquifer system of the Basin of Ouarzazate was performed using the numerical groundwater model MODFLOW PMWIN5. Simulations in steady state conditions were carried out.

The Basin of Ouarzazate is considered as an independent hydrogeological unit due to the presence of low permeable rocks bordering the basin such as the Precambrian rocks of the Jbel Saghro and the Skoura Mole and the Southern Atlas Marginal Zone. Therefore, the lateral groundwater flows from the High Atlas and the Anti-Atlas towards the basin are negligible for the simulation. Moreover, due to the arid conditions prevailing in the Basin of Ouarzazate, the recharge of the alluvial aquifers by the precipitation is negligible in comparison to the recharge occurring through the leakage of the wadis superficially draining the surrounding mountains.

Wadis with constant flow and wadis with rare surface flow are differently simulated in the model. While for the wadis with constant flow the "River package" was applied, different approaches were chosen to simulate the wadis with rare surface flow: "constant head cells", the "River package" and the "Well package". Two models are compared for the simulation of the recharge of the alluvial aquifer between Toundoute and Skoura: the first using a combination of "constant head cells" and the "River package" (model 1) and the second using the "Well package" (model 2).

The recharge by precipitation is fixed to 10 mm/a. Taking into account the result of several simulations with the model 1 and 2, the evapotranspiration rate is adjusted and then fixed to 316 mm/a.

In order to attribute the most accurate value of the riverbed hydraulic conductance (C_{RIV}), 6 simulations with various values of C_{RIV} are tested with model 1. It appears that the simulation taking into account a C_{RIV} = 0.01 m^2/s is the more adequate. This value of C_{RIV} corresponds to an effective hydraulic conductivity of the riverbed (K_{RIV}) equal to 1.6 $\cdot 10^{-6}$ m/s. This low value of K_{RIV} can be explained by clays deposited within the river bed material after flood events. According to this simulation, the effective recharge of the alluvial aquifers by riverbed infiltration over the whole model domain represents 85 % of the total recharge, respectively 27.54 $\cdot 10^6$ m^3/a. These values show that the alluvial aquifers are mainly recharged by the wadis. The effective recharge of the alluvial aquifer by riverbed infiltration of the Dades and M'Goun Wadis (based on a water budget calculated for an area including the Ifre, Ait Moutade and Tinouar stations) is equal to 10.3 $\cdot 10^6$ m^3/a. This result is in accordance to the losses of these wadis measured at the DRH monitoring stations, which averages 9.0 $\cdot 10^6$ m^3/a.

Three simulations with various values of the total discharge rate of the injection well (Q_W) are tested with model 2. It appears that the use of the "well package" creates huge error in the zone of injection. The simulation, taking into account a discharge rate of the injecting wells equal to 8.22 $\cdot 10^6$ m^3/a, is the more realistic.

Simulations for both models describe well the three main alluvial aquifers of Ouarzazate (115 km^2), Toundoute-Skoura (236 km^2) and Dades-M'Goun (131 km^2). At the scale of the basin, simulations are in accordance with the reality although some errors exist with groundwater levels above surface level. These errors are mainly due to the lack of precise data and to the accuracy of the digital elevation model. Also, local and very superficial aquifers located in the

north-western part of the basin along wadis from the north could not be simulated at the basin scale.

This study proposes different approaches to simulate the alluvial aquifer system of the Basin of Ouarzazate where the recharge depends strongly on wadis with no constant flow. First simulations in steady state are tested. In order to improve the models and to simulate the alluvial aquifer system in unsteady state, several recommendations can be suggested. In fact, it appears to be necessary to:

- Create three independent models in order to simulate separately each alluvial aquifer at a local scale and in this way to avoid computing problems due to the presence of dry cells in the model domain.
- Organise more field work in order to map details in the limits of the alluvial aquifers and to draw a precise permeability map based on pumping tests.
- Install a monitoring network measuring continuously the groundwater level within the alluvial aquifer which can be used for calibration and validation phases.
- Estimate more accurately the evapotranspiration rate.
- Estimate the pumping rate of groundwater for the irrigation use.

10 HYDROGEOLOGICAL RESULTS AND IMPLICATION IN IMPETUS INVESTIGATION

10.1 Sustainability in water resources management

The growing population and the development of sectors such as agriculture, industry and tourism increase the needs for water, which represents a considerable pressure on water resources in arid and semi-arid areas. Consequently, a water resource can be considered as sustainable for the development of a region (MARGANE, 2003):

- *If water for human beings and the environment is provided in sufficient amount and quality.*
- *If water resources are allocated in such a way that no negative long-term effects for the society, the economy and the environment occur.*
- *If the emission of hazardous substances into the environment is minimized.*
- *And if the water resources are protected against pollution.*

Groundwater is an important factor in the water resource management due to its availability even in areas with scarce or even none surface water. Additionally, groundwater resources are less dependent on seasonal climatic changes, particularly in arid area. Therefore, the sustainability of the groundwater needs to be estimated. In order to assess the groundwater resources the following steps are needed (MARGANE, 2003):

- *Determination of extent, thickness and saturation limits of aquifers and aquitards in the groundwater system.*
- *Determination of hydraulic properties and characterization of groundwater flow.*
- *Assessment of the groundwater quality.*
- *Identification of groundwater exploitation potentials (accessibility and renewability).*

Additional steps such as the groundwater vulnerability to pollution and/or the assessment of socio-economic factors influencing water management policies have to be taken into account too.

This study has focused on the mains steps such as the assessments of physical information (geology, determination of extensions and boundaries of aquifers, set up of average hydraulic conductivity maps etc.), hydrological information (water budgets, location of recharge areas, variability of piezometric head, estimation of the groundwater age at selected locations in the aquifers, stream-groundwater relations etc.) and chemical information (geochemical characteristics, spatial distribution of water quality in aquifers, temporal changes in water quality particularly for potentially vulnerable unconfined aquifers, stream flow quality etc.).

10.2 Groundwater resources of the Upper Drâa catchment

Investigations focused on the groundwater system of the Upper Drâa catchment (15,200 km^2), which corresponds to the northern part of the basin until the Mansour Eddahbi reservoir. With the integration of hydrogeological, hydrophysical and hydrochemical methods (water balances, hydrochemistry, stable isotope, ^{14}C and ^{3}H analyses as well as the groundwater flow model), this work attempts to give specific insights into the hydrogeology of the Upper Drâa catchment.

10.2.1 Main features of the aquifer systems

The aquifer system of the Upper Drâa catchment is divided in three main hydrogeological units: the Anti-Atlas Mountains, the High Atlas Mountains and the Basin of Ouarzazate (Fig. 10.1).

Anti-Atlas

The Anti-Atlas domain shows poor groundwater storage capacity mainly developed in very limited alluvial aquifer overlaying the low permeable formations of the Precambrian basement.

High Atlas

The folded and thrusted Liassic limestone unit of the High Atlas, covering 20 % of the Upper Drâa catchment, represents clearly the main aquifer system of the region in regard to its aquifer qualities, its volume and its recharge. In order to identify the main characteristics of this aquifer system, investigations focused at different scales on two catchments: the Assif-n'Ait-Ahmed catchment (110 km^2) and the Ifre catchment (1,240 km^2) (Fig. 10.1). The Liassic limestones and dolomites of the Toundoute Nappe cover 60 % of the Assif-n'Ait-Ahmed catchment. The 400 m thick formations show karstic features such as dolines and poljes and represent the main aquifer of the Assif-n'Ait-Ahmed catchment with a potential groundwater volume ranging from 0.19 km^3 to 0.38 km^3. Triassic formations (basalt and clays), underlying the Liassic formations, act as aquitard of the Liassic aquifer.

Almost 50% of the Ifre catchment is covered by the Liassic aquifer (305 km^2 of massive limestones and dolomites of the Lotharagian and 300 km^2 of limestones alternating with marls of Domerian). Based on its geological framework, hydrogeochemistry of the groundwater and on a precise water-head map, two types of aquifers are revealed: the Liassic aquifer of the Toundoute Nappe and the overlaying alluvial aquifer developed within the Quaternary-Mio-Pliocene formations of the Ait Kandoula Basin (Fig. 10.1-A). The alluvial aquifer of the Ait Kandoula Basin is shallow and mainly recharged by the riverbed infiltration of the Wadis. Additionally, a significant part of the recharge originates from the Liassic carbonates.

Basin of Ouarzazate

In the tertiary infilling of the Basin of Ouarzazate, various aquifers can be distinguished:

- Shallow aquifers developed in Quaternary alluvium and in reworked Mio-Pliocene deposits.
- And semi-deep or deep aquifers of the Mio-Pliocene, Eocene and Cretaceous formations.

The alluvial aquifers provide the first groundwater resources for irrigation or domestic uses. These superficial aquifers are regionally divided into the alluvial aquifer of Ouarzazate, the alluvial aquifer between Toundoute and Skoura and the alluvial aquifer stretching along the M'Goun and the Dades Wadis in northeast of the basin (Fig. 10.1). The water-head map shows a general groundwater flow direction from the northern range of the Basin of Ouarzazate to the south-west, revealing an active recharge of the alluvial aquifers from the High Atlas Mountains. The alluvial aquifers are developed in alluvium deposits (sand, gravel, pebble and conglomerates) with a thickness varying between few meters to 30 m and overlaying either the clayey formations of the Miocene or the marls of Senonian (Tikirt area).

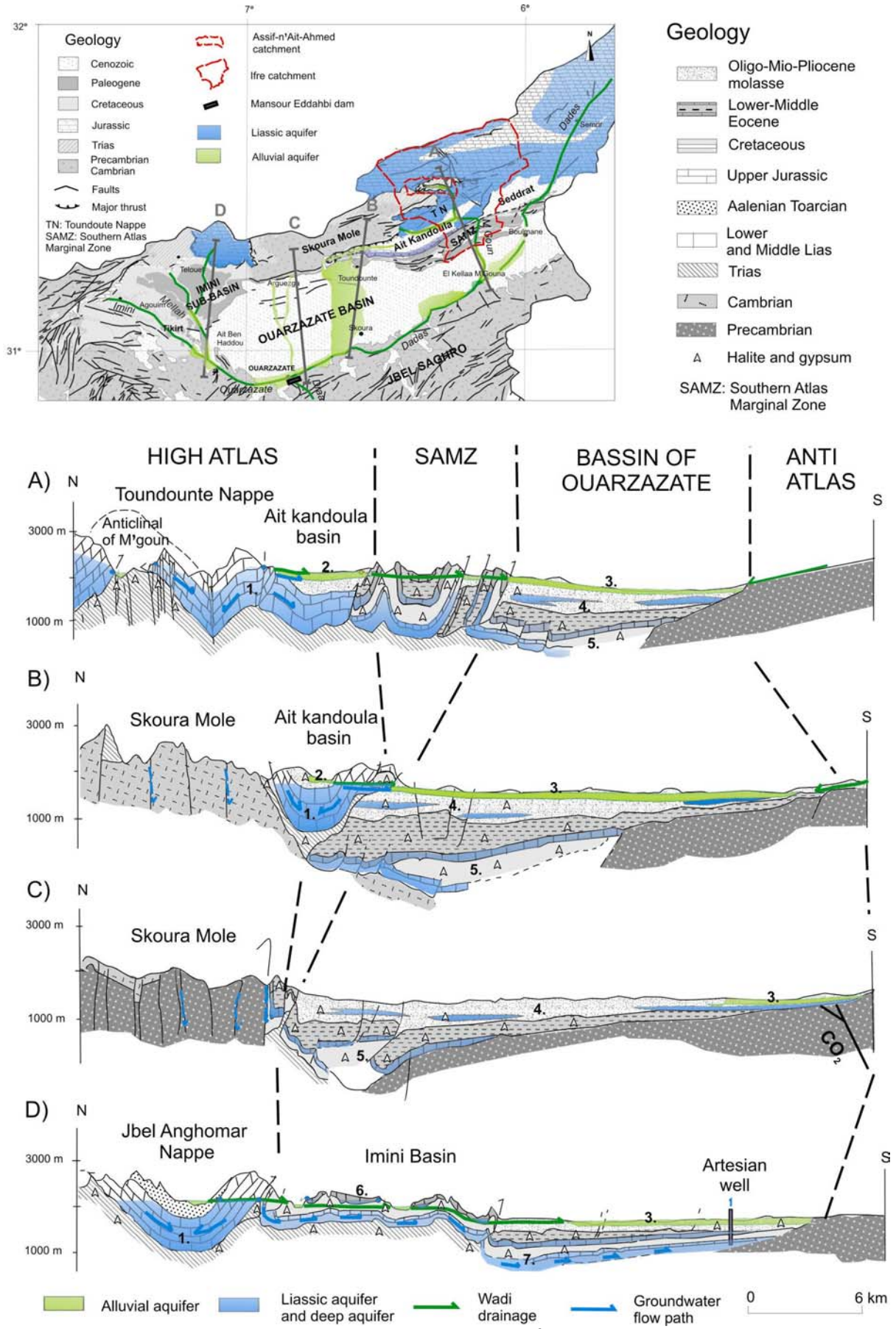

Fig. 10.1: Conceptual hydrogeological model of the Upper Drâa catchment; 1. Liassic aquifers, 2. alluvial aquifer of the Ait Kandoula Nappe, 3. alluvial aquifer of the Basin of Ouarzazate, 4. multi layer aquifer of Mio-Pliocene, 5. deep aquifers of Lower Eocene and Cenomanian-Turonian, 6. perched aquifer of Eocene and 7. confined aquifer of Infracenomanian. (geological profiles modified after JOSSEN & FILALI, 1988)

The Mio-Pliocene sediments were deposited in a pro-grading alluvial fan system, thus a multi-layer aquifer is developed today. The sediments are often clayey, which excludes good aquifer qualities. But local semi-deep aquifers in sand and conglomerates are observed at some boreholes. For instance, a thickness of almost 50 m of sand is described between Ouarzazate and Skoura. Limits of these aquifers are not known but their recharges are obviously not efficient, although some hydraulic connections to the alluvial aquifers are possible.

In the Basin of Ouarzazate, the carbonates, sandstones and conglomerates of the Lower Eocene and Cretaceous (Infracenomanian- Cenomanian-Turonian) may constitute some deep aquifers (Fig. 10.1), but due to the depth of those aquifers and to the obviously low productivity by lack of active recharge, these aquifers do not represent exploitable groundwater resources.

The Eocene carbonates (20 to 30 m of thickness) crop out in the Imini sub-basin of the Basin of Ouarzazate (Fig. 10.1-D). Some small perched aquifers, drained by boundary springs, are developed in those formations. In the same area, clays and marls of Senonian act as an aquitard between the overlaying perched Eocene aquifers and a confined aquifer (50 m of thickness) developed in conglomerates, sandstones and sand of the Infracenomanian and in carbonates of the Cenomanian-Turonian. The groundwater of the confined aquifer flows from the north to the south, where artesian wells are observed.

10.2.2 Hydrogeochemical characterization

Groundwater

The groundwater in the Upper Drâa catchment is strongly affected by high mineralization due to the leaching of evaporitic minerals naturally present in various formations (Trias, Cretaceous, Eocene and Mio-Pliocene).

In the Anti Atlas, the groundwater is of Ca-Mg-Na-HCO_3-SO_4 type with observed electric conductivity (EC) varying between 800 µs/cm and 2,200 µs/cm.

In the High Atlas, some springs draining the Liassic carbonates show groundwater of Ca-Mg-HCO_3 type with low conductivities between 150 µS/cm and 300 µS/cm. These springs are used by the population as drinking water supply. At the contact of the Triassic formations (aquitard), the carbonated groundwater evolves rapidly to Ca-SO_4-Mg or Na-Ca-Cl-SO_4 types due to the leaching of gypsum and halite. The leaching of evaporitic minerals increases considerably the mineralization of the groundwater, as observed at some springs in Ifre catchment with high conductivities up to 5,500 µS/cm.

The quality of the groundwater varies broadly within the Basin of Ouarzazate. While relative low mineralised groundwater (EC about 500 µS/cm) prevails in the eastern part of the basin, saline groundwater is observed at Ouarzazate town (EC up to 7,000 µS/cm). Regionally, rapid changes of the groundwater types are observed throughout the basin, which is difficult to link to the general flow direction. The groundwater chemistry in the Basin of Ouarzazate shows no correlation with the changes of the groundwater level and no clear seasonal variations during the period of investigation (2001 to 2005). The hydrochemical characteristic of groundwater mainly depends on the degree of hydraulic connection to the Wadis.

The confined aquifer of Infracenomanian shows high spatial differences in regard to the chemistry. Two artesian wells in a distance of 10 km have been investigated in the Tikirt area.

While one well (166art) represents a Ca-Mg-Na-HCO_3-Cl water type with a mean conductivity of 1,100 µS/cm, the other (167art) is a Ca-Mg-SO_4 water type with a significant higher mean conductivity of 2,600 µS/cm. Thus the first one is used for drinking water supply by some NGOs and the second one is unfit for the human consumption.

Surface water

A high spatial variation of the surface water chemistry is observed. The Dades River at the north-western range of the Basin of Ouarzazate shows the lowest mineralization with a mean conductivity of 700 µS/cm and a Ca-Mg-HCO_3 water type. Downstream nearby Ouarzazate, the mineralization of the Dades River increases (EC = 2,100 µS/cm) and the facies of water changes to Ca-Na-Mg-SO_4-Cl due to the drainage of the alluvial aquifer displaying more mineralised groundwater. In the western part of the Basin of Ouarzazate, the Mellah wadi has brackish water with a conductivity of 16,000 µS/cm, unfit for the human consumption. The facies of the Mellah Wadi water is of Na-Ca-Cl type due to the leaching of halite cropping out in the north-west of the catchment.

Saturation indexes

The Saturation Index (SI) of various minerals is calculated in order to characterise the chemical evolution of the groundwater. Although aquifers in Anti-Atlas are developed in magmatic and volcanic rocks, the groundwater is more saturated in regard to calcite ($SI_{calcite}$ = 0.32) and dolomite ($SI_{dolomite}$ = 0.52) than the carbonated aquifers of the High Atlas (Tab. 10.1). This characteristic reveals a relative long residence time of the groundwater in the Anti Atlas compared to the High Atlas, which is confirmed by a slightly over-saturation of quartz (SI_{quartz} = 0.27).

Tab. 10.1: Saturation Indexes of calcite, dolomite, gypsum and quartz observed in the Anti-Atlas, High Atlas and the Basin of Ouarzazate (extremes, mean and standard deviation (SD))

		Anti Atlas	High Atlas		Basin of Ouarzazate
		Jbel Sagrho 20 samples	Assif-n'Ait-Ahmed 156 samples	Ifre 60 samples	 277 samples
$SI_{calcite}$	min	-0.16	-0.35	-0.3	-0.58
	max	0.78	0.94	0.88	1.00
	mean	**0.32**	**0.19**	**0.29**	**0.40**
	SD	0.28	0.32	0.25	0.25
$SI_{dolomite}$	min	-0.43	-0.97	-1.23	-1.18
	max	1.39	2.31	1.22	1.82
	mean	**0.52**	**0.10**	**0.30**	**0.64**
	SD	0.54	0.62	0.55	0.50
SI_{gypsum}	min	-0.81	-3.41	-3.18	-2.43
	max	-1.77	-0.20	-1.04	-0.06
	mean	**-1.33**	**-1.91**	**-1.99**	**-0.95**
	SD	0.27	0.83	0.57	0.54
SI_{quartz}	min	-0.02	-0.76	-0.46	-0.51
	max	0.42	0.32	0.22	1.24
	mean	**0.27**	**-0.11**	**-0.06**	**0.24**
	SD	0.11	0.24	0.20	0.23

Aquifers of the Basin of Ouarzazate show more evolved groundwater with slightly over-saturation of calcite ($SI_{calcite}$ = 0.40), dolomite ($SI_{dolomite}$ = 0.64) and quartz (SI_{quartz} = 0.24). The

saturation of gypsum in the Basin of Ouarzazate (SI_{gypsum} = -0.95) exhibits the importance of gypsum leaching in regard to quality of the groundwater.

Characterization of the main hydrochemical processes

Some chemical processes occurring in the aquifers have been identified. A dedolomitization process associated with gypsum dissolution in the Assif-n'Ait-Ahmed catchment, which explains the observed correlation between Mg^{2+} and SO_4^{2-} in the groundwater of springs. The influences of CO_2 gas coming up along faults from the Precambrian rocks nearby Ouarzazate town (Fig. 10.1-C). The dissolution of CO_2 gas produces protons in the solution, which decreases the pH and increases the HCO_3^- concentration. This explains the anti-correlation between pH and HCO_3^- observed in some wells of the Basin of Ouarzazate. Moreover, the presence of CO_2 gas in groundwater increases the capacity of carbonate dissolution.

10.2.3 Recharge processes and origin of groundwater

The investigations of the northern Drâa Basin in the High Atlas and the Basin of Ouarzazate show complex recharge conditions due to the hydrogeological setting. The precipitation in the Upper Drâa catchment shows high spatial variability. In the Jbel Saghro, the precipitation with a mean of 160 mm/a (at the IMPETUS station of Bouskour for the years 2002 and 2003) proves that the Anti-Atlas is clearly under arid conditions. Contrarily, the High Atlas shows semi-arid conditions with precipitation reaching 900 mm/a above 2,500 m of altitude. The precipitation decreases significantly at the foothills of the High Atlas Mountains and reach only 107 mm/a at the Ouarzazate town. Consequently, the High Atlas Mountains represent the main recharge area of the Upper Drâa catchment.

Estimations of the water balance in the High Atlas in two different scales (110 km^2: Assif-n'Ait-Ahmed catchment and 1,240 km^2: Ifre catchment) reveal groundwater recharge rates between 4 % (Assif-n'-Ait Ahmed) and 11 % (Ifre) of the total precipitation. Due to scare available data, evapotranspiration is only roughly estimated either after TURC (1963) for the Assif-n'-Ait-Ahmed catchment or Jensen-Haise for the Ifre catchment (JENSEN & HAISE 1963). Thus the recharge rates given reflect only a general view, but clearly prove that the recharge of the Liassic carbonated aquifer is effective and that only a part of this recharge is drained by Wadis (base flow).

Role of the "Southern Atlas Marginal Zone"

The discharge of the Liassic aquifer of the High Atlas into the Basin of Ouarzazate is not well known. The "Southern Atlas Marginal Zone" (SAMZ), a compressional deformation zone, (Fig. 10.1) acts as a hydrogeological barrier between the aquifers of the High Atlas Mountains and the Basin of Ouarzazate. Therefore, the Wadis draining the High Atlas have a primordial role in the recharge processes of the aquifer system of the Basin of Ouarzazate.

Isotopic characterization of precipitation and groundwater

The origin of groundwater is assessed by natural labelling with stable isotopes ($\delta^{18}O$, $\delta^{2}H$). In order to understand the recharge processes, the isotopic signature of rainwater are defined based on series of rain water sampled at 10 meteorological IMPETUS stations between summer 2002 and autumn 2004. A Local Meteoric Water Line (LMWL) lying slightly above the

Global Meteoric Water Line (GMWL) with the following relationship was found (**$^2H = 8\ \delta^{18}O + 10.6$** ($R^2$=0.92)).

Seasonal variations of the isotopic composition of rain are observed. Compared to the humid season (October to April), an enrichment in the heavy isotopes during the dry season (May to September) is observed due to more recycled rainwater condensed at warmer temperatures. Additional "amount effects" characterised by clear depletion of heavy isotopes in the context of extreme rain events over the whole catchment are proved. Those rain events are important for the characterization of the local recharge by precipitation in the Basin of Ouarzazate.

Groundwater in the aquifers of the Anti-Atlas are clearly enriched in heavy isotopes ($\delta\ ^{18}O_{mean}$ = -6.5 ‰) due to strong evaporation effects (d-excess = 8.6) (Tab. 10.2). The groundwater of High Atlas's aquifers is relatively depleted in heavy isotopes (Assif-n'Ait-Ahmed: $\delta\ ^{18}O_{mean}$ = -9.1 ‰, d-excess = 12.8) plotting slightly above the Local Meteoric Water Line (d-excess = 10.6) due to the altitude effect. In the Basin of Ouarzazate, the alluvial aquifer systems show small evaporation effects (d-excess = 9.8). Hence, the high mineralization observed in the groundwater results only of the leaching of evaporitic minerals. In general, the groundwater of the alluvial aquifers in the Basin of Ouarzazate shows isotopic signatures ($\delta\ ^{18}O_{mean}$ = -8.2 ‰) close to the groundwater of the aquifers in High Atlas, which reveals an active recharge from those mountains.

Tab. 10.2: Statistical description of the stable isotopes (extremes, mean and standard deviation (SD)) observed in the Anti Atlas, High Atlas and the Basin of Ouarzazate.

		Anti Atlas	High Atlas		Basin of Ouarzazate
		Jbel Sagrho 20 samples	Assif-n'Ait-Ahmed 156 samples	Ifre 60 samples	262 samples
$\delta^{18}O$ [‰]	min	-7.3	-10.8	-9.9	- 9.7
	maxi	-5.5	-7.6	-6.6	-5.5
	mean	**-6.5**	**-9.1**	**-8.6**	**-8.2**
	SD	0.5	0.5	0.6	0.8
δ^2H [‰]	min	-49	-71	-66	-69
	max	-38	-53	-49	-37
	mean	**-43**	**-60**	**-58**	**-56**
	SD	4	3	2	5
d-excess	min	5.7	5.7	3.4	3
	max	11.8	16.6	16.0	14
	mean	**8.6**	**12.8**	**10.8**	**9.8**
	SD	1.6	1.8	2.8	2.1

Estimation of the mean altitude of the recharge area based on isotopic data

Based on weighted mean of rain $\delta^{18}O$, a local altitude gradient of 0.20 ‰ $\delta^{18}O$ per 100 m is calculated for the High Atlas. This gradient takes into account the isotopic characteristics of the snow which plays a primordial role in the recharge of groundwater in the High Atlas. The snow cover is relatively more depleted in heavy isotopes ($\delta^{18}O$ = -10.3 ‰, δ^2H = -70 ‰ and d-excess = 12.2) than the rainwater. Calculations based on the Digital Elevation Model compared with the isotopic composition of selected springs approve the local altitude gradient by finding a relationship of $\delta^{18}O$ = -0.002 · "altitude" - 3.0 (R^2 = 0.97). This method allows the estimation of the mean altitude of the recharge area with an error of +/- 50 m. While for the recharge area of the Assif-n'Ait-Ahmed a mean altitude between 2,650 m to 3,400 m prevails, which displays the

main outcropping area of the Liassic limestones, the recharge areas of the Ifre catchment's aquifers have mean altitudes between 2,200 m and 3,450 m. The estimated mean altitude of the groundwater recharge area of the alluvial aquifers in the Basin of Ouarzazate ranges between 2,400 m to 2,900 m. As the maximum elevation of the Basin of Ouarzazate is about 1,800 m the results clarify that there is no significant groundwater recharge within the basin. The recharge of the confined Infracenomanian aquifer is estimated between 2,500 m and 2,800 m, which localises the recharge area in the High Atlas. Differences in isotopic signatures between the artesian wells reveal some local infiltrations from the alluvial aquifer of the Imini Wadi.

Semi-deep aquifers in the Basin of Ouarzazate

Nearby Kelaa M'Gouna, a well (40) shows a particular hydrochemistry which may reveal a hydraulic connection with a local sandy semi-deep aquifer of the Mio-Pliocene formation (Fig. 10.1). The groundwater of this well shows relative low mineralised groundwater (mean EC = 1,100 µS/cm) of Na-Ca-Cl-SO_4 to Na-Ca-SO_4-Cl facies with particular low contents of Mg^{2+} (9.8 mg/l < Mg^{2+} < 18.0 mg/l). Thus excluding a long transit from the High Atlas where dolomites are prevailing. The groundwater is also slightly oversaturated in regard to the quartz (SI_{quartz} = 0.46), which proves the passage of groundwater within a silicate aquifer such as quartz sand, sandstones, quartzite or magmatic rocks with a relative high residence time. Moreover, the stable isotopic composition shows the highest depletion in heavy isotope observed in the whole Drâa catchment (mean: $\delta^{18}O$ = -9.4 ‰, $\delta^{2}H$ = -67 ‰ and d-excess= 8.0). The strong isotopic depletion can be explained by two assumptions:

- The recharge of this small aquifer occurs only through the local precipitation which is isotopically depleted due to the amount effect affecting the heavy rain events.
- No current effective recharge occurs and the isotopic composition of the groundwater reveals old groundwater.

Some other wells in the Basin of Ouarzazate also reveal the influence of a semi-deep aquifer due to elevated Na^+ and Cl^- content:

- Well 43 nearby Skoura: 1,318 mg/l < $[Na^+ + Cl^-]_{43}$ < 1739 mg/l.
- Well 37 nearby Ouarzazate: 2,533 mg/l < $[Na^+ + Cl^-]_{37}$ < 3157 mg/l.

At well 43, the over-saturation in regard to calcite ($SI_{calcite}$ = 0.63), dolomite ($SI_{dolomite}$ = 1.09) and quartz (SI_{quartz} = 0.40) reveals a relative high residence time. At well 37 the calcite and dolomite are in perfect equilibrium ($SI_{calcite}$ = 0.08 and $SI_{dolomite}$ = 0.03) due to the presence of CO_2 in groundwater. But the saturation of quartz at this well (SI_{quartz}=0.94) reveals the presence of long residence time groundwater. Contrarily to well 40, the isotopic composition of the wells 43 and 37 reveals a recharge from the High Atlas.

The exploitation of the semi-deep aquifers in the Basin of Ouarzazate is limited due to either the quality with the presence of saline groundwater or to the low recharge of these aquifers.

The perched aquifer of the Eocene aquifer

The perched aquifer of Eocene in Imini sub-basin (Fig. 10.1-D) shows low mineralization with no influences of leaching of evaporitic minerals (spring 51: $[Na^+ + Cl^-]$ = 48 mg/l and $[Ca^{2+} + SO_4^{2-}]$ = 141 mg/l). The isotopic composition of the groundwater shows some strong depletion in heavy

isotopes (-9.6 ‰ < $\delta^{18}O$ < -8.9‰; -66 ‰ < $\delta^{2}H$ < -61 ‰), which proves a local recharge during extreme rain events affected by strong “amount effect”. The low recharge of these perched aquifers does not allow an efficient exploitation of theses groundwater resources.

Confined aquifer of Infracenomanian

The confined aquifer of the Infracenomanian in Imini sub-basin (Fig. 10.1-D) shows clear spatial variations in regard to the geochemistry and isotopic composition (166art $_{mean}$: $\delta^{18}O$ = -8.7‰, $\delta^{2}H$ = -59 ‰ and excess = 9.9 and 167art $_{mean}$: $\delta^{18}O$ = -8.0‰, $\delta^{2}H$ = -55 ‰ and d-excess = 9.2), which reveals the inhomogeneous character of this aquifer. The lower contents of Na^+ and Cl^- (153 mg/l < $[Na^+ + Cl^-]_{Infracenomanian}$ < 302 mg/l) in comparison to the alluvial aquifer of the Mellah Wadi (700 mg/l < $[Na^+ + Cl^-]_{Mellah\ alluvial\ aquifer}$ < 4,000 mg/l) proves that no infiltration occurs from the superficial aquifer of the Mellah Wadi into the confined aquifer.

10.2.4 Residence time

For the estimation of groundwater age, tritium and carbon-14 analyses were performed. Saturation Indexes of quartz is related with tritium values in groundwater of the Upper Drâa catchment, which confirms the interpretations of the estimation of residence time (Fig. 10.2).

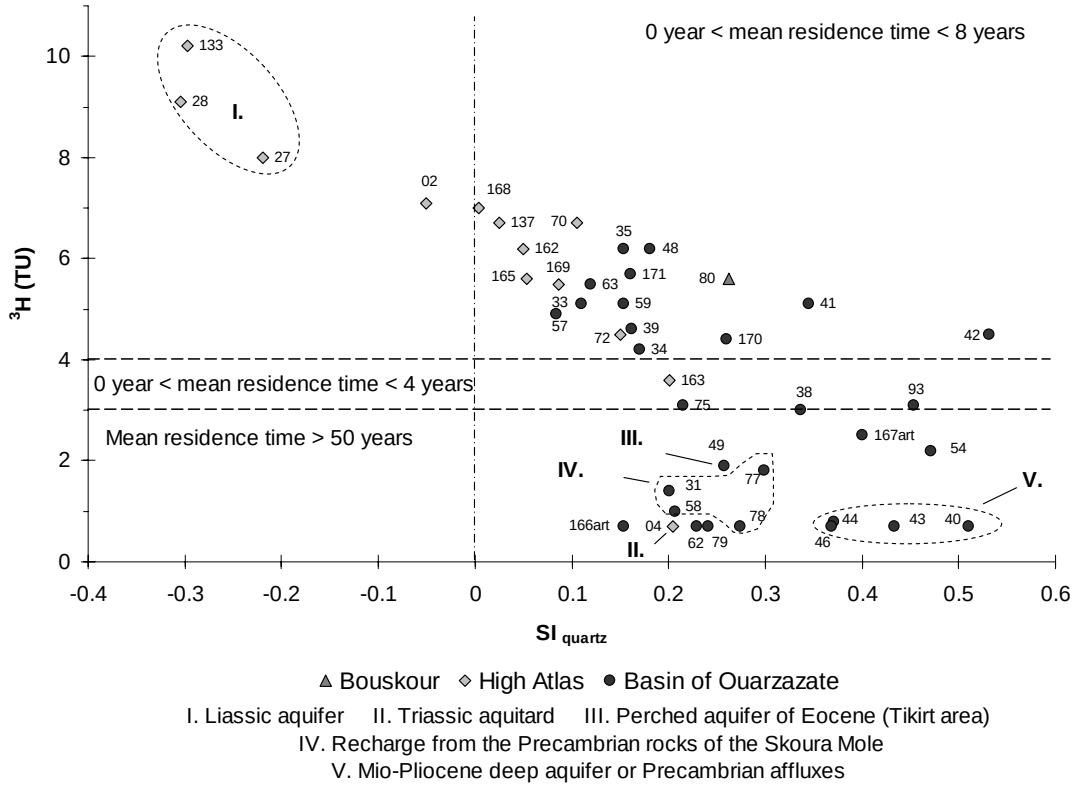

Fig. 10.2: Groundwater residence time in the Upper Drâa catchment represented by tritium values versus saturation index of quartz.

Tritium signatures of the groundwater from the Liassic carbonates and from the alluvial aquifers in the High Atlas as well as of the alluvial aquifers in the Basin of Ouarzazate (Fig. 10.1) indicate ages younger than 10 years and thus recent recharge processes (Fig. 10.2). In the semi-deep aquifers of the Basin of Ouarzazate (wells 40, 43, 44 and 46) the mean residence time of the groundwater is older than 50 years (Fig. 10.2). The confined aquifer of the Infracenomanian in Imini sub-basin (artesian wells 166art and 167art) provides groundwater than 50 years (Fig. 10.1 and 10.2). Due to the fact that the volume of this confined aquifer is

small, the groundwater dating shows that the productivity of this aquifer is not suitable for exploitation. Groundwater from the Precambrian rocks of the Skoura Mole located in the northern part of the basin (Fig. 10.1-B and C) as well as groundwater from Triassic basalt in the Assif-n'Ait-Ahmed valley appears to be older than 50 years (Fig. 10.2). The unproductive character of those fissured aquifers is explained by a low rate of infiltration and a low permeability. Moreover, groundwater of the Precambrian rocks (well 31) shows old groundwater dated between 500 to 2,800 years with the carbon-14 method. The perched aquifers of the Eocene unit in Imini sub-basin (Fig. 10.1-D) show also groundwater older than 50 years (Fig. 10.2), which is due in this case to the low recharge rate by precipitation occurring in the Basin of Ouarzazate.

10.2.5 Numerical model of the alluvial aquifers of the Basin of Ouarzazate

The simulation in steady state of the alluvial aquifer system of the Basin of Ouarzazate has been performed using the numerical groundwater model MODFLOW PMWIN5. The recharge by precipitation is fixed to 10 mm/a according to the water balance defined in the Ifre catchment. Taking into account the result of several simulations, both the evapotranspiration rate as well as the effective hydraulic conductivity of the riverbed (K_{RIV}) are adjusted and fixed to 316 mm/a, and 1.6 $\cdot 10^{-6}$ m/s respectively. This low value of K_{RIV} can be explained by clays deposited within the river bed material after flood events.

Simulations describe well the three main alluvial aquifers of Ouarzazate (115 km^2), Toundoute-Skoura (236 km^2) and Dades-M'Goun (131 km^2), although some errors remain in the calculation of the groundwater level due to the scarcity of data and to calculation problems caused by the presence of dry cells in the model. These errors should be resolved with the development of three distinct models considering separately each alluvial aquifer.

The total recharge displays a summation of recharge by rain infiltration and recharge by river bed infiltration. According to the model results the effective recharge of the alluvial aquifers by river bed infiltration over the whole model domain represents 85 % (~ 27 Mio m^3/a) of the total recharge. These values demonstrate that the main recharge process in the Basin of Ouarzazate is the river bed leakage. As an example, the effective recharge of the alluvial aquifers by the river bed infiltration of the Dades and the M'Goun Rivers averages 10 Mio m^3/a. This result is in the same ranges as the losses of the discharge measured by the DRH monitoring stations, which are about 9 Mio m^3/a.

10.3 Outlook

The groundwater resources in the Upper Drâa catchment are limited due to the small dimension of prevailing aquifers, their low recharge rate and their often natural low quality of the groundwater. The scarcity of water resources in this region represents clearly the main limitation factor for the development. Under the given conditions, future changes of the climate or of the water uses (increasing of irrigation, development of tourisms etc.) will have a strong impact on the groundwater availability and quality. This study allowed the identification of the potentiality of the groundwater resources and their interactions with the surface water of the two of the given three sub-regions defined by IMPETUS project from demographical, economical and natural framework conditions. The sub-regions are (SPETH et al. 2005):

- High Atlas: characterized as a marginalised mountain region with a poorly developed infrastructure where water availability is relatively good and is thus only a weak limiting factor for agricultural production.
- Ouarzazate Basin: characterized by a well-developed infrastructure and strong urban centres where the water resources are limited but still sufficient for the actual conditions.

The results of the hydrogeological investigation will support the development of an “IMPETUS Decision Support System” (IDSS) (SPETH et al. 2005, IMPETUS Westafrika 2006). The IDSS includes a Geographic Information System (GIS), which will display spatially the characteristics of aquifers (e.g. lithology, stratigraphy, geochemical rocktype and hydraulic parameters), the groundwater availability and its quality. Additionally, the hydrogeological model applied on the alluvial aquifer system of the Basin of Ouarzazate will be coupled with other models (e.g. hydrogeological model in the Middle Drâa catchment, hydrological model, climatological model etc.). With the IDSS the various water-related problems having an important impact on the development of this region (such as availability and access of fresh water, climate and land-use changes, food security, and demographic development) can be analysed.

The elucidated amount of available groundwater as well as the model can provide a sufficient basis for the third phase of IMPETUS. But the model can be used only as a starting point. Further refinements are required e.g. additional investigations in the field with detailed mapping of the alluvial aquifer limits and pumping test at selected wells. Installations of a monitoring network in the Basin of Ouarzazate including continueous groundwater level measurements and chemical analyses are required to obtain long time series of data necessary for an appropriate calibration of the model.

REFERENCES

AGUTTES, J.; RJIMATI, E.-C.; TABIT, L. & ZAJACZKOWSKI, W. (1993): Optimisation de la prospection géochimique régionale. Etude méthodologique (Jbel Saghro, Anti- Atlas). – Mines, Géologie et Energie, 53, 69-74.

APPELO, C.A.J. & POSTMA, D. (1999³): Geochemistry, groundwater and pollution. Rotterdam: Balkema-Publisher.

BAKALOWICZ, M. (1979): Contribution de géochimie des eaux à la connaissance de l'aquifère karstique et de la karstification. Thèse de Doctorat d'Etat ès Sciences Naturelles. Université Pierre et Marie Curie, Paris, France.

BAKALOWICZ, M. (1994): Water geochemistry: Water quality and dynamics. – Groundwater Ecology, 97- 127.

BEAUCHAMP, J. (1988): Triassic sedimentation and rifting in the High Atlas (Morocco). In: MANSPEIZER, W. (Ed.): Triassic- Jurassic rifting: continental breakup and the origin of the Atlantic Ocean and passive margins. Amsterdam, Oxford, New York: Elsevier, 477-497.

BEAUCHAMP, J. & PETIT, J.P. (1983): Sédimentation et taphrogenèse triassique au Maroc: l'exemple du Haut Atlas de Marrakech. – Bulletin Centres Recherche Exploration. Elf-Aquitaine, 7, 1, 389-397.

BEAUCHAMP, W.; ALLMENDINGER, R.W.; BARANZAGI, M.; DEMNATI, A.; EL ADJI, M. & DAHMANI M. (1999): Inversion tectonics and the evolution of the High Atlas Mountains, Morocco, based on a geological-geophysical transet. – Tectonics 18, 2, 163-185.

BELL, S. (2005): Geologische Kartierung der IMPETUS-Testfläche Tichki und hydrogeologische Bewertung des Assif-n'Ait-Ahmed Einzugsgebietes, Region M´Goun, südlicher Hoher Atlas, Marokko. Unveröffentlicht. Diplomarbeit. Geologisches Institut. Universität Bonn.

BOYER, C.; CHIKHAOUI, M.; DUPUY, C. & LEBLANC, M. (1978): Le volcanisme calco-alcalin précambrien terminal de l'Anti-Atlas (Maroc) et ses altérations. Interprétations géodynamique. –Comptes Rendus Hebdomadaires des Séances de l´Académie des Sciences, Série D: Sciences Naturelles, 287, 5, 427- 430.

BREDE, R.; HAUPTMANN, M.; HERBIG, H. (1992): Plate tectonics and intracratonic mountain ranges in Morocco. The Mesozoic-Cenozoic development of the Central High Atlas and the Middle Atlas. – Geologische Rundschau. International Journal of earth sciences, 81, 1, 127- 141.

BUDEWIG, T. (in progress): Geologische Kartierung der IMPETUS-Testfläche Tichki, Region M´Goun, südlicher Hoher Atlas, Marokko. Unveröffentlicht. Diplomarbeit. Geologisches Institut. Universität Bonn.

CAPPETTA, H.; JAEGER, J.-J.; SIGE, B.; SUDRE, J. & VIANEY-LIAUD, M. (1987): Compléments et précisions biostratigraphiques sur la faune paléocène à Mammifères et Sélaciens du bassin d'Ouarzazate (Maroc). – Tertiary Res. 8, 4, 147-157.

CAPPY, S. (2001): Impact de l'activité anthropique sur les sources karstiques du Larzac septentrional pour la mise en place d'un réseau de surveillance. Non publié. Rapport de DEA. Université de Montpellier.

CASTANY, G. (1963): Traité pratique des eaux souterraines. Paris: Dunod.

CHAMAYOU, J.; COMBE, M. & DUPUY, J.C. (1977): Moyenne vallée du Dra. In: Royaume du Maroc. Ministère du commerce, de l´industrie, des mines et de la marine marchande. Direction des mines, de la géologie et de l´énergie. Division de la géologie (Ed.): Ressources en Eau du Maroc. Tome 3. Domaines atlasique et sud-atlasique. Notes et Mémoires du service géologique N° 231.Rabat: Service géologique du Maroc, 262-298.

CHIANG, W.H.; KINZELBACH, W. & RAUSCH, R. (1998): Aquifer Simulation Model for Windows. Stuttgart: Gebrüder Bornträger.

CHIANG, W.H. & KINZELBACH, W. (2000): 3D-groundwater modelling with PMWIN- a simulation system for modelling groundwater flow and pollution. New York: Springer-Verlag.

CHOUBERT, G. (1948): Essai sur la paléogéographie du Mésocrétacé marocain. – Livre jubilaire Soc. Sci. Nat. Maroc, 307-365.

CHOUBERT, G. (1963): Histoire géologique du Précambrien de l'Anti Atlas. Royaume du Maroc. Ministère du commerce, de l´industrie, des mines et de la marine marchande. Direction des mines, de la géologie et de l´énergie. Division de la géologie. Notes et Mémoires du service géologique N° 162. Tome 1. Rabat: Service géologique du Maroc.

CLARK, I. & FRITZ, P. (1997): Environmental Isotopes in Hydrogeology. New York: Lewis Publishers.

CRAIG, H. (1961): Isotopic variations in meteoric waters. – Science 133, 3465, 1702-1703.

DE JONG, C.; MACHAUER, R.; REICHERT B.; CAPPY S.; VIGER R. & LEAVESLEY, G. (2004): An integrated geomorphological and hydrogeological MMS modelling framework for a semi-arid mountain basin in the High Atlas, southern Morocco. In: Pahl-Wostl, C.; Schmidt, S.; Rizzol A.E. & Jakeman, A.J. (Eds.): Complexity and Integrated Resources Management, Transactions of the 2nd Biennial Meeting of the International Environmental Modelling and Software Society, iEMSs: Manno, Switzerland, 736-741.

DESTOMBES, J. (1963): Données stratigraphiques sur l'Ordovicien de l'Anti-Atlas (Maroc). – Revue de l'Institut Français du Pétrole, 18, 10, 1464- 1471.

DESTOMBES, J. (1968): sur la présence d'une discordance générale de ravinement d'âge Ashgill supérieur dans l'Ordovicien terminal de l'Anti-Atlas (Maroc). – Comptes Rendus Hebdomadaire des Séance de l´Académie des Sciences, Série D : Sciences Naturelles, 267, 6, 565- 567.

DIRECTION DE LA RECHERCHE ET DE LA PLANIFICATION DE L'EAU (Eds.) (1994): Etude du plan directeur de l'aménagement des eaux des bassins du Guir, Ziz, Rheris et Drâa: étude des schémas d'aménagement. Volume II. Rabat.

DOUGLAS, M. (1997): Mixing and temporal variations of groundwater inflow at the Con Mine. Yellowknife, Canada. Unpublished. Master Science Thesis. University of Ottawa, Canada.

DRESNAY, DU R. (1979): Sédiments Jurassiques du domaine des chaînes Atlasiques du Maroc. – Symposium Sédimentation Jurassique W. Européen. 345-365.

DVWK (DEUTSCHER VERBAND FÜR WASSERWIRTSCHAFT UND KULTURBAU E.V.) (1999): Methoden für die Beschreibung der Grundwasserbeschaffenheit. DVWK- Schriften, 125. Bonn: Wirtschafts- und Verl.- Ges. Gas und Wasser.

DYCK, S. & PESCHKE, G. (1995³): Grundlagen der Hydrologie. Berlin: Verlag für Bauwesen.

EL BOUARI, A. (1990): Modélisation des précipitations et des apports au niveau du barrage Mansour Eddahbi. Mémoire de fin d'étude. Institut agronomique et vétérinaire Hassan II. Rabat.

EL HARFI, A. (1994): Dynamique sédimentaire des séries continentales tertiaires au Sud du Haut-Atlas (bassins de Ouarzazate et Anzal, Maroc). Faciès et milieux de dépôts. Evolution diagénétique et pédogénétique. Thèse. Université Bourgogne. Dijon.

EL HARFI, A.; LANG, J.; SALOMON, J. (1996): Le remplissage continental cénozoique du basin d'avant-pays de Ouarzazate. Implications sur l'évolution géodynamique du Haut Atlas central (Maroc). – Comptes Rendus de l´Académie des Sciences. Serie II. Sciences de la Terre et des Planètes. 323, 7, 623-630.

EL HARFI, A.; LANG, J.; SALOMON, J. & CHELLAI, E. H. (2001): Cenozoic sedimentary dynamics of the Ouarzazate foreland basin (Central High Atlas Mountains, Morocco). – Geologische Rundschau. International Journal of Earth Science, 90, 2, 393-411.

EL OUALI, A.; MUDRY, J.; MANIA, J.; CHAUVE, P.; ELYAMINE, N. & MARZOUK, M. (1999): Present recharge of an aquifer in a semi-arid region: an example from the Turonian limestones of the Errachidia basin, Morocco. – Environmental Geology, 38, 2, 171-176.

ERRARHOUI, K. (1997): Structure du Haut Atlas: Plis et chevauchements du socle et de couverture (interpretations des données géophysiques et géologiques). Thèse. Université Paris-Sud. Orsay, France.

FONTES, J.C. (1976): Isotopes du milieu et cycles des eaux naturelles: quelques aspects. Thèse de doctorat d'état. Université Paris.

FONTES, J.C. (1985): Some considerations on groundwater dating using environmental isotopes. – IAHS-AISH Publication, 154, 1, 118-154.

FONTES, J.C.; TAYLOR, R.E.; LONG, A. & KRA, R.S. (Eds.) (1992): Chemical and isotopic constraints on ^{14}C dating of groundwater. United States: Springer-Verlag.

FONTES, J.C. & GARNIER, J.M. (1979): Determination of the initial ^{14}C activity of total dissolved carbon: a review of existing models and a new approach. – Water resources Research, 15, 2, 399-413.

FRAISSINET, C.; ZOUINE, E. M.; MOREL, J.L.; POISSON, A.; ANDRIEUX, J.; FAURE-MURET, A. (1988): Structural evolution of the southern and northern central High Atlas in Paleogene and Moipliocene times. In: Jacobshagen, V. (Ed.): The System of Marocco. Lecture Notes Earth Science. Volume 15. New York: Springer, 273-292.

FRIEDLI, H.; LOTSCHER, H.; OESCHGER, H.; SIEGENTHALER, U. & STAUFFER, B. (1986): Ice core record of the 13C/12C ratio of atmospheric CO2 in the past two centuries. – Nature London, 324, 6094, 237-238.

FRITZ, P. & FONTES, J.C. (Eds.) (1980): Handbook of environmental isotope geochemistry. Volume 1-3. Amsterdam, Oxford, New York: Elsevier.

FRIZON DE LAMOTTE, D.; SAINT BEZAR, B.; BRACENE, R. & MERCIER, E. (2000): The two main steps of the Atlas building and geodynamics of the western Mediterranean. – Tectonics 19, 4, 740-761.

GAT, J.R.; MOOK, W.G. & MEIJER, H.A.J. (2001): Environmental isotopes in the hydrological cycle. Principles and applications. Volume II: Atmospheric water. IHP-V, Technical Documents in Hydrology, No. 39. Unesco. Paris.

GAUTHIER, H. (1957): Contribution à l'étude géologique des formations post-liasiques du bassin du Dadès et du Haut-Todra (Maroc méridional). – Notes et Memoires du Service Geologique Rabat, 119.

GEYH, M. (2000): Environmental isotopes in the hydrological cycle. Principles and applications. Volume IV. Surface Water. IHP-V. Technical Documents in Hydrology, No. 39, Vol. IV. Unesco: Paris.

GENTIL, L. (1915): Le Crétacé moyen et supérieur dans le Haut Atlas occidental (Maroc). In : Comptes Rendus de l´Académie des Sciences. Sciences de la Terre et des Planètes. 160. Paris: Gauthier- Villars, 774.

GIBSON, J.J.; EDWARDS, T.W.D. & PROWSE, T.D. (1993): Runoff generation in a high boreal wetland in northern Canada. – Nordic Hydrol. 24, 213-224.

GONFIANTINI, R.; FRÖHLICH, K.; ARAGAS, L.A. & ROZANSKI, K. (1998): Isotopes in Groundwater Hydrology. In: Kendall, C. & McDonnell, J.J. (Eds.): Isotope Tracers in Catchment Hydrology. Amterdam: Elsevier, 203-246.

GÖRLER, K. & ZUCHT, M. (1986): Stratigraphie und Tektonik des kontinentalen Neogens im Süden des Zentralen Hohen Atlas, Provinz Ouarzazate (Maroko). Berliner Geowissenschaftliche Abhandlungen, Reihe A: Geologie und Palaeontologie, 66, 2, 471-494.

GÖRLER, K.; JACOBSHAGEN, V.H. (ED.); HELMDACH, F.F.; GAEMERS, P.; HEISSIG, K.; HINSCH, W.; MÄDLER, K.; SCHWARZHANS, W. & ZUCHT, M. (1988): The uplift of the central High Atlas as deduced from Neogene continental sediments of the Ouarzazate province, Morocco. – Lecture Notes in Earth Sciences 15, 361- 404.

GÜLER, C.; THYNE, G.D.; MCCRAY, J.E. & TURNER, A.K. (2002): Evaluation of graphical and multivariate statistical methods for classification of water chemistry data. – Hydrogeology Journal 10, 4, 455-474.

HERBIG, H.G. (1986): Lithostratigraphisch-fazielle Untersuchungen im marinen Alttertiär südlich des zentralen Hohen Atlas (Marokko). – Berliner Geowissenschaftliche Abhandlungen, Reihe A: Geologie und Palaeontologie, 66, 2, 343-380.

HERBIG, H.G. (1991): Das Paläogen am Südrand des zentralen Hohen Atlas und im Mittleren Atlas Marokkos. Stratigraphie, Fazies, Paläogeographie und Paläotektonik. – Berliner Geowissenschaftliche Abhandlungen, Reihe A: Geologie und Paläontologie, 135, 1-289.

HERBIG, H.-G. & TRAPPE, J. (1994): Stratigraphy of the subatlas Group (Maastrichian-Middle Eocene, Morocco). – Newsletter on Stratigraphy, 30, 3, 125-165.

HOFMANN, H. (2002): Geologische Kartierung und hydrogeologische Bewertung der IMPETUS-Testfläche Ameskar, Region M´Goun, südlicher Hoher Atlas, Marokko. Unveröffentlicht. Diplomarbeit. Geologisches Institut. Universität Bonn.

HUNEAU, F. (2000): Fonctionnement hydrogéologique et archives paléoclimatologies d'un aquifère profond méditerranéen: Etude géochimique et isotopique du bassin miocène de Valréas (Sud-Est de la France). Thèse de doctorat. Université d´Avignon (France).

IAEA (1980): Arid zone hydrology: investigations with isotope techniques. TecDoc. Vienna: AIEA.

IAEA (1987): Isotope techniques in water resources development. Proceedings of a symposium, Vienna: AIEA.

IAEA (1991): Isotope techniques in water resources development. Proceedings of a symposium. Vienna: AIEA

IAEA (1995): Isotopes in water resources management. Proceedings of a symposium, Vienna: AIEA

IAEA (2001): Isotope techniques in water resource investigations in arid and semi-arid regions. TecDoc-1207. Vienna: AIEA

IMPETUS WESTAFRIKA (2006): Fallstudien für ausgewählte Flusseinzugsgebiete in unterschiedlichen Klimazonen. Sechster Zwischenbericht. Köln.

JACOBSHAGEN, V.; BREDE, R.; HAUPTMANN, R.M.; HEINITZ, W. & ZYLKA, R. (1988): Structure and post-Paleozoic evolution of the Central High Atlas. In: Jacobshagen, V. (Ed.): The Atlas system of Morocco. Berlin: Springer Verlag, 245-271.

JENSEN, M.E. & HAISE, H.R. (1963): Estimating evapotranspiration from solar radiation. – J. Irrig. Drainage Div. ASCE, 89, 15-41.

JENNY, J.; LE MARREC, A. & MONBARON, M. (1981): Les couches rouges du Jurassique moyen du Haut Atlas central (Maroc): correlations lithostratigraphiques, éléments de datation et cadre-tectono-sédimentaire. – Bulletin de la Societé Géologique de France, série 7, 23, 6, 627-639.

JENNY, J. (1988): Les décrochements de l'Atlas de Demnat, Haut Atlas central (Maroc): Prolongation orientale de la Zone de décrochement du Tizi n'Test et clef de la comprèhension de la tectonique atlasique. – Eclogae Geologicae Helvetiae, Volume 76, 1, 243-251.

JOSSEN, J.-A. & FILALI, J. (1988): Le bassin de Ouarzazate, synthèse stratigraphique et structurale. Contribution à l'étude des aquifères profonds. Progr. Nations Unies Dévelop. Dep Coop Techn., Dévelop Projet MOR 86/004, 1-36.

KENDALL, C. & CALDWELL, A.J.J. (1998): Fundamentals of Isotope Geochemistry. In: Kendall, C. & McDonnell, J.J. (Eds.): Isotope Tracers in catchment Hydrology. Amsterdam: Elsevier, 51-86.

KHALIL, J. & RACHACH, A. (1986): Etude géologique et hydrogéologique du secteur ouest du bassin de Ouarzazate (région Ouarzazate Tikirt). Diplom d'Ingénieur d'Etat. Rabat.

KINZELBACH, W. & RAUSCH, R. (1995): Grundwassermodellierung. Eine Einführung mit Übungen. Berlin [u.a.]: Bornträger.

KINZELBACH, W.; AESCHBACH, W.; ALBERICH, C.; GONI, IB.; BEYERLE, U.; BRUNNER, P.; CHIANG, WH.; RUEEDI, J. & ZOELLMANN, K. (2002): A survey of Methods for Groundwater Recharge in Arid and Semi-arid regions. Early Warning and Assessment Report Series, UNEP/DEWA/RS.02-2. United Nations Environment Programme. http://www.unep.org/water/groundwater/. (2006-07-30).

KNIPPERTZ, P.; FINK, A.; REINER, A. & SPETH, P. (2003): Three late summer/early autumn cases of tropical-extratropical interactions causing precipitation in Northwest Africa. – Monthly Weather Review, 131, 1, 116-135.

LANGMUIR, D. (1971): The geochemistry of some carbonate groundwaters in central Pennsylvania. – Geochimica et Cosmochimica Acta, 35, 10, 1023- 1045.

LAVILLE, E., LESAGE, J.C. & SEGURET, M. (1977): Géométrie, cinématique (dynamique) de la tectonique atlasique sur le versant sud du Haut Atlas marocain. Aperçu sur les tectoniques hercyniennes et tardi-hercyniennes. Bulletin de la Société géologique de France, 19, 3, 527-539.

LAVILLE, E. (1980): Tectonique et microtectonique d'une partie du versant sud du Haut Atlas marocain (Boutonnière de Skoura, Nappe de Toundoute). – Notes Mém. Serv. géol. Maroc, 41, 285, 81-183.

LAVILLE, E. & PETIT, J.P. (1984): Role of synsedimentary strike-slip faults in the formation of Moroccan Triassic basins. – Geology 12, 7, 424-427.

LAVILLE, E. (1988): A multiple releasing and restraining stepover model for the Jurassic strike-slip basin of the Central High Atlas (Morocco). In: Manspeizer, W. (Ed.): Triassic-Jurassic Rifting, Continental Breakup and the Origin of the Atlantic Ocean. New York: Elsevier, 499-523.

LAVILLE, E. & PIQUE, A. (1991) : La distension crustale atlantique et atlasique au Maroc au début du Mésozoique: le rejeu des structures hercyniennes. – Bulletin de la Société Géologique de France, Huitième Série, 162, 6, 1161- 1171.

LAWRENCE, J.R. (1987): Use of contrasting D/H ratios of snows and groundwater of eastern New York State in watershed evaluation. – Water Resource Res. 23, 519-521.

LEBLANC, M. (1976): Proterozoic oceanic crust at Bou Azzer. – Nature London, 261, 5555, 34-35.

LEVESQUE, R. (2004): SPSS programming and data management – a Guide for SPSS and SAS users. Second Edition SPSS.

LEVIN, I.; GRAUL, R. & TRIVETT, N.B.A. (1995): Long term observations of atmospheric CO2 and carbon isotopes at continental sites in Germany. – Tellus Series B-chemical and physical meteorology, 47, 1-2, 23- 24.

MALOSZEWSKI, P. & ZUBER, A. (1993): Principles and practice of calibration and validation of mathematical models for the interpretation of environmental tracer in aquifers. – Advances in Water Resources, 16, 3, 173- 190.

MANSPEIZER, W.; PUFFER, J. H. & COUSMINER, H. L. (1978): Separation of Morocco and eastern North America: A Triassic-Liassic stratigraphic record.– Geological Society of America Bulletin, 89, 6, 901-920.

MARGANE, A. (2003): Management, protection and sustainable use of groundwater and soil resources in the Arab Region. Volume 6: Guideline for sustainable groundwater resources Management. Damascus: ACSAD-BGR Technical Cooperation Project.

MARINI, F. & OUGUIR, H. (1990): Un nouveau jalon dans l'histoire de la distension pré: panafricaine au Maroc: le Précambrien II des boutonnière du Jbel Saghro nord-oriental (Anti Atlas, Maroc). – Comptes Rendus de l´Académie des Sciences, Série 2, Mecanique, Physique, Chimie, Sciences de l´Univers, Sciences de la Terre, 310, 5. Paris : Gauthier- Villars, 577- 582.

MARTAU, R. (2002): Geologie des Gebietes um Taoujgalt, (Hoher Atlas, Marokko) unter besonderer Berücksichtigung der triassischen und kretazischen Schichtenfolge. Unveröffentlicht. Diplomarbeit. Geologisches Institut. Universität Bonn.

MATTAUER, M. ; TAPPONNIER, P. & PROUST, P. (1977): Sur le mécanisme de formation de chaînes intracontinentales. L'exemple des chaînes atlasiques du Maroc. – Bulletin Societé géologique France, 7, 19, 3, 521-526.

MCDONALD, M.G. & HARBAUGH, A.W. (1988a): MODFLOW, A modular three-dimensional finite-difference groundwater flow model. U. S. Geological Survey. Open-file report 83-875. chapter A1.

MCDONALD, M.G. & HARBAUGH, A.W. (1988b): A modular three-dimensional finite-difference groundwater flow model. Techniques of water resources. Invests. Of the, U.S. Geol. Survey. Book 6. C. Al.

MICHARD, A. (1976): Elément de géologie marocaine, – Notes et mémoires du Service géologique du Maroc, 252, 369- 408.

MINISTERE DE L' EQUIPEMENT, DGH, DRPE & DRH DU SOUSS MASSA ET DRAA (2002) : Elaboration du schéma directeur de la province de Ouarzazate pour l'approvisionnement en eau potable des populations rurales et la définition des projets. Mission 1: analyse de la situation existante. Etude des ressources en eau. Agadir.

MORET, L. (1933) : Compléments stratigraphiques de la zone subatlasique méridionale de l'Atlas de Marrakech. – Comptes Rendus somm. Societé géologique de France. 16, 257- 258.

MOOK, W.G. (Ed.) (2000): Environmental isotopes in the hydrological cycle. Principles and applications. Volume I. Introduction. IHP-V, Technical Documents in Hydrology, No. 39, Vol. I. Paris: Unesco.

OLIVE, P. (1999): La datation des eaux souterraines à long temps de résidence par le radiocarbone. Mode d'emploi. – Hydrogéologie, 1, 3-19.

OSTERHOLT, V. (2002): Geologische Kartierung der IMPETUS-Testfläche Ameskar, Region M´Goun, südlicher Hoher Atlas, Marokko. Unveröffentlicht. Diplomarbeit. Geologisches Institut. Universität Bonn.

PARKHURST, D.L. & APPELO, C.A.J. (1999): User's guide to PHREEQC (Version 2): A computer program for speciation, batch reaction, one dimensional transport, and inverse geochemical calculations. U.S. Geological Survey Water Ressources Investigations Report 99-4259.

PIQUÉ, A.; BOSSIERE, G.; BOUILLIN, J.P.; CHALOUAN, A.; HOEPFFNER, C. (1993): Southern margin of the Variscan belt: The north-western Gondwana mobile zone (eastern Morocco and northern Algeria).– Geologische Rundschau, 82, 432-439.

PIQUÉ, A. (2001): Geology of Northwest Africa. Berlin: Borntraeger.

RAVENGA, C. (1998): Watersheds of the world. Ecological value and vulnerability. A joint publication of the World Resources Institute and the Worldwatch Institute, Washington, USA.

ROZANSKI, K.; FROEHLICH, K. & MOOK, W.G. (ED.) (2001): Environmental isotopes in the hydrological cycle. Principles and applications. Volume III. Surface Water. IHP-V. Technical Documents in Hydrology, No. 39, Vol. III. Unesco: Paris.

RUEEDI, J. (2002): A survey of Methods for Groundwater Recharge in Arid and Semi-arid regions. Early Warning and Assessment Report Series. UNEP/DEWA/RS.02-2. United Nations Environment Program. Nairobi. Kenya. 44- 56.

SALEM, O.; VISSER, J.H.; DEAY, M. & GONFIANTINI, R. (1980): Groundwater flow patterns in the western Lybian Arab Jamahiriaya evaluated from isotopic data. In: Panel Proceedings Series, STI/PUB/547. Austria: IAEA, 165-179.

SCHMIDT, M. (2003): Development of a fuzzy expert system for detailed land cover mapping in the Dra catchment (Morocco) using high resolution satellite images. Elektronische Dissertationen der Mathematisch-Naturwissenschaftlichen Fakultät der Universität Bonn.

SCHULZ, O. & DE JONG, C. (2004): Snowmelt and sublimation: field experiments and modelling in the High Atlas Mountains of Morocco. – Hydrology and Earth System Sciences, 8, 6, 1076-1089.

SCHULZ, O. (2006): Analyse schneehydrologischer Prozesse und Schneekartierung im Einzugsgebiet des Oued M'Goun, Zentraler Hoher Atlas (Marokko). Dissertation an der Mathematisch-Naturwissenschaftlichen Fakultät der Universität Bonn.

SPETH, P.; DIEKKRÜGER, B. & CHRISTOPH, M. (2002): an integrated approach to the efficient management of scarce water resources in West Africa- case studies for selected river catchments in different climatic zones, Intern Status report, April 2002.

SPETH, P.; DIEKKRÜGER, B.; CHRISTOPH, M. & JAEGER, A. (2005): An integrated approach to the efficient management of scarce water resources in West Africa – case studies for selected river catchments in different climatic zones. IMPETUS Report period: 01.05.2003-28.02.2005, Cologne.

SPITZ, K. & MORENO, J. (1996): A practical guide to groundwater and solute transport modelling. New York: John Wiley & Sons.

STAMM, R. (1981): Die Dolomitische Facies des Turon im Hohen Atlas zwischen Atlantik und Sahara (Marokko). Dissertation. Universität Bonn.

STETS, J. (1992): Mid-Jurassic events in the western High Atlas (Morocco). – Geologische Rundschau 81, 1, 69-84.

STETS, J. & WURSTER, P. (1977): Atlas and Atlantic – structural relations. Eos. Trans. AGU, 58, 908.

STETS, J. & WURSTER, P. (1981): Zur Strukturgeschichte des Hohen Atlas in Marokko.– Geologische Rundschau 70, 3, 801-841.

THEIN, J. (1985): Die Paläogeography of the High Atlas Marokkos – Ergebnisse Geochemischer und Mikrofazieller Untersuchungen. Habilitation. Universität Bonn.

THEIN, J. (1989): Paleogeography and Geochemisrty of the "Cenomano-Turonian" Formations in the Manganese District of Imini (Morocco) and their Relation to Ore Deposition. – Ore Geology Reviews, 5, 4, 257-291.

THORNTHWAITE, C. W. (1948): An approach toward a rational classification of climate. – Geographical Review 38, 55-94.

TÓTH, J. (1998): Groundwater as a geologic agent: An overview of the causes, processes, and manifestations. In: Hydrogeology Journal ,7, 1, 1-14.

TRAPPE, J. (1989): Das marine Alttertiär im Westlichen Hohen Atlas: Mikrofazies, Paläogeographie, Phosphoritgenese. Doktorarbeit. Bonn.

TRAPPE, J. (1991): Stratigraphy, facies distribution and paleogeography of the Marine Paleogene from the western High Atlas, Morocco. – Neues Jahrbuch für Geologie und Paläontologie. Abhandlungen, 180, 3, 279-321.

TURC, L. (1963): Evaluation des besoins en eau d'irrigation, évapotranspiration potentielle, formulation simplifié et mise à jour. – Ann. Agron., 12, 13-49.

USDA NATURAL RESOURCES CONSERVATION SERVICE (USDA NRSC) (1993): Channel transmission losses. Chapter 19. National Engineering Handbook. Number 4: Hydrology. Washington, D.C.: U.S. Department of Agriculture.

VAN HOUTEN, F.B. (1977): Triassic-Liassic deposits of Morocco and Eastern North America: comparison. – Bulletin Am. Assoc. Petrol. Geol., Volume 61, 79-99.

VOGEL, J.C. (1970): Carbon-14 dating of groundwater. In: Isotope Hydrology 1970. 225-239. IAEA Symposium 129. Vienna.

VOGEL, J.C. (1993): Variability of carbon isotope fractionation during photosynthesis. In: Ehleringer, J.R.; Hall, A.E. & Farquhar, G.D. (eds.): Stable Isotopes and Plant Carbon – Water relations. Academic Press. San Diego, 29-38.

WARME, J. (1988): Jurassic carbonate facies of the central and eastern High Atlas rift, Morocco. In: JACOBSHAGEN, V. (ed.): The Atlas System of Morocco. Berlin: Springer Verlag, 169-199.

YOUBI, L. (1990): Hydrologie du basin du Dadès. Ministère de l'Agriculture et de la réforme Agraire, ORMVAO. Ouarzazate.

ZUBER, A. (1986): Chapter 1. Mathematical models for the interpretation of environmental radioisotopes in groundwater systems. In: FRITZ, P. & FONTES, J. C. (Eds.): Handbook of environmental Isotope Geochemistry. Vol. 2. Amsterdam: Elsevier, 1-59.

ZUBER, A. & MALOSZEWSKI, P. (2001): Lumped parameter models., In: MOOK, W.G. (Ed.): Environmental isotopes in the hydrological cycle-Principles and applications. Volume VI: Modelling. IHP-V. Technical Documents in Hydrology, No. 39, Vol. IV. Unesco: Paris, 5-36.

GEOLOGICAL MAPS

FETHA, M.; BENSAID, M. & DAHMANI, A. (1990): Carte géologique du Maroc-Zawyat Ahancal. Scale 1/100,000. Rabat, Morocco : Minist. de l´Energie et del Mines.

SAADI, M.; HILALI, E.A. & BENSAID, M. (1977): Carte géologique du Maroc-Jebel Saghro-Dadés. N° 161. Scale 1/200,000. Rabat, Morocco : Minist. de l'Energie et des Mines.

SAADI, M. ; BENSAID, M. & DAHMANI, M. (1985): **C**arte géologique du Maroc-Azilal. 339. Scale 1/100,000. Rabat, Morocco : Minist. de l'Energie et des Mines.

CHOUBERT, G ; DESTOMBES, J. ; FAURE-MURET, A. ; GAUTHIER, H. ; HINDERMEYER, J. ; HOLLARD, H. & JOURAVSKY, G. (1971) : Carte géologique de l'Anti-Atlas central et de la zone synclinale de Ouarzazate : feuilles Ouarzazate-Alougoum et Telout Sud, N° 138. Scale 1/200,000. Rabat, Morocco : Minist. de l'Energie et des Mines.

CHOUBERT G. ; DESTOMBES, J. ; GAUTHIER, H. & HINDERMEYER, J. (1980): Carte géologique du Maroc Jbel Saghro-Dadès. 161 (Haut Atlas Central, sillon Sud-Atlasique et Anti-Atlas oriental). Scale 1/200,000. Rabat, Morocco : Minist. de l'Energie et des Mines.

CHOUBERT, G. (1959): Feuille de Ouarzazate. Carte géologique du Maroc. Scale 1/500,000. N°70 1978. Rabat, Morocco: Minist. de l'Energie et des Mines.

INTERNET LINKS

UNITED NATIONS ENVIRONMENT PROGRAMME (13/08/2006): http://www.unep.org

INTERNATIONAL ATOMIC ENERGY AGENCY (13/08/2006/): http://www.iaea.org